

**On the effect of tidal variations of turbulent mixing  
on flow and salt transport in estuaries**

**An idealised model study**



Yoeri Dijkstra  
Thesis Applied Mathematics  
November 2014



# On the effect of tidal variations of turbulent mixing on flow and salt transport in estuaries

An idealised model study

Final report

**Y.M. Dijkstra BSc.**

Master Thesis

Applied Mathematics, Specialisation Computational Science and Engineering,  
Faculty of Electrical Engineering, Mathematics and Computer Science,  
Delft University of Technology



**Thesis presentation November 14, 2014 15.30**

Assessment committee:	dr. H.M. Schuttelaars,	TU Delft
	prof. dr. J.D. Pietrzak,	TU Delft
	dr. ir. M.B. van Gijzen,	TU Delft
	dr. ir. R.E. Uittenbogaard,	Deltares
	ir. J.A.Th.M. van Kester,	Deltares

Cover photo: Trá Lí estuary and Blennerville windmill, Ireland  
By Aron Dijkstra, 2014



# Abstract

The intrusion of sea water into estuaries creates a complex flow that results from the density difference between fresh river run-off and salty sea water. In combination with other processes, such as tides, these complex flows are of interest because they affect the transport of e.g. salt, sediments and nutrients in water, which determine the future shape and ecology of the estuary. This research focusses on mechanisms that result in exchange flows and transport of salt.

The model study has led to new insights into the way in which tides and baroclinic pressure gradients contribute to the straining circulation, i.e. the exchange flow that is induced by the interaction of temporal variations of turbulence and velocity. The straining circulation is traditionally associated with the tidal flow. To make a distinction between this traditional view and the new findings, we will call this the *tidal straining circulation*. It is shown that the tidal straining circulation explains only a small part of the total straining circulation in a parameter space typical for well-mixed and partially stratified estuaries.

This research identifies a new and more important contribution to the straining circulation. This is caused by interactions between the gravitational circulation and temporal variations of turbulent mixing, which we will call the *gravitational straining circulation*. The gravitational straining circulation increases non-linearly with increasing temporal variations of turbulence. Large tidal variations of turbulent mixing are typically found in well-mixed and partially stratified estuaries. Such temporal variations of turbulence can be caused by strain-induced periodic stratification (SIPS), asymmetric mixing or symmetric variations of mixing, such as the variation of turbulence with the tide.

The dominant contribution of gravitational straining circulation to the total straining circulation explains why the straining circulation is larger than the gravitational circulation in partially stratified estuaries and why both the gravitational circulation and the straining circulation have the same dependency on the along-channel salinity gradient. It also explains why the straining circulation is much smaller in strongly stratified estuaries, where the tidal variations of turbulence are not as large as in partially stratified estuaries. The direction and magnitude of the gravitational straining circulation is additionally shown to be independent of the timing of temporal variations of turbulent mixing. The magnitude and direction of the tidal straining circulation depend not only on the timing of temporal variations of mixing, but are shown to also depend on the bed roughness and the rate of mixing. This implies that the tidal straining circulation can act in the opposite direction as is expected from current theory in certain model parametrisations.

Concerning the transport of salt, it is shown that temporal variations of turbulent mixing are able to create a strong salt transport. A potentially large salt transport is caused by temporal correlations of the salinity and the velocity. This salt transport contribution is shown to be highly sensitive to the phase of the salinity, which is strongly dependent on the phase of turbulent mixing. Accurate modelling of turbulence is therefore essential to obtaining accurate results for the salinity.



# Preface

Estuaries have captured my imagination ever since I first encountered them in my studies. Many estuaries are areas of great natural beauty and tranquillity. Others support some of the largest cities and harbours in the world and have become of essential economic value. It is therefore that human interventions in estuaries and the surrounding waters can have an enormous environmental and economical impact. The understanding of the physics that governs the flow in estuaries is of essential importance to evaluating and designing sustainable measures for managing estuaries. This research treats a number of important physical mechanisms that act in estuaries. These investigations are on an abstract level and will only contain the odd reference to real estuaries. Still, the idea of studying something so tangible and natural as estuaries inspires me on a daily basis.

The physics of flow in estuaries contains exactly those elements that have always intrigued me during my studies and that have led me take-up my studies in mathematics as well as in civil engineering. This physics includes turbulence and the complex interactions between flow and turbulence that lead to transitions between different states of the estuarine system. I am therefore happy that this thesis treats such interactions between flow and turbulence, to make a contribution to a further understanding of the physics of estuaries.

This research is my master thesis for Applied Mathematics and part of my double degree in Civil Engineering and Applied Mathematics. This research has been an excellent combination of both fields of study; using mathematical techniques to formulate and implement an idealised model and using understanding of the physical system to interpret the results. I hope that this work can be a bridge between the two fields, showing the use of idealised models to civil engineers and the mathematical challenges of estuarine physics to mathematicians.

I would like to thank Henk Schuttelaars for the great cooperation, good ideas and his endless enthusiasm in working on this thesis. This work would not be what it is without his great support. I would also like to thank Julie Pietrzak and Rob Uittenbogaard for their feedback during the writing of this thesis and Jan van Kester and Martin van Gijzen for their work on the assessment committee. I would like to express my gratitude to Deltares for giving me the opportunity to work with them for fourteen months during the work on both theses.

I hope that you will find as many new insights in reading this thesis as I did in the process of writing it.

Yoei Dijkstra,  
November 2014



# Contents

<b>Introduction</b>	<b>1</b>
<b>1 Flow in estuaries</b>	<b>5</b>
1.1 Propagation of the tide . . . . .	6
1.2 Baroclinic flow . . . . .	7
1.3 Turbulence and turbulence induced flows . . . . .	9
<b>2 Model formulation: hydrodynamics</b>	<b>13</b>
2.1 Assumptions and approach . . . . .	14
2.2 Model equations . . . . .	15
2.3 Solution method . . . . .	17
2.4 The $k - \varepsilon$ turbulence model . . . . .	24
<b>3 Model formulation: salinity</b>	<b>29</b>
3.1 Background and assumptions . . . . .	29
3.2 Model equations . . . . .	30
3.3 Solution method . . . . .	31
3.4 Salt balance decomposition . . . . .	32
<b>4 Results: hydrodynamics</b>	<b>37</b>
4.1 Reference case . . . . .	38
4.2 The effect of a parabolic eddy viscosity . . . . .	40
4.3 The eddy viscosity as calculated by the $k - \varepsilon$ model . . . . .	42
4.4 The interaction of the velocity and eddy viscosity . . . . .	45
4.5 The decomposition of the straining circulation . . . . .	50
4.6 The (un)importance of longitudinal eddy viscosity variations . . . . .	58
<b>5 Results: salinity</b>	<b>61</b>
5.1 Reference case . . . . .	61
5.2 Results with a $k - \varepsilon$ turbulence model . . . . .	63
5.3 Sensitivity to the phase of the eddy viscosity . . . . .	65
5.4 Limitations of the salinity model . . . . .	67
<b>6 Discussion</b>	<b>69</b>
6.1 Exchange flows . . . . .	69
6.2 Salt intrusion . . . . .	75
<b>Conclusions</b>	<b>77</b>
<b>Recommendations</b>	<b>79</b>
<b>Bibliography</b>	<b>81</b>
<b>A Derivation and solution hydrodynamics</b>	<b>85</b>
A.1 Scaling the equations . . . . .	85
A.2 Version 1: constant eddy viscosity . . . . .	89
A.3 Version 2: parabolic viscosity . . . . .	94
A.4 Version 3: time-varying viscosity . . . . .	95
A.5 Version 4: time- and space-varying viscosity . . . . .	101

---

A.6 Analytical solution to the Version 3 momentum equation . . . . .	102
A.7 Numerical aspects . . . . .	103
<b>B Salinity model</b>	<b>107</b>
B.1 Scaling and derivation of the model . . . . .	107
B.2 Vector form of salinity model . . . . .	110
<b>C Implementation of the <math>k - \varepsilon</math> turbulence model</b>	<b>113</b>
<b>D Model verification</b>	<b>117</b>
D.1 Required number of frequency components . . . . .	117
D.2 Validity of the scaling . . . . .	117
D.3 Model convergence and limitations . . . . .	118
D.4 Closure of the salt balance . . . . .	120
<b>E Approximate analytical solutions to the straining circulation</b>	<b>123</b>
E.1 Tidal straining circulation with a constant eddy viscosity profile . . . . .	123
E.2 Tidal straining circulation with an arbitrary eddy viscosity profile . . . . .	124
E.3 Phase independence of the gravitational straining circulation . . . . .	125

# Introduction

Estuaries are bodies of water where rivers meet the sea or ocean. The flow of water in estuaries is not only affected by the clearly visible external forcing of tides, river discharge and wind, but also by the internal forcing by density variations in the water. An example of such density variations are the density differences between the salty sea water that flows into the estuary and the fresh river water that flows out into the sea. These forcing mechanisms and the interaction between them give rise to complex flow patterns. A part of such density induced flows are exchange flows. Exchange flow is a term for the residual, i.e. time-averaged, flow of water, with a cross-sectionally-averaged velocity of zero, but with varying magnitude and direction over the estuarine cross-section. The exchange flow is of interest because it is important for the transport of constituents in the estuary such as salt, sediments, nutrients and algae, which in turn determine the development of the shape and ecology of the estuary.

The transport of salt in water is of particular interest because it is both affected by the flow and induces a flow. These interactions between water and salinity have such an effect on the flow dynamics, that the understanding of them is a requirement for understanding the transport of other substances in water. The transport of salt is also of interest in itself; the intrusion of salt water into the estuary can be a major problem for the agricultural and drinking water system in the often heavily populated areas around estuaries.

Mathematical models can be used to gain understanding of the exchange flows and salinity dynamics. There are several types of models that exist for this purpose, each with their own advantages. One clear distinction between model types is that between idealised and complex models ([Murray, 2003](#)). Idealised models are characterised by containing only those physical processes that are regarded as the essential physical processes for the subject under study. These models are, as a result, not capable of providing a quantitatively accurate representation of a real estuary. Their relative simplicity, however, makes them suitable for providing insight into the workings and importance of the physics that is included. Contrastingly, complex numerical models are capable of simulating estuarine dynamics at a more quantitative basis, but it is generally difficult to explain the model results in terms of the separate physical processes contained in the model.

Restricting our attention to idealised models, we see that these models have long mainly focussed on the net transport by residual flows in general and exchange flows in particular. The classical way ([Geyer and MacCready, 2014](#)) of analysis contains the residual flow which is due to the river flow, a baroclinic pressure gradient (i.e. pressure differences that are caused by density differences) and non-linear advection. Some or all of these residual velocity components are used to calculate the net transport of salt ([Hansen and Rattray, 1965](#); [MacCready, 2004](#); [Ralston et al., 2008](#)). The exchange flow which is caused by the baroclinic pressure gradient is called gravitational circulation and is considered by these authors to be the most important mechanism for the transport of salinity. The baroclinic pressure gradient arises from the fact that the salinity on the seaward side of the estuary is higher than on the landward side. This causes the typical gravitational circulation with water flowing into the estuary near the bed and water flowing out to sea near the water surface, see [Geyer \(2010\)](#) or Section 1.2.

The classical way of modelling residual flows does not consider an important class of exchange flows that is created by asymmetric mixing. Asymmetric mixing concerns differences in the amount of turbulent mixing of the water column over a tidal cycle. The occurrence of asymmetric mixing is often ascribed to strain-induced periodic stratification (SIPS). The SIPS mechanism was first published by [Simpson et al. \(1990\)](#) and concerns tidal asymmetries in the degree of mixing of salt and fresh water. This asymmetry works as follows: during ebb tide, the vertical velocity gradient causes fresh water from the riverine side of the estuary to flow over the more saline and denser water from the seaward side, thus creating a stably stratified water column. Such stable stratification acts to reduce the amount of turbulent mixing. This process is reversed during flood tide, when more saline water flows over lighter fresh water, creating an unstably stratified water column. The amount of

mixing increases in order to return to a stable situation. SIPS is, however, not the only mechanism that creates asymmetric mixing as asymmetries in the vertical gradient of the horizontal flow velocity can have a similar effect (Burchard and Hetland, 2010).

It was shown by Jay and Musiak (1994) that asymmetric mixing by SIPS causes an exchange flow of water by altering the vertical profile of the tidal flow. This exchange flow was later called straining circulation by Burchard et al. (2011) and Geyer and MacCready (2014) as a reference to the SIPS mechanism. Several studies have confirmed the importance of the straining circulation by measurements (Stacey et al., 2001), complex models in one vertical dimension (1DV) (Stacey et al., 2008; Burchard and Hetland, 2010) and idealised models (Prandle, 2004; Cheng et al., 2010). These studies have found that the straining circulation can be larger than the gravitational circulation for a wide range of parameters that describe well-mixed to partially stratified estuaries. Burchard and Hetland (2010) find that the straining circulation is about two times the magnitude of the gravitational circulation for a typical partially stratified estuary.

It remains a challenge to differentiate between straining circulation and gravitational circulation in measurements, because the straining circulation typically has the same shape as the gravitational circulation (Burchard and Hetland, 2010; Cheng et al., 2011). Burchard and Hetland (2010) have also shown that the straining circulation has a similar dependency on the horizontal salinity gradient as the gravitational circulation in well-mixed to partially stratified estuaries. On the other hand, Cheng et al. (2011) find that straining circulation is greatly diminished in strongly stratified estuaries and can adopt a different shape of the velocity profile. The current framework of explaining the straining circulation has not yet led to an explanation as to why these dependencies exist.

Tidal processes are, next to the exchange flows, also important for the net transport of salt. The correlations between vertical and temporal variations of the tidal velocity and the salinity can result in a significant or even dominant net transport of salt (Hughes and Rattray, 1980). The tidal contribution to the salt transport has been studied from measurements (Winterwerp, 1983; Bowen and Geyer, 2003; Lerczak et al., 2006) and in idealised model studies with constant turbulence (McCarthy, 1993; Wei et al., 2014). It has however not been studied separate from other salt transport mechanisms in models with variable mixing, so that little is known about the dependency of the tidal salinity transport on tidal variations of turbulence.

In this study we will explain the above dependencies of the exchange flow and we will make a first step in analysing the tidal salinity transport under conditions of tidally variable mixing in a well-mixed to partially stratified estuary. To this end, we will develop a two-dimensional longitudinal-vertical (2DV) model for hydrodynamics and salinity. The model is an idealised model based on a mathematical scaling and ordering of the equations, which allows us to study different physical mechanisms associated with tides, river discharge and density, separately and systematically. The turbulence modelling in the model allows for arbitrary variations of the turbulent mixing in space and time and the model is coupled to a  $k - \varepsilon$  turbulence model.

The inclusion of arbitrary temporal variations of the eddy viscosity is a novel feature to this type of idealised models. Previous studies with this class of models have used constant mixing (Ianniello, 1977, 1979; McCarthy, 1993) or small variations of mixing (Cheng et al., 2010; Chernetsky, 2012). The inclusion of arbitrary temporal variations of the turbulent mixing allows us to study the interactions between several tidal velocity constituents and the residual flow via correlations with the tidal variations of turbulent mixing. These interactions will prove essential to the establishment and dependencies of the straining circulation. The arbitrarily sized variations of mixing will also allow us to study the effects of turbulence variations on tidal salt transport; this has not been possible with small variations of mixing, because such variations do not appear in the scaled salinity model (Cheng et al., 2010).

This study centres around two research questions:

1. How does the flow velocity, and straining circulation in particular, depend on the interactions between tidal variations of turbulence and the flow velocity itself?
2. How does the tidally induced salt transport depend on tidal variations of turbulence?

This report starts with a short overview of the background theory on the propagation of the tide, density driven

exchange flows and turbulence in Chapter 1. The idealised 2DV model for hydrodynamics will be formulated in Chapter 2. This chapter will start along the lines of Ianniello (1977, 1979) with a constant turbulent mixing formulation. We will then extend the model to include vertical and temporal variations of turbulence. We will also treat the coupling of the hydrodynamic model to a  $k - \varepsilon$  turbulence model. The model will be extended with a model for salinity transport following on from McCarthy (1993) in Chapter 3. In a similar manner as with the hydrodynamics model, the salinity model will be extended to include vertical and temporal variations of turbulent mixing. Additional to the salt transport model, we will develop a tool to decompose the salt transport into contributions by different forcing mechanisms and convert the transport to equivalent values of a one-dimensional horizontal (1DH) salinity dispersion coefficient, inspired by Fischer (1972).

The results of the hydrodynamic model and the salinity model will be discussed separately. Chapter 4 discusses how spatial and temporal variations of turbulence affect the flow velocity and the exchange flow in particular. We will investigate the effects of vertical, horizontal and temporal variations of the eddy viscosity separately. This research focusses on temporal variations of turbulence, in light of which a framework is developed to explain the interactions between these temporal variations and the flow velocity. This framework will then be used to explain the nature of the straining circulation. The results of the salinity model will be treated in Chapter 5. We investigate the effect of temporal variations of turbulence on the tidal salt transport. The results include an analysis of the tidal salt transport with mixing calculated by the  $k - \varepsilon$  model and a sensitivity analysis of such transport to the phase and magnitude of turbulent mixing. A synthesis and discussion of the results is presented in Chapter 6. This report closes with conclusions and recommendations for further research.



# 1

## Flow in estuaries

Estuaries are defined as semi-enclosed basins with a free connection to the sea or ocean within which salt ocean water is diluted by fresh water (Valle-Levinson, 2010). The density differences between fresh riverine water and salty sea water result in interesting and complex flow patterns. Density differences in water can generally be caused by differences in salinity, sediment concentration or temperature. In this study, we will assume that all density differences are caused by differences in salinity. Estuaries here form the connection between the relatively narrow and shallow river and the wider and deeper sea, see Figure 1. They typically vary strongly in width and depth and generally do not consist of straight channels, but contain alternating patterns of deep meandering channels and shallow shoals or islands.

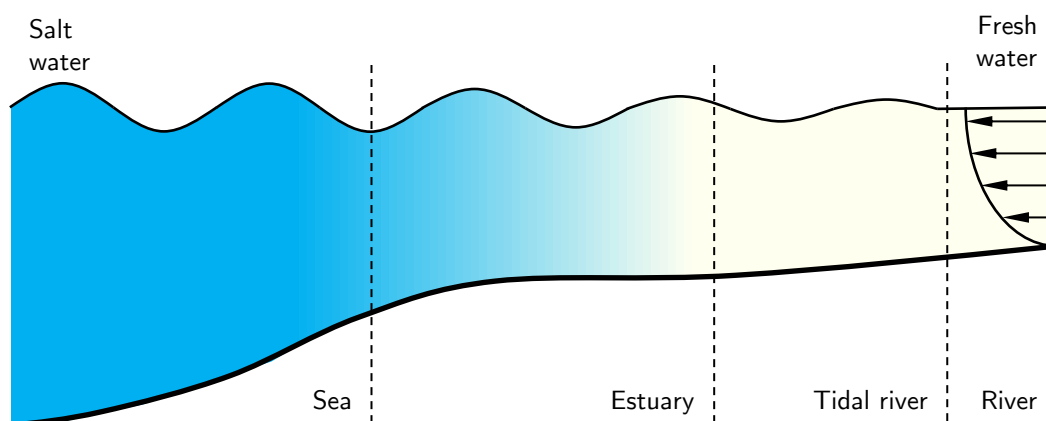


Figure 1: Conceptual image of the sea, estuary, tidal river and river.

The flow in an estuary is a combination of the fresh river water that flows out to sea, the oscillatory movement of the tide that propagates from the sea into the estuary, the flow and waves which are caused by the wind and the flow which is caused by the density differences between fresh and salt water. These forcing mechanisms can be divided in barotropic and baroclinic components. *Barotropic* concerns the flow in which density differences in the water are not taken into account. *Baroclinic* concerns that part of the flow that is driven by density differences, which are caused by differences in for example the salinity. The barotropic and baroclinic flow in the estuary will be treated in more detail below. The discussion on the barotropic flow in Section 1.1 concentrates on the propagation of the barotropic tide. The discussion on the baroclinic flow in Section 1.2 explains how baroclinic density gradients are capable of creating a time-average flow of water. This will be followed by an introduction to the meaning and role of turbulence in the estuary in Section 1.3.

## 1.1. Propagation of the tide

The global tide is created by the gravitational forces of the Sun and the Moon on the Earth. Such forces create a tidal wave that propagates through the oceans over the world. As this wave moves into shallower seas and estuaries it deforms under the effects of, among others, shoaling, funnelling, friction and reflection. Shoaling occurs when a wave moves from deep to shallow water. The energy contained in the wave in deep water needs to be transferred to the shallow water which results in an amplification of the wave height. Funnelling describes the same effect for a wave moving into a channel with a converging width; the principle of conservation of energy again results in an amplification of the wave height. The amplification is counteracted by friction, mainly from contact with the river or sea bed. The friction depends strongly on the water depth, bed composition, bed forms and vegetation and is therefore an intricate process to model accurately. Finally, reflection occurs when a wave hits a steep coastline, sea wall or tidal weir. The wave energy is reflected back, leading to an amplification of the wave height by up to a factor two.

The above discussion concerns what is sometimes called the *vertical tide*, the tidal wave height or amplitude. We will not use the word tide to denote the vertical tide, but use it to denote the *horizontal tide*, which describes the tidal flow velocity. The *ebb tide* is then defined as the period of time during which the tidal velocity has a seaward direction, while the *flood tide* is conversely defined as the period of time during which the tidal velocity has a landward direction.

We need to make a distinction between the flow velocity and the velocity of the wave. The tidal wave moves at a different rate than the water itself. The frictionless shallow water approximation for the barotropic wave velocity, denoted by  $c_E$ , is

$$c_E = \sqrt{gH}, \quad (1.1)$$

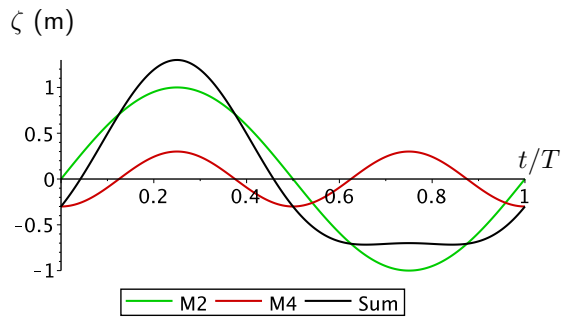
where  $g$  is the acceleration of gravity and  $H$  is the water depth. The wave velocity for a depth of 10 m is then 10 m/s, while the typical flow velocity is only 1 m/s.

The notion that the wave velocity is finite leads to the conclusion that a tidal wave must be at a different stage in its cycle at different locations along the estuary. This phenomenon is described by the phase of the wave. Let us define a phase of zero as the phase of the wave at the mouth of the estuary at some point in time  $t_0$ . The wave then takes time to travel up the estuary so that the phase of zero occurs at  $t_1 > t_0$  at a location inside the estuary. In other words, the phase of the tidal wave inside of the estuary is negative at time  $t_0$ . A negative phase of the wave at some location therefore means that the wave lags the wave at the mouth of the estuary.

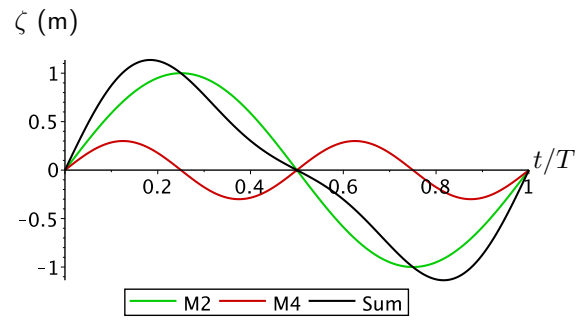
The tidal wave is generally not a simple sine wave, but consists of multiple frequency components. The frequency components are denoted by the combination of a letter that indicates the origin and a number that indicates the frequency. For example the  $M_2$  tide denotes the lunar tide (M for moon) with a period of 12 hours and 25 minutes, i.e. approximately twice a day. Some components are mainly forced externally by the Sun and the Moon, for example the lunar  $M_2$  and solar  $S_2$  tides and the lunar-solar interaction  $K_1$ . Other components are mainly generated internally in a shallow sea, estuary or tidal river by non-linear mechanisms like friction. Examples of such internally generated tidal constituents are the overtides  $M_4$ ,  $M_6$ ,  $S_4$  and  $S_6$ . In this thesis we will concentrate on the main tidal constituent in most parts of the world: the  $M_2$  tide and its internally generated overtides.

The combination of these constituents results in a tidal wave that is skewed and asymmetric. *Skewness* is used to describe a wave that has wave crests that are more peaked and wave troughs that are flatter than a sine wave, see Figure 2a. A skewed wave can be constructed by perturbing an  $M_2$  wave by a small  $M_4$  wave that is out of phase. *Asymmetry* is used to describe a wave that is 'pitched forward', see Figure 2b. An asymmetric wave is also constructed by perturbing the  $M_2$  wave by an  $M_4$  component, but the  $M_4$  component is now in phase with the  $M_2$  component.

The overtides also cause skewness and asymmetry of the horizontal tide. Such skewness and asymmetry is called *horizontal tidal asymmetry* or just *tidal asymmetry*. The complexity of all the causes of tidal asymmetry is often summarised by stating that the system is ebb dominant or flood dominant. The notion of ebb and



(a) Time record of a skewed wave.



(b) Time record of an asymmetric wave

flood dominance is generally associated with the study of sediment transport. Ebb dominance is therefore associated with a net landward directed sediment transport, while flood dominance is associated with a net seaward sediment transport. We will adopt the definition of [Friedrichs and Aubrey \(1988\)](#); [Friedrichs \(2010\)](#) here. This states that a system is *ebb dominant* if the period of time during which the water level falls is shorter than the period of time during which the water level rises. The converse holds for *flood dominant* estuaries. This definition is not conclusive about the direction of the net sediment transport, which depends on more factors than the tidal asymmetry. [Friedrichs \(2010\)](#) provides an overview of how the shape and bathymetry of the estuary influences tidal asymmetry and net sediment transport.

The non-linear tidal propagation in estuaries does not only induce overtides, but also residual flows. The *residual flow* or *subtidal flow* are terms that denote the current that remains after tidally averaging the along-channel velocity. Related to this, we will use the terms *exchange flow* or *estuarine circulation* for the part of the residual flow that has a cross-sectionally-averaged value of zero. The formal definitions of exchange flow and estuarine circulation do not make this clear distinction, but the terms are frequently used in this way ([Geyer and MacCready, 2014](#)).

Examples of tidally-averaged flows with a non-zero depth-averaged value are the river flow and the return flow that compensated for Stokes drift. The Stokes drift is a net transport that is caused by the differences in flow velocity under the crest and the trough of a wave. The flow velocity under a wave crest is higher than under a wave trough, resulting in a net inflow of water. The net inflow of water by Stokes drift needs to be counteracted in order to satisfy the law of conservation of mass. Such return flow is established by a subtidal water level gradient which causes a pressure gradient and therefore a flow directed out of the estuary. Other residual flows with a non-zero depth-averaged value can be present locally in certain channels or on certain shoals that favour either the ebb or the flood tide. The cross-sectionally averaged contribution of such residual flows is zero.

Exchange flows can be caused by a number of processes among which non-linear advection ([Li and O'Donnell, 2005](#)), baroclinic pressure, see Section 1.2, and interactions with asymmetric turbulent mixing, see Section 1.3.

## 1.2. Baroclinic flow

The baroclinic pressure induces a component of the exchange flow that is known as gravitational circulation. In this section it will be explained how this exchange flow is established.

First, however, we will look closer at the shape of the density profiles in an estuary. Baroclinic pressure is the pressure that is caused by density differences, which in this research are caused by salinity differences. The sea contains salt water, while river water is fresh. This causes salt water to be concentrated near the mouth of the estuary, while fresh water is concentrated further inland. This is referred to as *horizontal stratification*. Salt water is heavier than fresh water which leads to the tendency of salt water to be concentrated near the bed and fresh water to be concentrated near the surface. This is referred to as *vertical stratification*. The structure of the horizontal and vertical stratification differs between estuaries. [Pritchard \(1955\)](#) identifies the following classes:

- (a) **Salt-wedge.** Very pronounced horizontal and vertical stratification with a salt water flow which is concentrated near the bed and which moves back and forth through the estuary during the tidal cycle. The transition between saline and fresh water is strong and there is hardly any turbulent mixing at the interface between the two.
- (b) **Strongly stratified.** Horizontally and vertically stratified. The water column is stratified and remains stratified throughout the tidal cycle, with higher salinity concentrations near the bed than near the surface. Turbulent mixing is strongly damped by the stratification.
- (c) **Partially stratified.** Horizontally stratified and weakly vertically stratified. The water column is stably stratified during only a part of the tidal cycle. Turbulent mixing is damped during stratification, but is enhanced when the water column becomes fully mixed, causing strong variations in mixing throughout the tidal cycle.
- (d) **Well-mixed.** Horizontally stratified. The water column is well-mixed throughout the tidal cycle and turbulent mixing is hardly influenced by vertical stratification.

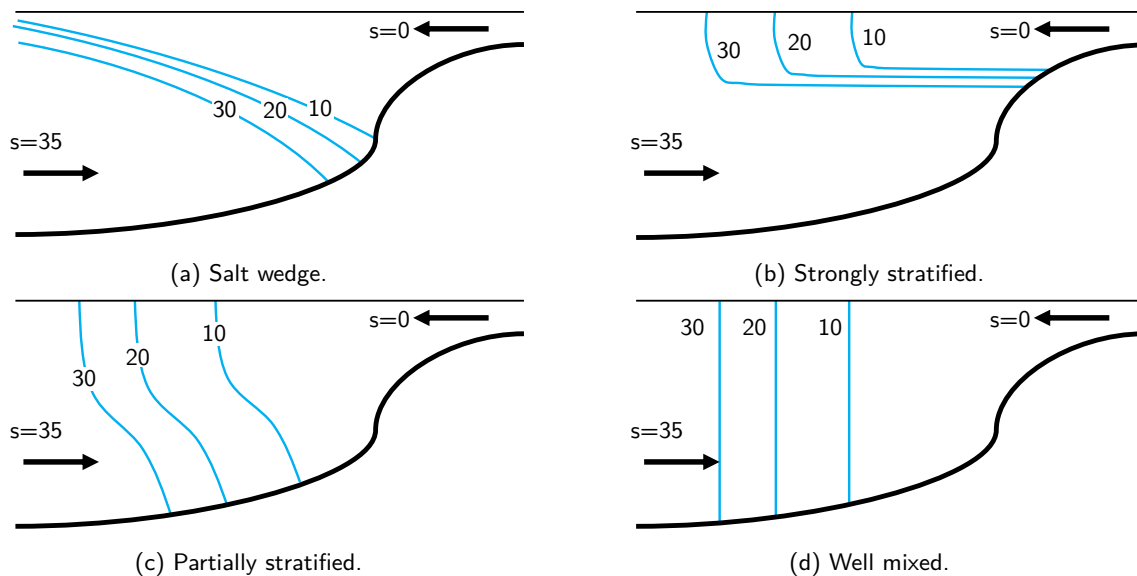


Figure 3: Typical salt distribution in the several classes of estuaries.

This research is restricted to partially stratified and well-mixed estuaries. In this section we will concentrate on the way in which the horizontal stratification induces the gravitational circulation. The vertical stratification can also induce exchange flows via asymmetries in turbulent mixing. This will be discussed in Section 1.3.

We will look closer at the definition of baroclinic pressure in order to derive the relation between horizontal stratification and gravitational circulation. The barotropic and baroclinic flow are driven by pressure gradients. The pressure is assumed to be hydrostatic, which means that it is determined according to

$$p = g\rho(\zeta - z) + p_0.$$

This equation describes that the pressure in water depends on the atmospheric pressure above the water  $p_0$  and the pressure under water. The latter is composed of the product of the density of water  $\rho$ , the acceleration of gravity  $g$  and the distance to the water surface  $\zeta - z$ . We use  $\zeta$  to denote the level of the water surface and  $z$  to denote the vertical coordinate. This coordinate ranges from the bed level  $z = -H$  to the surface  $z = \zeta$ .

We assume that atmospheric pressure is constant in the horizontal direction. We can then take the derivative of the pressure to find the pressure gradient along the estuary and obtain

$$p_x = \underbrace{g\rho\zeta_x}_{(1)} + \underbrace{g\rho_x(\zeta - z)}_{(2)},$$

where the subscript denotes the derivative in  $x$ -direction, i.e. along the length of the estuary. The first term on the right-hand side is known as the barotropic pressure, while the second part is the baroclinic pressure.

Whereas the barotropic pressure is constant in the vertical direction, the baroclinic pressure differs in the vertical direction. The baroclinic pressure varies linearly in the vertical direction if the density is constant in the vertical direction. The time-independent part of the baroclinic pressure causes a residual flow velocity. Similarly to what we have seen for the Stokes drift, the baroclinically induced velocity must be compensated for by a barotropic pressure gradient in order to ensure conservation of mass. We then have a linearly varying baroclinic pressure gradient and a counteracting constant barotropic pressure gradient. The net pressure gradient and the corresponding flow velocity are displayed in Figure 4. The velocity is an exchange flow which is called *gravitational circulation*. It has a cross-sectionally average value of zero, but is directed landward near the bed and directed seaward near the surface. It can therefore cause a net transport of constituents in water if such a constituent is non-uniformly distributed over the water column.

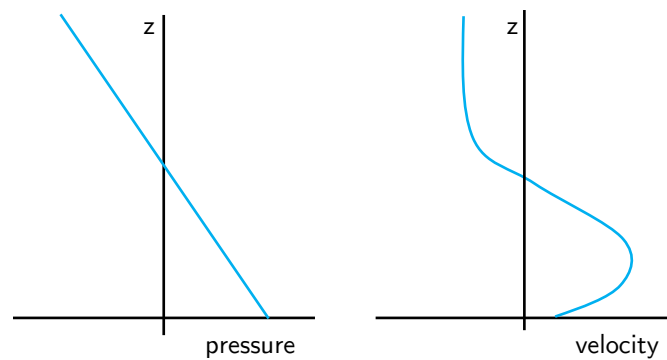


Figure 4: Net baroclinic pressure (left) and the resulting exchange flow: the gravitational circulation (right).

### 1.3. Turbulence and turbulence induced flows

This section provides a brief introduction to turbulence modelling by introducing the eddy viscosity hypothesis and then using this to describe how temporal variations of turbulence cause exchange flows. A more complete explanation of turbulence is given by [Tennekes and Lumley \(1972\)](#) and [Pope \(2000\)](#). Introductions to turbulence for applications in estuaries and coastal waters are provided by [Fischer et al. \(1979\)](#) and [Monismith \(2010\)](#).

Turbulence is the mixing of water by turbulent eddies, or vortices, that derive their energy from gradients of the velocity and density. Turbulent mixing acts on scales that become as small as 0.1 mm, the so called Kolmogorov scale. Such small scales cannot as yet be resolved by models for environmental flows (e.g. rivers or estuaries) or geophysical flows (e.g. oceans), because the computational time that would be required is too high. Such models therefore solve for the flow velocity on a much larger scale and parametrise turbulence as a diffusive mixing process.

Turbulence shows in a time record of the velocity as seemingly random fluctuations of the velocity. Such fluctuations of the velocity components in three dimensions  $u$ ,  $v$  and  $w$  are denoted by  $u'$ ,  $v'$  and  $w'$ . The model resolves the velocity signal without these fluctuations  $\bar{u}$ ,  $\bar{v}$  and  $\bar{w}$ . The fluctuating velocity components can, however, not be fully eliminated from the model, because the product of two fluctuating components results in a net shear stress on the large-scale flow. Such a shear stress, called the Reynolds stress, is typically dominated by the product of  $u'$  and  $w'$ . Its net contribution is denoted by

$$\tau = \overline{\rho u' w'},$$

where  $\tau$  is the Reynolds stress. This Reynolds stress is parametrised by a Fickian diffusion process according to the eddy viscosity hypothesis. This reads

$$\tau = \overline{\rho u' w'} = -\rho \nu_t u_z.$$

The diffusion coefficient  $\nu_t$  is called the *eddy viscosity*. The eddy viscosity is not a constant, but is a complex function of the flow properties. The modelling of turbulence is the process of finding expressions for the eddy viscosity in terms of mean flow quantities. In this thesis we will consider a number of such expressions ranging from prescribing a constant value to employing a complex non-linear  $k - \varepsilon$  model.

Turbulence is affected by velocity gradients and density gradients. Velocity gradients promote turbulence. This means that mixing increases during peak ebb and flood tide when the velocity, and therefore the velocity gradient, is largest. Stable density gradients (i.e. lighter water on top of heavier water) oppose this and decrease mixing. Such decrease of mixing is established by the potential energy gradient which accompanies the density gradient and which should be overcome by turbulent eddies. This process drains kinetic energy from the eddies and therefore reduces mixing. Partially stratified estuaries are only stably stratified (i.e. have a stable density gradient) during part of the tidal cycle, which causes variations in turbulent mixing.

We will call these variations of turbulence over the tidal time-scale *turbulence asymmetry*. Asymmetric turbulence is capable of changing the tidal propagation and the baroclinic flows by altering the oscillatory flow and creating a new exchange flow. The latter has particularly received a lot of attention in literature since the first time it was described by Jay and Musiak (1994). Their reasoning follows on from the strain-induced periodic stratification (SIPS) mechanism described by Simpson et al. (1990). Both will be explained below.

The SIPS mechanism describes the evolution of vertical stratification in well-mixed and partially stratified estuaries. Let us consider an estuary that is well mixed in the vertical direction and horizontally stratified. The tidal velocity is small near the bed, because of the effect of bed friction, and is larger near the surface. During ebb, this causes the fresh water from the landward side of the estuary to flow slowly near the bed and faster near the surface. The result is a water column that becomes stably stratified and therefore contains a reduced level of turbulence, see Figure 5. The converse happens during flood leading to unstable stratification with heavy salt water on top of light fresh water, which results in increased mixing.

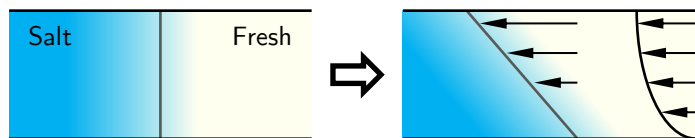


Figure 5: Straining of salinity by the ebb tide in a horizontally stratified estuary.

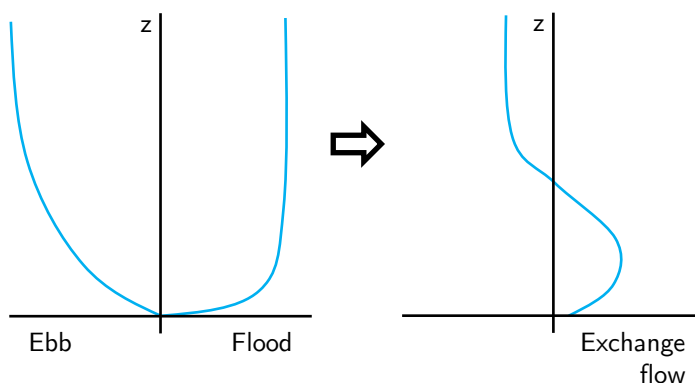


Figure 6: Vertical velocity profiles according to the theory by Jay and Musiak (1994) and the resulting time-averaged flow velocity.

Jay and Musiak (1994) reason that the variations of mixing caused by SIPS result in an exchange flow by describing the changes to the distribution of momentum. The momentum of a tidal flow is concentrated in the top part of the water column, because the flow velocity is larger there than near the bed. The increased mixing during flood acts to smooth this momentum distribution and so mixes momentum downward. This yields an increased flow velocity in landward direction near the bed and a decreased flow velocity near the surface. During ebb, the reduced mixing leads to the opposite effect on the momentum distribution resulting in an increase

of momentum near the surface and a decrease near the bed. This yields a decreased flow velocity in seaward direction near the bed and an increased flow velocity near the surface. This asymmetric flow during ebb and flood can be described by a symmetric tidal wave and a constant component or exchange flow. The exchange flow has a landward direction near the bed and a seaward direction near the surface, see Figure 6.

The SIPS induced exchange flow is not the only nor the most important exchange flow that is caused by temporal variations of turbulence. Turbulence asymmetry is not only created by an asymmetry in buoyancy, but also by an asymmetry in velocity shear (Burchard and Hetland, 2010). It is important to note that an asymmetry in velocity shear is not only created by an asymmetry in the depth-averaged velocity itself, but also by asymmetric contributions to the shear, which are not visible in the depth-averaged velocity. This will be a focal point of this research.

The asymmetry of the water level is another source of asymmetric turbulence. In the estuaries that will be considered here the effect will be that the turbulent length-scale can become larger during higher water than during low water. As a result the eddy viscosity is larger during high water than during low water.

It is additionally not only the tidal flow that interacts with asymmetric turbulence to induce an exchange flow. It will be shown for the first time in this research that the interaction of the baroclinic pressure with temporal variations of turbulence will also induce an exchange flow. This exchange flow will have a greater magnitude than the exchange flow caused by the interaction of the tide and SIPS in a wide parameter range.

All exchange flows caused by interactions of the velocity and temporal variations of turbulence will be called *straining circulation*, which is the name given by Burchard et al. (2011) to describe the SIPS induced exchange flow.



# 2

## Model formulation: hydrodynamics

The 2DV model for the hydrodynamics will be developed in this chapter. The model is named the two-dimensional point model (2DPM) model, because it solves the vertical dimension like a sequence of 1DV point models that are coupled horizontally. The solution method makes use of a mathematical perturbation approach and solves the equations in terms of Fourier components in time, the advantages of which will be discussed in Section 2.1.

Idealised modelling started with the one-dimensional horizontal (1DH) modelling of water levels in frictionally dominated tidal flows in the 19<sup>th</sup> century. Some of the main results are repeated by e.g. [Ippen and Harleman \(1961\)](#) for prismatic channels and by [Lanzoni and Seminara \(1998\)](#) and [Friedrichs \(2010\)](#) for converging channels. The analytical solution for the water motion found in these analyses is based on the balance between a barotropic tidal forcing and friction. The disadvantage of the 1DH approach is the lack of the vertical structure that is required for the modelling of exchange flows such as gravitational circulation. The depth-averaged velocity of the exchange flow is zero, so that a depth-averaged model cannot resolve this circulation. One-dimensional vertical (1DV) models were therefore developed to investigate the structure of the water column. [Hansen and Rattray \(1965\)](#) have developed analytical solutions for the gravitational circulation in such a 1DV model under the assumption of vertically constant turbulent mixing.

The combination of the 1DH and 1DV approaches results in an idealised 2DV model. [Ianniello \(1977\)](#) was the first to build such a model that computes the residual currents resulting from the combined effects of barotropic pressure, baroclinic pressure, river flow and momentum advection. The model was initially built for channels with a constant depth and width and later extended by [Ianniello \(1979\)](#) for channels of exponentially converging depth and width. Analytical solutions were developed for the case of a spatially and temporally constant eddy viscosity and vertically parabolic eddy viscosity. The latter profile is typical for barotropic river flows and results approximately in the classic logarithmic vertical velocity profile, which corresponds closely to observed profiles.

The model that will be developed in this chapter extends the model by [Ianniello \(1979\)](#). We will first introduce the assumptions which will be used in the model in Section 2.1. These assumptions are used to scale the equations in order to simplify them. We will present the equations and the scaling argument in Section 2.2. The system of equations that is obtained can be rewritten as a system of linear ordinary differential equations. The solution of this system can be written in terms of abstract linear operators that can be solved numerically. This procedure is explained in Section 2.3. Section 2.4 finally treats the coupling of the model to a  $k - \varepsilon$  turbulence model. The full details of the hydrodynamic model, including analytical solutions and its numerical implementation, are presented in Appendix A.

## 2.1. Assumptions and approach

The semi-analytical model is a 2DV model of a channel with a varying longitudinal bed profile and an exponentially decreasing width, see Figure 7. The processes that act in the lateral direction are parametrised in the model. The bed level, which is denoted by  $H(x)$ , is allowed to vary gradually (i.e. with length scales corresponding to the length of the tidal wave) over the  $x$ -direction. The width  $B$  is exponentially decreasing according to

$$B(x) = B_0 e^{-x/L_b},$$

where  $L_b$  denotes the convergence length. A straight channel is retrieved by imposing  $L_b = \infty$ . The model is forced by a tidal signal ( $M_2, M_4$ ) at the seaward side. A tidal weir is located at the landward end of the estuary. This weir acts as a reflecting wall over which a constant river inflow  $Q$  is prescribed. Short waves, swell and wind forcing are not included in the model.

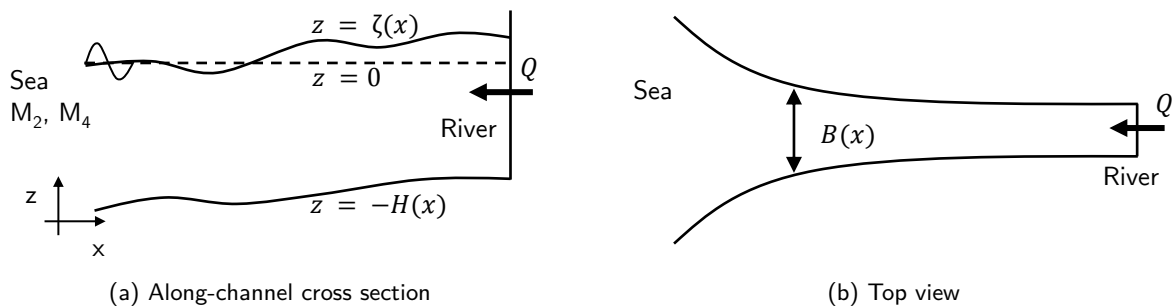


Figure 7: Schematic overview of the modelled system.

The estuary is assumed to be well-mixed to partially stratified. The meaning of these terms and the implication on modelling are discussed in Chapter 3. For the purposes of the hydrodynamic model it is sufficient to remark that the horizontal density gradient in these estuaries is approximately constant over the water column and is relatively small (see Section 2.2) throughout the estuary.

The linearisation of the model pivots around the assumption that the water level variations are small compared to the water depth. In this report the water level variations are related to the amplitude of the  $M_2$  tide as this is the main tidal component in most estuaries.

The above assumptions are used to simplify the hydrodynamic model equations using a perturbation approach. This approach involves the ordering of the equations and the solution in a small parameter  $\delta$ , here defined as the ratio of the amplitude of the  $M_2$  tide at the seaward entrance  $A_{M_2}$  and the water depth at the seaward entrance  $H_0$ ;

$$\delta = \frac{A_{M_2}}{H_0}. \quad (2.1)$$

The perturbation approach makes use of the idea that terms of at most  $\mathcal{O}(\delta)$  are negligible compared to terms of  $\mathcal{O}(1)$ . So a first approximation of the equations is obtained by removing the small terms from the equations. One then obtains a simplified equation with solely  $\mathcal{O}(1)$  terms. A better approximation of the solution of the equation can be obtained by solving the difference of the original equation and the  $\mathcal{O}(1)$ -equation. The terms in this new equation are at most of  $\mathcal{O}(\delta)$ . This equation can again be ordered in terms of  $\mathcal{O}(\delta)$  and terms of at most  $\mathcal{O}(\delta^2)$  and the procedure is repeated. The result is a sequence of equations at different orders. Each additional equation improves the accuracy of the approximation of the solution. For the above definition of  $\delta$ , the obtained set of simplified equations is linear and therefore easier to solve than the original equation.

The non-linear terms in the equations are not neglected by applying the perturbation approach. Instead, the non-linear interactions are expanded in a series expansion and the terms of this series expansion are spread over all higher-order equations. If  $\delta$  is indeed small (i.e.  $\delta \ll 1$ ), the series expansion converges quickly and it is sufficient to take only a few equations into account. If conversely  $\delta$  is not small (i.e.  $\delta$  close to, but smaller than

1), the perturbation approach is still valid, but the series converges slowly and many higher-order equations are needed for a reasonable approximation of the original equations.

As a consequence of the linearisation, the vertical and horizontal dimensions can be solved independently in the particular case of the momentum and depth-averaged continuity equations, which will be introduced in the next section. The time derivatives can be eliminated from these equations by solving the model for separate tidal constituents. As a result only ordinary differential equations (ODEs) in  $x$  or  $z$ -direction need to be solved. These ODEs can be solved analytically in some situations. Numerical solution methods are used otherwise.

The effect of turbulence modelling on the flow is investigated by comparing several formulations for the eddy viscosity  $\nu_t$ . Table 2.1 provides an overview of the eddy viscosity formulations in different versions of the 2DPM model. The amount of complexity is increased in consecutive versions by allowing the eddy viscosity to vary in more or different dimensions. The term *variable* in the table means that any function in the function space  $H^1$  (functions that have a weak derivative) is allowed.

Version number	$x$ -direction	$z$ -direction	time
1	variable	constant	constant
2	variable	parabolic	constant
3	variable	constant	variable
4	variable	variable	variable
5	$k - \varepsilon$	$k - \varepsilon$	$k - \varepsilon$

Table 2.1: Formulations of  $\nu_t$  in different versions of the 2DPM model. The profile of  $\nu_t$  in each dimension is denoted.

The above assumptions are used in the next section to obtain at the model equations. These equations are then scaled to obtain the ordered system.

## 2.2. Model equations

The solution to the hydrodynamic model consists of the water level  $\zeta(x, t)$  and the horizontal and vertical velocity  $u(x, z, t)$  and  $w(x, z, t)$ . The equations that describe the flow are the width-averaged continuity and momentum equations. The equations read

$$u_x + w_z - \frac{u}{L_b} = 0, \quad (2.2)$$

$$u_t + uu_x + wu_z = -g\zeta_x - g \int_z^\zeta \frac{\rho_x}{\rho_0} d\hat{z} + (\nu_t u_z)_z. \quad (2.3)$$

The continuity equation will also be used in depth-averaged form

$$\zeta_t + \left( \int_{-H}^\zeta u dz \right)_x - \frac{1}{L_b} \int_{-H}^\zeta u dz = 0. \quad (2.4)$$

In these equations  $\rho$  is the density,  $\rho_0$  is a constant reference density,  $g$  is the acceleration of gravity and  $\nu_t$  is the eddy viscosity. The subscripts  $x$ ,  $z$  and  $t$  are derivatives in the respective dimensions. The equations are based on the principles of conservation of mass and momentum. The conservation of momentum is a form of the second law of Newton, describing how mass accelerates if a force is exerted on it. The acceleration is described by the left-hand side of the momentum equation 2.3 by the inertia in the first term and the advection of momentum in the second and third terms. The 'forces' are found on the right-hand side of the equation and represent the barotropic pressure, baroclinic pressure and vertical Reynolds-stress divergence (i.e. turbulence) respectively.

The baroclinic pressure term in momentum equation 2.3 can be rewritten by using the assumption of a constant vertical density gradient. The term reads

$$g \int_z^\zeta \frac{\rho_x}{\rho_0} d\hat{z} = g \frac{\rho_x}{\rho_0} (\zeta - z).$$

The eddy viscosity is an arbitrary number or function in Versions 1, 3 and 4. For Version 2, however, the eddy viscosity is restricted to a parabolic profile of the form

$$\nu_t(x, z, t) = \nu_{t,0}(z_s(x) - z)(H(x) + z_b(x) + z), \quad (2.5)$$

where  $z_s$  and  $z_b$  are the surface and bottom roughness heights and  $\nu_{t,0}$  is a calibration parameter.

The equations are subject to the boundary conditions given below. At the free surface  $z = \zeta$ :

$$\begin{aligned} \nu_t u_z(x, \zeta, t) &= 0 && \text{(no stress),} \\ w(x, \zeta, t) &= \zeta_t(x, t) + u \zeta_x(x, t) && \text{(kinematic).} \end{aligned}$$

At the bed  $z = -H$ :

$$\begin{cases} \nu_t u_z(x, -H, t) = s_f u(x, -H, t) & \text{(partial slip, Version 1 and 3),} & \text{or} \\ u(x, -H, t) = 0 & \text{(no slip, Version 2, 4),} & \text{or} \\ \nu_t u_z(x, -H, t) = u_*^2 & \text{(quadratic friction, Version 5),} \\ w(x, -H, t) = -u(x, -H, t) H_x & \text{(kinematic).} \end{cases}$$

At the seaward side  $x = 0$ :

$$\zeta(0, t) = \text{Re} \left( \sum_{n=1}^p A_{M_{2n}} e^{ni\omega t + i\phi_n} \right).$$

This boundary condition prescribes a sum of the  $M_2$  tide and its overtides at the boundary. The amplitude of the  $n^{\text{th}}$  overtide at the boundary is denoted by  $A_{M_{2n}}$ , its angular frequency by  $n\omega$  and its phase by  $\phi_n$ . Finally, the boundary condition at the inland boundary  $x = L$  is

$$\int_{z=-H}^{\zeta} u(L, z, t) dz = \frac{Q}{B(L)},$$

which corresponds to a reflective weir over which a constant river flow discharges into the estuary.  $Q$  is the fresh water discharge in volume per second.

Note that the bed roughness formulation for the Versions 1 and 3 differs from that for the Versions 2 and 4 and that of Version 5. Versions 1 and 3 use a vertically constant eddy viscosity. The roughness is therefore specified in the boundary condition parametrised by a coefficient  $s_f$ . The roughness formulation is linearised so that the resulting system of equations is linear. For the Versions 2 and 4, the roughness is related to the shape of the vertical eddy viscosity profile. The bed roughness in Version 2 is parametrised by the roughness height  $z_b$  that appears in the eddy viscosity formulation 2.5. Version 4 uses either this parabolic profile or a different user-defined profile. The roughness does not have to be specified in the boundary conditions for Version 2 and 4, because the effect of the roughness is incorporated in the eddy viscosity profiles. A roughness height also exists for the roughness formulation in Version 5. However, a quadratic friction law will be used here instead of a no-slip condition as will be explained in Section 2.4.

A scaling analysis is used to find an ordering of the equations in the small parameter  $\delta$  defined in Equation 2.1. We will discuss the main results of this scaling here. The details of the scaling are given in Appendix A. The result of the scaling is that the advection terms  $uu_x$  and  $wu_z$  in momentum equation 2.3 are of order  $\delta$ . Additionally, the assumption that the horizontal density gradient is small has the consequence that the baroclinic pressure is also of order  $\delta$ . The condition on the density difference  $\Delta\rho$  over the length of the estuary to establish this scaling is

$$\frac{\Delta\rho}{\rho_0} = \mathcal{O}(\delta^2).$$

The final step before obtaining the ordered set of equations is to define an ordering of the solution:

$$\begin{aligned} u &= u^0 + u^1 + u^2 + \dots, \\ w &= w^0 + w^1 + w^2 + \dots, \\ \zeta &= \zeta^0 + \zeta^1 + \zeta^2 + \dots \end{aligned}$$

The superscripts denote the order of magnitude, i.e.  $u^0$ ,  $w^0$  and  $\zeta^0$  are of  $\mathcal{O}(1)$ ,  $u^1$ ,  $w^1$  and  $\zeta^1$  are of  $\mathcal{O}(\delta)$  etcetera. Throughout this report we will use superscripts to denote the order of a term.  $\mathcal{O}(1)$  terms will be called leading-order terms,  $\mathcal{O}(\delta)$  terms will be called first-order terms etcetera. Subscripts will be used in this report to denote the tidal constituent. A subscript 0 denotes residual flows, 1 denotes the  $M_2$  components and higher numbers denote the consecutive overtides of the  $M_2$  tide. The equation applies to all orders or all tidal constituents if superscripts or subscripts are omitted.

This scaling leads to the following leading-order equations

$$u_t^0 = -g\zeta_x^0 + (\nu_t u_z^0)_z, \quad (2.6)$$

$$u_x^0 + w_z^0 - \frac{u^0}{L_b} = 0, \quad (2.7)$$

$$\zeta_t^0 + \left( \int_{-H}^0 u^0 dz \right)_x = \frac{1}{L_b} \int_{-H}^0 u^0 dz. \quad (2.8)$$

The first-order system is given by

$$u_t^1 + u^0 u_x^0 + w^0 u_z^0 = -g\zeta_x^1 + g \frac{\rho_x}{\rho_0} z + (\nu_t u_z^1)_z, \quad (2.9)$$

$$u_x^1 + w_z^1 - \frac{u^1}{L_b} = 0, \quad (2.10)$$

$$\zeta_t^1 + \left( \int_{-H}^0 u^1 dz \right)_x + \zeta_x^0 u^0(x, 0, t) + \zeta^0 u_x^0(x, 0, t) = \frac{1}{L_b} \left( \int_{-H}^0 u^1 dz + \zeta^0 u^0(x, 0, t) \right). \quad (2.11)$$

The ordered boundary conditions are given in Appendix A.

## 2.3. Solution method

The leading-order model equations 2.6 to 2.8 will be solved first. This is done by first solving the coupled system of the momentum equation and the depth-averaged continuity equation. The continuity equation may then be used to obtain  $w$ . In this section we will focus on solving the coupled system and we will not use  $w$ . The solution to the leading-order system is used as input to the first-order equations 2.9 to 2.11.

It will be shown in this section that the leading-order and first-order systems have a similar structure and can therefore be solved in a similar manner. First, the solution procedure will be illustrated for the leading-order system of Version 1 and 2. Next, still restricting the discussion to the leading-order system, this procedure will be extended to cover also the model Versions 3 to 5 (see Table 2.1). Finally, the common structure of the leading-order and first-order systems is used to solve the first-order system. The details of the solution procedure for all model versions is given in Appendix A.

### 2.3.1. Illustration of the solution procedure for a time-independent eddy viscosity

The system is converted to a system of ODEs by solving for Fourier components  $e^{i\omega_{M_{2n}} t}$ , where  $i$  is defined such that  $i^2 = -1$  and  $\omega_{M_{2n}}$  is the angular frequency of the tidal constituent  $M_{2n}$ . The angular frequencies of the overtides of the  $M_2$  tide are simply multiples of the angular frequency of the  $M_2$  tide. We will therefore use  $\omega$  for the angular frequency of the  $M_2$  tide and write

$$\omega_{M_{2n}} = n\omega \quad (n = 0, 1, \dots)$$

The tidal constituents can be described by the projection of these Fourier components to the real numbers. So the horizontal velocity and water level signals can be described by taking a sum of Fourier components and

projecting them to the real numbers;

$$u(x, z, t) = \text{Re} \left( \sum_{n=0}^{\infty} \hat{u}_n(x, z) e^{in\omega t} \right),$$

$$\zeta(x, t) = \text{Re} \left( \sum_{n=0}^{\infty} \hat{\zeta}_n(x) e^{in\omega t} \right).$$

The symbol  $\hat{\cdot}$  denotes the complex valued amplitude. This complex amplitude contains information on both the real amplitude and the phase of the tidal constituent.

The model Versions 1 and 2 both use a temporally constant eddy viscosity. As a consequence, the system will only respond with a signal at those frequencies at which it is forced. It is assumed in these versions that the river discharge is small and does not appear in leading order. The system is then only forced by the tide, which is assumed to consist only of the  $M_2$  component in leading order. So the system responds with only one tidal constituent: the  $M_2$  tide. The velocity and water level formulations then simplify to

$$u(x, z, t) = \text{Re} \left( \hat{u}(x, z) e^{i\omega t} \right),$$

$$\zeta(x, t) = \text{Re} \left( \hat{\zeta}(x) e^{i\omega t} \right),$$

The Version 1 and 2 form of the Equations 2.6 and 2.8 in frequency space read

$$i\omega \hat{u}^0 - \nu_t \hat{u}_{zz}^0 - \nu_{t,z} \hat{u}_z^0 = -g \hat{\zeta}_x^0, \quad (2.12)$$

$$i\omega \hat{\zeta}^0 + \left( \int_{-H}^0 \hat{u}^0 dz \right)_x - \frac{1}{L_b} \int_{-H}^0 \hat{u}^0 dz = 0. \quad (2.13)$$

The first equation can be solved as a second-order ODE in  $z$  in terms of the unknown water level gradient  $\hat{\zeta}_x^0$ . The result can then be used in the second equation to obtain a second-order ODE in  $x$  which can be solved for  $\hat{\zeta}^0$ .

In order to obtain a better insight into the structure of the problem, the model is rewritten in a more abstract notation. This abstract notation helps to show the similarities between the model versions and the similarities between the leading-order and first-order systems. The notation is also practical for the numerical implementation of the model. We will use linear operator theory for this abstract notation. An elementary example is provided in Intermezzo 1.

Equation 2.12 can be rewritten by using the linear operator  $\mathcal{A}$ , which is defined as

$$\mathcal{A} = i\omega - \nu_t \frac{\partial^2}{\partial z^2} - \nu_{t,z} \frac{\partial}{\partial z}.$$

This equation is subject to homogeneous boundary conditions

$$\begin{aligned} \nu_t \hat{u}_z^0(x, 0) &= 0, \\ \nu_t \hat{u}_z^0(x, -H) - s_f \hat{u}^0(x, -H) &= 0 && \text{(Version 1), or} \\ \hat{u}^0(x, -H) &= 0 && \text{(Version 2).} \end{aligned}$$

The solution to the momentum equation is then

$$\hat{u}^0 = -g \mathcal{A}^{-1} \hat{\zeta}_x^0$$

This solution is then substituted in the depth-averaged continuity equation 2.13 and one obtains

$$i\omega \hat{\zeta}^0 - g \left( \int_{-H}^0 \mathcal{A}^{-1} \hat{\zeta}_x^0 dz \right)_x + \frac{g}{L_b} \int_{-H}^0 \mathcal{A}^{-1} \hat{\zeta}_x^0 dz = 0.$$

*Intermezzo 1 : linear operators*

We will illustrate the use of linear operators by a simple example. Consider the Poisson problem in one dimension in the domain  $[0, 1]$

$$u_{zz} = f, \quad (z \in (0, 1))$$

where  $f$  is an arbitrary real function and the problem is subject to homogeneous boundary conditions of a mixed type:

$$\begin{aligned} \alpha u(0) + \beta u_z(0) &= 0, & (\alpha, \beta \in \mathbb{R}) \\ \gamma u(1) + \delta u_z(1) &= 0, & (\gamma, \delta \in \mathbb{R}) \end{aligned}$$

We define the linear operator  $\mathcal{A} : H_m^1(0, 1) \rightarrow \mathbb{R}$  according to

$$\mathcal{A} = \frac{\partial^2}{\partial z^2}.$$

We then solve the problem

$$\mathcal{A}u = f.$$

The boundary conditions are incorporated in the linear function space in which solutions  $u$  are sought. For this case we seek for solutions in the space of all functions that possess a weak derivative, which is called  $H^1(0, 1)$ . This space is restricted to the boundary conditions. We therefore require

$$u \in H_m^1(0, 1) = \{H^1(0, 1) \mid \alpha u(0) + \beta u_z(0) = 0, \gamma u(1) + \delta u_z(1) = 0, \alpha, \beta, \gamma, \delta \in \mathbb{R}\}$$

In this research we will not focus on the function spaces that the solutions are in, because this is irrelevant to the analytical and numerical calculation of the solution. The function space is introduced here to explain how the abstract notation captures the boundary conditions.

Inhomogeneous boundary conditions cannot be incorporated in the function space, because this would make the space non-linear. In order to see this, consider the boundary conditions

$$\begin{aligned} \alpha u(0) + \beta u_z(0) &= a, & (\alpha, \beta, a \in \mathbb{R}) \\ \gamma u(1) + \delta u_z(1) &= b, & (\gamma, \delta, b \in \mathbb{R}) \end{aligned}$$

and let  $u_1$  and  $u_2$  be functions in  $H_m^1(0, 1)$ , but now with these boundary conditions. The sum of these solutions is not in the same space, because it does not satisfy the boundary conditions.

The solution is therefore separated into two parts. The first is a solution to the inhomogeneous differential equation with homogeneous boundary conditions, which has been treated above. We will call this the *internally forced* part. The second is a solution to the homogeneous differential equation with inhomogeneous boundary conditions. We will call this the *externally forced* part. The latter will be denoted by  $u_{bc1}(a)$  and  $u_{bc2}(b)$ .  $u_{bc1}(a)$  is the solution that satisfies the inhomogeneous boundary condition at  $z = 0$  and the homogeneous boundary condition at  $z = 1$ .  $u_{bc2}(b)$  satisfies the inhomogeneous condition at  $z = 1$  and the homogeneous condition at  $z = 0$ . The total solution to the problem reads

$$u = u_{bc1}(a) + u_{bc2}(b) + \mathcal{A}^{-1}f$$

Next, the linear operator  $\mathcal{B}$  is defined according to

$$\mathcal{B} = i\omega - g \left( \int_{-H}^0 \mathcal{A}^{-1} dz \right)_x \frac{\partial}{\partial x} - g \left( \int_{-H}^0 \mathcal{A}^{-1} dz \right) \frac{\partial^2}{\partial x^2} + \frac{g}{L_b} \left( \int_{-H}^0 \mathcal{A}^{-1} dz \right) \frac{\partial}{\partial x},$$

subject to a homogeneous boundary condition at  $x = L$  and an inhomogeneous boundary condition at  $x = 0$ :

$$\begin{aligned}\hat{\zeta}(0) &= A_{M_2}, \\ -g \int_{-H}^0 \mathcal{A}^{-1}(L, z) dz \hat{\zeta}_x(L) &= 0.\end{aligned}$$

The solution to this equation consists only of the externally forced part due to the boundary forcing at  $x = 0$ . This solution is denoted by

$$\hat{\zeta}^0 = \hat{\zeta}_{\text{tide}}^0(A_{M_2}).$$

The subscript 'tide' is used to denote this solution, because this solution reflects the effect of the tidal forcing at the boundary.

The solution for the velocity profile can be calculated analytically and is given by [Ianniello \(1977, 1979\)](#) for Version 1 and [McGregor \(1972\)](#) for Version 2. For a simple channel in which all parameters, except for the width, are uniform in the x-direction one can also obtain analytical solutions for the water level for both versions. The analytical solutions for velocity and water level are repeated in [Appendix A](#).

### 2.3.2. Solution for a time-dependent eddy viscosity

It was assumed in the above versions that the system is forced by a single frequency and responds with the same frequency. The Versions 3 and 4 are generalised versions of this and include multiple forcing frequencies and multiple response frequencies. Contrary to the previous section, the boundary forcing can now consist of an arbitrary number of tidal components, as long as they are overtides of the  $M_2$  tide. Additionally, the river discharge is not required to be small, so that it may act as a forcing in the leading-order equations. We will however restrict this study to small river discharges, because this is characteristic for well-mixed and partially stratified estuaries. The possibility of including a larger river discharge is included for generality. The response of the system consists of the same frequencies as the forcing frequencies, supplemented by additional non-forced response frequencies that originate from the interaction with the time-dependent eddy viscosity as will be shown in this section.

The eddy viscosity is assumed to consist of a finite number of Fourier modes

$$\nu_t(x, z, t) = \text{Re} \left( \sum_{n=0}^p \hat{\nu}_{t,n}(x, z) e^{ni\omega t} \right). \quad (2.14)$$

The angular frequency  $\omega$  again corresponds to the  $M_2$  tide. Hence, it is assumed that the eddy viscosity consists of a constant component and frequencies which are multiples of this  $M_2$  tidal frequency. We assume that the eddy viscosity is a known input to the model. In reality, the eddy viscosity depends on the solution  $u$  and  $\zeta$ . It will be treated at the end of this section how this dependency can be solved iteratively.

The velocity and water level responses to this eddy viscosity signal and a finite set of frequencies at the boundaries consist of infinitely many tidal constituents. We will truncate the solution after a finite number of constituents so that the model can be solved analytically or numerically. It will be shown in [Appendix D.1](#) that the high-frequency components are only small in the cases considered in this study.

It is practical to write the solution as a series of both positive and negative Fourier components

$$u = \text{Re} \left( \sum_{n=-p}^p \hat{u}_n e^{ni\omega t} \right), \quad (2.15)$$

$$\zeta = \text{Re} \left( \sum_{n=-p}^p \hat{\zeta}_n e^{ni\omega t} \right), \quad (2.16)$$

The momentum equation contains the product of the eddy viscosity and velocity derivatives. The product  $\nu_t u_{zz}$  is used as an example of how such products should be calculated in solving the equations. Substituting the Fourier series 2.14 and 2.15 we obtain another Fourier series. The components of this Fourier series are

$$\nu_{t,m} u_{zz,n} = \text{Re} \left( \frac{1}{2} \hat{\nu}_{t,m} \hat{u}_{z,n} e^{i(n+m)\omega t} + \frac{1}{2} \overline{\hat{\nu}_{t,m}} \hat{u}_{z,n} e^{i(n-m)\omega t} \right),$$

for  $m = 0, \dots, p$ ,  $n = -p, \dots, p$ . The overline denotes the complex conjugate. Note that this product creates response frequencies that are equal to the sum and difference of the interacting components. This has several consequences. Firstly, response frequencies other than the forcing frequencies may be present.

Secondly, the product of two positive Fourier components can create a negative Fourier component. These negative Fourier components represent the same tidal constituents as their positive counterparts. This can be seen from the following equality:

$$u_{-n} = \text{Re} (\hat{u}_{-n} e^{-ni\omega t}) = \text{Re} (\overline{\hat{u}_{-n}} e^{ni\omega t});$$

The expression on the right contains the positive frequency component  $e^{ni\omega t}$ . So it is possible to eliminate the negative Fourier components from the system and work with only positive components. This would reduce the number of components that need to be solved from  $2p + 1$  to  $p + 1$ . However, the elimination of the negative Fourier components would lead to a less well structured problem and would not benefit the computational costs of solving the equations. This will be shown in Appendix A. We will therefore retain the negative Fourier components in the computation.

Thirdly, the response signal contains an infinite number of tidal constituents, even when the forcing and eddy viscosity consist of a finite number of constituents. This can be seen by imagining a forced frequency, say  $M_2$ , that interacts with some eddy viscosity frequency, say  $M_4$ . This creates two new signals which are the sum and difference of these two components, i.e. the  $M_6$  and  $M_2$ . These components again interact with the  $M_4$  eddy viscosity frequency to create four more frequencies, one of which is a new  $M_{10}$  signal. The continuation of this reasoning yields one additional constituent with each step. The result is an infinite number of components.

The above reasoning also learns us that all frequencies are built up from many interactions. For example the  $M_2$  signal consists of the 'direct' boundary forced signal such as in Version 1 and 2. Additionally the interaction of this signal with the  $M_4$  eddy viscosity gives an  $M_2$  response. The  $M_6$  velocity that is created also interacts with the  $M_4$  eddy viscosity to create an  $M_2$  velocity component. This means that, even when one is interested in the low frequencies only, the cut-off point  $p$  should be chosen sufficiently large in order to get accurate results.

We can again solve the Equations 2.6 and 2.8 in frequency space. This is done for the set of positive and negative Fourier components, which are contained in the vectors  $\underline{\hat{u}}^0$  and  $\underline{\hat{\zeta}}^0$ :

$$\underline{\hat{u}}^0 = \begin{bmatrix} \hat{u}_{-p}^0 \\ \vdots \\ \hat{u}_0^0 \\ \vdots \\ \hat{u}_p^0 \end{bmatrix}, \quad \underline{\hat{\zeta}}^0 = \begin{bmatrix} \hat{\zeta}_{-p}^0 \\ \vdots \\ \hat{\zeta}_0^0 \\ \vdots \\ \hat{\zeta}_p^0 \end{bmatrix}.$$

The underline denotes a vector.

The resulting system of equation reads

$$D \underline{\hat{u}}^0 - \mathcal{N} \underline{\hat{u}}_{zz}^0 - \mathcal{N}_z \underline{\hat{u}}_z^0 = -g \underline{\hat{\zeta}}_x^0, \quad (2.17)$$

$$D \underline{\hat{\zeta}}^0 + \left( \int_{-H}^0 \underline{\hat{u}}^0 dz \right)_x - \frac{1}{L_b} \int_{-H}^0 \underline{\hat{u}}^0 dz = 0, \quad (2.18)$$

where  $D$  is a  $(2p + 1) \times (2p + 1)$ -diagonal matrix with entries  $ni\omega$  ( $n = -p, \dots, p$ ). The matrix  $\mathcal{N}$  is a band matrix that contains the eddy viscosity components. Details are provided in appendix A.

The scalar system 2.12, 2.13 and vector system 2.17, 2.18 have a similar structure. The vector system is therefore rewritten in the same abstract notation as the scalar system, with the linear operators  $\mathcal{A}$  and  $\mathcal{B}$  now defined as

$$\mathcal{A} = D - \mathcal{N} \frac{\partial^2}{\partial z^2} - \mathcal{N}_z \frac{\partial}{\partial z},$$

$$\mathcal{B} = D - g \left( \int_{-H}^0 \mathcal{A}^{-1} dz \right)_x \frac{\partial}{\partial x} - g \left( \int_{-H}^0 \mathcal{A}^{-1} dz \right) \frac{\partial^2}{\partial x^2} + \frac{g}{L_b} \left( \int_{-H}^0 \mathcal{A}^{-1} dz \right) \frac{\partial}{\partial x}.$$

The operator  $\mathcal{A}$  is again subject to the homogeneous boundary conditions

$$\begin{aligned} \mathcal{N} \hat{u}_z^0(x, 0) &= 0, \\ \mathcal{N} \hat{u}_z^0(x, -H) - s_f \hat{u}^0(x, -H) &= 0 && \text{(Version 3), or} \\ \hat{u}^0(x, -H) &= 0 && \text{(Version 4).} \end{aligned}$$

The operator  $\mathcal{B}$  has inhomogeneous boundary conditions at both boundaries

$$\begin{aligned} \hat{\zeta}(0) &= \underline{a}^0, \\ -g \int_{-H}^0 \mathcal{A}^{-1}(L, z) dz \hat{\zeta}_x(L) &= \frac{Q^0}{B(L)}. \end{aligned}$$

The vector  $\underline{a}^0$  consist of the boundary forcing amplitude and phase at the various frequencies. The second boundary condition contains the forcing by the constant river discharge, which only contributes to the subtidal flow and is zero for the other frequencies.

The solutions are then given by

$$\begin{aligned} \hat{u}^0 &= -g \mathcal{A}^{-1} \hat{\zeta}_x^0, \\ \hat{\zeta}^0 &= \hat{\zeta}_{\text{tide}}^0 + \hat{\zeta}_q^0 \end{aligned}$$

We again use the subscript 'tide' to denote the effect of the tidal external forcing. The subscript 'q' denotes the effect of the external forcing by the river discharge.

Analytical solutions for the inverse of  $\mathcal{A}$  exist for Version 3 and for Version 4 if parabolic profiles for all eddy viscosity components are used. Analytical solutions also exist for the  $x$ -direction in Version 3 for a simple channel in which all parameters, except for the width, are constant in the  $x$ -direction. The analytical solution method for Version 3 is given in Appendix A. Numerical solutions will be used in the remainder of this report. The details of the numerical solution procedure are also presented in Appendix A.

The eddy viscosity is assumed to be a known input to the model, while it depends on the solution  $u$  and  $\zeta$  in reality. This choice has been made to retain the linearity of the model. Several iterative procedures have been included in the model to capture the dependency of the eddy viscosity on the velocity. One such procedure, which is included in Version 3 and 4, concerns the phase of the eddy viscosity. A realistic approximation of an eddy viscosity signal in a homogeneous flow contains the components with twice the frequency of the tidal velocity components and is in phase with these components. In Version 3, where  $\nu_t$  is constant in the  $z$ -direction, it is therefore assumed that the phase of  $\hat{\nu}_{t,2n}$  corresponds to the depth-averaged phase of  $\hat{u}_n^0$ . In Version 4, where  $\nu_t$  is allowed to vary in the  $z$ -direction, the phase of  $\hat{\nu}_{t,2n}$  matches the phase of  $\hat{u}_n^0$ . The non-linear equations are solved by a Picard iteration. This means that the phase of the eddy viscosity is zero initially and adopts the phase of the previously calculated velocity in each consecutive iteration. The model is therefore linear in every iteration step. Experiments with the model show that this procedure converges monotonously and within a reasonable amount of iterations. A different iterative coupling is applied to the coupling to the  $k - \varepsilon$  turbulence model in Version 5. This is treated in Section 2.4.

### 2.3.3. Solution to the first-order system

The previous section illustrated the solution method for the leading-order equations. This section treats the extension of this solution method to the first-order momentum and depth-averaged equations. It will be shown

that this extension is simple, because of the similarity of the structure of the leading-order and first-order equations. The solution method is applied to model Versions 3 and 4.

In order to simplify the notation, the following symbols are introduced:

$$\begin{aligned}\eta(x, z, t) &= u^0(x, z, t)u_x^0(x, z, t) + w^0(x, z, t)u_z^0(x, z, t), \\ \gamma(x, t) &= \zeta^0(x, t)u^0(x, 0, t), \\ \chi(x, t) &= \zeta^0(x, t)u_{zz}^0(x, 0, t).\end{aligned}$$

The advection terms are thus represented by  $\eta$ . The function  $\gamma$  denotes the Stokes drift by the leading-order flow (see Section 1.1) and  $\chi$  denotes a flow correction which is due to the linearisation of the boundary condition at  $z = \zeta$  to  $z = 0$ .

The first-order equations 2.9, 2.11 are again solved in frequency space using the same definitions of  $\nu_t$ ,  $u$  and  $\zeta$  as in 2.14, 2.15 and 2.16. Similarly, Fourier series are defined for  $\eta$ ,  $\gamma$ ,  $\chi$  and  $\rho$ . The equations then read

$$D\hat{u}^1 - \mathcal{N}\hat{u}_{zz}^1 - \mathcal{N}_z\hat{u}_z^1 = -g\hat{\zeta}_x^1 - \hat{\eta} + \frac{g}{\rho_0}\hat{\rho}_x z, \quad (2.19)$$

$$D\hat{\zeta}_t^1 + \left( \int_{-H}^0 \hat{u}^1 dz \right)_x - \frac{1}{L_b} \int_{-H}^0 \hat{u}^1 dz = -\hat{\gamma}_x + \frac{\hat{\gamma}}{L_b}. \quad (2.20)$$

Equation 2.19 still satisfies homogeneous boundary conditions at the bed, but the condition at the surface has become inhomogeneous. The boundary conditions read

$$\mathcal{N}\hat{u}_z^1(x, 0) = -\mathcal{N}\hat{\chi}, \quad (2.21)$$

$$\mathcal{N}\hat{u}_z^1(x, -H) - s_f\hat{u}^1(x, -H) = \underline{0}, \quad (\text{Version 3}) \text{ or} \quad (2.22)$$

$$\hat{u}_z^1(x, -H) = \underline{0}. \quad (\text{Version 4})$$

Equation 2.20 satisfies the boundary conditions

$$\hat{\zeta}^1(0) = \underline{a}^1, \quad (2.23)$$

$$\int_{-H}^0 \hat{u}^1(L, z) dz = \frac{Q^1}{B(L)} - \hat{\gamma}. \quad (2.24)$$

Equations 2.19, 2.20 have the same structure as the leading-order equations 2.17, 2.18; both systems use the same operators on the left-hand side and both systems have known quantities on the right-hand side. Because the systems at both orders use the same operators, the definitions of  $\mathcal{A}$  and  $\mathcal{B}$  are exactly the same for the leading-order and first-order systems. The first-order momentum equation can thus be written in abstract notation as

$$\mathcal{A}\hat{u}^1 = -g\hat{\zeta}_x^1 - \hat{\eta} + \frac{g}{\rho_0}\hat{\rho}_x z,$$

With solution

$$\hat{u}^1 = \hat{u}_{\text{no-stress}}^1 - g\mathcal{A}^{-1}\hat{\zeta}_x^1 - \mathcal{A}^{-1}\hat{\eta} + \frac{g}{\rho_0}\mathcal{A}^{-1}\hat{\rho}_x z,$$

where the subscript 'no-stress' signifies the solution to the homogeneous equation with the inhomogeneous boundary condition 2.21 at the surface.

The first-order depth-averaged continuity equation becomes

$$\begin{aligned}\mathcal{B}\hat{\zeta}^1 &= \left( \int_{-H}^0 \mathcal{A}^{-1}\hat{\eta} dz \right)_x - \frac{1}{L_b} \int_{-H}^0 \mathcal{A}^{-1}\hat{\eta} dz - \frac{g}{\rho_0} \left( \int_{-H}^0 \mathcal{A}^{-1}\hat{\rho}_x z dz \right)_x + \frac{1}{L_b} \frac{g}{\rho_0} \int_{-H}^0 \mathcal{A}^{-1}\hat{\rho}_x z dz \\ &\quad + \left( \int_{-H}^0 \hat{u}_{\text{no-stress}}^1 dz \right)_x - \frac{1}{L_b} \int_{-H}^0 \hat{u}_{\text{no-stress}}^1 dz - \hat{\gamma}_x + \frac{\hat{\gamma}}{L_b}.\end{aligned}$$

The solution contains many terms. The notation is slightly simplified by rewriting terms containing  $L_b$  in terms of the width  $B$ .

$$\begin{aligned} \underline{\hat{\zeta}}^1 = & \hat{\zeta}_{\text{tide}}^1 + \hat{\zeta}_q^1 + \hat{\zeta}_{\text{return flow}}^1 + \hat{\zeta}_{s_x}^1 + \hat{\zeta}_{\text{adv}}^1 + \hat{\zeta}_{\text{no-stress}}^1 + \mathcal{B}^{-1} \left( \frac{B}{B_0} \int_{-H}^0 \mathcal{A}^{-1} \hat{\eta} dz \right)_x \\ & - \mathcal{B}^{-1} \frac{g}{\rho_0} \left( \frac{B}{B_0} \int_{-H}^0 \mathcal{A}^{-1} \hat{\rho}_x z dz \right)_x + \mathcal{B}^{-1} \left( \frac{B}{B_0} \int_{-H}^0 \hat{u}_{\text{no-stress}}^1 dz \right)_x - \mathcal{B}^{-1} \left( \frac{B}{B_0} \hat{\gamma} \right)_x \end{aligned}$$

The solutions to these equations can be written in a clearer way by grouping the right-hand side forcings by their physical meaning. The solution then takes the form

$$\hat{u}^1 = \hat{u}_{\text{tide}}^1 + \hat{u}_q^1 + \hat{u}_{\text{no-stress}}^1 + \hat{u}_{\text{adv}}^1 + \hat{u}_{s_x}^1 + \hat{u}_{\text{return flow}}^1, \quad (2.25)$$

$$\underline{\hat{\zeta}}^1 = \hat{\zeta}_{\text{tide}}^1 + \hat{\zeta}_q^1 + \hat{\zeta}_{\text{no-stress}}^1 + \hat{\zeta}_{\text{adv}}^1 + \hat{\zeta}_{s_x}^1 + \hat{\zeta}_{\text{return flow}}^1. \quad (2.26)$$

The partial solutions on the right-hand side consist of the solution to one or more forcing terms of the equations or boundary conditions. These partial solutions can simply be added to make the full solution because the equations are linear. The meaning of the subscripts is provided in Table 2.2.

Subscript	Physical component	Meaning
tide	External tidal forcing	External forcing of water level
$q$	River discharge	Externally forced residual flow
no-stress	Free surface mixing, $\chi$	Change of the velocity profile due to linearised no-stress condition
adv	Advective transport, $\eta$	Contribution of advection
$s_x$	Baroclinic pressure	Contribution of the salinity gradient
return flow	For residual flow: Gravitational circulation Return flow of Stokes drift, $\gamma$	See Section 1.1

Table 2.2: Physical mechanisms identified in the velocity and water level fields.

## 2.4. The $k - \varepsilon$ turbulence model

The previous sections described the model Versions 1 to 4 for hydrodynamics with prescribed profiles and time-dependency of the eddy viscosity. The fifth version of the model involves the coupling of the hydrodynamic model to a two-equation turbulence model. The turbulence model acts as a separate module, feeding its solution into the eddy viscosity formulation 2.14 of Version 4. Next, the Version 4 model is used to calculate the velocities and water levels as before and the result is used as input to the turbulence model. This iterative process is repeated until convergence is reached. This section will first present the  $k - \varepsilon$  model and some important properties and assumptions, after which the coupling of the hydrodynamic and turbulence models is discussed. The details on the numerical implementation of the  $k - \varepsilon$  model are presented in Appendix C.

### 2.4.1. Properties and assumptions of the $k - \varepsilon$ model

The  $k - \varepsilon$  model is a popular two-equation turbulence model that is used in many complex flow models. The version of the model that is used here is the buoyancy extended form of Rodi (1993). This section treats only some of the assumptions and properties of the  $k - \varepsilon$  model. Further details of the derivation of the model and some results of computations with the model can be found in Dijkstra (2014).

The  $k - \varepsilon$  model is a turbulence model that is based on the eddy viscosity closure hypothesis. In this hypothesis it is assumed that turbulent mixing has the form of a diffusion process that can be expressed by the diffusion term  $(\nu_t u_z)_z$ , in which the eddy viscosity  $\nu_t$  acts as a diffusion coefficient. This turbulent diffusion acts predominantly in the vertical direction, because the vertical velocity gradient is generally much larger than the horizontal velocity gradient.

The eddy viscosity is parametrised by the use of the mixing-length hypothesis. According to this hypothesis the value of the eddy viscosity is determined by the product of a typical length-scale and a typical velocity-scale of turbulent eddies. The eddy viscosity is then expressed as

$$\nu_t = c_\mu \sqrt{k} l_m,$$

where  $\sqrt{k}$  is the velocity-scale, with  $k$  representing the turbulent kinetic energy. The variable  $l_m$  denotes a length-scale of mixing and  $c_\mu$  is a constant. Several alternative definitions exist for the mixing-length. For the  $k - \varepsilon$  model it is assumed that the mixing-length can be expressed as

$$l_m = \frac{k^{3/2}}{\varepsilon},$$

where  $\varepsilon$  is the rate of dissipation of turbulent eddies. The resulting expression for the eddy viscosity is

$$\nu_t = c_\mu \frac{k^2}{\varepsilon}$$

The two unknown quantities  $k$  and  $\varepsilon$  are calculated by the  $k - \varepsilon$  model, which consists of two coupled non-linear transport equations. The  $k - \varepsilon$  model by Rodi (1993) is adapted by using the additional assumption that the horizontal gradient of turbulence are much smaller than the vertical gradients. This reduces the model to the following 1DV model:

$$k_t = ((\nu + \nu_t) k_z)_z + \nu_t u_z^2 - \frac{\nu_t}{\sigma_\rho} N^2 - \varepsilon, \quad (2.27)$$

$$\varepsilon_t = \left( \left( \nu + \frac{\nu_t}{\sigma_\varepsilon} \right) \varepsilon_z \right)_z + c_1 \frac{\varepsilon}{k} \nu_t u_z^2 - c_3 \frac{\varepsilon}{k} \frac{\nu_t}{\sigma_\rho} N^2 - c_2 \frac{\varepsilon^2}{k} \quad (2.28)$$

The symbol  $\nu$  represents the molecular diffusion of  $10^{-6} \text{ m}^2/\text{s}$ . The terms on the right-hand side of both equations represent the diffusive vertical transport, production of turbulence by velocity gradients, production or dissipation of turbulence by stratification and viscous dissipation of turbulence. The quantity  $N$  in the equations is the buoyancy frequency which is defined as

$$N = \sqrt{-\frac{g}{\rho} \rho_z}.$$

The expressions  $\frac{\nu_t}{\sigma_\varepsilon}$  and  $\frac{\nu_t}{\sigma_\rho}$  denote dispersion coefficients for the dispersive transport of turbulence dissipation  $\varepsilon$  and density differences respectively. The constants  $\sigma_\varepsilon$  and  $\sigma_\rho$  are Prandtl-Schmidt numbers that are used to relate these diffusion coefficients to the eddy viscosity. The constants  $c_1$ ,  $c_2$  and  $c_3$  are calibrated constants. Table 2.3 presents the values of the parameters such as calibrated by Launder et al. (1972), Rodi (1993) and in the numerical model Delft 3D - FLOW (Deltares, 2014).

Parameter	$c_1$	$c_2$	$c_3$ (stable stratification)	$c_3$ (unstable stratification)	$c_\mu$	$\sigma_\rho$	$\sigma_\varepsilon$
Value	1.44	1.92	0	1.44	0.09	0.7	1.3

Table 2.3: The values of the parameters in the  $k - \varepsilon$  model.

The boundary conditions of the model are

$$\begin{aligned} k(x, \zeta, t) &= 0, \\ k(x, -H, t) &= \frac{u_*^2}{\sqrt{c_\mu}}, \\ \frac{\partial \varepsilon}{\partial z}(x, \zeta, t) &= 0, \\ \frac{\partial \varepsilon}{\partial z}(x, -H, t) &= \frac{|u_*^3|}{9z_0 \kappa}, \end{aligned}$$

where  $z_0$  is the roughness height,  $\kappa$  is the Von Kármán constant of 0.4 and  $u_*$  is the friction velocity which is defined as

$$u_* = \frac{\tau}{|\tau|} \sqrt{\frac{|\tau|}{\rho_0}},$$

where  $\tau$  is the bed shear stress.

The  $k - \varepsilon$  model derives ultimately from physical conservation laws and we will quickly outline the derivation of the model. An exact equation for  $k$  can be derived from the principle of energy conservation. Equation 2.27 follows from this exact equation by assuming that turbulent transport terms can be described by diffusion terms. This is a generally accepted assumption (Mellor and Yamada, 1982). It makes no sense physically to formulate an exact conservation equation for turbulence dissipation  $\varepsilon$ , because there is no such law as conservation of dissipation. Still, it is possible to derive an exact transport equation for  $\varepsilon$  from energy and momentum conservation. This equation, however, involves some unknown quantities and the equation needs to be closed. The validity of these closure assumptions is contested and leads to a range of turbulence models that make different closure assumptions. From a pragmatic point of view, the  $k - \varepsilon$  model is a turbulence model that contains the complexity to reproduce some of the influence of velocity gradients, friction and stratification on turbulent mixing, while it is still sufficiently simple to solve within a reasonable computational time. This is why the model is implemented in many complex numerical models for large-scale applications, such as Delft 3D-FLOW.

The  $k - \varepsilon$  model is solved numerically according to the implementation in Delft 3D-FLOW. Details of this implementation are given in Appendix C and by Dijkstra (2014). Note that the  $k - \varepsilon$  model is solved as a partial differential equation in  $z$  and  $t$  instead of solving it using Fourier components. We chose this method here in order to be able to use the well-tested Delft 3D-FLOW implementation of the turbulence model, rather than to make a new implementation of which the accuracy is not yet known. It is possible to solve the system in terms of Fourier components, but it is unknown whether this yields accurate results within a reasonable amount of computational time.

### 2.4.2. Bed friction formulation

In theory, the bottom boundary conditions should require no-slip conditions so that  $u$  and  $\nu_t$  are zero at the bed. However, all information on bed friction is then contained in the gradient of the eddy viscosity at the bed, which cannot be accurately simulated with a resolution that yields reasonable computational times with the 2DPM model or in fact any large-scale 2D or 3D model. On the small scale that would be required in order to use no-slip conditions, it is no longer realistic to regard the bed as a flat plate. Instead, it contains ripples and dunes (also called bed forms) and possible vegetation or fluidised mud, which determine the roughness of the bed.

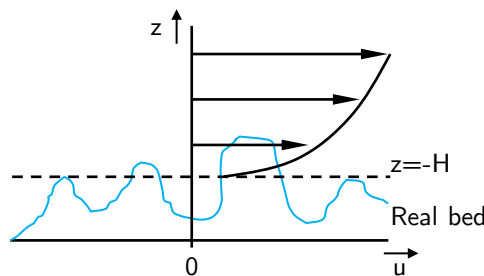


Figure 8: Definition of the bed level  $z = -H$  on a rough bed.

In order to circumvent the use of high resolution grids and highly detailed bed topography, the boundary conditions are applied at a constant level which is a small distance from the real bed (Hinze, 1975), see Figure 8. This newly defined bed level  $z = -H$  is then a smoothly varying surface that possesses a certain roughness, which is parametrised by a roughness height. Consistent with this definition, the velocity and eddy viscosity

are non-zero at this bed level. Such boundary conditions are derived from a combination of idealised modelling and empiricism. This yields the boundary conditions of the  $k - \varepsilon$  model given above and the quadratic-slip boundary condition for the velocity, which reads

$$\nu_t(-H)u_z(-H) = u_*^2,$$

The bed friction  $u_*$  depends on the velocity near the bed, see Appendix C. The effect of bed friction is now incorporated in the boundary conditions of the  $k - \varepsilon$  model and the boundary condition for the velocity.

The non-linear boundary condition is linearised according to Picard's method, i.e. by taking one factor  $u_*$  explicitly from the previous iteration level and one implicitly in the current iteration. A solution to the non-linear boundary condition is obtained by the iterative solution method.

### 2.4.3. Coupling of the turbulence and hydrodynamic models

The turbulence model is a non-linear model that is solved in time, while the hydrodynamic model is a linear model that is solved in frequency space. Both models are therefore implemented as separate modules. The coupling between these modules is presented here. Because the turbulence and hydrodynamic models together form a non-linearly coupled system, the equations are solved iteratively. To explain this solution procedure we will treat consecutively the initialisation phase, the iteration phase and the convergence criterion.

The notation is simplified by using the following abstract notation of both modules:

$$\begin{aligned} \nu_t &= f(u_z, u_*, \rho_z) && \text{for the turbulence model,} \\ \begin{bmatrix} u \\ \zeta \end{bmatrix} &= \underline{g}(\nu_t) && \text{for the hydrodynamic model.} \end{aligned}$$

The functions  $f$  and  $\underline{g}$  represent the models and the subscript  $n$  will be used below to denote a quantity after the  $n^{\text{th}}$  iteration.

An initial velocity and water level field are needed as input in order to calculate the eddy viscosity  $\nu_{t,1}(x, z, t)$ . This initial field, denoted by  $u_0$  and  $\zeta_0$ , is calculated by the hydrodynamic model using an assumed initial eddy viscosity  $\nu_{t,0}(x, z, t)$ .

The iteration between both modules starts by running the turbulence model, the result of which is an eddy viscosity field in  $x$ ,  $z$  and  $t$ . The turbulence model is run for 10 tidal cycles in the first iteration in order to eliminate spin-up. The final cycle is used as the initial eddy viscosity in the next iteration. The turbulence model is run for only two tidal cycles in subsequent iterations, which is sufficient because the turbulence field is not supposed to change much between two iterations. A fast Fourier transformation (FFT) algorithm is used to transform the last tidal cycle of the eddy viscosity field to frequency space in every iteration. The hydrodynamic model Version 4 then uses the constant component and the first  $p$  overtides of the  $M_2$  tidal frequency, including the  $M_2$  frequency itself. So the hydrodynamic model does not use the full eddy viscosity signal, but an abstraction of it. It will be shown in the results and Appendix D.1 that this abstraction captures a large part of the eddy viscosity signal for reasonably small values of  $p$ .

The coupling makes use of the under-relaxation method. This means that the hydrodynamic model uses a fraction  $\lambda \in [0, 1]$  of the eddy viscosity from the previous iteration and a fraction  $1 - \lambda$  of the eddy viscosity from current iteration. This method can prevent certain instabilities that the model may display, because the changes in the model from one iteration to the other are kept small when  $\lambda$  is close to 1. A value  $\lambda = 0.9$  is used in this research, which means that only 10% of the newly calculated value of the eddy viscosity is used in every iteration.

To be more precise the iteration is given by

$$\begin{aligned}\nu_{t,n} &= f(u_{z,n-1}, u_{*,n-1}, \rho_{z,n-1}), \\ \tilde{\nu}_{t,n} &= (1 - \lambda)\nu_{t,n}^{FFT} + \lambda\nu_{t,n-1}^{FFT}, \\ \begin{bmatrix} u_n \\ \zeta_n \end{bmatrix} &= \underline{g}(\tilde{\nu}_{t,n}),\end{aligned}$$

where  $\nu_t^{FFT}$  is the eddy viscosity signal that results after the fast Fourier transform described above.

The above procedure of using a number of Fourier components to approximate the eddy viscosity does not ensure positivity of the eddy viscosity. The positivity of  $\tilde{\nu}_{t,n}$  is therefore checked and the value is corrected if it becomes negative by reducing the amplitude of the oscillating components.

The convergence of  $\tilde{\nu}_{t,n}$  is measured by the supremum-norm in  $x$ ,  $z$  and  $t$  of the difference between the eddy viscosity in consecutive iterations before the FFT, i.e.

$$\Delta\nu_{t,n} = |\nu_{t,n} - \nu_{t,n-1}|_{\infty}. \quad (2.29)$$

The iteration is assumed to have converged when  $\Delta\nu_{t,n} < \mathcal{O}(10^{-5} \text{ m}^2/\text{s})$ , which is much smaller the typical value of the eddy viscosity.

# 3

## Model formulation: salinity

The 2DPM hydrodynamics model is extended in this chapter by a salinity model which makes use of the perturbation approach. The assumptions behind this model make it suitable only for well-mixed estuaries. Section 3.1 explores in more detail what this restriction means and how this compares to other studies. The salinity model will be explained in Section 3.2. This model is again solved by using abstract linear operators as will be explained in Section 3.3. In order to gain understanding of the physical mechanisms that drive the salinity model, a method for analysis is presented in Section 3.4.

### 3.1. Background and assumptions

The balance of the various physical mechanisms that govern the salinity transport depends strongly on the vertical salinity structure (Jay and Smith, 1990b). The idealised model that is used in this research is restricted to the processes and the vertical salinity structure that are seen in well-mixed estuaries. This means that the model is not capable of modelling strongly stratified and salt wedge estuaries, and only partially capable of modelling partially stratified estuaries. Strongly stratified and salt-wedge estuaries are characterised by a high river discharge and little to moderate tidal influence. The persisting strong stratification diminishes the influence of turbulent mixing and mixing is dominated by internal wave breaking and Kelvin-Helmholtz instabilities (Jay and Smith, 1990b). Conversely, well-mixed and partially stratified estuaries have a smaller river discharge and a larger tidal influence and turbulent mixing is important.

Most previous idealised model studies into the transport of salinity have been restricted to well-mixed estuaries (Jay and Smith, 1990c; MacCready, 2004; Burchard and Hetland, 2010). An exception to this is the study done by Jay and Smith (1990b) who use a two-layer model to study salt-wedge estuaries. This model is, however, not suitable for other classes of estuaries and so to date no idealised model exists that is capable of simulating the transition between partially stratified and salt-wedge estuaries. In order to model this transition it is vital to include the effect of stratification on turbulent mixing (Geyer and MacCready, 2014). It is therefore possible that the inclusion of a  $k - \varepsilon$  turbulence model as is done in this study makes the model capable of modelling the transition. However, it is outside the scope of this thesis to explore this possibility.

The restriction to well-mixed estuaries allows us to assume that the longitudinal salinity gradient is rather small. In the derivation of the salinity model in Appendix B this is made slightly more precise by stating that the typical length-scale along which the salinity varies should be of the same order of magnitude as the length-scale of the tidal wave. A consequence of this assumption is that the vertical stratification is weak, which agrees with the initial restriction of the study to well-mixed and partially stratified estuaries. It is further assumed that the river discharge appears in the first-order velocity component. This assumption also agrees with well-mixed estuaries.

### 3.2. Model equations

The transport equation for salinity in 2DV is given by the following advection-diffusion equation:

$$s_t + us_x + ws_z = \frac{1}{BH} (BHK_H s_x)_x + (K_V s_z)_z. \quad (3.1)$$

In this equation  $K_H$  and  $K_V$  are dispersion coefficients. The coefficient  $K_H$  parametrises all unresolved processes. These include most notably lateral processes and lateral variations of longitudinal processes. It is expected that this value is small in narrow estuaries with a rectangular cross-section, but it is dominant over the other processes in many estuaries (Fischer, 1972; Burchard et al., 2011).  $K_V$  parametrises vertical mixing and can be related to the eddy viscosity through the Prandtl-Schmidt number according to

$$K_V = \frac{\nu_t}{\sigma_\rho}.$$

The Prandtl-Schmidt number  $\sigma_\rho$  is assumed to be a constant, but may also be chosen to vary with stratification (Burchard and Hetland, 2010).

The salinity is related to the density through an equation of state. It is sufficient to use a linear relation between density and salinity for the range of salinity concentrations that is applied in this study. The equation of state reads

$$\rho = \rho_0(1 + \beta s),$$

where  $\beta = 7.7 \cdot 10^{-4}$  1/psu and  $\rho_0 = 1000$  kg/m<sup>3</sup> is a reference density. The acronym psu is the unit for salinity and stands for *practical salinity unit*.

The boundary conditions to Equation 3.1 are no-flux conditions at the surface and bed

$$K_V s_z = 0 \quad \text{at } z = \zeta \text{ and } z = -H.$$

A fixed salinity is prescribed at the mouth and a no-flux condition is prescribed at the landward boundary

$$\begin{aligned} \frac{1}{H} \int_{-H}^0 s \, dz &= s_{\text{sea}} & \text{at } x = 0, \\ Q \frac{1}{H} \int_{-H}^0 s \, dz &= BHK_L \frac{1}{H} \int_{-H}^0 s_x \, dz. & \text{at } x = L. \end{aligned}$$

The perturbation approach again uses a scaling and an ordering of the solution. The scaling is given in detail in Appendix B, the main result being that the advective terms in Equation 3.1 are of  $\mathcal{O}(\delta)$  and the horizontal dispersion term is of  $\mathcal{O}(\delta^2)$ . The ordering of  $s$  is written as

$$s = s^0 + s^1 + s^2 + \dots,$$

where  $s^0$  is of  $\mathcal{O}(1)$ ,  $s^1$  is of  $\mathcal{O}(\delta)$  etcetera.

The resulting leading-order and first-order equations are then

$$s_t^0 = (K_V s_z^0)_z, \quad (3.2)$$

$$s_t^1 + u^0 s_x^0 + w^0 s_z^0 = (K_V s_z^1)_z. \quad (3.3)$$

The ordered boundary conditions are given in Appendix B.

The solution to Equation 3.2 with its no-flux boundary conditions is that  $s_0$  is an unknown function of  $x$ -only. This implies that the leading-order salinity field is well-mixed and constant in time. An additional closure equation is required, because  $s_0$  remains an unknown function. This closure equation is the depth-averaged, time-averaged second-order salinity equation. The derivation is again given in the appendix. The equation reads:

$$\left( B \int_{-H}^0 \langle u^0 s^1 \rangle dz \right)_x + \left( B \int_{-H}^0 \langle u^1 s^0 \rangle dz \right)_x + (B \langle \zeta^0 u^0(x, 0, t) s^0(x, 0, t) \rangle)_x = (BHK_H s_x^0)_x. \quad (3.4)$$

### 3.3. Solution method

The Equations 3.2, 3.3 and 3.4 are again solved as systems of ordinary differential equations by using the superposition of Fourier components. The salinity model will be applied to the vector form of Versions 3 to 5 of the hydrodynamic model, the scalar solutions will be omitted. The details of the solution procedure are given in Appendix B. The main results are presented below.

Before substituting the Fourier series we consider the leading-order equation. It can be shown that this equation with no-flux boundary conditions at the bed and linearised surface stipulates

$$s^0(x, z, t) = s^0(x). \quad (3.5)$$

So the leading-order salinity field is well-mixed, time-independent and unknown. Therefore the depth-integrated time-integrated second-order equation 3.4 is used as closure according to the method by McCarthy (1993).

The first-order equation 3.3 is solved in frequency space. To this end, the first-order salinity is written as the truncated Fourier series

$$s^1(x, z, t) = Re \left( \sum_{n=-p}^p \hat{s}_n^1(x, z) e^{ni\omega t} \right).$$

The equation can then be written in a matrix form similar to the hydrodynamic model. This equation reads

$$D\hat{s}^1 - \frac{1}{\sigma_\rho} \mathcal{N}_z \hat{s}_z^1 - \frac{1}{\sigma_\rho} \mathcal{N} \hat{s}_{zz}^1 = -\hat{u}^0 s_x^0,$$

where  $D$  and  $\mathcal{N}$  are the same matrices as in the hydrodynamic model and it is used that  $K_V = \frac{\nu_t}{\sigma_\rho}$ . The leading-order salinity in this equation is a scalar quantity, because it consists only of the subtidal salinity. This equation can be rewritten in a more abstract notation by using the linear operator  $\mathcal{R}$  which is defined as

$$\mathcal{R} = D - \frac{1}{\sigma_\rho} \mathcal{N}_z \frac{\partial}{\partial z} - \frac{1}{\sigma_\rho} \mathcal{N} \frac{\partial^2}{\partial z^2}.$$

We obtain the equation

$$\mathcal{R}\hat{s}^1 = -\hat{u}^0 s_x^0,$$

subject to no-flux boundary conditions

$$\begin{aligned} \mathcal{N} \hat{s}_z^1(x, 0) &= 0, \\ \mathcal{N} \hat{s}_z^1(x, -H) &= 0. \end{aligned}$$

The solution for  $\hat{s}^1$  only has an internally forced part (see Intermezzo 1 in Chapter 2):

$$\hat{s}^1 = -\mathcal{R}^{-1} \hat{u}^0 s_x^0. \quad (3.6)$$

The linear operator  $\mathcal{R}$  is singular and requires a compatibility condition. This compatibility condition is obtained by integrating the residual component of Equation 3.3 over the water depth. This condition then prescribes that there is no net (i.e. time-averaged and depth-averaged) salt transport in this first-order equation. More details are given in Appendix B.

Next, the second-order depth-averaged time-averaged equation 3.4 is solved. This equation can be rewritten by using the vertical uniformity of  $s^0$  and the depth-averaged continuity equation. This allows one to eliminate  $u^1$  from the equation, i.e. the salinity model only uses the leading-order velocity as input. The resulting equation reads

$$\left( B \int_{-H}^0 \langle u^0 s^1 \rangle dz \right)_x + s_x^0 Q^1 = (BHK_H s_x^0)_x. \quad (3.7)$$

This is a scalar equation, because  $s^0$  is only the subtidal component by Equation 3.5. The equation is also real because the subtidal salinity component does not contain phase information.

The equation is a real, scalar equation, but contains correlations of tidal components of the velocity and first-order salinity. The equation is therefore solved in frequency space. This requires the conversion of the product  $\langle u^0 s^1 \rangle$  to frequency space. This product becomes

$$\langle u^0 s^1 \rangle = \text{Re} \left( (\hat{u}^0)^T \hat{s}^1 \right) = -\text{Re} \left( (\hat{u}^0)^T \mathcal{R}^{-1} \hat{u}^0 s_x^0 \right).$$

By using Equation 3.6, the equation in frequency space becomes

$$-\left( B s_x^0 \int_{-H}^0 (\hat{u}^0)^T \mathcal{R}^{-1} \hat{u}^0 dz \right)_x + s_x^0 Q^1 = (BHK_H s_x^0)_x.$$

This equation is rewritten to an abstract notation by defining the linear operator  $\mathcal{S}$  as

$$\begin{aligned} \mathcal{S} = & - \left( B \int_{-H}^0 (\hat{u}^0)^T \mathcal{R}^{-1} \hat{u}^0 dz \right)_x \frac{\partial}{\partial x} - B \int_{-H}^0 (\hat{u}^0)^T \mathcal{R}^{-1} \hat{u}^0 dz \frac{\partial^2}{\partial x^2} + Q^1 \frac{\partial}{\partial x} \\ & - (BHK_H)_x \frac{\partial}{\partial x} - BHK_H \frac{\partial^2}{\partial x^2}. \end{aligned}$$

The equation then simplifies to

$$\mathcal{S} s^0 = 0,$$

subject to the following boundary conditions:

$$s^0(0) = s_{\text{sea}},$$

$$Q^1 s^0(L) - BHK_H s_x^0(L) - B \int_{-H}^0 \langle (\hat{u}^0)^T \mathcal{R}^{-1} \hat{u}^0 \rangle dz s_x^0(L) = 0.$$

The solution to this equation only contains one externally forced part from the inhomogeneous boundary condition at the seaward side:

$$s^0 = s_{bc}(s_{\text{sea}}).$$

### 3.4. Salt balance decomposition

The depth-averaged time-averaged second-order salinity Equation 3.7 describes the amount of salt intrusion. In this section two decompositions of the salt balance will be developed to analyse the different mechanisms that are responsible for this salt intrusion. These decompositions will express the salt transport in terms of equivalent dispersion coefficients such as are used in 1DH studies into salt intrusion (e.g. [Savenije \(2005\)](#), [Kuijper and Van Rijn \(2011\)](#) and references therein). First, such 1DH approach is introduced and it is shown how the results of the 2DV model can be converted to 1DH. Next, both decomposition techniques are introduced. Finally, the salt balance is compared to the salinity model that was developed above.

#### 3.4.1. The 1DH dispersion coefficient

The salt transport in 1DH is often described by the following equation ([Ippen and Harleman, 1961](#))

$$BH(\bar{s})_t + Q\bar{s}_x = (BHK\bar{s}_x)_x,$$

where  $K$  is the dispersion coefficient for salt and the overline ( $\bar{\cdot}$ ) denotes depth-averaging over the time-averaged depth, i.e.

$$\bar{s} = \frac{1}{H} \int_{-H}^{\zeta} s dz.$$

This is not the proper equation for describing conservation of salinity, because  $BH$  denotes the linearised time-averaged cross-section; interactions between the free surface variations, salinity and velocity are implicitly contained in  $K$ . This equation will be used here so that the definition of  $K$  is consistent with the general definition that is used in literature. The time-averaged form of this salt transport equation reads

$$Q\langle\bar{s}\rangle_x = (BHK\langle\bar{s}_x\rangle)_x. \quad (3.8)$$

This equation describes the balance between the river discharge flushing saline water from the estuary and the dispersion pumping saline water into the estuary.

Rather than considering the 1DH equation, one can also calculate the salt transport from a 2DV perspective. This is done by the salt balance, which describes the salt flux through a cross-section. We will consider the time-averaged depth-averaged flux  $M_t$ . The total salt flux must equal zero in a stationary situation. We thus obtain

$$M_t = B\langle(H + \zeta)\bar{u}\bar{s}\rangle - BHK_{\text{closure}}\langle\bar{s}\rangle_x = 0. \quad (3.9)$$

The mass transport equation contains two terms. The first describes the transport by salinity advection, i.e. the product of  $u$  and  $s$ . This is the model resolved transport, because both the velocity and the salinity are calculated by the model. The second term is a salt dispersion term that is parametrised by a dispersion coefficient  $K_{\text{closure}}$ . This term describes the unresolved transport, because the dispersion coefficient is not calculated by the model. The unresolved transport contains for example the transport by lateral processes or laterally varying longitudinal processes.

The salt balance 3.9 can be related to the 1DH salinity equation 3.8 by assuming that the model-resolved salt flux can be written according to

$$B\langle(H + \zeta)\bar{u}\bar{s}\rangle = Q\langle\bar{s}\rangle - BHK_u\langle\bar{s}\rangle_x,$$

where  $K_u$  is a dispersion coefficient. The 1DH dispersion coefficient  $K$  is equal to

$$K = K_u + K_{\text{closure}},$$

so that the salt balance then reads

$$M_t = Q\langle\bar{s}\rangle - BH(K_u + K_{\text{closure}})\langle\bar{s}\rangle_x = 0.$$

This is the integrated form of the 1DH salt transport equation.

An expression for the unknown 1DH dispersion coefficient  $K$  in terms of output of 2DV model data can be found by rewriting the latter expression to

$$K = -\frac{\langle(H + \zeta)\bar{u}\bar{s}\rangle}{H\langle\bar{s}\rangle_x} + \frac{Q}{B} \frac{\langle\bar{s}\rangle}{H\langle\bar{s}\rangle_x} + K_{\text{closure}}. \quad (3.10)$$

The only unknown in this equation is the closure coefficient  $K_{\text{closure}}$  which needs to be prescribed or parametrised. It will be shown in Section 3.4.4 that this closure coefficient corresponds approximately to the lateral dispersion coefficient  $K_H$  in the 2DV salinity model.

### 3.4.2. Decomposition in physical contributions

The expression for  $K$  can be decomposed into the contribution by the various forcing mechanisms in the hydrodynamic model such as the tide, river discharge and baroclinic pressure, described in Table 2.2. This requires the decomposition of the velocity and salinity into components that can be attributed to these forcing mechanisms, such as was done in Equation 2.25 for the velocity. A similar decomposition could be constructed for the salinity. However, such a decomposition would not be trivial nor unambiguous, because of the structure of the depth-averaged time-averaged salinity equation. In order to see this, consider the abstract operator notation of this equation:  $\mathcal{S}s^0 = 0$ . The solution consists of a single term forcing at the seaward boundary. All

information on the forcing mechanisms is contained in the operator  $\mathcal{S}$ , instead of in the forcing of the equation or the boundary conditions. So a decomposition would require that both operator  $\mathcal{S}$  and the solution  $s^0$  are separated in the various physical mechanisms. The equation  $\mathcal{S}s^0 = 0$  would then be non-linear in the physical forcing mechanisms, even though it is linear in  $s^0$ .

For our present purposes it is sufficient to use a decomposition of the velocity and use the full salinity signal as calculated by the model. This means that the decomposition of the dispersion coefficient is calculated according to

$$K_i = -\frac{\langle (H + \zeta) \overline{u_i s} \rangle}{H \langle \overline{s} \rangle_x},$$

with  $i \in \{\text{tide, no-stress, adv, } s_x, \text{ return flow}\}$  (see Table 2.2). The river discharge needs a separate definition for the dispersion coefficient. Consistent with Equation 3.10 this expression should read

$$\begin{aligned} K_{\text{river}} &= -\frac{\langle (H + \zeta) \overline{u_{\text{river}} s} \rangle}{H \langle \overline{s} \rangle_x} + Q \frac{\langle \overline{s} \rangle}{BH \langle \overline{s} \rangle_x}, \\ &= -\frac{\langle (H + \zeta) (\overline{u_{\text{river}} - \langle \overline{u_{\text{river}} \rangle}) s} \rangle}{H \langle \overline{s} \rangle_x}. \end{aligned}$$

This represents the salt transport by the depth-varying or time-varying component of the river discharge. Time-variations of the river discharge can occur even when the prescribed discharge at the boundary is constant. These result from interactions with the temporal variations of the eddy viscosity.

From the scaling analysis for the 2DV salinity model it is expected that the tidal contribution to  $K$  will be much larger than the contribution of the other mechanisms. It is therefore expected that the results will not change much if the above decomposition were to contain a decomposition of the salinity.

### 3.4.3. Fischer (1972) decomposition

The above decomposition makes specific use of the linearity of the 2DV model that is used in this thesis. The decomposition that is explained below is more general and could also be applied to analyse the output of a complex non-linear flow model. The approach that will be used here is the approach by Fischer (1972). First, we make the following decomposition of the velocity and salinity

$$u = u_a + u_b + u_c + u_d, \tag{3.11}$$

$u_a = \langle \overline{u} \rangle$	cross-sectionally-averaged time-averaged velocity
$u_b = \overline{u} - u_a$	cross-sectionally-averaged time-varying velocity
$u_c = \langle u \rangle - u_a$	cross-sectional variation of the time-averaged velocity
$u_d = u - u_a - u_b - u_c$	cross-sectional variation of the time-varying velocity
$= u - \langle u \rangle - \overline{u} + \langle \overline{u} \rangle$	

A similar decomposition is made for the salinity. Fischer (1972) continues by dividing the terms  $u_c$ ,  $s_c$ ,  $u_d$  and  $s_d$  in a vertically varying part and a laterally varying part. The 2DV approach in this thesis assumes that these terms vary only in the vertical direction.

This decomposition can now be used to find a decomposition of the resolved salt transport  $B \langle (H + \zeta) \overline{u s} \rangle$ . The full decomposition results in an equation containing 16 terms. In order to simplify this equation, some of these terms are put together in one term with comparable physical meaning. The resulting equation is

$$B \langle (H + \zeta) \overline{u s} \rangle = Q s_a + BH \langle u_b s_b \rangle^* + BH \overline{u_c s_c}^* + BH \langle \overline{u_d s_d} \rangle^*. \tag{3.12}$$

The asterisks \* denote that the term is not exactly equal to the term that one would expect from the decomposition, but that it is corrected for the Stokes drift. Appendix D.4 provides the details of these terms.

The dispersion coefficient can then be decomposed as follows

$$\begin{aligned} K_{Qs_a} &= 0, \\ K_{BH\langle u_b s_b \rangle^*} &= -\frac{\langle u_b s_b \rangle^*}{\langle \bar{s} \rangle_x}, \\ K_{BH\overline{u_c s_c}} &= -\frac{\overline{u_c s_c}}{\langle \bar{s} \rangle_x}, \\ K_{BH\langle \overline{u_d s_d} \rangle^*} &= -\frac{\langle \overline{u_d s_d} \rangle^*}{\langle \bar{s} \rangle_x}. \end{aligned}$$

These terms may seem abstract, but they have a physical interpretation. The terms are also used in several studies that discuss measurements of salinity in estuaries, e.g. that by [Lerczak et al. \(2006\)](#) in the Hudson River, by [Jay and Smith \(1990a\)](#) in the Columbia River and by [Winterwerp \(1983\)](#) in the Rotterdam Waterway.

The component  $\langle u_b s_b \rangle^*$  could be called *tidal oscillatory mean dispersion*. It is the transport due to the interaction of the cross-sectionally-averaged tidal velocity and salinity, which can potentially yield a large contribution. In literature this term is generally either neglected ([Fischer, 1972](#)) or used together with the terms containing  $u_d$  ([Lerczak et al., 2006](#)). However, this is unjustly done so. [Fischer \(1972\)](#) reasons that the term is negligible in well-mixed to partially stratified estuaries, because  $s_b$  is much smaller than  $s_a$ . However,  $u_b$  (the typical tidal velocity) is generally much larger than  $u_a$  (the typical residual velocity) so that this argument does not hold. It will be shown in Section 5.2 that  $\langle u_b s_b \rangle$  is not negligible. It is useful to consider this term separately from the terms containing  $u_d$ , because it is generally known from measurements what the typical magnitudes of the average tidal velocity and tidal variation of salinity are. The magnitude of  $\langle u_b s_b \rangle$  can thus be estimated from only a few measurements. On the other hand, the variations of velocity and salinity over the cross-section are often unknown.

It is particularly interesting to look at the phase of  $u_b$  compared to the phase of  $s_b$ . It will be shown in Sections 5.1 and 5.2 that this phase difference is important for the salt transport.

The term  $\overline{u_c s_c}$  is the *steady shear dispersion* ([Taylor, 1953](#)), also known as transport due to estuarine circulation. This contains most notably the transport by gravitational circulation and straining circulation.

Finally the term  $\langle \overline{u_d s_d} \rangle^*$  is the *tidal oscillatory shear dispersion*. It denotes the net transport of salt due to shearing of the velocity and salinity profiles. The term reflects many subtle properties of the flow, such as the degree and the timing of vertical stratification and the shape of the vertical velocity profile.

The above described transport mechanisms are not the only nor the most important mechanisms that act in a real estuary. Lateral and bathymetric variations have shown to be very important for the total longitudinal mass transport of salt ([Fischer, 1972](#); [Burchard and Schuttelaars, 2012](#)). These variations are, however, not included in the model.

#### 3.4.4. Relation of the salt balance to the 2DV model

The 2DV salinity model is an approximation to the complete salt transport equation. The differences between the 2DV model and the salt balance are derived below. The second-order salinity equation 3.7 can be integrated in  $x$ -direction to obtain

$$Qs^0 + B \int_{-H}^0 \langle u^0 s^1 \rangle dz - BHK_H s_x^0 = C.$$

This equation describes that the salt flux through a cross-section is constant. It is assumed that the salt flux through the landward boundary is zero or negligibly small so that  $C = 0$ .

The differences between this 2DV model and the salt balance can be expressed in terms of a contribution to the closure term  $K_{\text{closure}}$ . To this end the 2DV equation is set equal to the salt balance, Equation 3.9. The

models can be related by noting that  $\hat{s}^0 = \langle \bar{s} \rangle$ . This yields

$$K_{\text{closure}} = K_H + \left( \left\langle \frac{1}{H} \int_{-H}^{\zeta} us^1 dz \right\rangle - \frac{1}{H} \int_{-H}^0 \langle u^0 s^1 \rangle dz \right) \frac{1}{s_x^0}. \quad (3.13)$$

This means that  $K_{\text{closure}}$  is equal to  $K_H$  plus the error that is made by the salinity model, so that  $K_{\text{closure}}$  can be used to verify the validity of the scaling argument.

One part of the error that is contained in Equation 3.13 should not be taken into account. This error is caused by the salt balance which calculates the Stokes drift from the interactions of  $u^1$  and  $\zeta^0$ ,  $u^0$  and  $\zeta^1$  and  $u^1$  and  $\zeta^1$ . The compensating return flows of these Stokes drift transports appear only in the second-order and third-order velocity and are not resolved. For reasons of consistency, the above Stokes terms should not be taken into account in the salt balance for analysing the 2DPM model, see also Appendix D.4.

# 4

## Results: hydrodynamics

This chapter will present the results regarding the first research question: *how does the flow velocity, and straining circulation in particular, depend on the interactions between tidal variations of turbulence and the flow velocity itself?* The results are obtained by using the hydrodynamic model described in Chapter 2. The salinity model will not be used in this chapter; the salinity is prescribed.

Not only exchange flow will be treated, but also oscillatory velocity components will be discussed. The interactions between oscillatory tidal components and turbulent mixing are important for understanding exchange flows. The complexity of turbulence modelling is varied by using the different versions of the hydrodynamic model. The different model versions are applied to one case and are calibrated on the water level. The case parameters and calibration procedure are discussed below.

One set of parameters for the shape and forcing of the estuary is used to illustrate the interactions between turbulent mixing and the flow velocity. The parameters are representative for the Western Scheldt estuary, which is situated in the South-West of the Netherlands and the North-West of Belgium. The Western Scheldt is characterised by an alternating pattern of channels and shoals, which are not included in the presently used model. The model is therefore not used to predict water levels and velocities in the Western Scheldt estuary, but only to show the importance of specific physical mechanisms in an estuary of these typical dimensions. The values of the parameters are given in Table 4.1.

Parameter	Symbol	Value
Length	$L$	100 km
Width at mouth	$B_0$	2500 m
Depth (constant along the estuary)	$H_0$	25 m
Convergence length	$L_b$	30 km
$M_2$ tidal amplitude at mouth	$A_{M_2}$	2.0 m
$M_4$ tidal amplitude at mouth	$A_{M_4}$	0.2 m
Phase difference between $M_2$ and $M_4$ tides at mouth	$\phi_{M_4}$	180 degrees
River discharge	$Q$	100 m <sup>3</sup> /s

Table 4.1: Parameter values for estuary dimensions and forcing.

The five model versions contain different parametrisations of the roughness coefficient and eddy viscosity that cannot unambiguously be related to one another. This means that each model version should be calibrated for that the results to be comparable. Version 5, with the  $k - \varepsilon$  turbulence model, is the starting point for this calibration procedure. It uses a roughness height  $z_s = 0.004$  m, which corresponds to a Chézy value of 60 m<sup>1/2</sup>/s. In versions 2 and 4, the parabolic eddy viscosity profiles are calibrated. These versions use the same roughness height, but need a calibration of the eddy viscosity magnitude. This magnitude varies in the

$x$ -direction in Version 5, but is assumed to be a constant in the other versions. The eddy viscosity magnitude in Version 2 and 4 is determined such that the depth-averaged eddy viscosity is the same in Version 5 at one location along the estuary. This location is determined by requiring that the  $M_2$  leading-order water level at the end of the basin has a similar amplitude and phase in the different model versions. This requirement is in accordance with common practice, in which the water level is used as a calibration criterion, because this is the best measured quantity. Versions 1 and 3 use the same depth-averaged eddy viscosity as in Version 2 and 4. The roughness coefficient in these two versions is calibrated using the water level at the end of the basin.

The results of this case with the Version 1 model will be discussed in Section 4.1, presenting an overview of the results with the simplest turbulence formulation. Section 4.2 discusses the most important changes to the velocity assuming a parabolic eddy viscosity profile. Next, the eddy viscosity is allowed to vary in time. This introduces multiple significant changes to the flow velocity which will be discussed in Sections 4.3 to 4.5. In these sections, the results of the  $k - \varepsilon$  model will be used to present the model result, while Versions 3 and 4 will be used for detailed analyses of the results. Finally, Section 4.6 discusses the importance of longitudinal variations of the eddy viscosity on the model results.

## 4.1. Reference case

We start the discussion of the results by presenting the results of the reference case by using the model of Version 1. This model uses a constant eddy viscosity and roughness coefficient

$$\begin{aligned}\nu_t &= 0.078 \text{ m}^2/\text{s}, \\ s_f &= 0.004 \text{ m/s}\end{aligned}$$

The value of the eddy viscosity is equal to the depth-averaged eddy viscosity at  $x = 26$  km in the  $k - \varepsilon$  model result, see also Section 4.3.

The leading-order solution is only forced by an  $M_2$  tide and will therefore only contain an  $M_2$  signal. The first-order is forced by an  $M_4$  tide and a constant river discharge. It will therefore respond with an  $M_4$  and residual signal. Additionally, the first-order is forced by a constant horizontal salinity gradient. The salinity is assumed to be uniform in the vertical direction. The salinity is prescribed according to a simple exponential profile, which is typical for well-mixed estuaries with a limited degree of tidal salt transport (Savenije, 2005);

$$s(x) = s_{\text{sea}} e^{-x/L_s},$$

where  $s_{\text{sea}} = 30$  psu is the salinity at the mouth and  $L_s = 30$  km is a length-scale of salt intrusion.

Figure 9 shows the absolute value and phase of the surface level elevation  $\zeta$  plotted against the longitudinal distance, with  $x = 0$  being the mouth of the estuary. The  $M_2$  water level amplitude increases with  $x$ . This amplification is caused by the funnelling effect of the estuary due the decreasing width, and the reflection of the tidal wave at the end of the basin. The amplification is opposed by bed friction, but this is not sufficient here to counteract the amplifying effects. Such an amplification of the tidal wave is seen in many estuaries among which the Western Scheldt. The phase of the leading-order water level decreases in upstream direction. This means that the water level signal upstream lags the water level signal at the seaward side, because the tidal wave takes time to travel up the estuary. This means that the phase  $\phi$  in a Fourier component is defined as  $e^{i\omega t + i\phi}$ .

The subtidal (denoted by  $M_0$  in the figure) and  $M_4$  contributions to the velocity originate from the first-order equations and are clearly smaller than the leading-order  $M_2$  water level elevation. Both first-order frequencies are partly forced externally at the boundaries and partly generated internally. The boundary forced part originates from the  $M_4$  tidal forcing at the seaward side and the river discharge at the landward boundary. Internal contributions are caused by advection, baroclinic pressure and interactions of the  $M_2$  flow velocity with the  $M_2$  water level elevation (the no-stress boundary condition and return flow). The separate contributions to the water level amplitude by each of these physical components are presented in Figure 10. Each panel in the figure displays the contribution to the water level by one forcing contribution in Equation 2.26 and Table 2.2. The results show that the internal forcing by the baroclinic pressure  $\zeta_{s_x}$  is the main contributor to the subtidal

water level elevation, while the external tidal forcing  $\zeta_{\text{tide}}$  is the most important contributor to the  $M_2$  and  $M_4$  water level elevation.

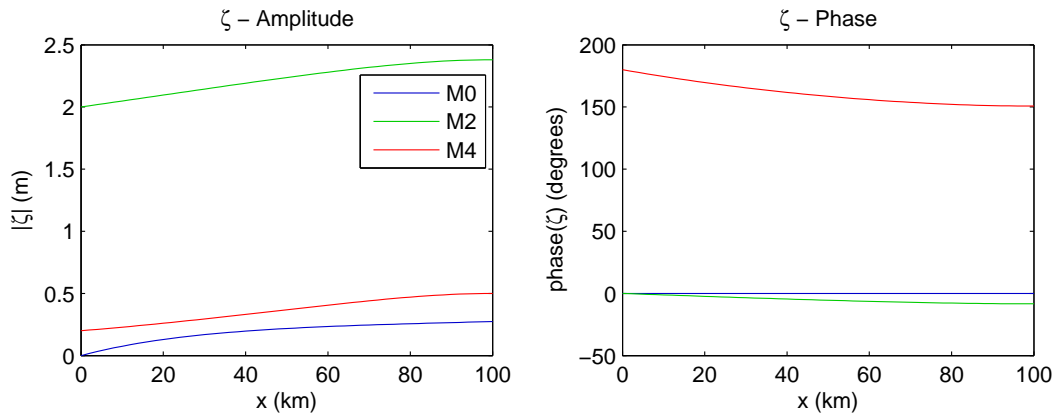


Figure 9: The water level amplitude and phase using model Version 1, separated in frequency components. The results of the leading order and first order are added.

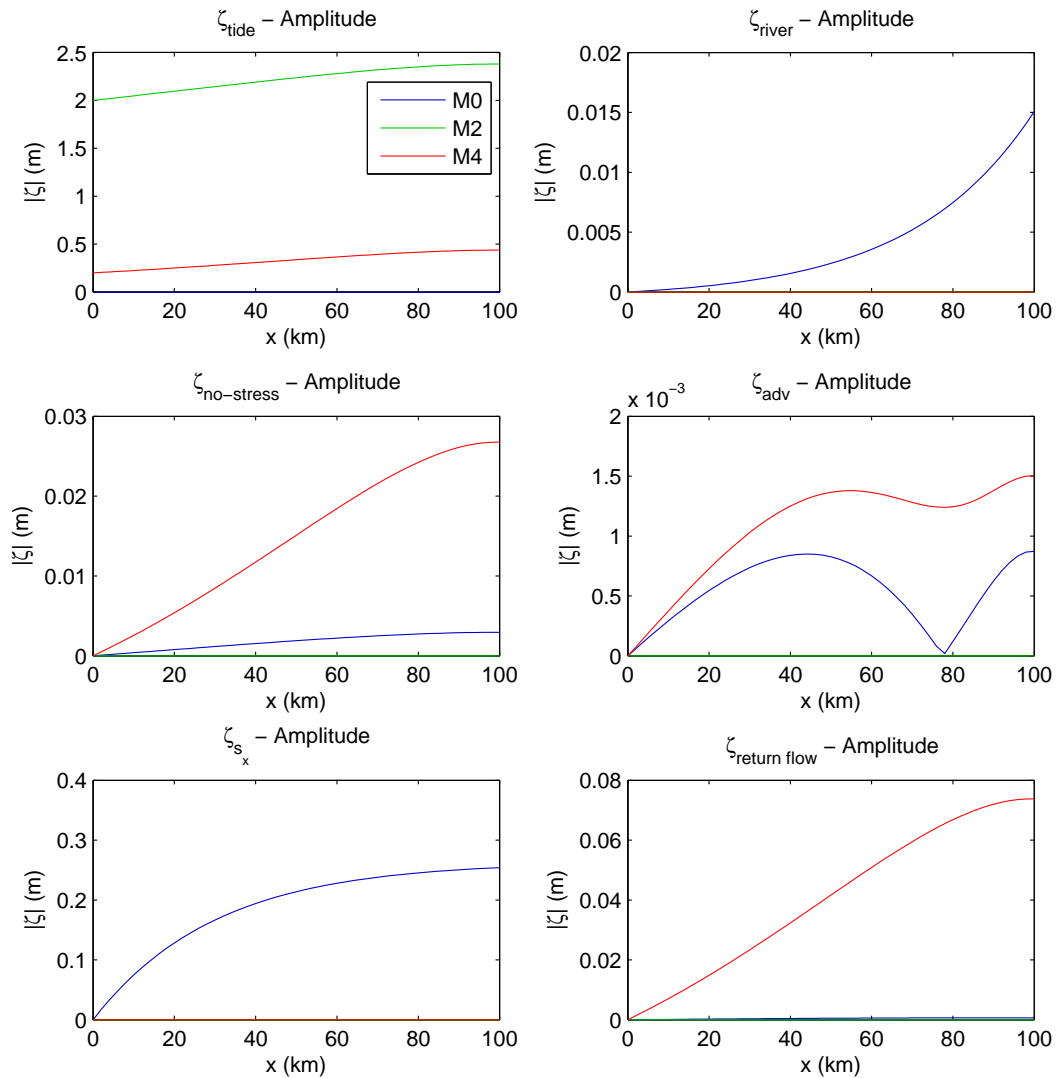


Figure 10: The water level amplitude separated in six forcing mechanisms using Version 1. The subscripts are explained in Table 2.2.

It can be argued that the assumed scaling of the model fails, because the  $M_4$  component at the landward boundary is smaller, but not much smaller than the  $M_2$  component. However, it is shown in Appendix D.2 that the results change little if the  $M_4$  component is moved to the leading order.

The horizontal velocity of the flow is presented in Figure 11. This figure shows the magnitude of the velocity in the  $(x, z)$ -plane at four instances during the tidal cycle. Tidal slack, i.e. the point in time where the depth-average velocity reverses, occurs around  $t = 0$  and  $t = 0.5T$  near the mouth of the estuary. The flow at these instances is dominated by the gravitational circulation, which shows as the circulating flow in the figure. The maximum outflow velocity occurs at  $t = 0.34T$  and is called peak ebb. Conversely, the maximum inflow velocity, or peak flood, occurs around  $t = 0.7T$ . So peak ebb and peak flood are not symmetrically distributed over the tidal cycle.

We can analyse the importance and vertical structure of each of the six forcing mechanisms by making a decomposition of the velocity, see Figure 12. The figure shows the velocity profile at peak ebb tide at 10 km from the mouth of the estuary. The most important forcing mechanisms are the tide and the baroclinic pressure. The tide provides the most important  $M_2$  and  $M_4$  signals, while the gravitational circulation (i.e. the baroclinically induced residual flow) provides the most important residual flow. These results are consistent with the results of the surface level elevation. The shapes of the profiles of the tide and gravitational circulation are distinctly different. The tidal flow profile has a uniform direction with the smallest velocity near the bed and the highest velocity near the surface. The river flow and return flow share the same type of profiles. The direction of the gravitational circulation is strongly curving and is bidirectional: landward near the bed and seaward near the surface. This is conform the theory that was introduced in Section 1.1. The profiles of the velocity which are due to advection and the no-stress surface condition also show curving bidirectional profiles. These will not be discussed in detail, because the magnitude of these terms is small.

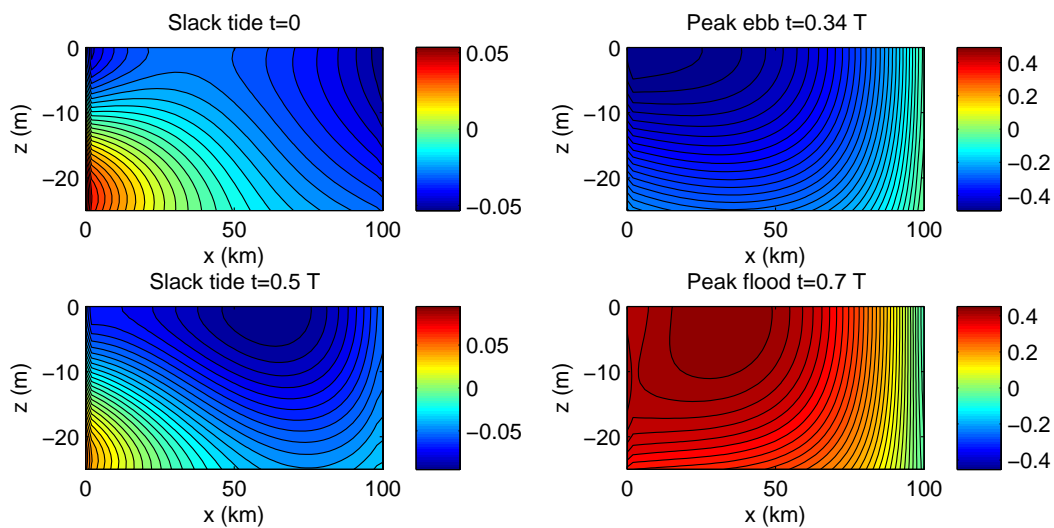


Figure 11: Total horizontal velocity (leading-order and first-order) in the estuary at four instances during the tidal cycle.

## 4.2. The effect of a parabolic eddy viscosity

In this section we will consider the influence of a parabolic eddy viscosity profile on the water motion. The parabolic vertical eddy viscosity is a good approximation of the result of the  $k - \varepsilon$  turbulence model as will be shown in Section 4.3. In order to calibrate the model, the friction parameters  $z_s$  and  $z_b$  (see Equation 2.5) are fixed at the same value as in Version 5 and the magnitude of the eddy viscosity is calibrated so that the water levels show the best correspondence with the results of Version 5. The differences between the results of the reference case and the results in this section amount to one centimetre in amplitude and 0.1 degree in phase for the  $M_2$  water level. The  $M_4$  and residual water level show differences of the same order of magnitude. The

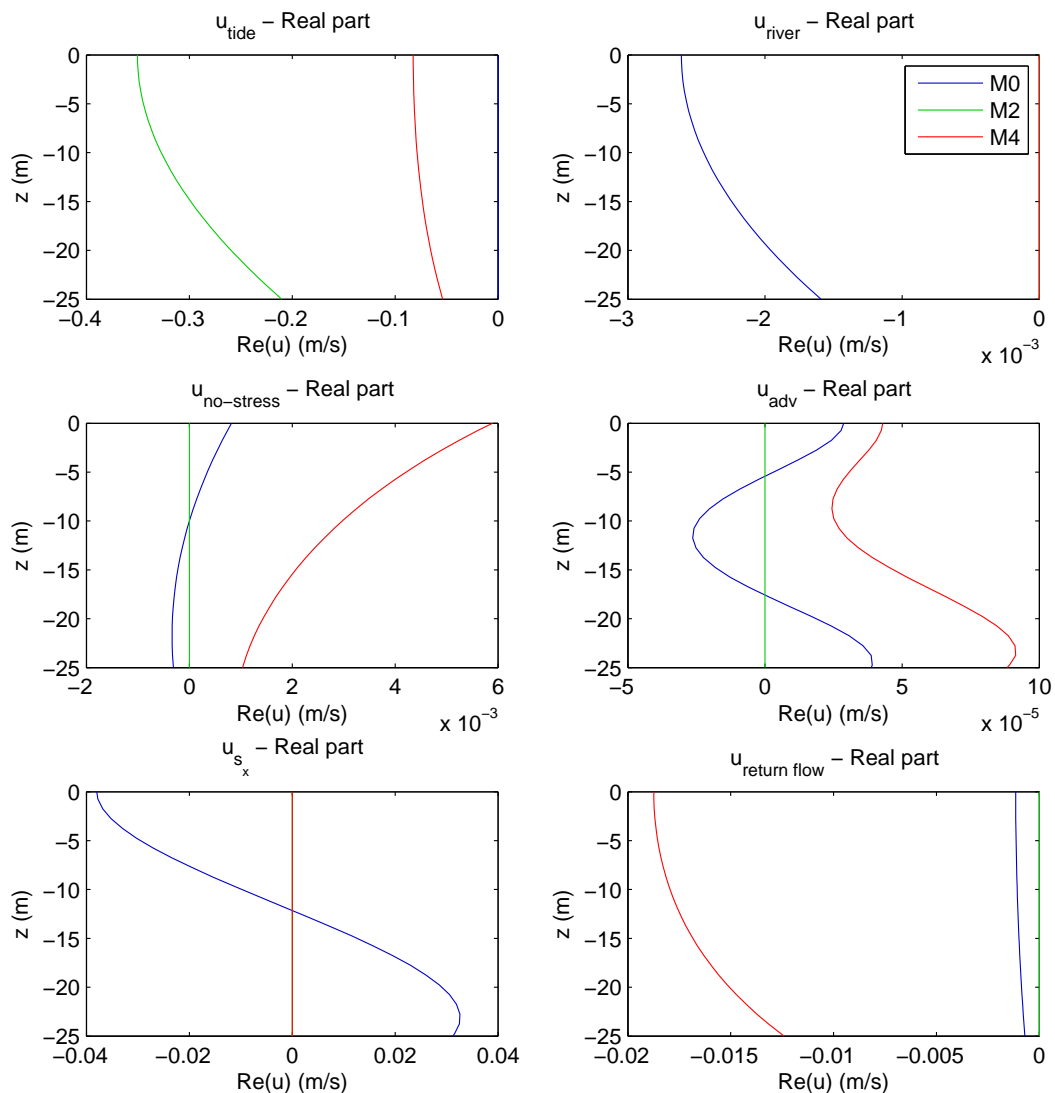


Figure 12: Horizontal velocity at  $x = 10$  km and at peak ebb  $t = 0.34T$  separated in six forcing mechanisms using Version 1. Subscripts are explained in Table 2.2.

calibration yields the following values:

$$\nu_{t,0} = 0.00075 \text{ m}^2/\text{s},$$

$$z_s = z_b = 0.004 \text{ m}.$$

The effect of the parabolic eddy viscosity on the tidal velocity profile is the formation of a strong boundary layer at the bed with a more uniform velocity in the rest of the water column. The velocity profile resembles the logarithmic velocity profile that is often associated with tidal flow. This shape is clearest in the profiles of the tidal velocity, river velocity and return flow in Figure 13. The figure again shows the decomposition of the velocity signal, but now with both the results of a constant and parabolic eddy viscosity. The formation of clear bed boundary layers are also visible in the profiles of the gravitational circulation and advection. The magnitude of almost all contributions is similar with a constant and parabolic eddy viscosity profile. The contribution from the no-stress boundary condition forms an exception. The changes to the tidal velocity profile near the surface lead to a different magnitude of this term. However, it is still small compared to the most important flow contributions.

The shape of the velocity profile is important to, for example, predicting the bed-load sediment transport. The

impact of the change from Version 1 to Version 2 on the bed-load sediment transport can be estimated by looking at the difference of the bed shear stress in both versions. The bed shear stress was defined in Section 1.3 as  $\tau = \rho \nu_t u_z$ . The maximum value of this bed shear stress is  $6 \cdot 10^{-2} \text{ N/m}^2$  in Version 2, while the maximum is  $1.2 \text{ N/m}^2$  in Version 1; a factor 20 difference between the two. One can use a constant eddy viscosity to analyse the qualitative behaviour of the flow velocity, but one should be careful in using it even for qualitative studies into sediment transport.

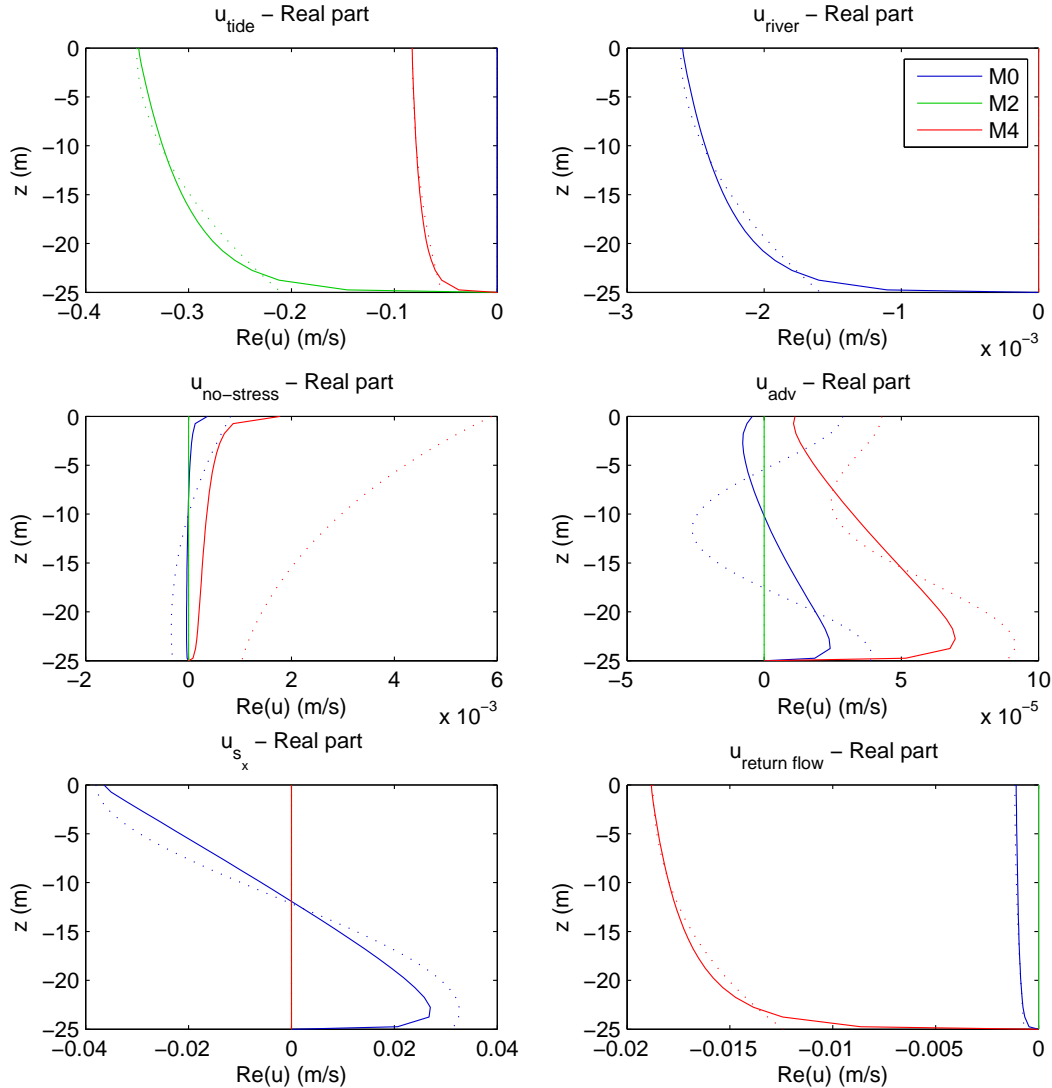


Figure 13: Components of the first order velocity at  $x = 10 \text{ km}$  and at peak ebb ( $t = 0.34T$ ) using model Version 2 (solid line) compared to Version 1 (dotted line).

### 4.3. The eddy viscosity as calculated by the $k - \varepsilon$ model

The  $k - \varepsilon$  model in Version 5 is used to calculate a realistic temporally and spatially varying eddy viscosity. This section will discuss the properties of the calculated eddy viscosity signal. The effects of the temporal and spatial variations of the eddy viscosity will then be discussed in the next sections. The Version 5 model is calibrated with the roughness height  $z_s = 0.004 \text{ m}$ , which corresponds to a Chézy value of  $60 \text{ m}^{1/2}/\text{s}$ .

The eddy viscosity amplitude is separated in four frequencies and is presented in Figure 14. The figure shows that the profiles of the eddy viscosity are similar to the parabolic profile in all frequencies and at all locations along the estuary. We will discuss the along-channel distribution and the time-dependence in more detail below.

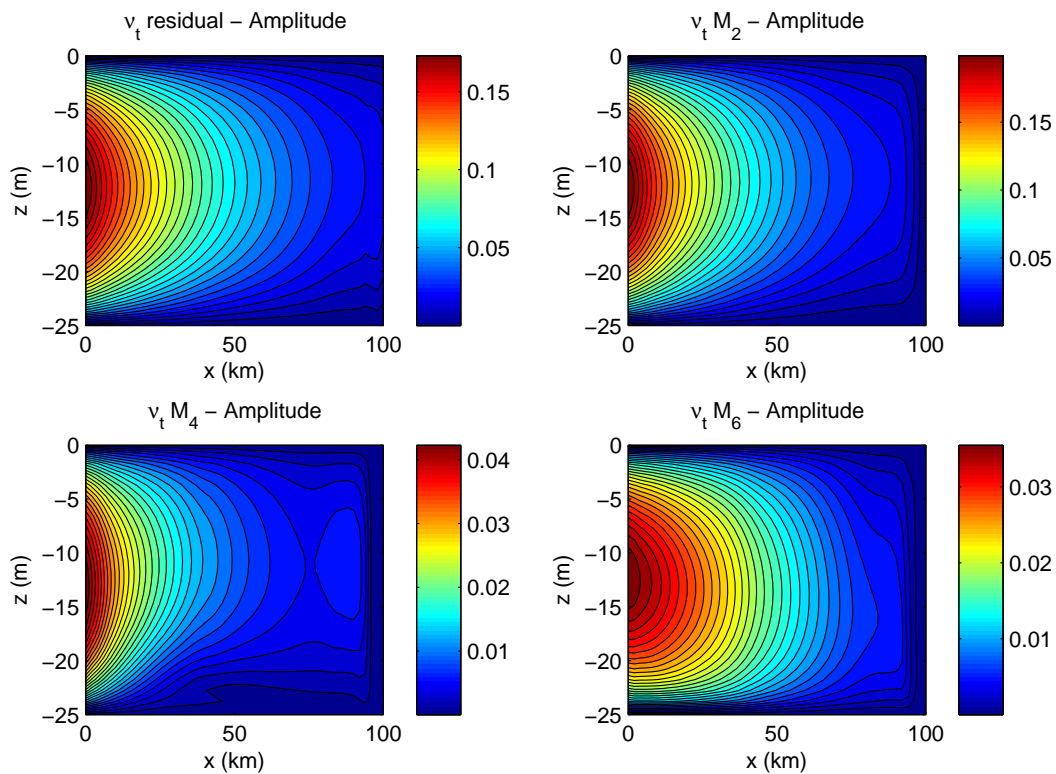


Figure 14: Eddy viscosity amplitude for the several frequency components using Version 5.

We will first discuss the along-channel distribution of the subtidal eddy viscosity. Many simple relations assume that the eddy viscosity can be estimated from the magnitude of the depth-averaged velocity. Such a relation is used for example in the idealised model studies of [Ianniello \(1977\)](#) and [Cheng et al. \(2010\)](#). The eddy viscosity does, however, not depend on the velocity, but on the velocity gradient. This gradient is contained in the production term of turbulent kinetic energy in the  $k - \varepsilon$  turbulence model. The distribution of the velocity and velocity gradient along the estuary are not the same. Figure 15 displays the along channel distributions of the depth-averaged time-averaged absolute velocity, velocity gradient and eddy viscosity, i.e.

$$\int_{-H}^0 \langle |u| \rangle dz, \int_{-H}^0 \langle |u_z| \rangle dz, \text{ and } \int_{-H}^0 \langle |\nu_t| \rangle dz.$$

The trend of the velocity is different to the trend of the velocity gradient and eddy viscosity. The velocity shear is therefore a better estimator of the eddy viscosity in a homogeneous water column.

The gravitational circulation is the most important source of the disparity between the velocity and its gradient. The gravitational circulation has a depth-averaged velocity of zero, but produces a significant amount of velocity shear. This is shown in Figure 16. The gravitational circulation produces a similar amount of velocity shear as the tide at the seaward boundary, even though the magnitude of the gravitational circulation is much smaller than the magnitude of the tidal velocity.

Figure 14 also shows that the  $M_2$  component of the eddy viscosity is of a similar magnitude as the subtidal component. This results in a strong asymmetry in the amount of turbulence during ebb and flood. Figure 18 shows this clearly with a time-series of the depth-average eddy viscosity. Such an asymmetry with a large eddy viscosity during flood and a small eddy viscosity during ebb would be the expected result of SIPS (see Section 1.3), which relates to an asymmetry in density stratification. The present case does however assume a homogeneous density in the water column. Other sources are therefore responsible for the turbulence asymmetry. One source is the asymmetry in the amount of velocity shear. The combination of gravitational circulation and tidal flow result in a profile that is more sheared during flood than during ebb ([Burchard and Hetland, 2010](#)), see Figure 17. The river flow and return flow counteract this by increasing the shear during ebb and decreasing

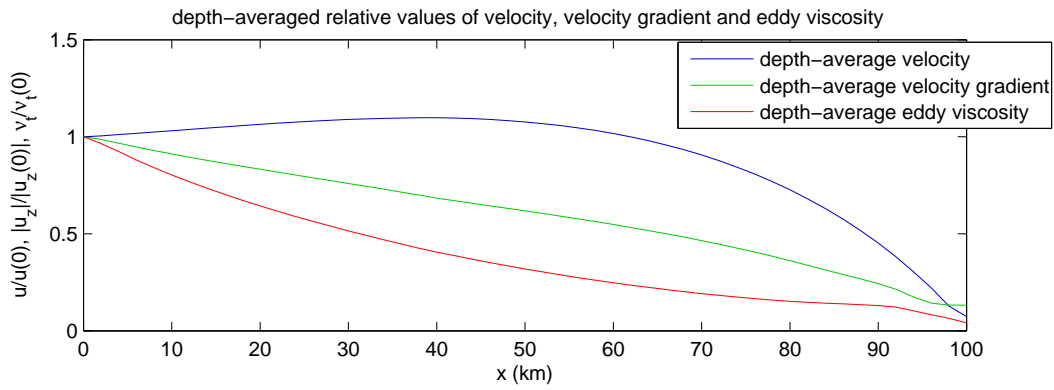


Figure 15: The along-channel distributions of the depth-average time-average absolute velocity, velocity shear and eddy viscosity. The values are scaled with the value at the seaward boundary.

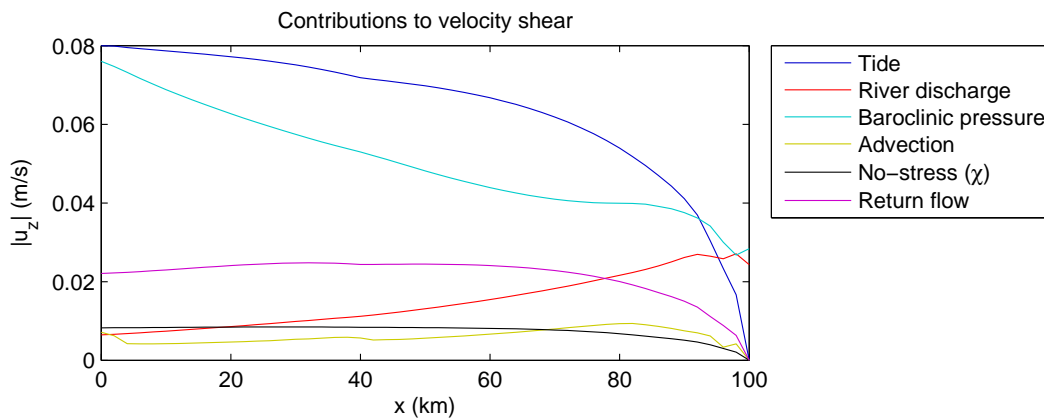


Figure 16: The contribution of the six forcing mechanisms to the depth-average time-average absolute velocity shear.

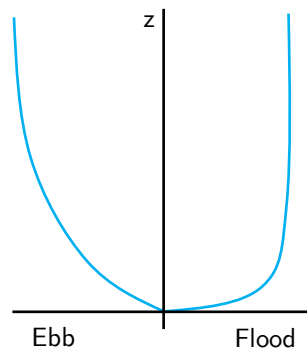


Figure 17: Schematic representation of the velocity profile that results from the combination of gravitational circulation and tidal flow.

it during flood, but this effect is small in this case. The turbulence asymmetry is further amplified by the tidal asymmetry. The present case is flood dominant. The flood velocity is therefore larger than the ebb velocity. This leads to more velocity shear during flood than during ebb. Finally, it is generally possible that the water level is higher during either ebb or flood. The eddy viscosity grows larger in deeper water than in shallower water, adding to the turbulence asymmetry. This does not play a role in the present simulation, because the water level and velocity are approximately 90 degrees out of phase; the average water level is the same during ebb and flood.

These sources of turbulence asymmetry lead to a velocity shear squared, i.e the production of turbulence, which is 1.5 times larger during flood than during ebb. Additionally, they lead to a bed friction which is 8 times larger

during flood than during ebb.

The  $M_4$  and  $M_6$  components also have a considerable magnitude. The phase of these components is such that the eddy viscosity is almost constant during ebb and has a strong peak during flood. The small peak of the eddy viscosity around  $t = 0.25T$  in Figure 18 is a model artefact which is caused by the limited number of Fourier components. However, the overall pattern of the eddy viscosity is well captured by these Fourier components.

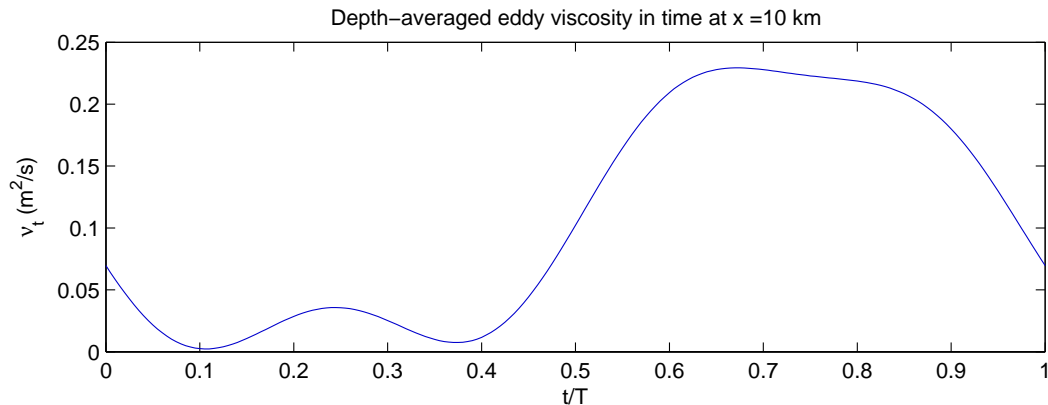


Figure 18: Depth-averaged eddy viscosity versus time at  $x = 10$  km.

#### 4.4. The interaction of the velocity and eddy viscosity

The interaction of temporally varying components of the eddy viscosity and velocity result in the creation of new velocity frequencies and changes to the amplitudes and phases of the velocity already present. In this section it will be analysed how large the effect of such interactions is on the velocity signal and how this depends on the magnitude of the temporally varying eddy viscosity.

The way in which new frequencies are created is best illustrated by considering the momentum equation. Let us assume that the eddy viscosity consists of a subtidal and an  $M_2$  component. We will consider the leading-order momentum equation of the  $M_2$  component:

$$i\omega\hat{u}_1^0 - (\hat{\nu}_{t0}\hat{u}_{1,z}^0)_z = -g\hat{\zeta}_{1,x}^0 + \frac{1}{2}(\hat{\nu}_{t1}\hat{u}_{2,z}^0)_z + \frac{1}{2}(\overline{\hat{\nu}_{t1}}\hat{u}_{0,z}^0)_z.$$

The terms on the left-hand side involve the  $M_2$  tide. They form the system response to the forcing terms on the right-hand side by the water level gradient and the other frequency components. The subtidal eddy viscosity appears in a system response term, while the time-varying eddy viscosity appears in the forcing terms. So the time-varying eddy viscosity controls the interaction between the different frequency components. The interaction of the  $M_2$  eddy viscosity and the subtidal and  $M_4$  tide act as a forcing on the  $M_2$  velocity. The residual and  $M_4$  velocity components are themselves influenced by other velocity components so that all velocity frequency components are coupled. It will be shown below that it is often sufficient to take only a few interacting components into account. This justifies the assumption of including only a limited number of frequency components in the calculation.

In Section 4.4.1 a theoretical framework will be developed that explains dependence of the velocity on the magnitude of the temporally varying eddy viscosity. This is then applied to analyse the results of Version 5 in Section 4.4.2.

##### 4.4.1. Theoretical framework for the strength of the interactions

Let us assume that the eddy viscosity consists of a subtidal and an equally large  $M_2$  component. The eddy viscosity is in phase with the  $M_2$  velocity. The Version 4 model has been used to obtain the model results in this section.

We will first consider the effects of the interaction between the eddy viscosity and the velocity on the leading-order velocity. This interaction creates new residual,  $M_4$  and higher frequency components. It is observed from the model output, see Figure 19, that the newly created residual and  $M_4$  velocity components are mainly due to the interaction of the  $M_2$  velocity and the  $M_2$  eddy viscosity. It is also found that  $M_2$  velocity is almost unaffected by the interaction of these new velocity components and the  $M_2$  eddy viscosity. So the frequency components form a weakly interacting system; the  $M_2$  velocity affects the residual and  $M_4$ , but their feedback to the  $M_2$  velocity is negligible.

We can explain this observation by looking at the magnitude of the terms in the momentum equation. Consider the momentum equation of the leading-order  $M_4$  velocity component:

$$2i\omega\hat{u}_2^0 - (\hat{v}_{t0}\hat{u}_{2,z}^0)_z = -g\hat{\zeta}_{2,x}^0 + \frac{1}{2}(\hat{v}_{t1}\hat{u}_{1,z}^0)_z, \quad (4.1)$$

where  $(\hat{v}_{t1}\hat{u}_{1,z}^0)_z$  is treated as a known forcing term that does not depend on the  $M_4$  velocity. We have seen above that this is a reasonable approximation, because the  $M_2$  velocity is only weakly affected by the  $M_4$  velocity.

The magnitude of the forcing term  $(\hat{v}_{t1}\hat{u}_{1,z}^0)_z$  can be estimated from a scaling argument. The expected magnitude, using the scales in Appendix A.1, is

$$\frac{gA_{M_2}}{L_{tide}} \approx 2 \cdot 10^{-4} \text{ m/s}^2.$$

The actual depth-averaged value of the forcing term is only  $3 \cdot 10^{-5} \text{ m/s}^2$ , see Figure 20. This is one order of magnitude smaller than the scaling suggests. So the forcing has the magnitude of an  $\mathcal{O}(\delta)$  term, instead of an  $\mathcal{O}(1)$  term. The reason for this difference is that the scaling argument assumes that the velocity gradient scales with the typical velocity magnitude over the typical water depth. The actual depth-averaged velocity gradient is larger than this scale near the bed, but quickly decreases and is small in the rest of the water column. The depth-averaged value of  $(\hat{v}_{t1}\hat{u}_{1,z}^0)_z$  is therefore much smaller than the scaling suggests.

The first-order velocity components interact differently than the leading-order components. The first-order velocity contained only residual and  $M_4$  components in Versions 1 and 2. These components create an  $M_2$  velocity component of similar magnitude ( $\mathcal{O}(\delta)$ ) through the interaction with the  $M_2$  eddy viscosity in Versions 3 and 4. This  $\mathcal{O}(\delta)$   $M_2$  velocity in turn affects the residual and the  $M_4$  components through the interaction with the  $M_2$  eddy viscosity, inducing an  $\mathcal{O}(\delta)$  change to the residual and  $M_4$  components. So the first-order velocity forms a system with mutual interactions of the same order of magnitude between the different components, see Figure 19. We will call such a system a strongly interacting system.

These results can be explained by using the same ideas that were used above for the leading-order velocity. We will consider the part of the momentum equation of the first-order  $M_2$  velocity component that is associated with the baroclinic pressure:

$$i\omega\hat{u}_1^1 - (\hat{v}_{t0}\hat{u}_{1,z}^1)_z = \frac{g}{\rho_0}\hat{\rho}_{0,x}^0 z + \frac{1}{2}(\hat{v}_{t1}\hat{u}_{0,z}^0)_z + \frac{1}{2}(\overline{\hat{v}_{t1}}\hat{u}_{2,z}^0)_z, \quad (4.2)$$

It is again assumed that the tidal components do not interact, so that the forcing terms  $\frac{1}{2}(\hat{v}_{t1}\hat{u}_{0,z}^0)_z$  and  $\frac{1}{2}(\overline{\hat{v}_{t1}}\hat{u}_{2,z}^0)_z$  are known from the plain gravitational circulation and first-order tide that was also found in Section 4.2. It will be shown why this assumption does not hold.

The forcing terms are plotted in Figure 20. The depth-average values of these forcing terms are

$$\int_{-H}^0 \left| \frac{1}{2}(\hat{v}_{t1}\hat{u}_{0,z}^0)_z \right| dz = 3 \cdot 10^{-5} \text{ m/s}^2,$$

$$\int_{-H}^0 \left| \frac{1}{2}(\overline{\hat{v}_{t1}}\hat{u}_{2,z}^0)_z \right| dz = 1 \cdot 10^{-5} \text{ m/s}^2.$$

The scaling argument states that these terms should be approximately  $2 \cdot 10^{-5} \text{ m/s}^2$ . So these terms are of the same order as the scaling suggests. The result is that they induce an  $M_2$  component which is of

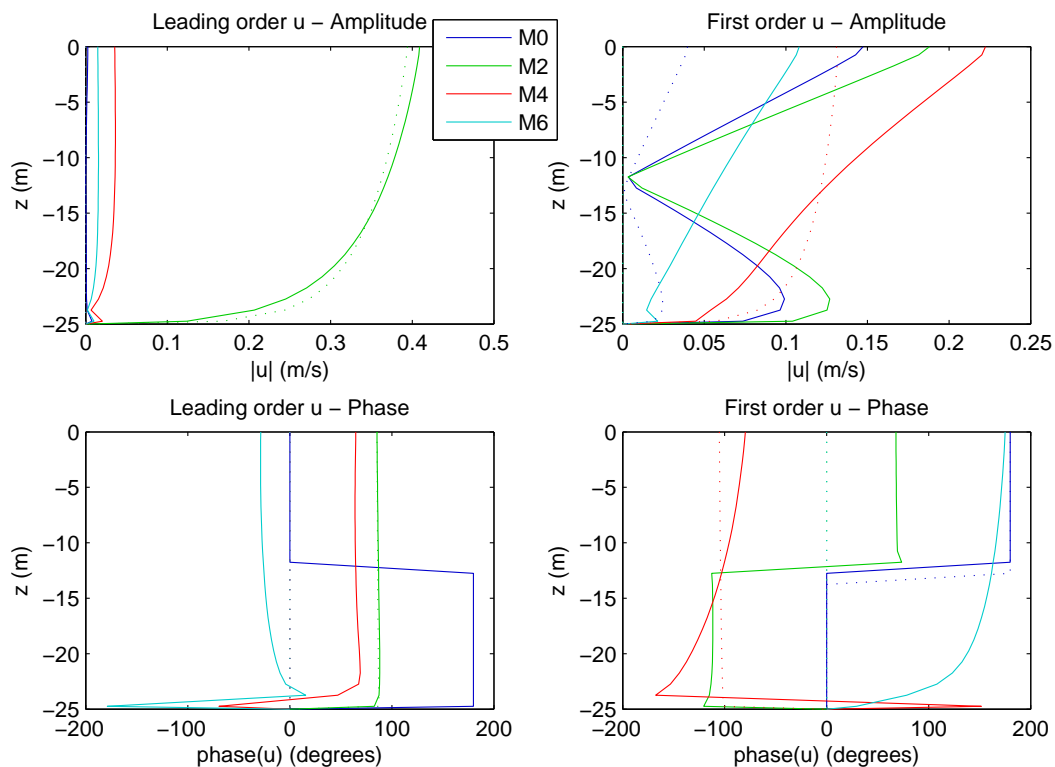


Figure 19: Amplitude and phase of the velocity at  $x = 10$  km with model Version 4. Solid line: results of subtidal and  $M_2$  eddy viscosity. Dotted line: results of subtidal eddy viscosity only (Version 2).

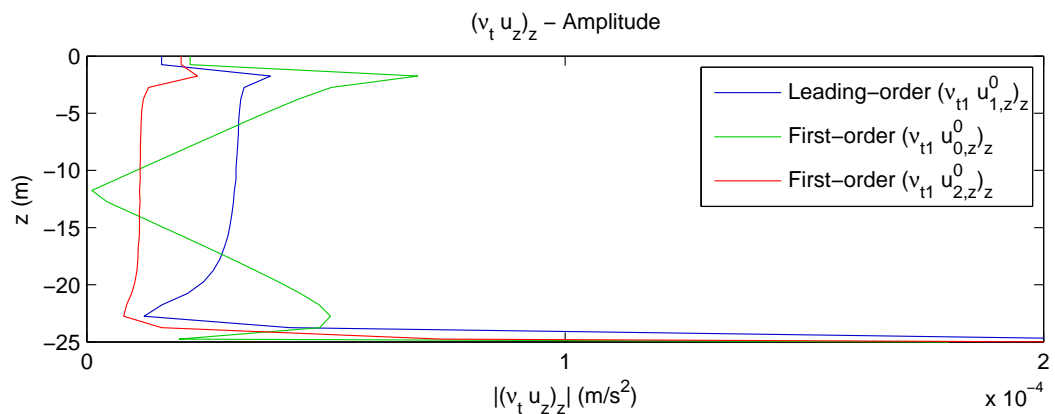


Figure 20: Amplitude of the forcing terms  $(\hat{v}_{t1}\hat{u}_{1,z}^0)_z$ ,  $(\hat{v}_{t1}\hat{u}_{0,z}^1)_z$  and  $(\hat{v}_{t1}\hat{u}_{2,z}^0)_z$  under the assumption that tidal components do not interact.

similar magnitude as the gravitational circulation and first-order tide. Essential in this is that the shape of the gravitational circulation induces an  $M_2$  component with a similar vertical structure as the gravitational circulation itself, see Figure 19. This strongly curving  $M_2$  components has a large velocity gradient. The forcing terms  $\int_{-H}^0 \frac{1}{2} (\hat{v}_{t1}\hat{u}_{1,z}^0)_z dz$  and  $\int_{-H}^0 \frac{1}{2} (\hat{v}_{t1}\hat{u}_{1,z}^0)_z dz$  that appear in the momentum equations of the residual and  $M_4$  components are therefore also of the same order as the scaling suggests. This forcing amplifies the residual and  $M_4$  components. It follows that the velocity components are strongly interacting; the assumption that components do not interact, does not hold.

The curvature of the gravitational circulation is essential for this interaction. The interaction between the residual and  $M_2$  component can be so strong because the interactions amplify the curved profiles, which generate velocity shear. This velocity shear adds to the interaction, so that a positive feedback loop is established. The

interaction between the first-order tidal  $M_4$  velocity component and the  $M_2$  component generates less shear so that the interaction is much weaker. This is also the case for the interaction between the first-order tidal  $M_4$  component and the  $M_6$  component; the interaction is weaker so that the  $M_6$  component is about two times smaller than the  $M_4$  component in first order, see Figure 19.

The above reasoning constitutes a theoretical framework that is summarised conceptually in Figure 21. This framework distinguishes between weakly and strongly interacting systems on the basis of two axes. The two axes can be made more exact with the following definitions

$$\text{temporal variations of turbulence} = \frac{|\hat{\nu}_{tn}|}{\hat{\nu}_{t0}},$$

$$\text{vertical curvature of the velocity profile} = \frac{|(\nu_{tn}\hat{u}_{m,z})_z|}{\mathcal{N}U/H^2},$$

where  $n, m \neq 0$  denote some tidal constituent and  $\mathcal{N}$ ,  $U$  and  $H$  are typical eddy viscosity, velocity and water depth scales. One finds a strongly coupled system if the turbulence is strongly asymmetric and the curvature of the velocity is of a similar or greater magnitude than the typical scale. The strongly interacting system is characterised by a positive feedback loop between tidal components. This leads to an amplification of the components that depends super-linearly on the temporal variations of turbulence. The interactions become weak when either the temporal variations of mixing or the curvature is small. Weakly interacting systems show hardly any feedback between the components, so that the interactions depend linearly on the turbulence asymmetry.

Examples of the linear and super-linear dependencies on turbulence asymmetry are shown in Figure 22. The figure shows the normalised velocity magnitude as a function of the temporal variations of turbulence. The left panel shows the results in the weakly coupled leading-order system. The magnitude of the  $M_2$  and  $M_4$  components depends linearly on  $\nu_{t1}/\nu_{t0}$  and the residual and  $M_6$  components show a weak super-linear trend. The right panel shows the results of the strongly coupled first-order system. The velocity components show a fairly linear trend for small values of  $\nu_{t1}/\nu_{t0}$  and a super-linear trend for larger values of this variable.

It is not required that the temporal variations of turbulence are caused by an  $M_2$  component or that the vertical curvature originates from gravitational circulation. This reasoning works for any source of vertical curvature and any temporally varying eddy viscosity that fits within a hydrostatic model.

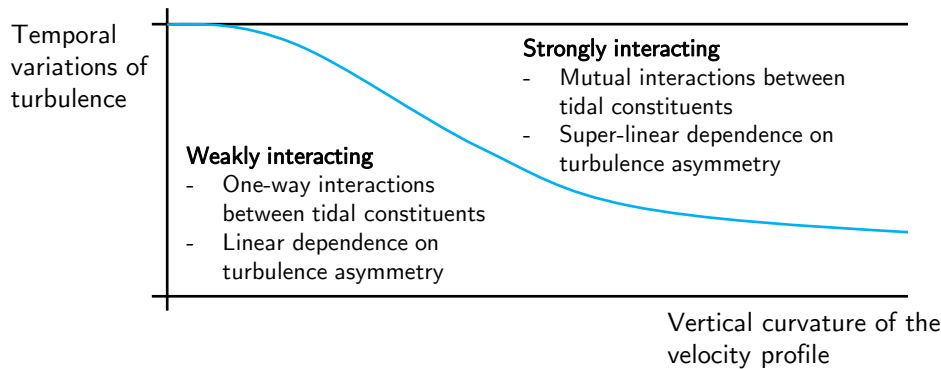


Figure 21: Conceptual representation of the types of velocity-eddy viscosity interactions.

#### 4.4.2. Results with Version 5

The above results carry over to the results of the simulations with the  $k - \varepsilon$  turbulence model. The velocity profiles simulated by this model are displayed in Figure 23. The results form an excellent example of the application of the above framework. It was already shown in Section 4.3 that the  $k - \varepsilon$  model simulated a strongly asymmetric turbulence profile which can be ascribed to a large  $M_2$  eddy viscosity. The curvature of the velocity profiles therefore determines whether the interactions with other frequency components are weak or strong. The leading-order tide is again a weakly coupled system, because the  $M_2$  tide shows little velocity

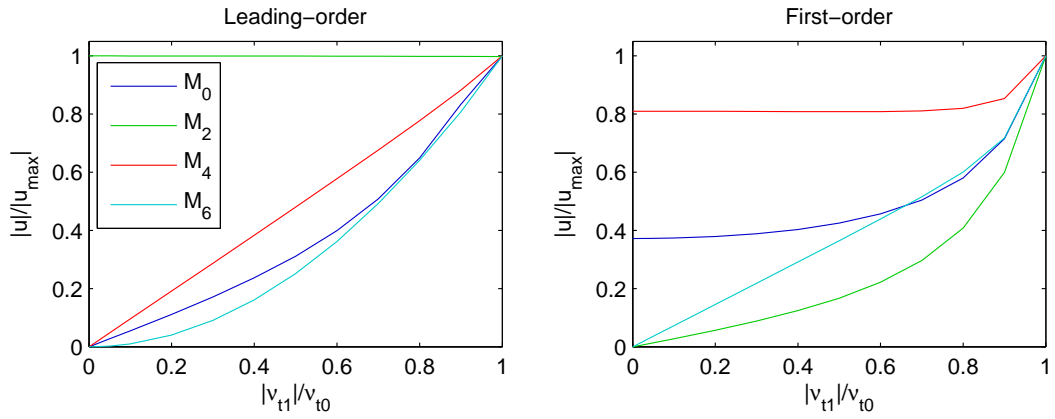


Figure 22: Dependence of velocity magnitude on magnitude of the  $M_2$  eddy viscosity amplitude. The right figure shows the weakly coupled situation for the leading order ( $(\nu_{t0}u_z^0)_z$  small). The left figure shows the strongly coupled situation for the first order ( $(\nu_{t0}u_z^1)_z$  large).

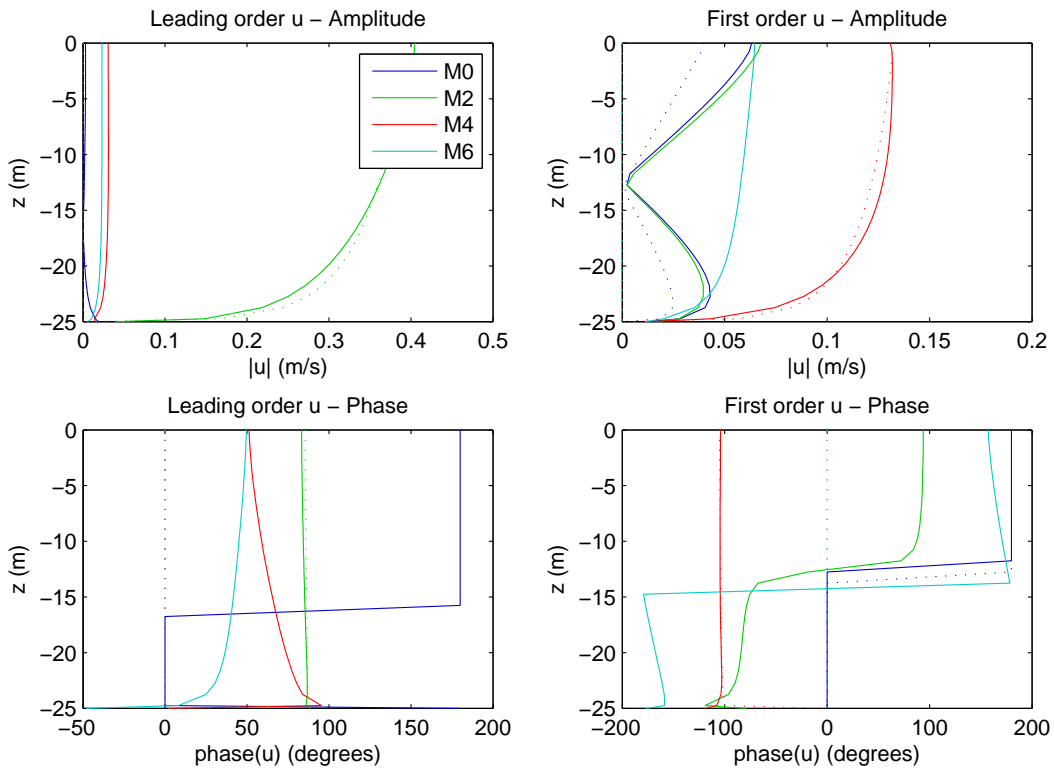


Figure 23: Amplitude and phase of the velocity at  $x = 10$  km with model Version 5. Solid line: results of Version 5. Dotted line: results of subtidal eddy viscosity only (Version 2).

shear. The same also holds for the first-order  $M_4$  tide. The comparison between the dotted line (subtidal eddy viscosity only) and the solid line ( $k - \varepsilon$  model) shows that the temporal variations of the eddy viscosity hardly influence the  $M_4$  velocity. The gravitational circulation on the other hand is strongly amplified due to its strong interactions with the temporally varying eddy viscosity and first-order  $M_2$  velocity.

The results show that both the leading-order tide and the gravitational circulation induce a residual flow or an amplification of this residual flow. This will be discussed in more detail in the next Section.

## 4.5. The decomposition of the straining circulation

The analysis of the previous section has resulted in two types of straining circulation, i.e. two types of flows that result from interactions between the velocity and temporal variations of turbulence. The first originates from the weakly interacting system of the barotropic tidal flow and will therefore be called *tidal straining circulation*. This contribution corresponds to the straining circulation that fits within the conceptual reasoning of Jay and Musiak (1994). The tidal straining circulation is much weaker than the tidal flow that induces it. It also requires variations of turbulence at the same frequency as the main tidal constituent, in this case  $M_2$ .

The second type of straining circulation originates from the strongly interacting system of the gravitational circulation. This will therefore be called the *gravitational straining circulation*. This research is the first time that the gravitational straining circulation is identified as such. Its magnitude is potentially larger than the gravitational circulation. It also does not require a specific frequency of turbulence variations; the gravitational circulation amplifies through mutual interactions with any frequency of varying turbulence.

In this section we will show some properties and dependencies of these two contributions to the straining circulation. We will show for the tidal straining circulations that the flow magnitude and direction depend on the magnitude and phase of the eddy viscosity and the roughness formulation in Section 4.5.1. These dependencies cannot be explained by the conceptual reasoning of Jay and Musiak (1994). We will show that there is an additional mechanism that also affects the tidal straining circulation that can explain these dependencies. It will be shown in Section 4.5.2 how the gravitational straining circulation depends on the eddy viscosity, the salinity gradient and the frequency of the temporally varying eddy viscosity. Section 4.5.3 will present the magnitudes of the different contributions to the straining circulation in the results of the model including  $k - \varepsilon$  turbulence model.

### 4.5.1. Straining circulation induced by $M_2$ barotropic tide

Jay and Musiak (1994) describe the exchange flow that would later be called straining circulation, as the interaction of SIPS induced asymmetric turbulence and the tidal flow. This process was explained in Section 1.3. In summary their reasoning is that periodic stratification leads to damping of turbulence during the ebb tide and strong mixing during the flood tide. The decreased ebb mixing is reasoned to lead to a less uniform tidal velocity profile, while the increased flood mixing leads to a more uniform tidal velocity profile. This asymmetry of the velocity profiles can be described by a symmetric  $M_2$  tide and an exchange flow with seaward flow near the surface and landward flow near the bed.

We will investigate this interaction in more detail by looking at the influence of the phase of the velocity and eddy viscosity and by looking at the influence of the roughness formulation. The motivation for such detailed analysis is presented in Figure 24, which zooms in on the result of Section 4.4.1. The model results are obtained with model Version 4 with an  $M_2$  eddy viscosity with three different phases. These phases are represented by the variable  $\Delta\phi$ , which is defined as the phase difference between the depth-averaged phase of the eddy viscosity and velocity and is positive when the  $M_2$  eddy viscosity lags the  $M_2$  velocity. The upper-left panel shows that the  $M_2$ - $M_2$  straining circulation is directed out of the estuary near the bed and into the estuary near the surface if  $\Delta\phi$  is zero. This direction is opposite to the direction that is generally associated with straining circulation. The flow reverses when  $\Delta\phi$  is increased, i.e. when the eddy viscosity lags the velocity.

These results will first be discussed by making a further decomposition of the straining circulation and providing a physical explanation to this decomposition.

#### Effect of bed friction on the straining circulation

There is a mechanism that is not taken into account in the reasoning of Jay and Musiak (1994) that could explain the circulation that was found in Figure 24: the effect of bed friction. If the effect of bed friction on mixing is reduced during ebb, this would result in a smaller boundary layer with a more uniform velocity profile in the rest of the water column. This situation is reversed during flood, so that the velocity profile is steeper during ebb than during flood. We then find a subtidal circulation in opposite direction; landwards near the

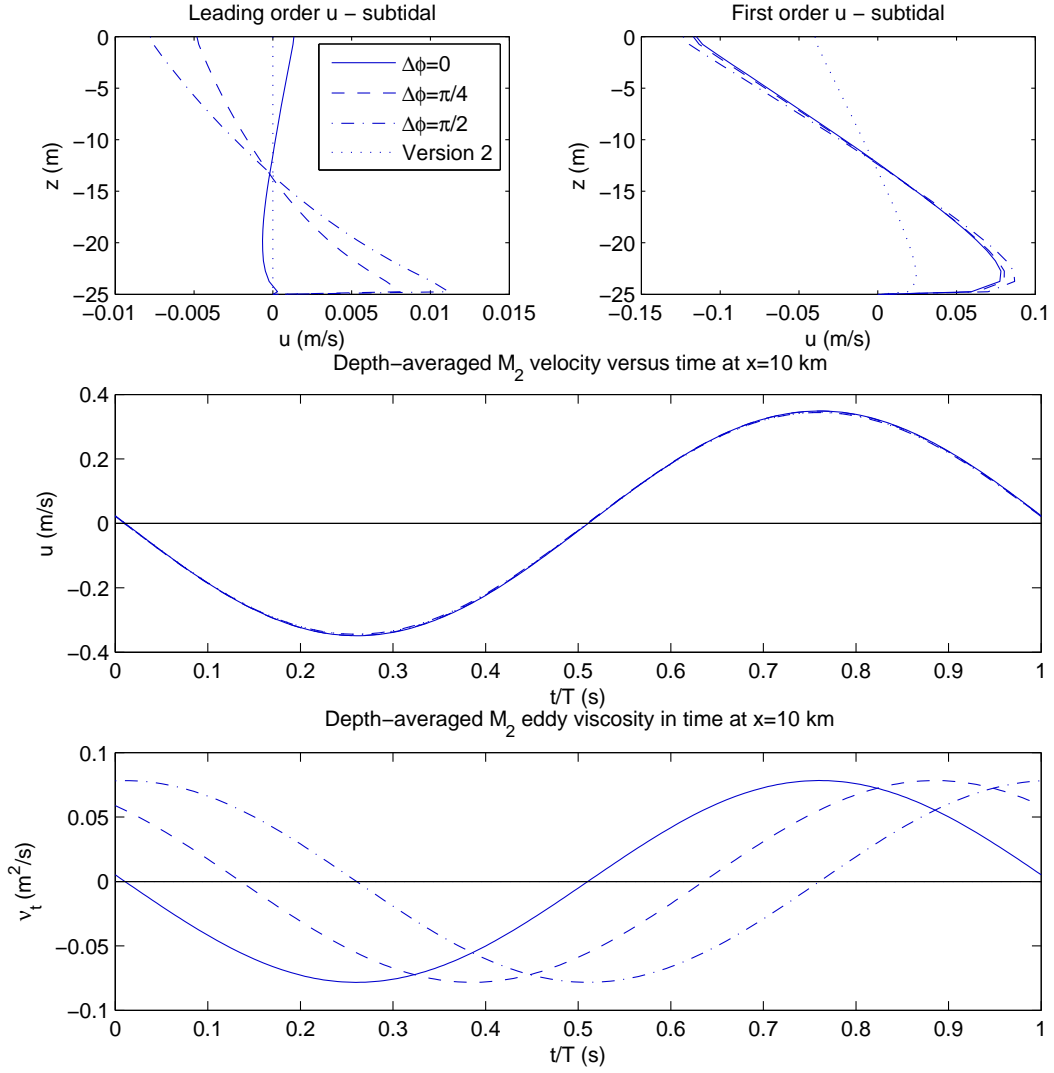


Figure 24: Results of the Version 4 model with several timings of the  $M_2$  turbulence signal. The results of Version 2 are given as comparison.  $\Delta\phi$  denotes the phase difference between the eddy viscosity and velocity. Top: the leading-order and first-order residual velocity profiles at  $x = 10$  km. Middle: depth-averaged  $M_2$  velocity versus time at  $x = 10$  km. Bottom: depth-averaged eddy viscosity versus time at  $x = 10$  km.

surface and seawards near the bed. The bed friction does not necessarily have to change for such effect to take place. It is the behaviour of the frictional boundary layer that is of importance. This frictional boundary layer extends through the whole water column in estuarine tidal flow and depends on both the bed friction and the eddy viscosity that propagates this bed friction up through the water column.

The opposing effects of the turbulent mixing and bed friction discussed above can be distinguished in the analytical solutions of the leading-order momentum equations, which are derived in Appendix E. These solutions are derived under the assumption of a weakly interacting system, i.e. the  $M_2$  velocity is not affected by the temporally varying eddy viscosity and the straining circulation is caused by  $M_2$ - $M_2$  interactions of the velocity and eddy viscosity only. We will repeat the solution for the exchange flow velocity from the appendix:

$$\hat{u}_0^0 = Re \left( \frac{\overline{\hat{v}_{t1}}}{\hat{v}_{t0}} \left( \underbrace{\frac{1}{H} \int_{-H}^0 \hat{u}_1^0 dz}_{(1)} - \hat{u}_1^0 + \kappa(z) \underbrace{\left( \frac{1}{H} \int_{-H}^0 \hat{u}_1^0 dz \right)}_{(2)} \right) \right). \quad (4.3)$$

The function  $\kappa(z)$  equals

$$\kappa(z) = -\frac{\frac{1}{H} \int_{-H}^0 f(z) dz - f(z)}{\frac{1}{H} \int_{-H}^0 f(z) dz - f(-H)},$$

$$f(z) = \int \frac{z}{\hat{\nu}_{t0}} dz.$$

This function  $\kappa(z)$  is equal to  $-1$  at the bed and is positive near the surface.

The first part of Equation 4.3 corresponds to the well-known mixing effect of the eddy viscosity that was described by Jay and Musiak (1994). This can be better understood by separating the phases of the eddy viscosity in a depth-mean and depth-varying part, denoted by overlines and apostrophes respectively, and rewriting this part to

$$\hat{u}_{0(1)}^0 = Re \left( \frac{|\hat{\nu}_{t1}|}{\hat{\nu}_{t0}} \left( \frac{1}{H} \int_{-H}^0 |\hat{u}_1^0| e^{i\phi'_{u1}} dz - |\hat{u}_1^0| e^{i\phi'_{u1}} \right) e^{i(\bar{\phi}_{u1} - \phi_{\nu t})} \right).$$

Let us assume that the eddy viscosity is in phase with the depth averaged velocity phase so that the last exponential vanishes. This corresponds to reduced mixing during ebb and increased mixing during flood. The velocity amplitude at the surface is larger than the depth-averaged velocity so that the resulting residual flow is negative there. The vertical phase variations of the  $M_2$  velocity are generally small enough for this reasoning to hold. A similar argument yields a positive residual velocity near the bed, see also Figure 25. The result is an exchange flow with seaward flow near the surface and landward flow near the bed. This part corresponds to the mixing effect of turbulence, because it describes the correlation between the phase difference between the velocity and the eddy viscosity on the one hand, and the uniformity of the velocity profile on the other hand.

Part two corresponds to the effect of the bed friction, which is contained within the function  $\kappa(z)$ . The bed friction creates a bottom boundary layer that affects the shape of the velocity profile in the water column. This effect is not contained in part 1. This can be understood intuitively by considering the ebb tide with a strong damping of turbulence. Part 1 describes that the velocity profile becomes less uniform as a result of this turbulence damping. However, at a very low degree of turbulence, the bed friction cannot propagate up the water column. This means that there is no source of velocity shear and the velocity profile must become uniform. So we find a balance between the effect of turbulence and an opposing effect that describes how bed friction is 'felt' in the water column.

The effect of part 2 is examined more closely by rewriting the term in a similar form as part 1:

$$\hat{u}_{0(2)}^0 = Re \left( \frac{|\hat{\nu}_{t1}|}{\hat{\nu}_{t0}} \kappa(z) \left( \frac{1}{H} \int_{-H}^0 |\hat{u}_1^0| e^{i\phi'_{u1}} dz \right) e^{i(\bar{\phi}_{u1} - \phi_{\nu t})} \right).$$

Again consider the eddy viscosity to be in phase with the depth-averaged velocity. The last exponential then vanishes. The integral is generally a positive number, because the vertical phase difference is typically small. So the function  $\kappa(z)$  is multiplied by a positive constant. This function is negative at the bed and positive at the surface, so that the residual flow is also positive at the surface and negative at the bed, see Figure 25.

The function  $f$  defined above suggests that there is a connection to the shape of the boundary layer. Let us consider the typical magnitude of the function  $f$ , which will be denoted by  $\mathcal{F}$  and uses a typical eddy viscosity scale  $\mathcal{N}$ . The magnitude of  $\mathcal{F}$  can be expressed as

$$\mathcal{F} = \int \frac{z}{\mathcal{N}} dz = \frac{1}{2} \frac{H^2}{\mathcal{N}}.$$

This is a time-scale which we will scale by the  $M_2$  tidal frequency to obtain a dimensionless parameter which is equal to the inverse square of the Stokes number

$$S_{tk}^{-2} = \mathcal{F}\omega = \frac{1}{2} \frac{\omega H^2}{\mathcal{N}}.$$

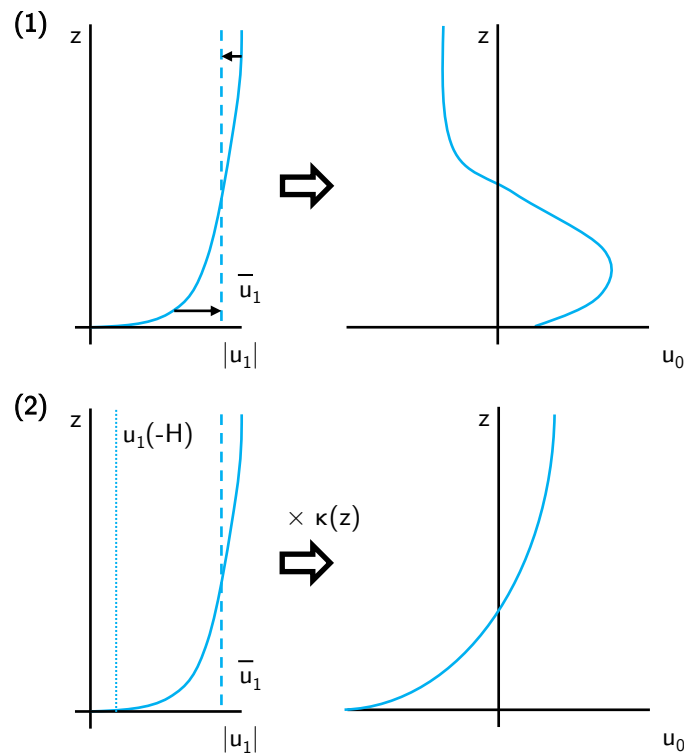


Figure 25: Schematic representation of the two opposing contributions to the residual circulation: (1) the effect of turbulent mixing and (2) the effect of bed friction.

The Stokes number is used to study the depth of frictional influence in oscillating flows and is defined as the ratio of this depth and the water depth (Souza, 2013). The quantity  $\mathcal{F}$  can therefore be regarded as a time-scale of frictional influence, so that the Stokes number becomes the ratio of a time-scale of frictional influence and the tidal time-scale.

The interpretation of  $\mathcal{F}$  as a time-scale is difficult here, because we are considering the creation of a residual flow. The creation of this residual flow does not depend on  $\omega$  and does therefore not depend on any tidal time-scale. Yet, the parameter  $\mathcal{F}$  has a meaning that is connected to the structure of the boundary layer. It therefore supports the earlier intuitive reasoning that part 2 reflects the effect of this boundary layer. More research is required to provide a better understanding of the opposing effects of turbulent mixing and bed friction on the velocity profile.

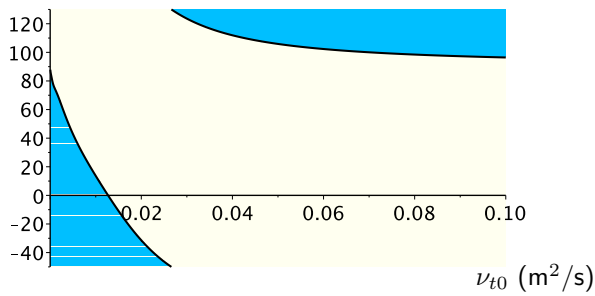
### Sensitivity to the roughness and eddy viscosity

We will study the sensitivity of the direction of the tidal straining circulation to three parameters in Versions 3 and 4 of the model. In Version 3 these parameters are the roughness parameter  $s_f$ , the vertically constant subtidal eddy viscosity  $\nu_{t0}$  and the phase difference between the depth-averaged leading-order  $M_2$  velocity and  $M_2$  eddy viscosity. The latter parameter will be denoted by  $\Delta\phi$  and is positive if the  $M_2$  eddy viscosity lags the  $M_2$  velocity. The results in this section are obtained from the analytical solution for the residual flow, derived in Appendix E. This solution uses the solution for  $\hat{u}_1^0$  which is calculated analytically. It is assumed that the  $M_2$  velocity is not affected by the  $M_2$  eddy viscosity.

Figure 26 shows the direction of the tidal straining circulation as a function of  $s_f$ ,  $\nu_{t0}$  and  $\Delta\phi$ . The white area in the figure represents the expected flow direction; with outflow near the surface and inflow near the bed. Figure 26c shows how the direction of the circulation depends on  $s_f$  and  $\nu_{t0}$  if  $\Delta\phi$  is zero; the relation between the input parameters and the circulation direction if the  $M_2$  eddy viscosity is in phase with the  $M_2$  velocity. Figures 26a and 26b show how the direction of the circulation changes with  $\Delta\phi$ . It is expected that the phase difference is positive in reality, simulating stable stratification during late ebb and enhanced mixing during late

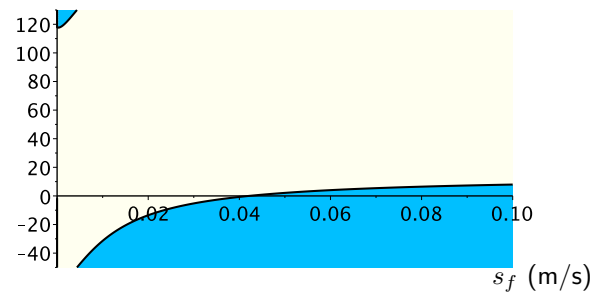
flood.

$\Delta\phi$  (degrees)



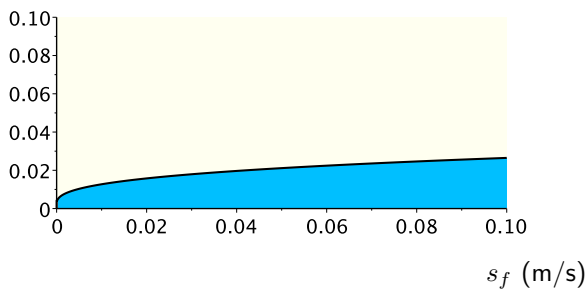
(a) Direction of the straining circulation in  $(\nu_{t0}, \Delta\phi)$  space with  $s_f = 0.1$  m/s and  $H = 25$  m.

$\Delta\phi$  (degrees)



(b) Direction of the straining circulation in  $(s_f, \Delta\phi)$  space with  $\nu_t = 0.02$  m<sup>2</sup>/s and  $H = 25$  m.

$\nu_{t0}$  (m<sup>2</sup>/s)



(c) Direction of the straining circulation in  $(s_f, \nu_{t0})$  space with  $\Delta\phi = 0$  and  $H = 25$  m.

Figure 26: Sensitivity of the direction of the tidal straining circulation to the three parameters  $s_f$ ,  $\nu_{t0}$  and  $\Delta\phi$  in Version 3. The white area represents the expected flow direction; outflow at the surface and inflow near the bed.

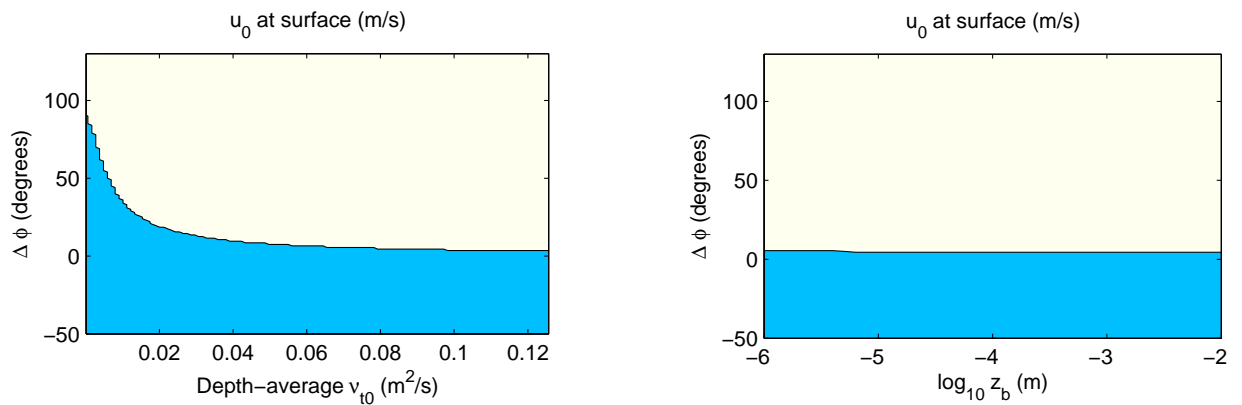
The parameters used in this research,  $\hat{\nu}_{t0} = 0.078$  m<sup>2</sup>/s and  $s_f = 0.004$  m/s, result in the expected direction of the straining circulation if the phase difference between the eddy viscosity and the velocity is zero, see Figure 26c. It is therefore that the Figures 26a and 26b use values of  $s_f$  and  $\nu_t$  that are different to the values used in the rest of this research. It illustrates the possible effect of the bed friction of the flow direction for other parameter settings.

The figure shows that it is required to have some phase difference  $\Delta\phi$  in order to get the expected direction of the circulation for many reasonable combinations of  $\nu_t$  and  $s_f$ , such as that used by (Chernetsky et al., 2010). It also shows that a positive value of  $\Delta\phi$ , which is expected from a physical point of view, yields the expected direction of the residual circulation for more values of  $\nu_t$  and  $s_f$  than a negative value of  $\Delta\phi$ .

The sensitivity study supports the physical explanation given above. The small value of the bed friction coefficient  $s_f$  used in the Version 3 simulations diminishes the effect of bed friction and therefore yields the expected flow direction.

A similar sensitivity study in Version 4, with the parabolic eddy viscosity profile, yields results which differ at a few points. At a phase difference  $\Delta\phi = 0$  no configuration of the parameters  $z_b$  and  $\nu_{t0}$  exists so that the straining circulation is in the expected direction. Figure 27 shows the other results of the sensitivity study. The left panel of this figure compares well to Figure 26a for small values of the eddy viscosity, but has a horizontal asymptote just above  $\Delta\phi = 0$  for larger values of the eddy viscosity. The right panel shows that the direction of the straining circulation is independent of the bed roughness  $z_b$  as long as this value is higher than  $10^{-6}$  m.

So the balance between the two parts that make up the tidal straining circulation depends on the type of roughness formulation as well as the value of the roughness parameter and  $\nu_{t0}$ . It can be seen from the



(a) Direction of the tidal straining circulation in  $(\nu_{t0}, \Delta\phi)$  space with  $z_b = 0.004$  m/s and  $H = 25$  m.

(b) Direction of the tidal straining circulation in  $(z_b, \Delta\phi)$  space with  $\frac{1}{H} \int_{-H}^0 \hat{\nu}_{t0} dz = 0.078$   $m^2/s$  and  $H = 25$  m.

Figure 27: Sensitivity of the direction of the tidal straining circulation to the three parameters  $z_b$ , depth-averaged  $\nu_{t0}$  and  $\Delta\phi$  in Version 4. The white area represents the expected flow direction; outflow at the surface and inflow near the bed.

analytical solutions to the tidal straining circulation that the depth of the estuary is the only other parameter that influences the direction of the tidal straining circulation in Version 3 and 4. This means that the amplitude of the  $M_2$  eddy viscosity and the magnitude of the  $M_2$  velocity are not important for the direction of the circulation.

This research is the first time that such dependencies are found. It is not known whether the possible reversal of the tidal straining circulation can also occur in reality or whether it is a model artefact. Experimental studies are required to investigate this.

#### 4.5.2. Straining circulation induced by the gravitational circulation

It was shown in Section 4.4 that the residual circulation in the first-order is amplified by the strong interactions between the velocity and the eddy viscosity. The most important interaction is that of the gravitational circulation with the  $M_2$  eddy viscosity. This interaction involves the gravitational circulation which interacts with the  $M_2$  eddy viscosity to create an  $M_2$  velocity. This  $M_2$  velocity has the same velocity profile as the gravitational circulation. It also has a similar magnitude, because the turbulence is strongly varying in time and the gravitational circulation profile has a strong curvature. The interaction of the  $M_2$  velocity and the  $M_2$  eddy viscosity provide a strong feedback to the exchange flow.

In this section we will show how the straining circulation induced by the gravitational circulation can be distinguished from the momentum equations and how the straining circulation depends on the along-channel salinity gradient, the phase of the eddy viscosity and the frequency of the temporal variations of the eddy viscosity.

The parts of the momentum equations that are associated with this interaction between the baroclinic residual and  $M_2$  velocity are

$$\begin{aligned} -\hat{\nu}_{t0} \hat{u}_{0,zz}^1 &= -g \hat{\zeta}_{0,x,s_x}^1 + Re(\overline{\hat{\nu}_{t1} \hat{u}_{1,zz}^1}) + g\beta s_{0,xz}, \\ i\omega \hat{u}_1^1 - \hat{\nu}_{t0} \hat{u}_{1,zz}^1 &= -g \hat{\zeta}_{1,x,s_x}^1 + \frac{1}{2} \hat{\nu}_{t1} \hat{u}_{0,zz}^1. \end{aligned}$$

The equations are restricted to the baroclinic forcing under the assumption of a constant salinity gradient. This exchange flow contains the effect of the gravitational circulation and the gravitational straining circulation. These two components can be distinguished in the equations by separating the subtidal water level gradient in a part associated with the gravitational circulation (GC) and a part associated with the gravitational straining

circulation (GSC);

$$\hat{\zeta}_{0,x,s_x}^1 = \hat{\zeta}_{0,x,GC}^1 + \hat{\zeta}_{0,x,GSC}^1,$$

The  $M_2$  water level gradient is only due to the gravitational straining circulation, because it is not forced directly by the salinity gradient. The equations then read

$$\begin{aligned} -\hat{\nu}_{t0}\hat{u}_{0,zz}^1 &= \underbrace{-g\hat{\zeta}_{0,x,GSC}^1 + Re(\overline{\hat{\nu}_{t1}\hat{u}_{1,zz}^1})}_{(GSC)} \underbrace{-g\hat{\zeta}_{0,x,GC}^1 + g\beta s_{0,x}z}_{(GC)}, \\ i\omega\hat{u}_1^1 - \hat{\nu}_{t0}\hat{u}_{1,zz}^1 &= \underbrace{-g\hat{\zeta}_{1,x,s_x}^1 + \frac{1}{2}\hat{\nu}_{t1}\hat{u}_{0,zz}^1}_{(GSC)}. \end{aligned}$$

The equation contains separate parts for GSC and GC. The only external forcing to this system is the along-channel salinity gradient. This induces the gravitational circulation, which enters in the equations for the  $M_2$  velocity. This  $M_2$  velocity feeds back into the residual velocity, see Figure 28. The equations are linear. This means that the solution depends linearly on the salinity gradient, i.e. both the gravitational circulation and the gravitational straining circulation depend linearly on the salinity gradient.

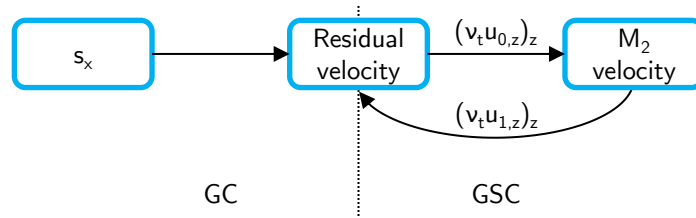


Figure 28: Schematic figure of the interactions in the system of gravitational circulation (GC) and gravitational straining circulation (GSC).

This dependence is verified in model Version 4 with a parabolic subtidal and  $M_2$  eddy viscosity of equal magnitude, see Figure 29. The magnitude of the exchange flow is measured as an absolute depth-average, see the definition of Equation 4.4 in the next section. The gravitational straining circulation and the gravitational circulation are indeed both linearly dependent on  $s_x$ , with this component of the straining circulation being 2.2 times greater than the gravitational circulation in this case.

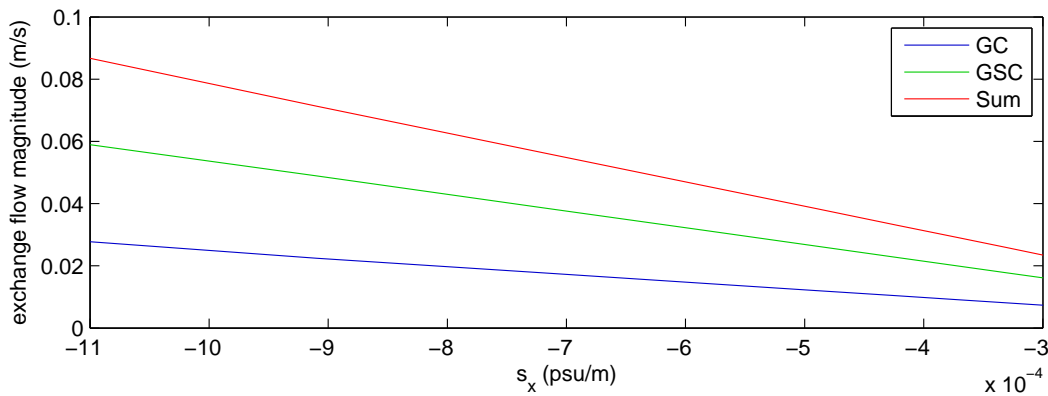


Figure 29: Magnitude (see Equation 4.4) of the gravitational circulation (GC) and gravitational straining circulation (GSC) as a function of the along-channel salinity gradient. The linear dependence has also been proved analytically.

It is proved in Appendix E.3 that the magnitude and direction of the gravitational straining circulation is independent of the phase of any temporally varying eddy viscosity. The gravitational straining circulation therefore does not depend on the timing of the eddy viscosity, but only on its magnitude. This is unlike the magnitude and direction of the tidal straining circulation, which was shown in the previous section to depend on the phase of the  $M_2$  eddy viscosity.

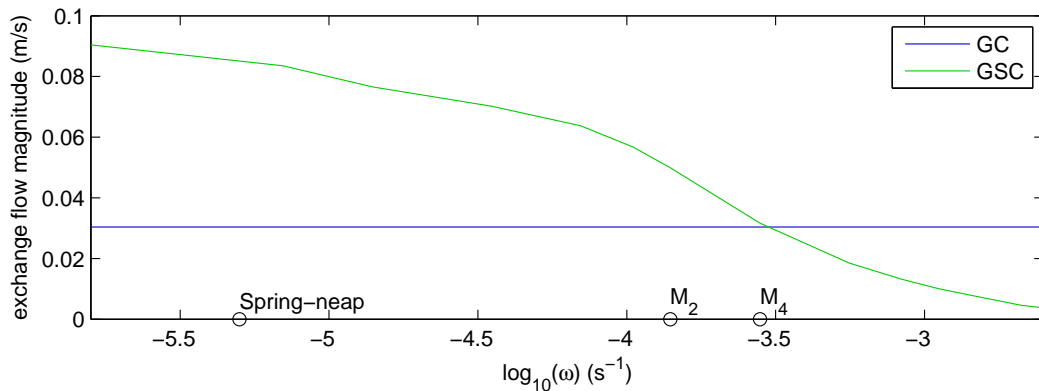


Figure 30: Magnitude (see Equation 4.4) of the gravitational circulation (GC) and gravitational straining circulation (GSC) as a function of the angular frequency of the tidal wave.

It is found in all experiments for this research that the gravitational straining circulation acts in the direction of the gravitational circulation. It could be possible that configurations of the bed roughness and eddy viscosity exist that produce a straining circulation in the opposite direction. Further research is required to prove whether such a reversal of direction is possible.

The interaction between the residual and  $M_2$  velocity components via an  $M_2$  eddy viscosity have been investigated above. We will now investigate the effectiveness of interactions between the gravitational circulation and other frequency components in creating the gravitational straining circulation. We will assume that the gravitational circulation interacts with one frequency component of the eddy viscosity and therefore with the same frequency component of the velocity. The temporal variation of the eddy viscosity has the same amplitude as the subtidal eddy viscosity. The angular frequency  $\omega$  of this frequency component is varied. The magnitude of the gravitational straining circulation as a function of  $\omega$  is presented in Figure 30. The figure shows that a smaller frequency results in a stronger exchange flow. This means that  $M_2$  variations of the eddy viscosity are more effective in creating the gravitational straining circulation than  $M_4$  variations or higher overtones. The  $M_4$  variations are, however, still capable of inducing a gravitational straining circulation that has the same magnitude as the gravitational circulation in this case. The variations of the eddy viscosity on the spring-neap cycle are more effective in creating the gravitational straining circulation than the  $M_2$  variations. It is outside the scope of this research to look into the effect of spring-neap variations.

### 4.5.3. Results with Version 5

The previous two sections have showed that the exchange flow in the present case consists of three important contributions. The first contribution is the straining circulation induced by the interaction of the  $M_2$  tide and  $M_2$  eddy viscosity. The second is the straining circulation induced by the strongly coupled system of gravitational circulation and  $M_2$  baroclinic velocity component via the  $M_2$  eddy viscosity. The final important contribution to the exchange flow is the gravitational circulation itself. We will compare the magnitude of the three contributions in the results with the  $k - \varepsilon$  turbulence model.

Figure 31 displays these contributions to the exchange flow. The magnitude of the contributions is measured in a similar way as Burchard and Hetland (2010):

$$\|u_0\|_1 = \frac{1}{H} \int_{-H}^0 |u_0 - \bar{u}_0| dz, \quad (4.4)$$

The total straining circulation contributes to 63% of the total exchange flow. The gravitational circulation contributes 36%. Other sources of exchange flows are for example the advection and the vertical variation of the river velocity. These contribute only 1% of the exchange flow. These results correspond to the results of Burchard and Hetland (2010), who have found that the straining circulation amounts to approximately 2/3 of

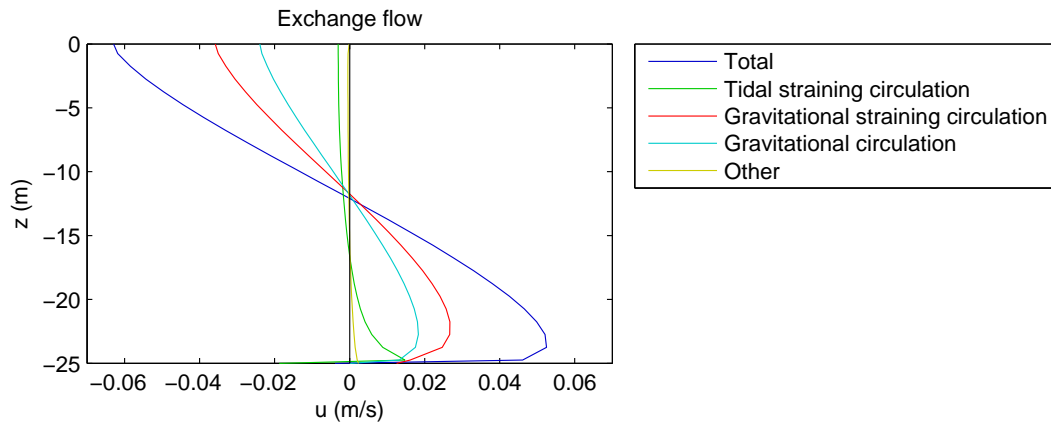


Figure 31: The three most important contributions to the exchange flow and the total exchange flow in the Version 5 simulation at  $x = 10$  km.

the exchange flow, while the gravitational circulation is responsible for the other 1/3 in their test cases. They have used an 1DV model with a  $k - \varepsilon$  model and have included salt transport.

The straining circulation consists for 85% by the gravitational straining circulation. Only 15% of the straining circulation is attributable to the tidal straining circulation. In literature it is assumed that the tidal straining explains the straining circulation, but it is shown here that this is not necessarily the case. The straining circulation is a result of the interaction of both the tidal and gravitational contributions. The gravitational straining circulation is capable of providing the largest contribution to the straining circulation. This contribution is also independent of the phase of the eddy viscosity, while the tidal straining circulation depends on the phase of the eddy viscosity and may even reverse direction.

#### 4.6. The (un)importance of longitudinal eddy viscosity variations

It was discussed in Section 4.3 that the eddy viscosity varies strongly in longitudinal direction and that these variations can be related to the velocity shear that is caused by the tidal velocity and the exchange flow. In this section it will be discussed what importance these longitudinal variations have on the flow velocity. To this end we compare the results of the full  $k - \varepsilon$  model (Version 5) with the results that are obtained by choosing an along-channel uniform eddy viscosity (Version 4). The vertical and temporal variations of the eddy viscosity are the same in both cases. The along-channel uniform profile of the eddy viscosity is chosen so that the  $M_2$  water level amplitude and phase at the end of the basin are similar in both cases.

The  $M_2$  tidal velocity and the exchange flow are used to compare both cases in Figure 32. This figure presents the differences in amplitude of the  $M_2$  tide and differences in magnitude of the exchange flow, see Equation 4.4. The tidal velocity is hardly affected by the longitudinal variations of the eddy viscosity, while the exchange flow magnitude changes up to 100% when longitudinal variations of the eddy viscosity not included.

The results in Figure 32 show the uncertainty in the model results when it is calibrated on the water level. The  $M_2$  and subtidal water level at the end of the estuary differ only 5 cm between the case of the longitudinally varying and constant eddy viscosity. This results in very small differences in the  $M_2$  velocity, but very large differences in the exchange flow magnitude. Calibration on the  $M_2$  water level as is done here is clearly not sufficient to get accurate results for the exchange flow.

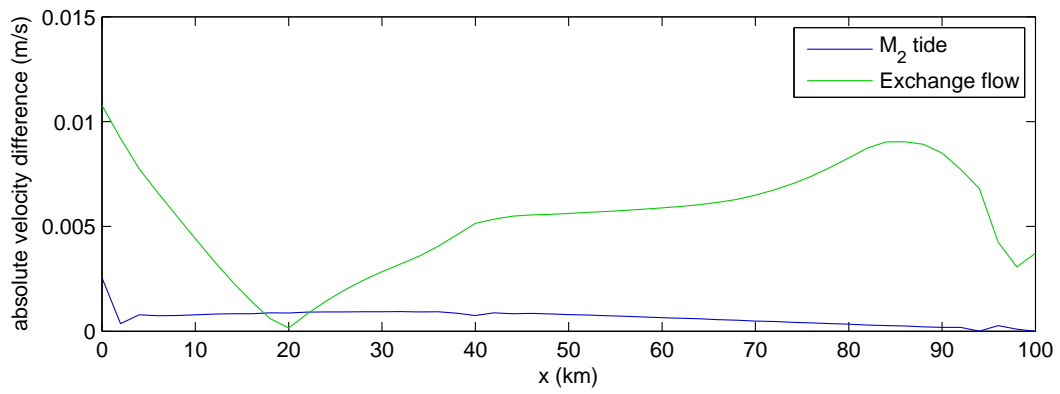


Figure 32: Absolute differences between the velocities as calculated by the  $k-\varepsilon$  model with and without longitudinal variations of the eddy viscosity. The differences are given for the  $M_2$  tide and the exchange flow.



# 5

## Results: salinity

This chapter considers the coupling of the hydrodynamic model and the salinity model, and the effect of turbulent mixing on this coupled model. The central question to be addressed in this chapter is the second research question: "how does the tidally induced salt transport depend on tidal variations of turbulence?" The structure of the salinity model is ideal for studying the salt transport, because one equation of the salinity model separates the mechanisms that are responsible for salt transport. The salinity model consists of two equations that are repeated here

$$\left( B \int_{-H}^0 \langle u^0 s^1 \rangle dz \right)_x + Q^1 s_x^0 - BH (K_H s_x^0)_x = 0,$$
$$s_t^1 - (K_V s_z^1)_z = -u^0 s_x^0.$$

The first equation describes the salt transport of the depth-averaged time-averaged salinity  $s^0$ . The transport in this equation comes from the leading-order tidal flow, which is contained in  $u^0$ , the river discharge  $Q$  and the unresolved dispersion, parametrised by  $K_H$ . The other forcing mechanisms of the flow, such as the baroclinic pressure or momentum advection, are unimportant according to the scaling procedure. The second equation describes the temporal and vertical variations of salinity  $s^1$ . This equation is forced by the along-channel advection of salt by the leading-order tide.

In this chapter we will focus on the tidal salinity transport. The dependency of this tidal transport on turbulence is explored by increasing the complexity of the turbulence modelling by using the different versions of the model. Special attention is paid to the effect of temporal variations of the eddy viscosity. The salt balances that were introduced in Section 3.4 will be used throughout this chapter to analyse the results.

This chapter uses the same estuary dimensions and tidal and river forcing as were used in the previous chapter, see Table 4.1. We will first discuss the results of the salinity model in the case of a temporally constant eddy viscosity (Version 1 and 2) in Section 5.1. Next, the  $k - \varepsilon$  model will be applied in Section 5.2. In Section 5.3 we will go further into the effect of a temporally varying eddy viscosity on the salt intrusion and timing of stratification.

### 5.1. Reference case

This section will present the results of the salinity model in the reference case. This case will use the estuary dimensions, tidal forcing and river discharge that were used in Chapter 4. The eddy viscosity is assumed to be constant in time and either constant or parabolic in the vertical direction (Version 1 and 2).

Figure 33 shows the depth-averaged, time-averaged salinity over the length of the estuary for Version 1 and Version 2. The results are presented for three different values of the horizontal dispersion coefficient  $K_H$ . A

smaller value of this coefficient results in less salt intrusion, while a larger value leads to more salt intrusion. This can be explained by looking at the 1DH salinity equation

$$Qs_x - (HBKs_x)_x = 0.$$

The 1DH equation is an advection-dispersion equation. This equation can be rewritten by using the product rule

$$Qs_x - HBK_x s_x - HBK s_{xx} = 0. \quad (5.1)$$

The dispersive component has a dispersion coefficient  $K$ . The dispersion spreads the salinity from the seaward boundary into the estuary and results in an exponential decay of the salinity with the distance from this boundary. The advective component transports salinity with a 'velocity'  $K_x$ . The salinity profile that results from advection does not decay with distance. The gradient of  $K$  therefore indicates the deviation of the salinity from the exponentially decaying profile.

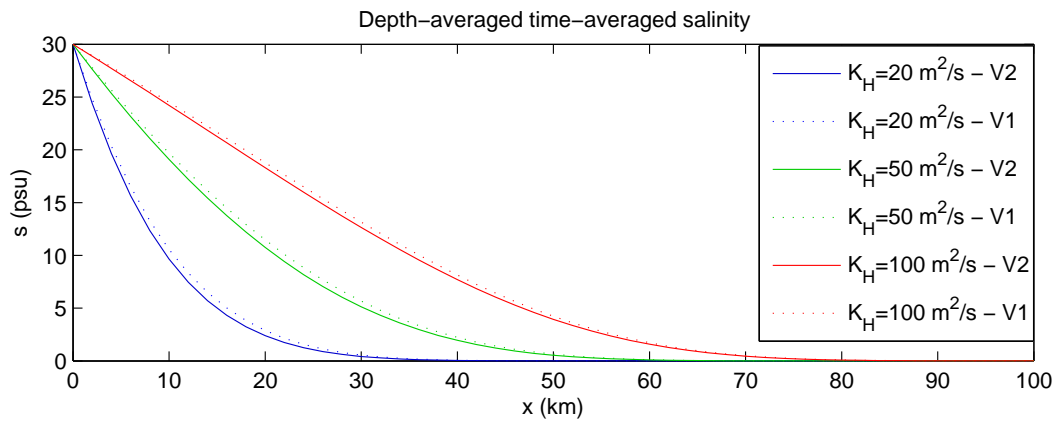


Figure 33: Depth-averaged time-averaged salinity versus longitudinal distance for Version 1 (dotted line) and Version 2 (solid line).  $K_H = 20, 50$  and  $100 \text{ m}^2/\text{s}$ .

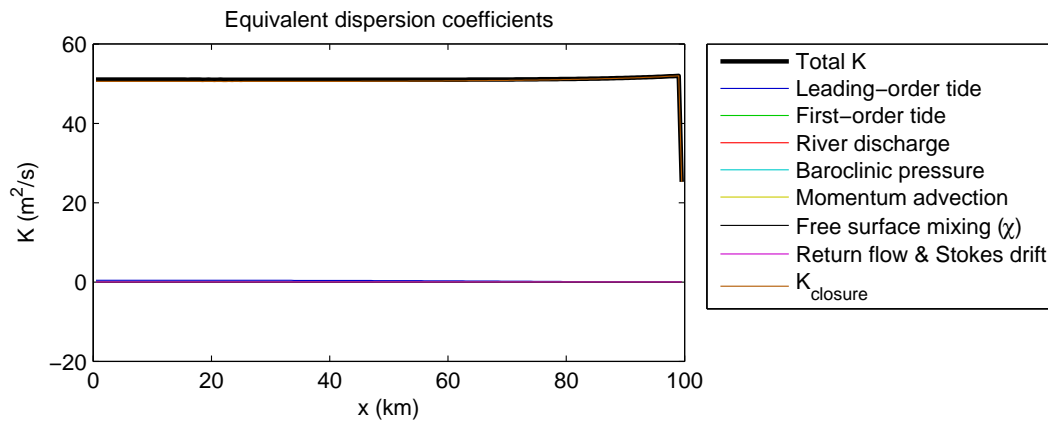


Figure 34: Equivalent dispersion coefficients separated in physical mechanisms. Model Version 2,  $K_H = 50 \text{ m}^2/\text{s}$ .

The dispersion coefficient is decomposed into the different forcing mechanisms in Figure 34. The decomposition is made according to the method presented in Section 3.4.2. The dispersion coefficients are calculated in post-processing so that the contribution of, for example, baroclinic pressure can be estimated even though it is not included in the salinity model. For the validity of the model it is required that the leading-order tidal contribution and the closure term are much larger than the other contributions.

The salt intrusion is almost solely established by the parametrised dispersion. The dispersion coefficient of this parametrised dispersion is  $K_{\text{closure}}$ , which equals the sum of  $K_H$  and any disparity between the 2DV model and the salt balance equation. Such differences can be caused by model errors, e.g. because the model does not

take baroclinic salinity transport into account. Differences between the model and the salt balance can also occur if the calculated salinity profile cannot be described by a dispersion coefficient. In this case, the  $K_{\text{closure}}$  almost equals the prescribed  $K_H$ .

We will look closer at the tidal contribution of the salinity transport and explain why it is negligible in this case. If the eddy viscosity is constant in time, this transport is induced by the  $M_2$ - $M_2$  interactions of velocity and salinity. The negligible contribution of the tide can be explained by considering the first-order salinity equation

$$i\omega \hat{s}_1^1 - (K_{V0} \hat{s}_{1,z}^1)_z = -\hat{u}_1^0 \hat{s}_x^0. \quad (5.2)$$

The first-order salinity contains the  $M_2$  frequency, which will be broken down into a depth-averaged part and a depth-varying part. To this end, the forcing on the right-hand side of the equation is also split into a depth-averaged part  $-\hat{u}_1^0 \hat{s}_x^0$  and a depth-varying part  $-(\hat{u}_1^0)' \hat{s}_x^0$ . The depth-averaged part indicates the excursion of salt over the  $M_2$  tide. Its magnitude is easily calculated by solving Equation 5.2 with only this part of the forcing. This yields the solution

$$\hat{s}_{1,\text{depth-averaged}}^1 = -\frac{\overline{\hat{u}_1^0} \hat{s}_x^0}{i\omega}.$$

The amplitude of  $\hat{s}_{1,\text{depth-averaged}}^1$  is about 3 psu at the mouth for the present situation. More importantly, it is always 90 degrees out of phase with the leading-order velocity. As a result, the product of  $\hat{s}_{1,\text{depth-averaged}}^1$  and  $\overline{\hat{u}_1^0}$  is zero and there is no contribution to the salt-intrusion.

So vertical stratification is, in this simplified model, the only model-resolved forcing mechanism for salt intrusion. The vertical stratification is negligible ( $\sim 0.01$  psu) in the present simulation due to the high value of the eddy viscosity. The vertical stratification would be larger if the parameter settings were different. The vertical stratification is only 11 degrees out of phase with the depth-average  $M_2$  velocity in this case. A higher level of vertical stratification would therefore lead to a more significant tidal salt transport.

A sensitivity study using the constant eddy viscosity model results in a maximum of  $2 \cdot 10^3 |\hat{s}_x^0|$  psu salinity difference between the surface and the bed, which is approximately 2 psu for a uniform salinity gradient  $\hat{s}_x^0$  of 30 psu over 30 km. This maximum value is found for  $\nu_t \approx 0.004$  m<sup>2</sup>/s and roughness coefficient  $s > 0.1$  m/s if the depth is 25 m and we consider the  $M_2$  tide, see Figure 35. At its maximum the vertical stratification is capable of a salt transport with an equivalent dispersion coefficient of approximately 50 m<sup>2</sup>/s with the estuary dimensions that are considered here. This is a significant amount. So the transport by the tide can be a dominant factor for salt transport, but the settings in this reference case produce hardly any tidal salt transport.

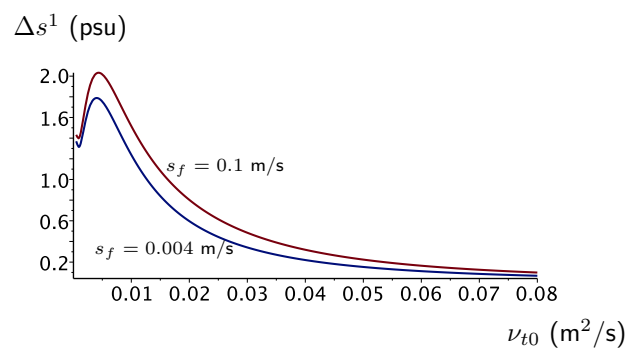


Figure 35: Maximum top-bottom salinity difference  $\Delta s^1$  during a tidal cycle in Version 1 with model parameters  $\hat{s}_x^0 = -10^{-3}$  psu/m and  $s_f = 0.004$  (blue line) or  $s_f = 0.1$  (red line).

## 5.2. Results with a $k - \varepsilon$ turbulence model

The tide can only transport salt by interactions with the vertical stratification if the eddy viscosity is constant. If the eddy viscosity were to vary in time, however, the tide would also transport salt by interactions with the depth-averaged salinity. This will be shown in this section.

We will therefore employ the  $k - \varepsilon$  turbulence model to calculate the eddy viscosity. The results in this section use the  $k - \varepsilon$  model without buoyancy effects, i.e. vertical stratification has no effect on turbulence. This restriction is necessary for the model to converge. These convergence problems are discussed in Appendix D.3. It is expected that the stratification has a profound effect on the eddy viscosity. However, the results presented in this section are still useful to illustrate the effects that any temporally and longitudinally varying eddy viscosity might have on the tidal salt transport.

The salt intrusion and equivalent dispersion coefficient as functions of  $x$  are presented in Figures 36 and 37. The tip of the salt curve has not progressed much further into the estuary than in the reference case, but the shape of the salt intrusion curve has changed to a more convex shape near the mouth of the estuary, causing increased salinity levels throughout the estuary. Figure 37 reveals that this change of the salinity is caused by the tidal salt transport, which is significant near the mouth of the estuary.

The changed shape of the salt intrusion curve appears in Figure 37 as the gradient of the tidal dispersion coefficient. This gradient indicates an advective type of transport, as was explained in the previous section. The combination of advective and dispersive transport of salt yields the more convex salinity profile near the seaward boundary.

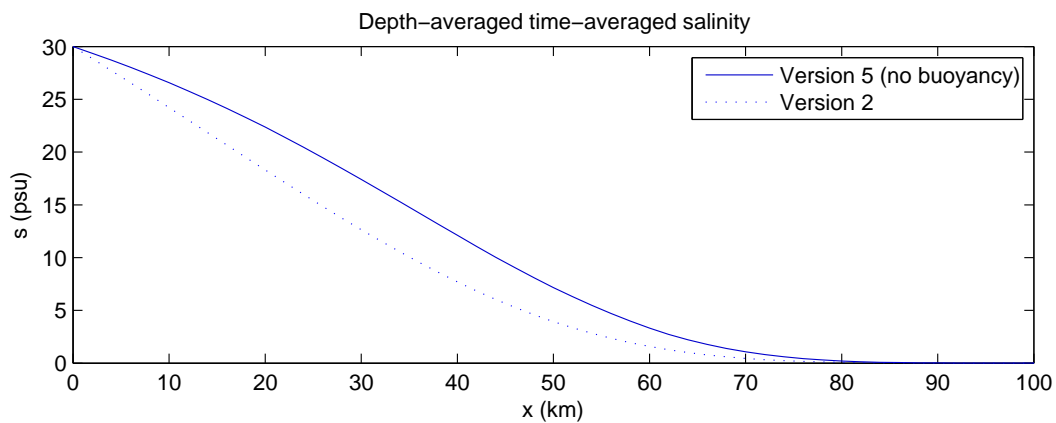


Figure 36: Depth-averaged time-averaged salinity versus longitudinal distance for Version 5 without buoyancy effects in the  $k - \varepsilon$  model (solid line). The result of Version 2 is given as reference (dotted line).  $K_H = 100 \text{ m}^2/\text{s}$ .

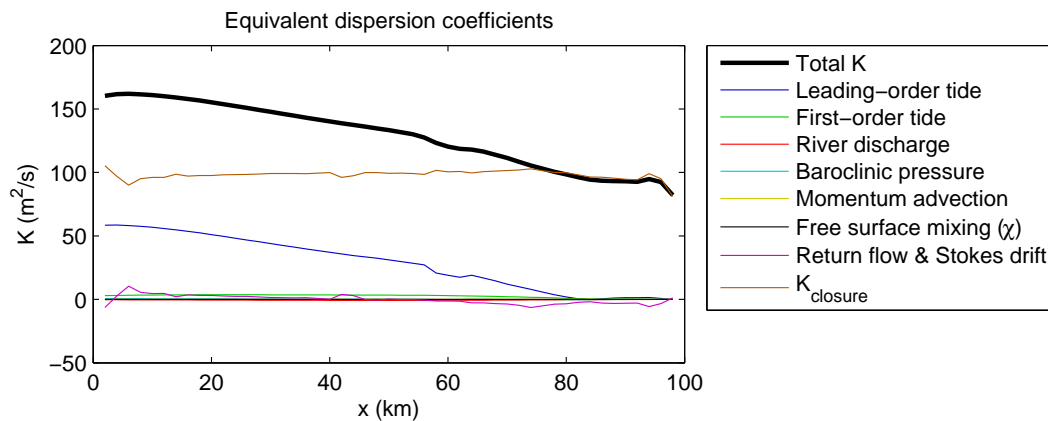


Figure 37: Equivalent dispersion coefficient separated in physical mechanisms. Model Version 5 without buoyancy effects in the  $k - \varepsilon$  model.  $K_H = 100 \text{ m}^2/\text{s}$ .

The tidal salinity transport is caused for 95 % by the interaction of the  $M_2$  tidal velocity with the depth-averaged  $M_2$  salinity. This type of salinity transport was absent in the reference case, because the depth-averaged  $M_2$  salinity and tidal velocity were out of phase. This is different if the eddy viscosity is allowed to vary in time. The phase difference between the depth-averaged  $M_2$  salinity and tidal velocity is now 82 to 86 degrees. So the two components are still almost out of phase, but this is sufficient to produce a significant tidal salt dispersion.

This means that the potential of the tide to transport salt is enormous even if the level of vertical stratification is limited.

The tidal salinity transport can be analysed further by looking closer at the first-order salinity equation. We will look at the  $M_2$  and  $M_4$  components and assume that these are the only components to illustrate the behaviour of this equation. The eddy viscosity is assumed to consist of a subtidal and an  $M_2$  component. The equations then read

$$i\omega\hat{s}_1^1 - (K_{V0}\hat{s}_{1,z}^1)_z = -\hat{u}_1^0\hat{s}_x^0 + \frac{1}{2}(\overline{K_{V1}}\hat{s}_{2,z}^1)_z,$$

$$2i\omega\hat{s}_2^1 - (K_{V0}\hat{s}_{2,z}^1)_z = -\hat{u}_2^0\hat{s}_x^0 + \frac{1}{2}(K_{V1}\hat{s}_{1,z}^1)_z.$$

The  $M_4$  salinity is forced by a weak  $M_4$  tidal velocity. The forcing of the  $M_4$  salinity by the  $M_2$  salinity via the term  $\frac{1}{2}(K_{V1}\hat{s}_{1,z}^1)_z$  is also small, because the vertical gradient of the  $M_2$  salinity is small, see Figure 38. Conversely, the  $M_4$  salinity has little influence on the  $M_2$  salinity as its vertical gradient is small. Note however, that the gradient of the  $M_4$  salinity is of similar magnitude as the gradient of the  $M_2$  salinity. The effect of the  $M_4$  salinity on the  $M_2$  salinity can therefore not be neglected completely. Nevertheless it can be concluded that the first-order salinity equation is a weakly interacting system; the interactions between different salinity components are small.

Still, the interactions between the components are strong enough to cause a shift of 6 degrees of the depth-averaged  $M_2$  salinity compared to the reference case, see Figure 38. This small phase shift is sufficient to induce a significant amount of salt transport. This makes salt transport especially difficult to model; even weak interactions between components that are small can be important for the prediction of the total salt transport.

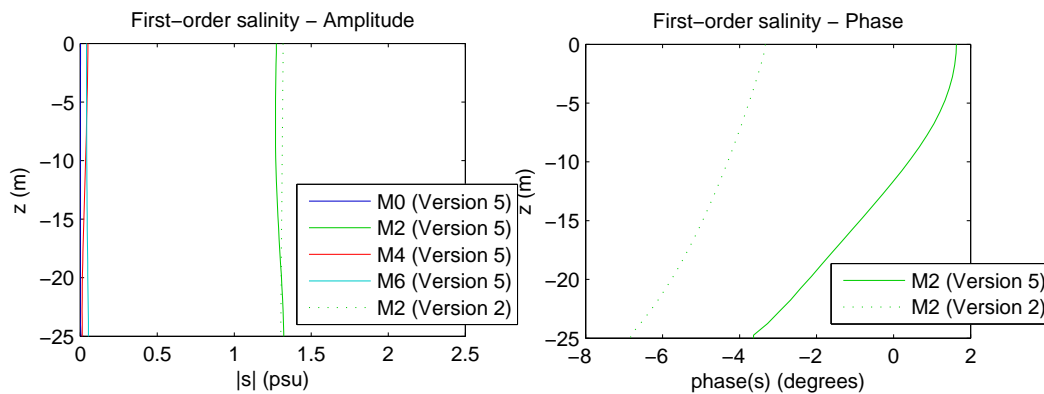


Figure 38: Vertical profiles of the first-order salinity at  $x = 30$  km with the  $k - \varepsilon$  model (solid line) and parabolic temporally constant eddy viscosity (dotted line).

Whereas the vertical stratification was most stable after peak ebb in the reference case, its  $M_2$  component is 30 degrees ahead of the  $M_2$  velocity here. This means that the water column is at its most stable stratification during early ebb. It could be questioned whether this is realistic. The eddy viscosity is higher during peak ebb than during early ebb, because buoyancy effects are not taken into account in the  $k - \varepsilon$  model. This increased mixing during peak ebb shifts the maximum stratification to early ebb.

So it is expected that the phase of the eddy viscosity changes when buoyancy effect are taken into account. This is likely to affect the salt transport. We will therefore investigate how the phase of the eddy viscosity and the phase of stratification are related in Section 5.3.

### 5.3. Sensitivity to the phase of the eddy viscosity

It was found in Section 4.3 that the eddy viscosity without salinity model mainly consists of a subtidal and an  $M_2$  component. It is further expected that the inclusion of buoyancy effects in the eddy viscosity would induce

a strong  $M_2$  component of the eddy viscosity, because of the tidally asymmetric SIPS phenomenon. We will therefore describe the eddy viscosity by a subtidal and an  $M_2$  component and investigate the sensitivity of the results to the magnitude and phase of the  $M_2$  eddy viscosity. First, it will be investigated how the phase of the vertical stratification depends on the phase of the eddy viscosity. Next, the dependency of the salt transport on the phase of the eddy viscosity is investigated. We will use model Version 4 with a parabolic eddy viscosity profile in this section.

When prescribing an  $M_2$  eddy viscosity, it is preferred that the phase of the stratification is not too sensitive to the chosen phase of the eddy viscosity. If the phase of the stratification is highly sensitive to the phase of the eddy viscosity, this would put strong demands on the accuracy with which the eddy viscosity is prescribed. This sensitivity is tested in Figure 39.

The phase of the stratification is independent of the phase of the eddy viscosity if the  $M_2$  eddy viscosity is only 1 % of the subtidal value. The value of  $\phi_{\text{strat}}$  is just negative, which means that the strongest stratification occurs just after peak ebb. The results change when the magnitude of the  $M_2$  eddy viscosity is increased to 10% of the subtidal eddy viscosity. The phase of the stratification is now equal to the phase of the eddy viscosity at a positive value. This means that the stratification is already at its maximum before peak ebb. The results change even more when the  $M_2$  eddy viscosity is increased further. The phase of the stratification becomes strongly dependent on the phase of the eddy viscosity.

The validity of the assumed simplified eddy viscosity is challenged by the highly fluctuating behaviour of the timing of the stratification with the phase of the eddy viscosity. It is likely that the addition of a small  $M_4$  eddy viscosity component affects the timing of the stratification quite significantly, because of the strong sensitivity. This means that the accuracy of turbulence modelling is essential in order to find the correct timing of stratification. One should furthermore be careful in using approximations of the full turbulence signal, because a small change in the turbulence prescription may result in a strong change in the timing of stratification.

A similar sensitivity is found when plotting the phase of the  $M_2$  eddy viscosity against the tidal salt dispersion coefficient, see Figure 40. The transport is almost solely established by the interaction of the  $M_2$  tidal velocity and  $M_2$  depth-averaged salinity. The phase difference between these two components is highly dependent on the phase of the eddy viscosity. Especially the strong change of the transport for  $\nu_{t1}/\nu_{t0} = 1$  around  $\phi_{\nu_t} = 0$  puts very strong requirements on the accuracy of turbulence modelling.

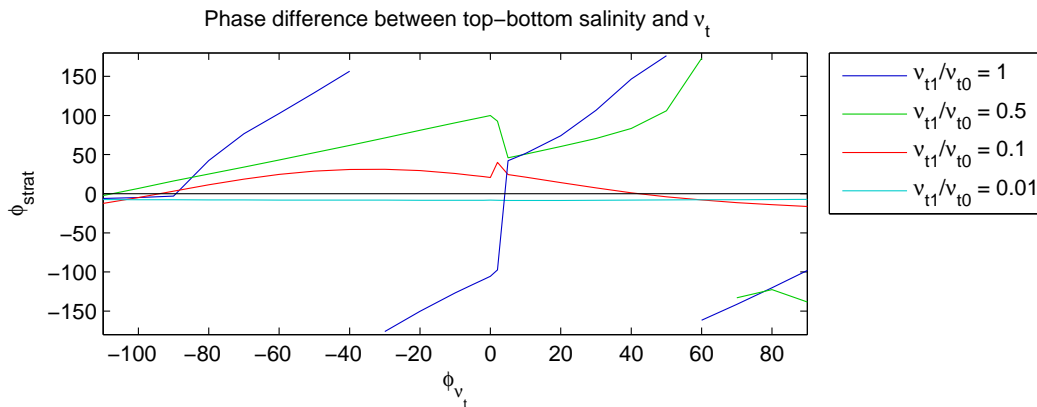


Figure 39: Phase difference (degrees) at  $x = 10$  km between the top-bottom salinity difference and the eddy viscosity as a function of the eddy viscosity. This phase is relative to the phase of the  $M_2$  velocity, i.e.  $\phi_{\nu_t} - \phi_u$ .

The reasons for these strong fluctuations are not fully understood. It was found in the previous section that the effect of small  $M_4$  and residual salinity components can result in large changes in the tidal salt transport. This leaves the possibility that small numerical errors are responsible for the strong fluctuations that were observed. The exclusion of small higher-order velocity and salinity components in the model can similarly have resulted in the strong fluctuations. More research is needed to investigate these dependencies of the tidal salt transport on the turbulence modelling.

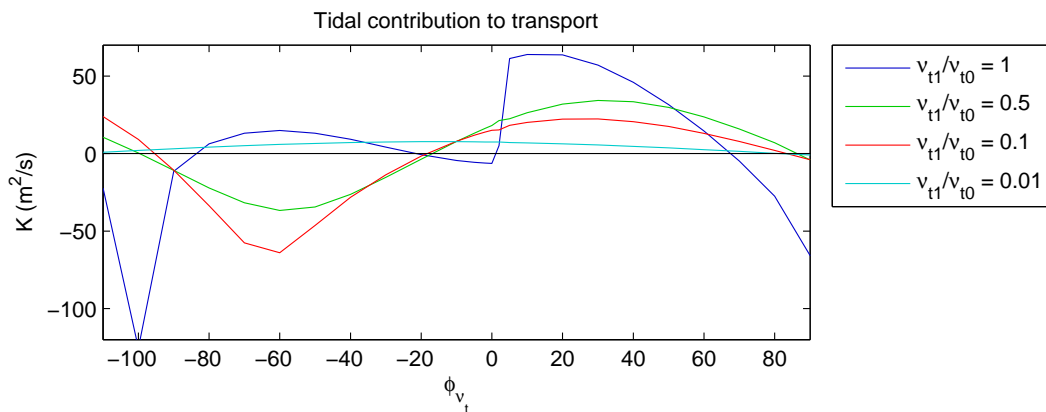


Figure 40: Tidal salt transport expressed by a dispersion coefficient at  $x = 10$  km as a function of the prescribed phase of the eddy viscosity. This phase is relative to the phase of the  $M_2$  velocity, i.e.  $\phi_{v_t} - \phi_u$ .

It can be concluded that, in this 2DV model, it is virtually impossible to prescribe an  $M_2$  eddy viscosity with the right phase so that the stratification and eddy viscosity are in phase or almost in phase. The correct phase is strongly dependent on the magnitude of the eddy viscosity. It is therefore not realistic to describe the effects of stratification on the eddy viscosity by a single  $M_2$  components and more complex turbulence modelling methods are required.

## 5.4. Limitations of the salinity model

The scaling of the salinity and the inclusion of only the leading-order and first-order salinity pose strong restrictions on the range of applicability of the salinity model. The model is only applicable to well-mixed estuaries and the results rely strongly on the parametrised dispersion with coefficient  $K_H$ . We will consider a number of limitations of the model and possible extensions of the salinity model within this idealised modelling framework.

It is argued that the present model scaling is only suitable for well-mixed estuaries and does not apply for partially stratified estuaries, because it does not take the baroclinically induced salt transport into account. It is hypothesised that the baroclinic pressure is capable of producing a salt transport of the same order of magnitude as the tide in partially stratified estuaries. This transport is thought to be caused by the gravitational circulation and gravitational straining circulation, which are the dominant contributions to the exchange flow in the present case. The hypothesis is motivated below.

Let us assume that the velocity, eddy viscosity and salinity can be described by a residual and an  $M_2$  component which are caused by the  $M_2$  tide and the exchange flow. The salt transport can then be described as

$$\langle \hat{u} \hat{s}^1 \rangle = \underbrace{\overline{\hat{u}_1^0 \hat{s}_1^1}}_{M_2 \text{ tidal transport}} + \underbrace{\hat{u}_0 \hat{s}_0^0}_{\text{transport by exchange flows}}.$$

It has been shown that the transport by the  $M_2$  tide consists of two parts: the transport by vertical correlations of  $\hat{u}_1$  and  $\hat{s}_1$  and the transport by temporal correlations of the depth-averaged  $\hat{u}_1$  and  $\hat{s}_1^1$ . The transport by vertical correlations was small in the present case, but can be larger in partially stratified estuaries when the vertical salinity gradient is larger. However, the vertical variation of the tidal velocity is not of  $\mathcal{O}(1)$ , but of  $\mathcal{O}(\delta)$  in most parts of the water column, except for near the bed. It could therefore be argued that the transport by vertical correlations of the tidal flow and salinity is not of  $\mathcal{O}(\delta^2)$ , as is assumed, but of  $\mathcal{O}(\delta^3)$ . Additionally, the vertical stratification and tidal velocity are not completely in phase, but have a small phase difference, which also reduces the transport. The transport by temporal correlations of the tidal velocity and salinity was shown to be highly dependent on the phase difference between the two components. The transport can therefore be of  $\mathcal{O}(\delta^2)$ , but also much smaller.

The transport by the exchange flow is caused by the vertical correlations of the exchange flow and subtidal

salinity. The vertical variation of the exchange flow is of  $\mathcal{O}(\delta)$ . Provided that the exchange flow induces an  $\mathcal{O}(\delta)$   $\hat{s}_0^0$ , the transport by the exchange flow is of  $\mathcal{O}(\delta^3)$ .

There are several factors that can lead to an amplification of the transport by the exchange flow. Firstly, there exists a positive feedback mechanism, which increases the salt transport by exchange flows. The straining of the salt field by the exchange flow induces stronger turbulence asymmetry through strain-induced periodic stratification (SIPS). The straining circulation depends super-linearly on this turbulence asymmetry and is therefore strongly amplified by SIPS. This stronger exchange flow again causes more straining of the salinity field. Secondly, the  $M_2$  salinity can increase the subtidal salinity. To see this, we will solve the first-order salinity equation for the subtidal salinity. The equation, under the above assumptions, reads

$$-(\hat{v}_{t0} \hat{s}_{0,z}^1)_z - (\overline{\hat{v}_{t1}} \hat{s}_{1,z}^1)_z = -u_0^0 s_x^0.$$

The solution to this equation is

$$\hat{s}_0^1 = \int \left( \frac{1}{\hat{v}_{t0}} \int u_0^0 s_x^0 + c_1 \right) - \int \frac{\overline{\hat{v}_{t1}}}{\hat{v}_{t0}} \hat{s}_{1,z}^1 + c_2,$$

where  $c_1$  and  $c_2$  are constants that can be determined with the boundary conditions and the compatibility relation. So the subtidal first-order salinity is determined by the exchange flow and the  $M_2$  salinity.

From the above reasoning it must be concluded that the scaling of the salinity model does not necessarily hold. The salt transport by the tide and exchange flow should therefore be included in the model to test their magnitudes for a parameter space typical for well-mixed and partially stratified estuaries.

If the above hypothesis holds, it can be used to construct a new definition of well-mixed and partially stratified estuaries. This new definition distinguishes both types by the governing physics for salt transport. Well-mixed estuaries can be defined as those estuaries where the exchange flows lead to little salt transport, i.e. a second-order contribution. The scaling of the salinity model holds in these cases. Partially stratified estuaries violate this scaling for the reasons described above. The exchange flows create a first-order contribution to the salt transport in this case. The two types of estuaries have the common property that the water column is well-mixed during part of the tidal cycle. Further research is needed to determine whether such new definitions would be meaningful if lateral salt transport is also taken in consideration.

A large part of the behaviour of the salinity model is determined by the parametrised dispersion. The parametrised dispersion consists mainly of lateral dispersion and lateral variations of longitudinal velocity components. Fischer (1972) has shown that these mechanisms are typically larger than the longitudinal dispersion on the basis of scaling laws and simplified analytical solutions. The fraction of the total transport that is resolved by a 2DV model will therefore always be limited.

Another limitation of the salinity model is the assumption that the along-channel salinity gradient should be small, i.e. of order  $\delta$ . If the salinity gradient becomes too large, the  $M_2$  salinity can become larger than the subtidal salinity at some points in the estuary. This does not only violate the scaling, i.e.  $s^0 \gg s^1$ , but it is also physically impossible, because it means that the salinity becomes negative for some period of time. This means that the requirement that  $\delta$  is small is quite strict. In contrast, this requirement is less strict in the hydrodynamic model, where the solution becomes less accurate when  $\delta$  is not small, but remains physically possible.

The salinity model can be improved by relaxing the assumption that  $s_x$  should be small. This would however bring the salinity advection term  $u s_x$  in the leading-order equations, so that the equations become coupled in the  $x$ -direction and  $z$ -direction. This makes the model more difficult to analyse. Some alternative improvements can be explored within the current scaling. More orders of magnitude can be included in the model. This would include the straining of the salt field by gravitational circulation and gravitational straining circulation in the second-order equation for salinity. It is expected however that the scaling will be violated, because the transport by the exchange flow is larger in partially stratified estuaries than the second-order would suggest. Another possibility would be to include the baroclinic pressure in the leading-order velocity. This would incorporate the straining by exchange flows in the first-order salinity, but would introduce a non-linearity between the hydrodynamics and salt model.

# 6

## Discussion

Since the work done by [Jay and Musiak \(1994\)](#), it is recognised that tidal variations of turbulence are essential for the prediction of exchange flows. A number of studies have investigated the sensitivity of these exchange flows to several estuarine parameters, such as the degree of stratification and bed friction ([Burchard and Baumert, 1998](#); [Stacey et al., 2001](#); [Burchard and Hetland, 2010](#); [Cheng et al., 2011](#)). It has been reported recently that the straining circulation forms the largest contribution to the exchange flow. [Burchard and Hetland \(2010\)](#) find that the exchange flow is composed of approximately 2/3 part by straining circulation and 1/3 part by gravitational circulation. They also find that both contributions to the exchange flow have a similar dependence on the Richardson number, i.e. the along-channel salinity gradient. It has not been explained why the exchange flow has this composition and why the exchange flow has this dependence on the Richardson number. These observations will be explained by providing a better understanding of the processes that govern the exchange flow. For the first time this research identifies the interactions of the gravitational circulation with temporal variations of turbulent mixing as one of the dominant sources of the exchange flow. These interactions will be discussed in Section [6.1](#).

Tidal variations of turbulence are also important for the transport of salt in estuaries. The dependence of salt intrusion on the flow has been investigated by many authors by using idealised models ([Hansen and Rattray, 1965](#); [Jay and Smith, 1990c](#); [McCarthy, 1993](#); [Prandle, 2004](#); [MacCready, 2004](#)) and measurements ([Hughes and Rattray, 1980](#); [Winterwerp, 1983](#); [Bowen and Geyer, 2003](#); [Lerczak et al., 2006](#)). The mechanisms by which tidal variations of turbulent mixing affect the salt intrusion have, however, not been studied systematically. This is partly because of the lack of a method to analyse the output of numerical models in terms of the different contributions to salt intrusion. Such a tool has been developed here. Additionally, a first step has been made in the systematic analysis of the interactions between tidal variations of turbulent mixing, flow and salinity. In Section [6.2](#) we discuss the salt transport induced by the barotropic tidal flow and give an outlook to the importance of exchange flows on salt transport.

### 6.1. Exchange flows

The exchange flows have been studied in a 2DV perturbation model. This model uses a scaling of the momentum equations to separate the solution, i.e. the velocity and water level, in contributions of different orders of magnitude indicated by the small parameter  $\delta$ . This parameter is defined as the ratio of the water level amplitude and the water depth. The model scaling results in a system of equations that is linear at each order of  $\delta$ . The linearity allows us to separate the contributions of different forcing mechanisms of the flow. We have distinguished the tidal flow, river discharge, baroclinic pressure, advection, return flow from Stokes drift and the free surface mixing, which is related to a linearisation of the surface level boundary condition. This research focusses on the contributions from the tidal flow and the baroclinic pressure, because these are the most important mechanisms for creating exchange flows in the parameter space under consideration.

The present model facilitates the investigation of the interactions between turbulence and the flow velocity by separating the interaction into two parts. The perturbation model takes the eddy viscosity as an input function, which is used to calculate the velocity and water level. Conversely, the turbulence model takes the velocity and water level as input and calculates the eddy viscosity on the basis of this velocity and water level. Interactions between the models can be included by iterating between the two models. We will discuss the perturbation model below. The dependence of the turbulence on the velocity and water level is outlined in Section 6.1.2

The perturbation model has been used earlier in combination with small, i.e.  $\mathcal{O}(\delta)$ , temporal variations of the eddy viscosity (Cheng et al., 2010; Chernetsky, 2012). An  $\mathcal{O}(\delta)$  temporal variation of the eddy viscosity adds an  $\mathcal{O}(\delta)$  forcing to the list above: the forcing by interactions of the leading-order velocity gradient and the temporally varying eddy viscosity. The straining circulation in these models is a result of such interactions between the  $M_2$  leading-order tide and the  $M_2$  variations of the eddy viscosity. This straining circulation is a first-order velocity, which will be called the *tidal straining circulation*.

This research takes a novel approach by allowing for large temporal variations of the eddy viscosity. The interactions between the eddy viscosity and the velocity gradient can now no longer be interpreted as a forcing mechanism that is of order  $\delta$ . Instead, the interactions can be an  $\mathcal{O}(1)$  term. Hence, the interactions induce an infinite number of velocity frequency components, some of which can be of the same order as the velocity component that entered in the interactions. The consequences of this can be better understood by looking at different frequency components, in this case the subtidal velocity, the  $M_2$  tide and its overtides. The interactions of for example an  $\mathcal{O}(\delta)$   $M_2$  velocity and the  $M_2$  temporally varying eddy viscosity induce a residual and an  $M_4$  velocity that are also of  $\mathcal{O}(\delta)$ . These residual and  $M_4$  velocity gradients themselves interact with the  $M_2$  eddy viscosity to induce an  $\mathcal{O}(\delta)$  change to the  $M_2$  velocity. The change to the  $M_2$  velocity is of the same order as the original  $M_2$  component. So the different frequency components are mutually coupled to one-another by the temporal variations of the eddy viscosity.

These arguments lead to two types of interactions between the velocity and eddy viscosity. We define the *weakly interacting system* as a system that behaves similar to a system with a small eddy viscosity as has been described above. The interactions between for example the  $\mathcal{O}(1)$   $M_2$  velocity and the  $M_2$  variations of the eddy viscosity induce a velocity of  $\mathcal{O}(\delta)$ . The  $M_2$  velocity itself is hardly changed by interactions between this  $\mathcal{O}(\delta)$  velocity and the temporally varying eddy viscosity. A system is weakly interacting when the interaction between the velocity gradient and the temporally varying eddy viscosity is small, i.e. when either the temporally varying eddy viscosity is of  $\mathcal{O}(\delta)$  or the vertical curvature of the velocity component under consideration is of  $\mathcal{O}(\delta)$ , see Figure 41. The curvature of the velocity component is defined here as  $(\overline{\nu_{tn} u_{m,z}})_z$ , where  $\nu_{tn}$  and  $u_{m,z}$  denote the time-varying frequency components that enter into the interaction and the overline denotes depth-averaging.

*Strongly interacting systems* are defined as those systems in which the different velocity frequency components create new frequency components of the same order via interactions of the velocity gradients and the temporal variations of turbulence. As a result, at least two frequencies of the same order have mutual interactions via the temporal variations of the eddy viscosity. A system is strongly interacting when both the temporal variations of the eddy viscosity and the vertical curvature of the various velocity frequency components are of  $\mathcal{O}(1)$ , see Figure 41. The effect of the interactions on the velocity has a super-linear dependence on the amplitude of the temporally varying eddy viscosity. This means that a small increase in the temporal variations of the eddy viscosity leads to a larger than proportional effect on the interactions.

Both types of systems are found in estuarine flow. The barotropic tidal flow is an example of a weakly interacting system. While the tidal velocity itself is of leading order, its vertical curvature is of first order. The almost logarithmic velocity profile that is associated with the barotropic tidal flow has a small average velocity gradient everywhere, except near the bed, where the eddy viscosity is typically small. This means that the residual flow that is induced by the interaction of the tidal flow and the temporally varying eddy viscosity, i.e. the tidal straining circulation, is much smaller than the tidal flow, see Figure 42. It is important to note that the magnitude and direction of the tidal straining circulation depend on the phase of the eddy viscosity and the bed roughness parametrisation. We will elaborate on this in Section 6.1.1.

The baroclinic flow that is driven by the longitudinal salinity gradient is an example of a potentially strongly

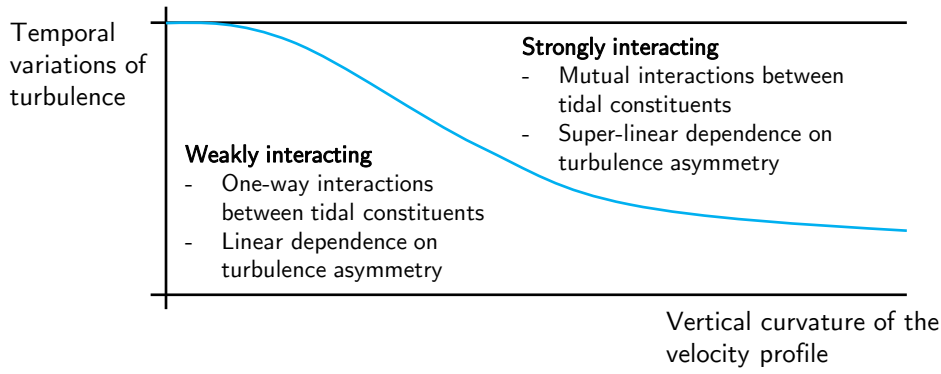


Figure 41: Conceptual representation of the types of velocity-eddy viscosity interactions.

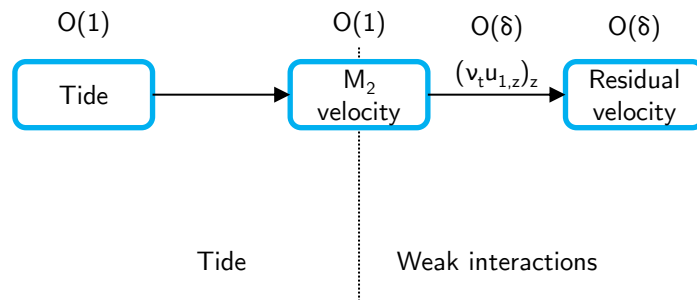


Figure 42: Conceptual visualisation of the weakly interacting tidal flow. TSC: tidal straining circulation.

interacting system. The  $\mathcal{O}(\delta)$  gravitational circulation has a large vertical curvature. So it will induce a strongly interacting system if the temporal variations of turbulence are of  $\mathcal{O}(1)$ . This strongly interacting system is visualised in Figure 43 assuming that the variations of turbulence have an  $M_2$  frequency. In a strongly interacting system, the gravitational circulation induces a velocity of  $\mathcal{O}(\delta)$  with the same frequencies as the temporal variations of mixing. This newly created velocity also has a large curvature and induces an  $\mathcal{O}(\delta)$  amplification of the exchange flow. This contribution to the exchange flow will be called the *gravitational straining circulation*. This gravitational straining circulation is independent of the phase of the eddy viscosity.

The strongly interacting system is most effective when the temporal variations of turbulence are asymmetric on the tidal time-scale. Such an asymmetry of turbulence can be caused by strain-induced periodic stratification (SIPS) (Simpson et al., 1990), but it has been shown that strong asymmetric turbulence can also be obtained without the effect of SIPS. This will be discussed in more detail in Section 6.1.2.

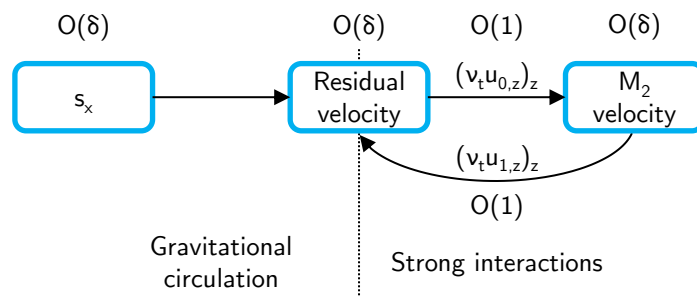


Figure 43: Conceptual visualisation of the strongly interacting baroclinic flow. GC: gravitational circulation. GSC: gravitational straining circulation.

Hence, the straining circulation is composed of at least two major  $\mathcal{O}(\delta)$  contributions if the eddy viscosity varies strongly over the tidal cycle: the tidal straining circulation and the gravitational straining circulation. For the case considered in this thesis, the contribution by the gravitational straining circulation is about 85 to 95% of

the total straining circulation and is therefore considerably greater than the contribution by the tidal straining circulation. So the common interpretation of the straining circulation as the tidal straining circulation describes only a small part of the full straining circulation in the situations under consideration. In these situations, the straining circulation should be interpreted as the gravitational straining circulation.

This new interpretation of the straining circulation offers an explanation for a result obtained by [Burchard and Hetland \(2010\)](#). They conclude that the straining circulation has approximately the same dependency on the Richardson number as the gravitational circulation. It is proved in this research that the gravitational straining circulation and the gravitational circulation have the same dependency on the Richardson number. The largest part of the straining circulation is formed by the gravitational straining circulation through the strong interactions, which explains the dependency.

This framework can also provide a possible explanation for the findings of [Cheng et al. \(2011\)](#) and a comment by [Geyer and MacCready \(2014\)](#). They conclude from model studies that the straining circulation is larger than the gravitational circulation in well-mixed estuaries, while the converse is true in strongly stratified estuaries. They also report that the temporal variations of the eddy viscosity are somewhat smaller in strongly stratified estuaries than in well mixed estuaries. By combining these findings and our results, it can be hypothesised that the strongly interacting system of the gravitational circulation and the temporally varying eddy viscosity creates a strong gravitational straining circulation in the partially stratified estuary. This circulation, however, collapses in strongly stratified estuaries. Hence, the small reduction of the temporal variations of the eddy viscosity in strongly stratified estuaries leads to a strong reduction of the straining circulation. This is consistent with the super-linear dependence of the gravitational straining circulation on the temporal variations of the eddy viscosity.

The exchange flow is decomposed into the contributions by the tidal straining circulation, gravitational straining circulation and gravitational circulation for the case of Chapter 4. This case describes a converging channel with a constant depth of 25 m, which is mainly forced by the tide and salinity. The advection and river discharge are small. The results are presented in Table 6.1. The results in the table are obtained by using a  $k - \varepsilon$  turbulence model and a prescribed salinity gradient. The density is uniform in the water column, so SIPS does not occur; strongly asymmetric turbulence is created by other factors that will be discussed in Section 6.1.2. We define the magnitude of the exchange flow in a similar way as [Burchard and Hetland \(2010\)](#):

$$\|u_0\|_1 = \frac{1}{H} \int_{-H}^0 |u_0 - \bar{u}_0| dz, \quad (6.1)$$

where  $u_0$  denotes the residual flow. This definition does not provide information on the direction of the exchange flow. The separate contributions to the exchange flow can therefore add-up to more than 100%, because some contributions cancel each other in the total exchange flow.

	Longitudinally varying $\nu_t$	Longitudinally constant $\nu_t$
Total exchange flow	0.034 m/s	0.039 m/s
Tidal straining circulation	8 %	3 %
Gravitational straining circulation	55 %	51 %
Gravitational circulation	37 %	44 %
Other	1 %	2 %

Table 6.1: Magnitude of the exchange flow (Equation 6.1) at  $x = 10$  km in the case of Chapter 4 with a  $k - \varepsilon$  turbulence model and a prescribed salinity gradient. The depth-average eddy viscosity at  $x = 10$  km is  $0.1 \text{ m}^2/\text{s}$  for the longitudinally varying eddy viscosity and  $0.078 \text{ m}^2/\text{s}$  for the longitudinally constant eddy viscosity.

Table 6.2 again shows the magnitude of the exchange flow in the same case, but now with the salinity resolved by the salinity model and  $K_H = 100 \text{ m}^2/\text{s}$ . This model uses the  $k - \varepsilon$  turbulence model without density effects.

Tables 6.1 and 6.2 show that the gravitational straining circulation is the dominant contribution to the exchange flow, sometimes explaining over half of the total exchange flow. It is much larger than the tidal straining circulation. The total straining circulation determines around 60% of the exchange flow, while the gravitational circulation explains most of the remaining 40%. These numbers are close to the distribution found by [Burchard](#)

	0 km	20 km	40 km	60 km
Total	0.026 m/s	0.028 m/s	0.029 m/s	0.023 m/s
Tidal straining circulation	18 %	11 %	2 %	3 %
Gravitational straining circulation	43 %	49 %	57 %	56 %
Gravitational circulation	37 %	38 %	39 %	39 %
Other	3 %	4 %	5 %	6 %

Table 6.2: Magnitude of the exchange flow (Equation 6.1) at several location in the case of Chapter 5 with the  $k - \varepsilon$  turbulence model without buoyancy effects in the turbulence model. Note that the percentages sum to more than 100% because of the definition of the magnitude of the exchange flow.

and Hetland (2010): 2/3 straining circulation and 1/3 gravitational circulation. Note that this distribution is not strongly dependent on the timing of the turbulence variations, because the gravitational straining circulation is independent of this timing.

### 6.1.1. Direction of the barotropic tidal straining circulation

The sign and magnitude of the barotropic tidal straining circulation depends on the timing of the eddy viscosity and the bed roughness formulation. The original theory by Jay and Musiak (1994) reasons that the barotropic tidal straining circulation has a velocity profile with two oppositely directed cells, similar to the gravitational circulation. Cheng et al. (2011) and Burchard et al. (2011) have found in model studies that this straining circulation can also possess a three-cell structure. It is found in this study that the barotropic tidal straining circulation can also have a two-cell structure with a reversed direction to the original theory, while the turbulent mixing still has the same time variation as described by Jay and Musiak (1994). A similar reversal has not been observed for the baroclinic pressure straining circulation, which is independent of the timing of the eddy viscosity.

It was already found by Stacey et al. (2008) and Cheng et al. (2010) that the direction of the barotropic tidal straining circulation changes if the eddy viscosity and velocity are over 90 degrees out of phase. This is still consistent with the original theory, because the principles of this theory can still be used to explain this; an increase in mixing leads to more uniform flow profiles and a decrease in mixing leads to less uniform profiles.

The flow reversal or three-cell structure that occurs when the eddy viscosity and velocity are less than 90 degrees out of phase cannot be described with the original theory. These changes are caused by changes to the frictional boundary layer, which act in addition to and opposite to the effect of asymmetric mixing described by Jay and Musiak (1994). It is hypothesised that decreased mixing during ebb leads to a reduction of the ability of bed friction to propagate through the water column, because less mixing is available to support this propagation. This leads to a more uniform velocity profile, instead of the less uniform profile that is created by asymmetric mixing. The converse situation applies to the flood tide. The development of the boundary layer therefore leads to an exchange flow that has an opposite direction to the exchange flow created by asymmetric mixing.

The balance between the two effects depends on the timing of the eddy viscosity and the bed friction formulation. The boundary layer development can lead to a reversal of the barotropic tidal straining circulation for realistic parameter settings, such as those of Chernetsky et al. (2010), if the  $M_2$  eddy viscosity and  $M_2$  velocity are in phase and the eddy viscosity profile is constant. Such a reversal can also occur if the  $M_2$  eddy viscosity and  $M_2$  velocity are in phase and the eddy viscosity profile is parabolic with a no-slip boundary condition. The reversal is found especially for small values of the eddy viscosity.

It is not known whether the reversal of the barotropic tidal straining circulation is a model artefact or that it also happens in real estuaries. The limited number of cases that has been tested with the  $k - \varepsilon$  turbulence model for this study have not shown such a flow reversal. It could therefore be that the flow reversal is a consequence of unrealistic combinations of the prescribed eddy viscosity and bed friction. It is possible that these parameters are modelled consistently in the  $k - \varepsilon$  turbulence model. The flow reversal has also not been observed in earlier model or measurement studies. However, this is probably because only the total straining circulation has been observed. This total straining circulation cannot reverse direction in most cases, because the gravitational straining circulation cannot reverse direction and is larger than the tidal straining circulation.

### 6.1.2. Sources of asymmetric and symmetric mixing

Asymmetric turbulence on a tidal time-scale is the most effective type of temporal variation of turbulence for inducing baroclinic pressure straining circulation. This is because the frequency of the temporally varying eddy viscosity affects the strength of the interacting system. The interactions are strong when the predominant frequency of the eddy viscosity is small. Within the  $M_2$  tidal period, this means that the  $M_2$  variations of the eddy viscosity are most effective for generating a baroclinic pressure straining circulation.

The asymmetric turbulence that is responsible for the straining circulation is often reasoned to originate from strain-induced periodic stratification (SIPS) (Simpson et al., 1990), which has been explained in Section 1. Three more causes of asymmetric turbulence are identified here: asymmetric shear, tidal asymmetry and asymmetric depth. The strongly asymmetric turbulence that has been obtained in this research is due to these factors, as SIPS is not included in the model.

The essential thought behind the asymmetric shear as a source of asymmetric turbulence is that the vertical velocity gradient is responsible for turbulence production, instead of the velocity itself. The gradient is not necessarily related to the magnitude of the depth-averaged velocity. This is especially clear in the case of exchange flows, which are characterised by strong gradients, but have a zero depth-averaged velocity. The combination of the tide and exchange flows is an important source of asymmetric shear (Burchard and Hetland, 2010). The combination of these two flow mechanisms typically results in a velocity profile that has a smaller average velocity gradient during flood than during ebb. This results in a higher degree of mixing during flood than during ebb, similar to the asymmetry that is caused by SIPS. Other sources of asymmetric turbulence are the river discharge, the return flow of Stokes drift and advection. The river discharge and return flow favour the velocity in the ebb flow direction and therefore the velocity gradient and mixing during the ebb tide. The effects of advection on mixing have not been investigated here.

Tidal asymmetry is a special case of asymmetric shear. The asymmetry of the depth-average tidal velocity causes an asymmetry of the velocity shear and therefore an asymmetry in turbulence production. It is insightful to distinguish between tidal asymmetry and asymmetric shear, because it provides an intuitive explanation for how the deformation of the tidal wave affects turbulent mixing. Asymmetric depth describes that the depth-averaged eddy viscosity depends on the water depth. A larger average depth during either ebb or flood will therefore lead to turbulence asymmetry.

The lowest-frequency symmetric variation of turbulence on the  $M_2$  tidal time-scale is the  $M_4$  frequency. Turbulence variations at this frequency can also be quite effective in promoting a strongly interacting system. The  $M_4$  variation of turbulence is for example created by any  $M_2$  velocity component, such as the tide or the  $M_2$  signal that is created by the baroclinic pressure. The  $M_4$  variation was small in the case considered in this research compared to the  $M_2$  variation. However, it tends to be strong in tidal channels if the turbulence asymmetry is less pronounced (Stacey et al., 2008; Burchard and Hetland, 2010; Stacey et al., 2010), because a major part of the turbulence production from the  $M_2$  tide is absent during slack tide. A strong turbulence asymmetry is therefore not essential to obtaining strongly interacting systems.

### 6.1.3. Exchange flows by other processes

A number of processes that have not been considered in this study are known to have an important effect on the exchange flows in certain cases. Lateral circulation can create a longitudinal exchange flow similar to the gravitational circulation, which is of the same or larger magnitude (Fischer, 1972; Lerczak and Geyer, 2004). Additionally the lateral circulation creates an additional contribution to straining circulation (Burchard and Schuttelaars, 2012).

Additional effects that can create exchange flows are wind (Scully et al., 2005), wind induced density straining (Burchard and Hetland, 2010), the Earth's rotation (Lerczak and Geyer, 2004; Huijts et al., 2006) and flow curvature (Chant, 2002). Li and O'Donnell (2005) have shown that advection can create a significant contribution to the exchange flow if a different parameter space is used than in this research.

## 6.2. Salt intrusion

The 2DV scaled salinity model that has been used provides a structure that is convenient for studying the transport of salt. The leading-order salinity is constant in time and in the vertical direction. Hence, the equation for this leading-order salinity takes the form of a 1DH transport equation that includes the net transport that is induced by vertical and temporal variations of the salinity. The equation resolves the transport that is caused by the river discharge and tide and contains a salinity dispersion term that parametrises all other processes (McCarthy, 1993). The first-order salinity describes the vertical and temporal variations of the salinity and is forced by the tidal straining of the along-channel salinity. We have focussed on the dependence of the tidal salinity transport on the complexity of the turbulence model.

The tidal transport in the present model is caused by two types of interactions that can be separated along the lines of Fischer (1972). The first is the interaction between the vertical salinity profile and the tidal velocity profile, the *tidal oscillatory shear transport*. The tidal oscillatory shear transport was negligible in the case considered in this research, because of the high degree of mixing. Significant contributions by this mechanism can be obtained with the present model with different parameter configurations, as is shown by Wei et al. (2014).

The second is the interaction between the temporally varying depth-averaged components of the salinity and tidal velocity, which could be called *tidal oscillatory mean transport*. This transport is zero if turbulent mixing is assumed to be constant in time, because the depth-averaged velocity and salinity are 90 degrees out of phase.  $\mathcal{O}(\delta)$  temporal variations of mixing have been applied to the salinity model by Cheng et al. (2010). These variations do not affect the salinity model up to the first-order salinity. This motivates the inclusion of large variations of turbulent mixing in order to study the tidal oscillatory mean transport.

The novel extension of the salinity model with  $\mathcal{O}(1)$  temporal variations of turbulence makes it possible to study this tidal oscillatory mean transport. The depth-averaged tidal velocity and salinity are still almost out of phase if the eddy viscosity varies strongly in time. However, a few degrees deviation from such 90 degrees phase difference already results in a significant salt transport. This makes the salt transport highly sensitive to small variations of the timing of the temporally varying salinity.

The small phase difference between the tidal velocity and salinity is caused by the interactions between the first-order salinity and the temporally varying eddy viscosity. The first-order salinity can be classified as a weakly interacting system in well-mixed to partially stratified estuaries, because the vertical curvature of the salinity is small. In the present case, the  $M_2$  salinity is the dominant component. The other salinity frequencies are also forced by small tidal constituents. These salinity frequencies are much smaller than the  $M_2$  salinity, but still strong enough to have a small effect on the  $M_2$  salinity via interactions with the eddy viscosity. This small effect manifests as a small change of the phase of the  $M_2$  salinity, which results in a significant salt transport.

The tidal oscillatory mean transport is also highly sensitive to the phase and magnitude of the temporally varying eddy viscosity. This stresses the importance of accurate turbulence modelling for the tidal transport. It also stresses the need for further research, as the dependency of the tidal transport on the temporal variations of the eddy viscosity are not well understood.

The importance of exchange flows for salt transport in well-mixed to partially stratified estuaries is a topic of ongoing debate. The transport by exchange flows is called *steady shear dispersion* (Taylor, 1953) and is by the correlation of vertical variations of the exchange flow velocity and salinity. The transport by gravitational circulation is the only model resolved transport mechanism opposing the river discharge in the models of Hansen and Rattray (1965), MacCready (2004) and Ralston et al. (2008). Prandle (2004) uses the same approach and extends this by taking a first step in adding straining circulation. Lerczak et al. (2006) support that the steady shear dispersion is the largest contribution to salt transport by analysing measurements in the Hudson River estuary. Fischer (1972) and McCarthy (1993), on the other hand, find from scaling arguments that transport by gravitational circulation is small.

First results of this research indicate that the scaling approach is only valid for well-mixed systems. The scaling approach is hypothesised to become inaccurate in partially stratified systems, because the steady shear

dispersion is not taken into account by the model, while it is as important as the salt transport by the tide. On the one hand the tidal salt transport can become smaller than  $\mathcal{O}(\delta^2)$ , which is the magnitude suggested by the scaling. The tidal oscillatory shear transport can become an  $\mathcal{O}(\delta^3)$  transport, because the vertical variation of the tidal velocity is small in a large part of the water column. The tidal oscillatory mean transport was shown to be highly sensitive to small phase changes of the salinity and can therefore be of  $\mathcal{O}(\delta^2)$ , but also much smaller. On the other hand the steady shear dispersion can become larger than the  $\mathcal{O}(\delta^3)$  suggested by the scaling. Steady shear dispersion is caused by the correlation of the exchange flow velocity and straining of the subtidal salinity. The straining of the subtidal salinity leads to a stronger asymmetry of turbulent mixing, which induces a stronger exchange flow and therefore more straining. This positive feedback increases the steady shear dispersion. Additionally, the interaction between the temporally varying salinity and turbulence can increase the straining of the subtidal salinity.

This hypothesis can be used to formulate a new definition of well-mixed and partially stratified estuaries which is based on the governing physics of salt transport. A well-mixed estuary can be defined as a system that has a well-mixed water column during a part of the tidal cycle and in which the salt transport by exchange flows is negligible. Well-mixed estuaries are therefore estuaries that comply with the present scaling approach for the salinity model. A partially stratified estuary also has a well-mixed water column during a part of the tidal cycle, but the salt transport by exchange flows is of the same order as the salt transport by the tide. The scaling of the salt model becomes invalid due to the importance of the velocity gradient and the feedback described above. These definitions fit within the estuarine classifications of [Hansen and Rattray \(1966\)](#), [Geyer \(2010\)](#) and [Geyer and MacCready \(2014\)](#), but have not been made explicit as is done here.

Further research is required to establish if these definitions are useful when considering salt transport by variations in the lateral dimensions. The salt transport by lateral processes and lateral variations of along-channel processes can form the dominant contribution to the salt transport ([Fischer, 1972](#)). Further research into these processes is therefore essential to obtaining a good understanding of salt transport in well-mixed and partially stratified estuaries.

Research into the mechanisms that are responsible for salt transport requires increasingly complex models. Suitable tools are required to study the contributions of the different physical forcing mechanisms to salt transport in these models. Decomposition techniques for analysing salt transport have been used for analysing measurements ([Hughes and Rattray, 1980](#); [Winterwerp, 1983](#); [Bowen and Geyer, 2003](#); [Lerczak et al., 2006](#)), but not so extensively for analysing model output of complex models. The framework by [Fischer \(1972\)](#) has been used here to develop two tools for analysing salt transport in models by dispersion coefficients. One tool is suitable for the idealised perturbation model and separates the salt transport in the contributions by different physical mechanisms. This is generally not possible for complex models, in which case the decomposition by [Fischer \(1972\)](#) can be used to find a useful decomposition.

The conversion of the salt transport contributions to equivalent dispersion coefficients establishes a connection between complex 2DV or 3D models or measurements and 1DH models. Dispersion coefficients in a 1DH sense are known for many estuaries around the world and have been widely studied ([Savenije, 2005](#); [Kuijper and Van Rijn, 2011](#)). Hence, the connection of complex models or measurements and 1DH models could provide more insight into the interpretation of complex model output.

# Conclusions

The novel extension of an idealised perturbation model for estuarine flow by a turbulence model has led to new insights into the mechanisms that create exchange flows and tidal salinity transport in well-mixed to partially stratified estuaries. A new mechanism that creates straining circulation has been identified and it is shown that this mechanism can explain most of the straining circulation and a dominant part of the total exchange flow in well-mixed to partially stratified estuaries. This new mechanism also provides an explanation for the open questions why the gravitational circulation and straining circulation have a similar dependence on the along-channel salinity gradient and why the straining circulation is strongly reduced in the transition from partially stratified to strongly stratified estuaries.

A new framework has been developed to explain the interactions between the temporal variations of the eddy viscosity and the flow velocity that induce straining circulation. We identify two types of interacting systems. The weakly interacting system is found if either the temporal variations of turbulence are small or the vertical curvature of the velocity profile is small. The latter condition applies for the barotropic tide, which' near-logarithmic velocity profile has a small rate of curvature. The weakly interacting system is characterised by small interactions between different frequency components of the flow velocity. Hence, the interactions between the  $M_2$  tidal velocity and the temporal variations of the eddy viscosity result in a residual velocity and overtides which are much smaller than the  $M_2$  tidal velocity itself. The  $M_2$  tidal velocity itself is hardly affected by interactions between other velocity frequency components and the eddy viscosity. The exchange flow that is created from this process is called the *tidal straining circulation*.

Conversely, the strongly interacting system is found if both the temporal variations of turbulent mixing and the vertical curvature of the velocity profile are large. The condition of a strongly curving velocity profile applies for gravitational circulation, so that a strongly interacting system is formed if the tidal variations of mixing are large. The strongly interacting system is characterised by mutual interactions between different velocity frequency components. Hence, the gravitational circulation interacts with the tidal variations of turbulence to create a velocity with the same frequencies as the tidal variations of turbulence. These velocity components have a curvature similar to the gravitational circulation and also interact with the temporally varying turbulent mixing to amplify other frequency components, among which the exchange flow. Such amplification of the residual flow is called the *gravitational straining circulation*.

Several factors have been identified that provide the strong tidal variations of mixing. Factors that cause an asymmetry of turbulence on the longest tidal time-scale, i.e.  $M_2$  frequency when considering the  $M_2$  tide, are the most effective for creating a strongly interacting system. Asymmetric turbulence is classically associated with SIPS. However, asymmetric shear has been shown to also cause strongly asymmetric turbulence. The exchange flow and flood dominance are important sources of asymmetric shear and create a similar asymmetric turbulence as is associated with SIPS. The river discharge, return flow of Stokes drift and ebb dominance create asymmetric turbulence with an opposite timing. Symmetric variations of turbulence, e.g.  $M_4$  frequency variations when considering the  $M_2$  tide, are often strong in tidally energetic estuaries with little asymmetric turbulence. These  $M_4$  variations can also lead to a strongly interacting system, but are less effective in doing so than the longer  $M_2$  variations.

So the tidal flow and baroclinic pressure result in three major contributions to the exchange flow:

1. the gravitational circulation,
2. the gravitational straining circulation, and
3. the tidal straining circulation.

These contributions have been quantified in a case study of a well-mixed estuary with the inclusion of the salinity model and a  $k-\varepsilon$  model without buoyancy effects. The gravitational circulation contributes about 40% of the exchange flow and the straining circulation about 60%. This distributions agrees with earlier findings. The gravitational straining circulation contributes up to 95% of the total straining circulation.

The gravitational straining circulation does not depend on the phase of the temporally varying turbulence. Its magnitude depends super-linearly on the amplitude of the temporally varying turbulence. This provides a possible explanation for the question why the straining circulation is dominant in partially stratified estuaries with strongly varying turbulence and much smaller in strongly stratified estuaries with only slightly less tidal variation of turbulence. The magnitude of the gravitational straining circulation and gravitational circulation both depend linearly on the along-channel salinity gradient. This explains that the straining circulation and gravitational circulation have a similar dependency on the salinity gradient.

We have separated the tidal straining circulation into two parts. The first is the well-known part that has a profile similar to the gravitational circulation and is caused directly by asymmetric mixing. A new part has been identified that is caused by a changing shape of the frictional boundary layer as a consequence of asymmetric mixing. This part has an opposite direction to the gravitational circulation and therefore opposes the first part. The balance between the two contributions is determined by a combination of the phase of the temporally varying eddy viscosity and the bed friction formulation. The second, newly identified effect can lead to a reversal of the direction of the tidal straining circulation for a realistic parameter space in parametrisations with a constant eddy viscosity or a parabolic eddy viscosity with no-slip boundary condition. Such a reversal has not been observed when using a  $k-\varepsilon$  turbulence model. It is unknown whether the reversal can occur in nature or whether it is a model artefact.

We have made a first step in analysing the tidal salt transport under tidal variations of turbulent mixing. Temporal variations of mixing create a process by which the tidal flow can transport salt that does not exist if the turbulent mixing is constant in time. This new transport is created by the correlation of the depth-averaged tidal salinity variations and the depth-averaged tidal velocity. Whereas these components are out of phase under the assumption of constant mixing, tidal variations of mixing can cause a phase shift of the tidal salinity. Even a small phase shift of the salinity can lead to a significant salt transport. The vertical and temporal variations of salinity form a weakly interacting system in well-mixed estuaries. The weak interactions are nevertheless sufficient to create a small phase shift of the tidal salinity and therefore a tidal contribution to the salt transport. This transport was the dominant source of transport in the well-mixed case considered in this research.

A sensitivity study has shown a very high sensitivity of the tidal salt transport to the phase and magnitude of a prescribed  $M_2$  eddy viscosity. Such a high sensitivity stresses the importance of accurate turbulence modelling to the modelling of salt transport. The sensitivity is not yet fully understood and more research is required to establish why these dependencies exist and what detail of turbulence modelling is needed to model salt transport to the desired accuracy.

# Recommendations

A robust and computationally efficient coupling of the hydrodynamic model and the turbulence model would provide the possibility to study the physics of complex interactions between flow and turbulence further. The coupling presently only converges if buoyancy is not taken into account, which is a serious limitation for further study into the physics of stratified estuaries. The iteration procedure additionally uses a strong under-relaxation method which is highly inefficient. It is therefore recommended to investigate stable ways of coupling the hydrodynamics model and turbulence model.

The robust coupling of the turbulence model to the flow model assists in the analysis of the sensitivity of the tidal salt transport to turbulence. The results of this research indicate a very strong sensitivity of the tidal salt transport to the timing of the turbulent mixing. However, this sensitivity is not yet well understood. More research into this would lead to a better understanding of salt transport. It would also lead to a better understanding of the complexity of turbulence modelling that is required in order to simulate the salt dynamics with a reasonable accuracy.

A question that is left open in this research is whether the flow reversal of the tidal straining circulation occurs in reality or whether it is a model artefact. An experiment would be required to test this. In either case the flow reversal is an interesting phenomenon and provides information about suitable choices for roughness parameters and eddy viscosity in idealised models and about the physical nature of the tidal straining circulation.

The hydrodynamic model provides possibilities to extend the research to the transition between partially stratified and strongly stratified estuaries. The river discharge and baroclinic pressure could easily be made leading-order effects in the equations. In order to model the full transition from partially stratified to strongly stratified estuaries, a salinity model and turbulence model should be coupled to the hydrodynamics model. A first step would, however, be to use the salinity and turbulence fields from complex models in the idealised model to study the importance of different physical forcing mechanisms.

This research also provides interesting clues for further research into spring-neap cycles. It has been shown that long tidal waves are most suitable for creating a strong straining circulation. It is therefore expected that spring-neap tidal cycles can play a significant role in the creation of straining circulation. This would have consequences for the validity of considering only one average  $M_2$  tide to determine the net transport in an estuary.

Concerning the salinity model, it has been hypothesised that the model scaling only holds for well-mixed estuaries. Interactions between flow, salinity and turbulence are expected to lead to a strong amplification of the salt transport by gravitational circulation in partially stratified estuaries. Such amplifications are not captured in the scaling of the equations. The salt transport by gravitational circulation can be captured in the model in two ways. The first is by including the second-order salinity. In view of the above described amplifications it is however expected that this second-order salinity is actually larger than expected from the scaling. The second is by including the gravitational circulation as a leading-order velocity. This would however lead to a non-linear coupling between the hydrodynamic and salinity model. It is recommended to look into the best way of incorporating the gravitational circulation into the salinity model to expand its range of applicability.

A different route of extending the salinity model would be to include the lateral dimension. It has been shown frequently that the lateral dimension contains many essential mechanisms that explain salt transport.

Idealised models tend more to complex models if they are extended by an increasing number of dimensions, physics and linear or non-linear interactions. In order to study increasingly complex processes, but still have an understandable idealised model, it is useful to look at a combination of idealised models, complex models and

measurements. This hybrid use of models allows one to use the strengths of each of these methods. A possible strategy is to use measurements to identify trends and patterns and to calibrate complex models. These complex model can then be used to identify a selection of physical mechanisms that are expected to be important for the process under consideration. Idealised models can then be used to study these physical mechanisms in detail and understand the possibly non-linear interactions between the mechanisms.

The further development of the methods for making a decomposition of the salt transport can also be regarded in light of the combined use of complex and idealised models. The analysis of salt fluxes in a 3D model in terms of 1D dispersion coefficients is likely to provide more insight into the results of complex models, as well as help the development of better idealised 1D models.

# Bibliography

- Bowen, M. M. and Geyer, W. R. (2003). Salt transport and the time-dependent salt balance of a partially stratified estuary. *Journal of Geophysical Research*, 108:3158.
- Burchard, H. and Baumert, H. (1998). The formation of estuarine turbidity maxima due to density effects in the salt wedge. a hydrodynamic process study. *Journal of Physical Oceanography*, 28:309–321.
- Burchard, H. and Hetland, R. D. (2010). Quantifying the contributions of tidal straining and gravitational circulation to residual circulation in periodically stratified tidal estuaries. *Journal of Physical Oceanography*, 40:1243–1262.
- Burchard, H., Hetland, R. D., Schulz, E., and Schuttelaars, H. M. (2011). Drivers of residual estuarine circulation in tidally energetic estuaries: Straight and irrotational channels with parabolic cross section. *Journal of Physical Oceanography*, 41:548–570.
- Burchard, H. and Schuttelaars, H. M. (2012). Analysis of tidal straining as driver for estuarine circulation in well-mixed estuaries. *Journal of Physical Oceanography*, 42:261–271.
- Chant, R. J. (2002). Secondary circulation in a region of flow curvature: relationship with tidal forcing and river discharge. *Journal of Geophysical Research*, 107:3131.
- Cheng, P., Valle-Levinson, A., and De Swart, H. E. (2010). Residual currents induced by asymmetric tidal mixing in weakly stratified narrow estuaries. *Journal of Physical Oceanography*, 40:2135–2147.
- Cheng, P., Valle-Levinson, A., and De Swart, H. E. (2011). A numerical study of residual circulation induced by asymmetric tidal mixing in tidally dominated estuaries. *Journal of Geophysical Research*, 116:C01017.
- Chernetsky, A. S. (2012). *Trapping of sediment in tidal estuaries*. PhD thesis, TU Delft.
- Chernetsky, A. S., Schuttelaars, H. M., and Talke, S. A. (2010). The effect of tidal asymmetry and temporal settling lag on sediment trapping in tidal estuaries. *Ocean Dynamics*, 60:1219–1241.
- Deltares (2014). *Delft 3D user manual*. Version 3.15.34158.
- Dijkstra, Y. M. (2014). Turbulence modelling in geophysical flows. Improving the numerical accuracy of the  $k - \varepsilon$  model by a mathematical transformation. Master's thesis, TU Delft.
- Fischer, H. B. (1972). Mass-transport mechanisms in partially stratified estuaries. *Journal of Fluid Mechanics*, 53:671–687.
- Fischer, H. B., List, E. J., Koh, R. C. Y., and Imberger, J. (1979). *Mixing in inland and coastal waters*. Academic press, New York.
- Friedrichs, C. T. (2010). *Contemporary issues in estuarine physics*, chapter Barotropic tides in channelized estuaries, pages 27–61. Cambridge University Press, Cambridge, UK.
- Friedrichs, C. T. and Aubrey, D. G. (1988). Non-linear tidal distortion in shallow well-mixed estuaries: a synthesis. *Estuarine Coastal and Shelf Science*, 27:521–545.
- Geyer, W. R. (2010). *Contemporary issues in estuarine physics*, chapter Estuarine salinity structure and circulation, pages 12–26. Cambridge University Press, Cambridge, UK.
- Geyer, W. R. and MacCready, P. (2014). The estuarine circulation. *Annual Review of Fluid Mechanics*, 46:175–197.

- Hansen, D. V. and Rattray, M. (1965). Gravitational circulation in straits and estuaries. *Journal of Marine Research*, 23:104–122.
- Hansen, D. V. and Rattray, M. (1966). New dimensions in estuary classification. *Limnology and Oceanography*, 11:319–326.
- Hinze, J. O. (1975). *Turbulence*. McGraw-Hill, New York.
- Hughes, F. W. and Rattray, M. (1980). Salt flux and mixing in the Columbia River estuary. *Estuarine and Coastal Marine Science*, 10:479 – 493.
- Huijts, K. M. H., Schuttelaars, H. M., De Swart, H. E., and Valle-Levinson, A. (2006). Lateral entrainment of sediment in tidal estuaries: and idealized model study. *Journal of Geophysical Research*, 111:C12016.
- Ianniello, J. P. (1977). Tidally induced residual currents in estuaries of constant breadth and depth. *Journal of Marine Research*, 35:755–786.
- Ianniello, J. P. (1979). Tidally induced residual currents in estuaries of variable breadth and depth. *Journal of Physical Oceanography*, 9:962–974.
- Ippen, A. T. and Harleman, D. R. F. (1961). One-dimensional analysis of salinity intrusion in estuaries. Technical report, Technical bulletin no. 5, Committee on tidal hydraulics, Corps of engineers, U.S. Army.
- Jay, D. A. and Musiak, J. D. (1994). Particle trapping in estuarine tidal flows. *Journal of Geophysical Research - Oceans*, 99:20445–20461.
- Jay, D. A. and Smith, J. D. (1990a). Circulation, density distribution and neap-spring transitions in the Columbia River estuary. *Progress in Oceanography*, 25:81 – 112.
- Jay, D. A. and Smith, J. D. (1990b). Residual circulation in shallow estuaries 1. Highly stratified, narrow estuaries. *Journal of Geophysical Research - Oceans*, 95:711–731.
- Jay, D. A. and Smith, J. D. (1990c). Residual circulation in shallow estuaries 2. Weakly stratified and partially mixed, narrow estuaries. *Journal of Geophysical Research - Oceans*, 95:733–748.
- Kuijper, K. and Van Rijn, L. C. (2011). Analytical and numerical analysis of tides and salinities in estuaries; part II: salinity distributions in prismatic and convergent tidal channels. *Ocean Dynamics*, 61:1743–1765.
- Lanzoni, S. and Seminara, G. (1998). On tide propagation in convergent estuaries. *Journal of Geophysical Research*, 103:30793–30812.
- Lauder, B. E., A. M., Rodi, W., and Spalding, D. B. (1972). The prediction of free shear flows - a comparison of the performance of six turbulence models. In *NASA conference on free shear flows, Langley*.
- Lerczak, J. A. and Geyer, W. R. (2004). Modelling the lateral circulation in straight, stratified estuaries. *Journal of Physical Oceanography*, 34:1410–1428.
- Lerczak, J. A., Geyer, W. R., and Chant, R. J. (2006). Mechanisms driving the time-dependent salt flux in a partially stratified estuary. *Journal of Physical Oceanography*, 36:2296–2311.
- Li, C. and O'Donnell, J. (2005). The effect of channel length on the residual circulation in tidally dominated estuaries. *Journal of Physical Oceanography*, 35:1826–1840.
- MacCready, P. (2004). Toward a unified theory of tidally-averaged estuarine salinity structure. *Estuaries*, 27:561–570.
- McCarthy, R. K. (1993). Residual currents in tidally dominated, well-mixed estuaries. *Tellus*, 45A:325–340.
- McGregor, R. C. (1972). Influence of eddy viscosity on vertical distribution of velocity in tidal estuary. *Geophysical Journal of the Royal Astronomical Society*, 29:103–108.
- Mellor, G. L. and Yamada, T. (1982). Development of a turbulence closure model for geophysical fluid problems. *Reviews of geophysics and space physics*, 20:851–875.

- Mohammadi, B. and Pironneau, O. (1994). *Analysis of the k-epsilon turbulence model*. Wiley.
- Monismith, S. G. (2010). *Contemporary issues in estuarine physics*, chapter Mixing in estuaries, pages 145–185. Cambridge University Press, Cambridge, UK.
- Murray, A. B. (2003). Contrasting the goals, strategies, and predictions associated with simplified numerical models and detailed simulations. In Wilcock, P. R. and Iverson, R. M., editors, *Prediction in Geomorphology*, pages 151–165. American Geophysical Union.
- Patankar, S. V. (1980). *Numerical Heat Transfer and Fluid Flow*. McGraw-Hill, New York.
- Pope, S. B. (2000). *Turbulent flows*. Cambridge university press, Cambridge, UK.
- Prandle, D. (2004). Saline intrusion in partially mixed estuaries. *Estuarine Coastal and Shelf Science*, 59:385–397.
- Pritchard, D. W. (1955). Estuarine circulation patterns. *Proceedings, American Society of Civil Engineers*, 81:1–11.
- Ralston, D. K., Geyer, W. R., and Lerczak, J. A. (2008). Subtidal salinity and velocity in the Hudson River estuary: observations and modelling. *Journal of Physical Oceanography*, 38:753–770.
- Rodi, W. (1993). *Turbulence models and their application in Hydraulics - a state of the art review*. IAHR, Delft, the Netherlands, 3rd edition. Balkema.
- Savenije, H. H. G. (2005). *Salinity and tides in alluvial estuaries*. Elsevier, Amsterdam, the Netherlands.
- Scully, M. E., Friedrichs, C. T., and Brubaker, J. M. (2005). Control of estuarine stratification and mixing by wind-induced straining of the estuarine density field. *Estuaries*, 28:321–326.
- Simpson, J. H., Brown, J., Matthews, J., and Allen, G. (1990). Tidal straining, density currents, and stirring in the control of estuarine stratification. *Estuaries*, 13:125–132.
- Souza, A. J. (2013). On the use of the Stokes number to explain frictional tidal dynamics and water column structure in shelf seas. *Ocean Science*, 9:391–398.
- Stacey, M. T., Brennan, M. L., Burau, J. R., and Monismith, S. G. (2010). The tidally averaged momentum balance in a partially and periodically stratified estuary. *Journal of Physical Oceanography*, 40:2418–2434.
- Stacey, M. T., Burau, J. R., and Monismith, S. G. (2001). Creation of residual flows in a partially stratified estuary. *Journal of Geophysical Research - Oceans*, 106:17013–17037.
- Stacey, M. T., Fram, J. P., and Chow, F. K. (2008). Role of tidally periodic density stratification in the creation of estuarine subtidal circulation. *Journal of Geophysical Research - Oceans*, 113:C08016.
- Taylor, G. T. (1953). Dispersion of soluble matter in solvent flowing slowly through a tube. *Proceedings of the Royal Society of London*, A219:186–203.
- Tennekes, H. and Lumley, J. L. (1972). *A first course in turbulence*. MIT press, Boston, MA.
- Tirao, J. A. (2003). The matrix-valued hypergeometric equation. *PNAS*, 100:8138–8141.
- Uittenbogaard, R. E., Van Kester, J. A. T. M., and Stelling, G. S. (1992). Implementation of three turbulence models in 3D-TRISULA for rectangular grids. Technical Report Z81, WL | Delft Hydraulics, Delft, the Netherlands.
- Valle-Levinson, A. (2010). *Contemporary issues in estuarine physics*, chapter Definition and classification of estuaries, pages 1–11. Cambridge University Press, Cambridge, UK.
- Wei, X., Schramkowski, G. P., and Schuttelaars, H. M. (2014). Salt dynamics in well-mixed estuaries: importance of advection by the tides. In *Proceedings of the 17th physics of estuaries and coastal seas (PECS) conference, Porto de Galinhas, Pernambuco, Brazil, 19-23 October 2014*.
- Winterwerp, J. C. (1983). Decomposition of the mass transport in narrow estuaries. *Estuarine Coastal and Shelf Science*, 16:627–638.



# A

## Derivation and solution hydrodynamics

This appendix presents the details of the hydrodynamics model that was introduced in Chapter 2. The assumptions regarding the shape of the estuary and the equations were introduced in that chapter. Section A.1 then treats the scaling of the equations and ends with an overview of the ordered set of equations. The subsequent sections treat the solution methods for the several versions of the model that were introduced in table 2.1 up to Version 4. The coupling of the model to the  $k - \varepsilon$  model in Version 5 is treated in Appendix C. Analytical solutions will be given for Version 1 and 2. The Versions 3, 4 and 5 are solved numerically, but the analytical solution procedure to Version 3 is provided in Section A.6. Finally, Section A.7 presents the numerical grid and discretisation methods.

### A.1. Scaling the equations

The three equations for continuity, momentum conservation and depth-averaged continuity in 2DV are repeated below

$$u_x + w_z - \frac{u}{L_b} = 0, \quad (\text{A.1})$$

$$u_t + uu_x + wu_z = -g\zeta_x - g \int_z^\zeta \frac{\rho_x}{\rho_0} dz + (\nu_t u_z)_z, \quad (\text{A.2})$$

$$\zeta_t + \left( \int_{-H}^\zeta u dz \right)_x - \frac{1}{L_b} \int_{-H}^\zeta u dz = 0. \quad (\text{A.3})$$

The equations are transformed to a dimensionless system by using a scaling argument in order to establish the order of magnitude of the several terms. The equations are scaled by using five typical scales, which are presented in Table A.1.

This table presents three more scales that are derived from the other five. The velocity scale  $U$  follows from the scaling of the depth-averaged continuity equations

$$\zeta_t + (H\bar{u})_x = \frac{H\bar{u}}{L_b}.$$

This equation can be expressed in dimensionless quantities according to

$$\frac{A_{M_2}}{T_{M_2}} \zeta_{t^*} + \frac{H_0 U}{L_{tide}} (H^* \bar{u}^*)_{x^*} = \frac{H_0 U}{L_b} H^* \bar{u}^*$$

Scale		Dimensionless quantity
$T_{M_2}$	$M_2$ tidal period	$t = T_{M_2} t^*$
$A_{M_2}$	$M_2$ tidal amplitude at the seaward side	$\zeta = A_{M_2} \zeta^*$
$H_0$	Average depth at seaward side	$z = H_0 z^*$
$L_{tide}$	Tidal wave length	$x = L_{tide} x^*$
$\mathcal{R}_x$	Typical density gradient	$\rho_x = \mathcal{R}_x \rho_x^*$
Derived scale		Dimensionless quantity
$U$	Typical horizontal velocity of the $M_2$ tide	$u = U u^*$
$W$	Typical vertical velocity of the $M_2$ tide	$w = W w^*$
$\mathcal{N}$	Typical eddy viscosity	$\nu_t = \mathcal{N} \nu_t^*$

Table A.1: Scales and derived scales for deriving the dimensionless equations.

In order to remain consistent, the velocity scale  $U$  is defined as

$$U = \frac{A_{M_2}}{T_{M_2}} \frac{\min(L_{tide}, L_b)}{H_0} \approx \frac{A_{M_2}}{T_{M_2}} \frac{L_{tide}}{H_0}$$

It is assumed that either  $L_b > L_{tide}$  or  $\frac{L_b}{L_{tide}} = \mathcal{O}(1)$ , such that  $\min(L_{tide}, L_b)$  can be replaced by  $L_{tide}$ . Similar to  $U$ ,  $W$  is derived from the continuity equation A.1. It follows that

$$W = \frac{H}{L_{tide}} U.$$

The typical eddy viscosity follows from the stationary barotropic momentum balance  $(\nu_t u_z)_z = g \zeta_x$ . It follows that

$$\mathcal{N} = \frac{H_0^2}{T_{M_2}}.$$

### A.1.1. Scaling the momentum equation

The dimensionless momentum equation is then given by

$$\begin{aligned} \frac{U}{T_{M_2}} u_{t^*}^* + \frac{U^2}{L_{tide}} u^* u_{x^*}^* + \frac{WU}{H_0} w^* u_{z^*}^* &= -g \frac{A_{M_2}}{L_{tide}} \zeta^* + \frac{g}{\rho_0} \mathcal{R}_x \rho_{x^*}^* (H_0 z^* - A_{M_2} \zeta^*) \\ &+ \frac{\mathcal{N}U}{H_0^2} (\nu_t^* u_{z^*}^*)_{z^*}. \end{aligned}$$

Rewriting this yields

$$\begin{aligned} u_{t^*}^* + \frac{A_{M_2}}{H_0} u^* u_{x^*}^* + \frac{A_{M_2}}{H_0} w^* u_{z^*}^* &= -g H_0 \frac{T_{M_2}^2}{L_{tide}^2} \zeta^* + \frac{g}{\rho_0} \frac{H_0 T_{M_2} \mathcal{R}_x}{U} \rho_{x^*}^* \left( z^* - \frac{A_{M_2}}{H_0} \zeta^* \right) \\ &+ H_0^2 (\nu_t^* u_{z^*}^*)_{z^*}. \end{aligned}$$

The factor  $\frac{A_{M_2}}{H_0}$  in front of the advection term is assumed to be much smaller than unity. This provides the motivation for ordering the equation around a small parameter  $\delta$  which is defined as

$$\delta = \frac{A_{M_2}}{H_0}.$$

The other factors that appear in the dimensionless momentum equation can be related to the magnitude of  $\delta$ . These factors are considered below. Firstly,  $g H_0 \frac{T_{M_2}^2}{L_{tide}^2}$  can be rewritten by using that  $\sqrt{g H_0}$  equals the

barotropic shallow-water wave velocity  $c_E$ . This wave velocity can also be estimated as  $c_E = \frac{L_{tide}}{T_{M_2}}$ . It follows that

$$gH_0 \frac{T_{M_2}^2}{L_{tide}^2} = 1.$$

Secondly,  $\frac{g}{\rho_0} \frac{H_0 T_{M_2} \mathcal{R}_x}{U}$  is simplified to

$$\frac{g}{\rho_0} \frac{H_0 T_{M_2} \mathcal{R}_x}{U} = \frac{c_I}{U} = \frac{\rho_x dx}{\rho_0} \frac{H_0}{A_{M_2}},$$

where  $c_I$  is the baroclinic (internal) wave velocity, defined as  $c_I = c_E \frac{\rho_x dx}{\rho_0}$ . The term  $\frac{c_I}{U}$  is also known as the internal Froude number and is assumed to be of order  $\delta$ . This gives an order-estimate for the allowable density difference  $\Delta\rho = \rho_x dx$  over the length of the estuary:

$$\frac{\Delta\rho}{\rho_0} = \mathcal{O}(\delta^2).$$

The dimensional momentum equation then has terms of the following order of magnitude:

$$\underbrace{u_t}_{\mathcal{O}(1)} + \underbrace{uu_x}_{\mathcal{O}(\delta)} + \underbrace{wu_z}_{\mathcal{O}(\delta)} = \underbrace{-g\zeta_x}_{\mathcal{O}(1)} + \underbrace{g \frac{\rho_x}{\rho_0} (z - \zeta)}_{\mathcal{O}(\delta)} + \underbrace{(\nu_t u_z)_z}_{\mathcal{O}(1)}$$

### A.1.2. Scaling the depth-averaged continuity equation

The dimensionless form of the depth-averaged momentum equation A.3 is

$$\zeta_{t^*} + \left( \int_{-H^*}^{\delta\zeta^*} u^* dz^* \right)_{x^*} = \frac{L_{tide}}{L_b} \int_{-H^*}^{\delta\zeta^*} u^* dz^*.$$

All terms are of the same order, except for the integration boundary  $\zeta$ . The integral is therefore linearised by a Taylor expansion according to

$$\int_{-H}^{\zeta} u dz = \int_{-H}^0 u dz + \zeta u(x, 0, t) + HOT^1$$

The dimensional equation then has terms of the following order of magnitude:

$$\underbrace{\zeta_t}_{\mathcal{O}(1)} + \underbrace{\left( \int_{-H}^0 u dz \right)_x}_{\mathcal{O}(1)} + \underbrace{\zeta_x u(x, 0, t) + \zeta u_x(x, 0, t)}_{\mathcal{O}(\delta)} = \frac{1}{L_b} \left( \underbrace{\int_{-H}^0 u dz}_{\mathcal{O}(1)} + \underbrace{\zeta u(x, 0, t)}_{\mathcal{O}(\delta)} \right).$$

### A.1.3. Scaling the boundary conditions

The momentum equation has boundary conditions which are applied on the bed and at the surface. The boundary condition  $\nu_t u_z(x, \zeta, t) = 0$  at the surface  $z = \zeta$  is linearised around  $z = 0$  by using a Taylor expansion

$$\nu_t u_z(x, \zeta, t) = \underbrace{\nu_t u_z(x, 0, t)}_{\mathcal{O}(1)} + \underbrace{\nu_t u_{zz}(x, 0, t)\zeta}_{\mathcal{O}(\delta)} + HOT.$$

<sup>1</sup>The acronym HOT means 'higher-order terms'.

The ordering of this boundary condition in terms of  $\delta$  is obtained by observing that  $z^* = \frac{A_{M_2}}{H_0} \zeta^* = \mathcal{O}(\delta)$ .

On the bed  $z = -H$  no-slip, partial slip or quadratic slip conditions may be applied, depending on the formulation for  $\nu_t$ . The boundary conditions read

$$\nu_t u_z(x, -H, t) = s_f u(x, -H, t) \quad (\text{partial slip}), \quad (\text{A.4})$$

$$u(x, -H, t) = 0 \quad (\text{no-slip}), \quad (\text{A.5})$$

$$\nu_t u_z(x, -H, t) = u_*(x, t)^2 \quad (\text{quadratic slip}), \quad (\text{A.6})$$

where  $s_f$  is a roughness parameter and  $u_*$  is the bed friction velocity, see Appendix C. These terms in these boundary conditions must all be of equal order in order to obtain balanced equations.

The horizontal boundary conditions are used for solving the water level  $\zeta$  from the depth-averaged continuity equation. An  $M_2$  and  $M_4$  tide is prescribed at the entrance  $x = 0$

$$\zeta(0, t) = \underbrace{A_{M_2} \cos(\omega t)}_{\mathcal{O}(1)} + \underbrace{A_{M_4} \cos(2\omega t - \phi)}_{\mathcal{O}(\delta)},$$

where the ordering follows from the dimensionless form  $\zeta^*(0, t) = \cos(t^*) + \frac{A_{M_4}}{A_{M_2}} \cos(2t^* - \phi)$ . It is assumed that  $\frac{A_{M_4}}{A_{M_2}}$  is of order  $\delta$ .

The landward boundary is modelled by a tidal weir. The tidal weir is a reflective boundary that allows a fixed river discharge over it. The boundary condition thus reads

$$\int_{-H}^{\zeta(L, t)} u(L, z, t) dz = \frac{Q}{B},$$

where  $Q$  is the river discharge in volume per second. The upper bound of the integral  $\zeta(L, t)$  is linearised around  $z = 0$  by using a Taylor expansion. It is further assumed that the river discharge is of order  $\delta$  in Version 1 and 2. This assumption is not necessary in Version 3 to 5. The results in this research use a river discharge of first order, but the general equations will be given. The equation then becomes

$$\underbrace{\int_{-H}^0 u(L, z, t) dz}_{\mathcal{O}(1)} + \underbrace{\zeta(L, t) u(L, 0, t)}_{\mathcal{O}(\delta)} + HOT = \underbrace{\frac{Q}{B}}_{\mathcal{O}(1), \mathcal{O}(\delta)}$$

#### A.1.4. Overview of equations

The solutions  $u$ ,  $w$  and  $\zeta$  are written as a power series of the small parameter  $\delta$

$$u = u^0 + u^1 + u^2 + \dots,$$

$$w = w^0 + w^1 + w^2 + \dots,$$

$$\zeta = \zeta^0 + \zeta^1 + \zeta^2 + \dots,$$

where  $u^1$ ,  $w^1$  and  $\zeta^1$  are assumed to be of order  $\delta$ ,  $u^2$ ,  $w^2$  and  $\zeta^2$  are of order  $\delta^2$  etcetera.

Substituting these series in the momentum, continuity and depth-averaged continuity equations yields the systems of equations in leading order and first order. The solution to the momentum equation yields  $u$ , the continuity yields  $w$  and the depth-averaged continuity equation yields  $\zeta$ .

The leading order system is given by

$$u_t^0 = -g \zeta_x^0 + (\nu_t u_z^0)_z, \quad (\text{A.7})$$

$$\bullet \nu_t u_z^0(x, 0, t) = 0, \quad (\text{A.8})$$

$$\bullet \nu_t u_z^0(x, -H, t) = s_f u^0(x, -H, t) \quad (\text{partial-slip}), \quad (\text{A.9})$$

$$\bullet u^0(x, -H, t) = 0 \quad (\text{no-slip}), \quad (\text{A.10})$$

$$\bullet \nu_t u_z^0(x, -H, t) = u_*(x, t)^2 \quad (\text{quadratic}). \quad (\text{A.11})$$

$$u_x^0 + w_z^0 - \frac{u^0}{L_b} = 0, \quad (\text{A.12})$$

$$\bullet w^0(x, 0, t) = \zeta_t^0(x, t), \quad (\text{A.13})$$

$$\bullet w^0(x, -H, t) = -u^0(x, -H, t)H_x. \quad (\text{A.14})$$

$$\zeta_t^0 + \left( \int_{-H}^0 u^0 \right)_x = \frac{1}{L_b} \int_{-H}^0 u^0, \quad (\text{A.15})$$

$$\bullet \zeta^0(0, t) = A_{M_2} \cos(\omega t), \quad (\text{A.16})$$

$$\bullet \int_{-H}^0 u^0(L, z, t) dz = \frac{Q^0}{B}. \quad (\text{A.17})$$

The first order system is given by

$$u_t^1 + u^0 u_x^0 + w^0 u_z^0 = -g \zeta_x^1 + g \frac{\rho_x}{\rho_0} z + (\nu_t u_z^1)_z, \quad (\text{A.18})$$

$$\bullet \nu_t u_z^1(0) + \nu_t \zeta(x, t)^0 u_{zz}^0(x, 0, t) = 0, \quad (\text{A.19})$$

$$\bullet \nu_t u_z^1(x, -H, t) = s_f u^1(x, -H, t), \quad (\text{partial-slip}), \quad (\text{A.20})$$

$$\bullet u^1(x, -H, t) = 0 \quad (\text{no-slip}), \quad (\text{A.21})$$

$$\bullet \nu_t u_z^1(x, -H, t) = u_*(x, t)^2 \quad (\text{quadratic}). \quad (\text{A.22})$$

$$u_x^1 + w_z^1 - \frac{u^1}{L_b} = 0, \quad (\text{A.23})$$

$$\bullet w^1(x, 0, t) + w_z^0(x, 0, t) \zeta^0(x, t) = \zeta_t^1(x, t) + u^0 \zeta_x^0, \quad (\text{A.24})$$

$$\bullet w^1(x, -H, t) = -u^1(x, -H, t)H_x. \quad (\text{A.25})$$

$$\zeta_t^1 + \left( \int_{-H}^0 u^1 \right)_x + \zeta_x^0 u^0(x, 0, t) + \zeta^0 u_x^0(x, 0, t) = \frac{1}{L_b} \left( \int_{-H}^0 u^1 + \zeta^0 u^0(x, 0, t) \right), \quad (\text{A.26})$$

$$\bullet \zeta^1(0, t) = A_{M_4} \cos(\omega t), \quad (\text{A.27})$$

$$\bullet \int_{-H}^0 u^1(L, z, t) dz = \frac{Q^1}{B} - \zeta^0(L, t) u^0(L, 0, t). \quad (\text{A.28})$$

## A.2. Version 1: constant eddy viscosity

Version 1 uses a vertically uniform and stationary eddy viscosity and linear friction law. The eddy viscosity and friction coefficient are allowed to change gradually in the  $x$ -direction. The river discharge is assumed to be of first-order magnitude. These assumptions allow for an analytical solution in vertical direction and an analytical solution in horizontal direction for some simple cases. Only these analytical solutions are treated in this section. The numerical solutions can be obtained as a specific case of Version 3.

### A.2.1. Leading order

The leading order equations are only forced by an  $M_2$  tidal component at the seaward boundary and the equations are linear. As a result the leading order velocity and water level can only consist of an  $M_2$  signal. So it is sufficient to consider one Fourier component with frequency  $\omega$ ;

$$\begin{aligned} u^0(x, z, t) &= Re(\hat{u}^0(x, z)e^{i\omega t}), & \hat{u}^0(x, z) &\in H^2 : (\mathbb{R} \times \mathbb{R}) \rightarrow \mathbb{C} \\ w^0(x, z, t) &= Re(\hat{w}^0(x, z)e^{i\omega t}), & \hat{w}^0(x, z) &\in H^2 : (\mathbb{R} \times \mathbb{R}) \rightarrow \mathbb{C} \\ \zeta^0(x, t) &= Re(\hat{\zeta}^0(x)e^{i\omega t}). & \hat{\zeta}^0(x) &\in H^2 : \mathbb{R} \rightarrow \mathbb{C} \end{aligned}$$

The momentum equation A.7 is then given by

$$i\omega\hat{u}^0 = -g\hat{\zeta}_x^0 + \nu_t\hat{u}_{zz}^0,$$

and the general solution is

$$\hat{u}(x, z) = -\frac{g\hat{\zeta}_x(x)}{r^2\nu_t} + C_1e^{rz} + C_2e^{-rz},$$

where

$$r(x) = \sqrt{\frac{i\omega}{\nu_t}}$$

The solution for  $\hat{u}$  is obtained by the substitution of the boundary conditions A.8 and A.9

$$\hat{u}(x, z) = -\frac{g\hat{\zeta}_x(x)}{i\omega} (1 - \alpha(x) \cosh(r(x)z)),$$

where

$$\alpha(x) = s_f (\nu_t r \sinh(rH) + s_f \cosh(rH))^{-1}$$

Next, the Fourier components and the solution for  $\hat{u}$  are substituted in the depth-averaged continuity equation A.15. This equation then gives a second-order linear ODE for  $\hat{\zeta}$ :

$$\begin{aligned} i\omega\hat{\zeta} + \frac{g}{i\omega} \left( \hat{\zeta}_{xx} - \frac{1}{L_b} \hat{\zeta}_x \right) \left( -H + \frac{\alpha}{r} \sinh(rH) \right) \\ + \frac{g}{i\omega} \sinh(rH) \hat{\zeta}_x \left( \alpha_x + \alpha r_x \left( H \frac{\cosh(rH)}{\sinh(rH)} - \frac{1}{r} \right) \right) - \frac{g}{i\omega} \hat{\zeta}_x (1 - \alpha \cosh(rH)) H_x = 0. \end{aligned}$$

This equation generally needs to be solved numerically because of the non-constant coefficients in the ODE. A case in which an analytical solution can be found is when all quantities are uniform in the  $x$ -direction. The ODE for  $\hat{\zeta}$  then reduces to

$$i\omega\hat{\zeta} + \frac{g}{i\omega} \hat{\zeta}_{xx} \left( -H + \frac{\alpha}{r} \sinh(rH) \right) = 0.$$

The solution of this equation is

$$\hat{\zeta}(x) = \frac{1}{2} A_{M_2} \left( \frac{e^{-RL}}{\cosh(RL)} e^{rx} + \frac{e^{RL}}{\cosh(RL)} e^{-Rx} \right),$$

where

$$R = \frac{\omega^2}{g \left( -H + \frac{\alpha}{r} \sinh(rH) \right)}$$

Finally, we find the solution for  $\hat{w}$  from the continuity equation A.12. This solution reads

$$\begin{aligned} \hat{w}(x, z) = \frac{g}{i\omega} \left( \hat{\zeta}_{xx} - \frac{1}{L_b} \hat{\zeta}_x \right) \left( z - \frac{\alpha}{r} \sinh(rz) \right) \\ + \frac{g}{i\omega r} \sinh(rz) \hat{\zeta}_x \left( -\alpha_x - \alpha r_x \left( z \frac{\cosh(rz)}{\sinh(rz)} - \frac{1}{r} \right) \right) + i\omega\hat{\zeta}. \end{aligned}$$

### A.2.2. First order

The first-order velocity and water level are forced externally by an  $M_4$  tidal component and a constant river discharge and internally by the salinity gradient, the leading-order advection, tidal return flow and water level. The forcing components span two frequencies: the residual ( $M_0$ ) and  $M_4$ . The equations for both frequencies are solved below.

Some simplifications in the notation are adopted for the first-order equations. The following quantities are introduced

$$\begin{aligned}\eta(x, z, t) &= u^0(x, z, t)u_x^0(x, z, t) + w^0(x, z, t)u_z^0(x, z, t), \\ \gamma(x, t) &= \zeta^0(x, t)u^0(x, 0, t), \\ \chi(x, t) &= \zeta^0(x, t)u_{zz}^0(x, 0, t).\end{aligned}$$

The following derivations make frequent use of products of Fourier components. Therefore a general derivation of such a product is given below. Let  $u_n = \hat{u}_n e^{ni\omega t}$  and  $w_m = \hat{w}_m e^{mi\omega t}$  be Fourier components of some quantities. Their product is given by

$$\begin{aligned}u_n w_m &= |\hat{u}_n| |\hat{w}_m| \left( \operatorname{Re} \left( e^{i \arg(\hat{w}_m)} \right) \cos(m\omega t) - \operatorname{Im} \left( e^{i \arg(\hat{w}_m)} \right) \sin(m\omega t) \right) \\ &\quad \left( \operatorname{Re} \left( e^{i \arg(\hat{u}_n)} \right) \cos(n\omega t) - \operatorname{Im} \left( e^{i \arg(\hat{u}_n)} \right) \sin(n\omega t) \right) \\ &= \frac{1}{2} |\hat{u}_n| |\hat{w}_m| \operatorname{Re} \left( e^{i(\arg(\hat{u}_n) + \arg(\hat{w}_m))} e^{i(n+m)\omega t} + e^{i(\arg(\hat{u}_n) - \arg(\hat{w}_m))} e^{i(n-m)\omega t} \right) \\ &= \operatorname{Re} \left( \frac{1}{2} \hat{u}_n \hat{w}_m e^{i(n+m)\omega t} + \frac{1}{2} \hat{u}_n \overline{\hat{w}_m} e^{i(n-m)\omega t} \right)\end{aligned}\tag{A.29}$$

#### Residual flow velocity

The equations for residual flow are obtained by taking the tide-averaged component of the first-order equations. Let  $\langle \cdot \rangle$  denote tide-averaging. The momentum equation with its boundary conditions is then given by

$$\begin{aligned}\nu_t \hat{u}_{0,zz}^1 &= \langle \hat{\eta} \rangle + g \hat{\zeta}_{0,x}^1 - g \beta \langle \hat{s}_x \rangle z, \\ \nu_t \hat{u}_{0,z}^1(x, 0) &= -\nu_t \langle \hat{\chi} \rangle, \\ \nu_t \hat{u}_{0,z}^1(x, -H) &= s_f \hat{u}_0^1(x, -H).\end{aligned}$$

The subscript 0 denotes the residual component.

For reasons of generality and ease of notation, we first solve the equation  $\nu_t \hat{u}_{0,zz}^1 = f(x, z)$  with the above boundary conditions. The solution to this equation reads

$$\hat{u}_0^1 = - \int_{-H}^z \int_{\bar{z}}^0 \frac{f(x, \hat{z})}{\nu_t} d\hat{z} d\bar{z} - \int_{-H}^0 \frac{f(x, z)}{s_f} dz - \langle \hat{\chi} \rangle \left( z + H + \frac{\nu_t}{s_f} \right).$$

The solution to  $\hat{u}_0^1$  can be written in the form

$$\begin{aligned}
 \hat{u}_0^1 &= u_1 - u_2 g \hat{\zeta}_{0,x}^1, & (A.30) \\
 u_1 &= u_{\text{no-stress}} + u_{\text{adv}} + u_{s_x}, \\
 u_2 &= -\frac{1}{2} \frac{z^2}{\nu_t} + \frac{1}{2} \frac{H^2}{\nu_t} + \frac{H}{s_f}, \\
 u_{\text{no-stress}} &= -\langle \hat{\chi} \rangle \left( z + H + \frac{\nu_t}{s_f} \right), \\
 u_{\text{adv}} &= -\int_{-H}^z \int_{\bar{z}}^0 \frac{\langle \hat{\eta} \rangle}{\nu_t} d\hat{z} d\bar{z} - \int_{-H}^0 \frac{\langle \hat{\eta} \rangle}{s_f} dz, \\
 u_{s_x} &= -g\beta \langle \hat{s}_x \rangle \left( \frac{1}{6} \frac{z^3}{\nu_t} + \frac{1}{6} \frac{H^3}{\nu_t} - \frac{1}{2} \frac{H^2}{s_f} \right),
 \end{aligned}$$

where the subscripts denote the part of the solution due to a particular forcing, see Table 2.2.

### Constant water level elevation

The equation for the constant water level elevation is obtained by using the decomposition A.30 for the residual flow velocity. It reads

$$\begin{aligned}
 -g \int_{-H}^0 u_2 dz \hat{\zeta}_{0,xx}^1 - g \left( \left( \int_{-H}^0 u_2 dz \right)_x - \frac{1}{L_b} \int_{-H}^0 u_2 dz \right) \hat{\zeta}_{0,x}^1 = \\
 - \left( \int_{-H}^0 u_1 dz \right)_x + \frac{1}{L_b} \int_{-H}^0 u_1 dz - \hat{\gamma}_x + \frac{1}{L_b} \hat{\gamma}.
 \end{aligned}$$

The expressions for  $u_1$  and  $u_2$  are then substituted and the terms in the resulting equation are grouped according to the forcing mechanism. The rewritten ODE for  $\hat{\zeta}_0^1$  reads

$$\begin{aligned}
 a \hat{\zeta}_{0,xx}^1 - b \hat{\zeta}_{0,x}^1 &= d, \\
 a &= -g \left( \frac{1}{3} \frac{H^3}{\nu_t} + \frac{H^2}{s_f} \right), \\
 b &= \left( \frac{\partial}{\partial x} - \frac{1}{L_b} \right) \left( -g \left( \frac{1}{3} \frac{H^3}{\nu_t} + \frac{H^2}{s_f} \right) \right), \\
 d &= \hat{\zeta}_{\text{no-stress}} + \hat{\zeta}_{\text{adv}} + \hat{\zeta}_{s_x} + \hat{\zeta}_{\text{return flow}}, \\
 \hat{\zeta}_{\text{no-stress}} &= \left( \frac{\partial}{\partial x} - \frac{1}{L_b} \right) \langle \hat{\chi} \rangle \left( \frac{1}{2} H^2 + \frac{\nu_t}{s_f} H \right), \\
 \hat{\zeta}_{\text{adv}} &= \left( \frac{\partial}{\partial x} - \frac{1}{L_b} \right) \left( \int_{-H}^0 \int_{-H}^z \int_{\bar{z}}^0 \frac{\langle \hat{\eta} \rangle}{\nu_t} d\hat{z} d\bar{z} dz + \frac{H}{s_f} \int_{-H}^0 \langle \hat{\eta} \rangle dz \right), \\
 \hat{\zeta}_{s_x} &= \left( \frac{\partial}{\partial x} - \frac{1}{L_b} \right) g\beta \langle \hat{s}_x \rangle \left( \frac{1}{8} \frac{H^4}{\nu_t} + \frac{1}{2} \frac{H^3}{s_f} \right), \\
 \hat{\zeta}_{\text{return flow}} &= - \left( \frac{\partial}{\partial x} - \frac{1}{L_b} \right) \langle \hat{\gamma} \rangle,
 \end{aligned}$$

The forcing mechanisms  $\hat{\zeta}_{\text{no-stress}}$ ,  $\hat{\zeta}_{\text{adv}}$ ,  $\hat{\zeta}_{s_x}$  and  $\hat{\zeta}_{\text{return flow}}$  originate from the effect of leading-order water level and their meaning is presented in Table 2.2.

There is no subtidal water level forcing at  $x = 0$ . The boundary condition thus reads

$$\hat{\zeta}_0^1(0) = 0.$$

The boundary condition at  $x = L$  is

$$\int_{-H}^0 \hat{u}_0^1(L, z) dz = \frac{Q^1}{B} - \langle \hat{\gamma}(L) \rangle.$$

This can be rewritten to an expression for  $\hat{\zeta}_0^1$ :

$$\hat{\zeta}_{0,x}^1(L) = \left( -g \int_{-H}^0 u_2(L, z) dz \right)^{-1} \left( \frac{Q^1}{B} - \langle \hat{\gamma}(L) \rangle - \int_{-H}^0 u_1(L, z) dz \right)$$

Note that the river discharge is a negative number, which reflects that the flow is in the negative  $x$ -direction.

#### $M_4$ flow velocity

Let  $[\cdot]$  denote the operation of taking the  $M_4$  component of a signal. The equation and the boundary conditions for the  $M_4$  velocity then read

$$\begin{aligned} 2i\omega \hat{u}_2^1 - \nu_t \hat{u}_{2,zz}^1 &= -[\hat{\eta}] - g\hat{\zeta}_{2,x}^1, \\ \nu_t \hat{u}_{2,z}^1(x, 0) &= -\nu_t [\hat{\chi}], \\ \nu_t \hat{u}_{2,z}^1(x, -H) &= s_f \hat{u}_2^1(x, -H) \end{aligned}$$

where the subscript 2 denotes the  $M_4$  frequency, i.e. the second overtide of the  $M_2$  tidal constituent.

The general solution to this equation is

$$\hat{u}_2^1 = \frac{1}{2\nu_t r} \left( - \int_z^0 [\hat{\eta}] e^{r\hat{z}} d\hat{z} e^{-rz} + \int_z^0 [\hat{\eta}] e^{-r\hat{z}} d\hat{z} e^{rz} \right) - \frac{g}{2i\omega} \hat{\zeta}_x + c_1 e^{rz} + c_2 e^{-rz}$$

Substituting the boundary conditions yields the following equation

$$\begin{aligned} \hat{u}_2^1 &= u_1 - u_2 g \hat{\zeta}_{2,x}^1, \\ u_2 &= \frac{1}{2i\omega} (1 - \alpha \cosh(rz)), \\ u_1 &= u_{\text{no-stress}} + u_{\text{adv}}, \\ u_{\text{no-stress}} &= -\frac{\alpha}{s_f} [\hat{\chi}] \left( \nu_t \cosh(r(z+H)) + \frac{s_f}{r} \sinh(r(z+H)) \right), \\ u_{\text{adv}} &= \frac{1}{2\nu_t r} \left( \int_z^0 [\hat{\eta}] e^{r\hat{z}} d\hat{z} e^{-rz} - \int_z^0 [\hat{\eta}] e^{-r\hat{z}} d\hat{z} e^{rz} \right) - \left( \int_{-H}^0 [\hat{\eta}] e^{r\hat{z}} d\hat{z} e^{rH} \left( \frac{1}{2} + \frac{s_f}{2\nu_t r} \right) \right. \\ &\quad \left. + \int_{-H}^0 [\hat{\eta}] e^{-r\hat{z}} d\hat{z} e^{-rH} \left( \frac{1}{2} - \frac{s_f}{2\nu_t r} \right) \right) \frac{\alpha}{s_f} \cosh(rz). \end{aligned}$$

where

$$\begin{aligned} r &= \sqrt{\frac{2i\omega}{\nu_t}}, \\ \alpha &= s_f (\nu_t r \sinh(rH) + s_f \cosh(rH))^{-1}. \end{aligned}$$

### $M_4$ water level

The  $M_4$  water level equation can be derived in a similar manner as the constant water level elevation. The ODE for  $\hat{\zeta}_2^1$  reads

$$\begin{aligned}
 a\hat{\zeta}_{2,xx}^1 - b\hat{\zeta}_{2,x}^1 - c\hat{\zeta}_2^1 &= d, \\
 a &= -\frac{g}{2i\omega} \left( H - \frac{\alpha}{r} \sinh(rH) \right), \\
 b &= \left( \frac{\partial}{\partial x} - \frac{1}{Lb} \right) \frac{g}{2i\omega} \left( H - \frac{\alpha}{r} \sinh(rH) \right), \\
 c &= -2i\omega, \\
 d &= \hat{\zeta}_{\text{no-stress}} + \hat{\zeta}_{\text{adv}} + \hat{\zeta}_{\text{return flow}}, \\
 \hat{\zeta}_{\text{no-stress}} &= \left( \frac{\partial}{\partial x} - \frac{1}{Lb} \right) \frac{\alpha}{r^2 s_f} [\hat{\chi}] (\nu_t r \sinh(rH) + s_f \cosh(rH) - s_f) \\
 \hat{\zeta}_{\text{adv}} &= \left( \frac{\partial}{\partial x} - \frac{1}{Lb} \right) \left\{ -\frac{1}{2\nu_t r} \left( \int_{-H}^0 \int_z^0 [\hat{\eta}] e^{r\hat{z}} d\hat{z} dz e^{-rz} - \int_{-H}^0 \int_z^0 [\hat{\eta}] e^{-r\hat{z}} d\hat{z} dz e^{rz} \right) \right. \\
 &\quad \left. + \left( \int_{-H}^0 [\hat{\eta}] e^{r\hat{z}} d\hat{z} e^{rH} \left( \frac{1}{2} + \frac{s_f}{2\nu_t r} \right) + \int_{-H}^0 [\hat{\eta}] e^{-r\hat{z}} d\hat{z} e^{-rH} \left( \frac{1}{2} - \frac{s_f}{2\nu_t r} \right) \right) \frac{\alpha}{rs} \sinh(rz) \right\}, \\
 \hat{\zeta}_{\text{return flow}} &= -\left( \frac{\partial}{\partial x} - \frac{1}{Lb} \right) [\hat{\gamma}]
 \end{aligned}$$

An  $M_4$  tide is applied on the boundary at  $x = 0$ . This boundary condition reads

$$\hat{\zeta}_2^1(0) = A_{M_4} e^{i\phi},$$

where  $A_{M_4}$  is the amplitude of the  $M_4$  tide and  $\phi$  is the phase of the tide relative to the  $M_2$  tide.

The boundary condition at  $x = L$  reads

$$\int_{-H}^0 \hat{u}_2^1(L, z) dz = -[\hat{\gamma}(L)].$$

This boundary condition is rewritten to a relation for  $\hat{\zeta}_{2,x}^1$  by substituting the expression for  $\hat{u}_2^1$

$$\hat{\zeta}_{2,x}^1(L) = \left( -g \int_{-H}^0 u_2(L, z) dz \right)^{-1} \left( -[\hat{\gamma}(L)] - \int_{-H}^0 u_1(L, z) dz \right).$$

### A.3. Version 2: parabolic viscosity

The parabolic eddy viscosity profile in vertical direction is of interest, because it is a good approximation for the eddy viscosity in homogeneous tidal flows. Such eddy viscosity profile also allows one to find an analytical solution for  $u$  and, for the case of a simple channel, the water level. These analytical solutions will be presented in this section. This analysis is restricted to the leading-order velocity. The analytical solutions for the first-order velocity are omitted, because they are complicated expressions that provide little insight into the properties of the solutions.

The parabolic profile for  $\nu_t$  is given by the following equation:

$$\nu_t = \nu_{t,0}(x)(z_s(x) - z)(H(x) + z_b(x) + z).$$

In this equation  $z_s$  and  $z_b$  represent surface and bottom roughness heights, which replace the roughness coefficient in Version 1. Moreover, the model no longer needs the partial-slip friction law, but instead uses the no-slip boundary condition. The river discharge is again assumed to be of first order.

### A.3.1. Leading order

The leading-order momentum equation A.7 reduces to

$$i\omega\hat{u}^0 + \nu_{t,0}(H + z_b - z_s + 2z)\hat{u}_z + \nu_{t,0}(z - z_s)(H + z_b + z)\hat{u}_{zz} = -g\hat{\zeta}_x^0.$$

The general solution to this ODE is

$$\hat{u} = -\frac{g}{i\omega}\hat{\zeta}_x + C_1H_1(z - z_s)^{-r_1} + C_2H_2(z - z_s)^{-r_2},$$

where

$$H_1 = \text{Hypergeometric} \left( [r_1, r_1], 2r_1, \frac{z_s + z_b + H}{z_b - z} \right),$$

$$H_2 = \text{Hypergeometric} \left( [r_2, r_2], 2r_2, \frac{z_s + z_b + H}{z_b - z} \right),$$

$$r_1 = \frac{1}{2} + \sqrt{\frac{1}{2} - \frac{i\omega}{\nu_t}},$$

$$r_2 = \frac{1}{2} - \sqrt{\frac{1}{2} - \frac{i\omega}{\nu_t}}.$$

The 'constants'  $C_1$  and  $C_2$ , which are still allowed to be functions of  $x$ , follow from the boundary conditions A.8 and A.10. It can be derived that  $C_1$  and  $C_2$  depend linearly on  $g\hat{\zeta}_x$ . The constants are therefore rewritten according to

$$C_1(x) = a_1(x)g\hat{\zeta}_x,$$

$$C_2(x) = a_2(x)g\hat{\zeta}_x,$$

for some functions  $a_1$  and  $a_2$ . The solution for  $u$  is

$$\hat{u} = g\hat{\zeta}_x \left( a_1H_1(z - z_s)^{-r_1} + a_2H_2(z - z_s)^{-r_2} - \frac{1}{i\omega} \right).$$

This solution can be substituted in the depth-averaged continuity equation A.15 to obtain the water level  $\zeta$ . The resulting ODE generally needs to be solved numerically. For the simple channel the ODE for  $\zeta$  can be solved analytically. The ODE for this case reads

$$\left( a_1 \int_{-H}^0 H_1(z - z_s)^{-r_1} + a_2 \int_{-H}^0 H_2(z - z_s)^{-r_2} - \frac{1}{i\omega}H \right) \hat{\zeta}_{xx} + \frac{i\omega}{g}\hat{\zeta} = 0$$

The integrals of the hypergeometric functions in this equations are evaluated analytically and the ODE is solved in a similar manner as in Version 1.

## A.4. Version 3: time-varying viscosity

The solutions for Version 3, 4 and 5 are obtained numerically. This section therefore presents the numerical solution method. An alternative, analytical, solution method to Version 3 is presented in Section A.6.

Consider an eddy viscosity which is constant in the vertical direction and variable in time according to a truncated Fourier series

$$\nu_t(x, t) = \text{Re} \left( \sum_{m=0}^p \hat{\nu}_{t,m}(x) e^{mi\omega t} \right).$$

The velocity and water level responses consists of an infinite Fourier series, but the series is truncated for numerical computation. These responses originate from the product of  $\nu_t$  and  $u_z$  in the momentum equation. It follows from Equation A.29 that these responses do not only consist of positive Fourier components but also of negative components. The velocity and water level are therefore approximated by

$$\begin{aligned} u &= \operatorname{Re} \left( \sum_{n=-p}^p \hat{u}_n e^{ni\omega t} \right), \\ w &= \operatorname{Re} \left( \sum_{n=-p}^p \hat{w}_n e^{ni\omega t} \right), \\ \zeta &= \operatorname{Re} \left( \sum_{n=-p}^p \hat{\zeta}_n e^{ni\omega t} \right). \end{aligned}$$

It is assumed that the phase of the eddy viscosity at a location  $x$  corresponds to the average phase of the leading order horizontal velocity at the same location. The vertically averaged phase has to be used in order for  $\nu_t$  to remain independent of  $z$ . This coupling of the phase of the velocity and eddy viscosity introduces a non-linearity in the model. The model is therefore solved iteratively.

#### A.4.1. Leading order

The momentum equation A.7 involves the product  $\nu_t u_z$ . This term introduces additional Fourier components to the system compared to previous versions of the model according to Equation A.29. It follows from this expression that the product of two positive Fourier components  $m$  and  $n$  can induce a negative Fourier component. Therefore, both positive and negative components will be used. The following equation follows from the momentum equation for the Fourier modes

$$ni\omega \hat{u}_n = -g \hat{\zeta}_{x,n} + \frac{1}{2} \sum_{m=0}^p (\hat{\nu}_{t,m} \hat{u}_{zz,n-m} + \overline{\hat{\nu}_{t,m}} \hat{u}_{zz,n+m}), \quad n = -p, \dots, p$$

So we solve a system of  $2p + 1$  ODEs of the form

$$D \hat{u} - \mathcal{N} \hat{u}_{zz} = -g \hat{\zeta}_x, \quad (\text{A.31})$$

where

$$D = \begin{bmatrix} -pi\omega & & & \emptyset \\ & -(p-1)i\omega & & \\ & & \ddots & \\ \emptyset & & & pi\omega \end{bmatrix}, \quad \underline{\hat{u}} = \begin{bmatrix} \hat{u}_{-p} \\ \hat{u}_{-(p-1)} \\ \vdots \\ \hat{u}_p \end{bmatrix},$$

$$\mathcal{N} = \frac{1}{2} \begin{bmatrix} 2Re(\hat{v}_{t,0}) & \overline{\hat{v}_{t,1}} & \cdots & \overline{\hat{v}_{t,p}} \\ \hat{v}_{t,1} & 2Re(\hat{v}_{t,0}) & \ddots & \vdots & \ddots & \emptyset \\ \vdots & \ddots & \ddots & \overline{\hat{v}_{t,1}} & \ddots & \\ \hat{v}_{t,p} & \cdots & \hat{v}_{t,1} & 2Re(\hat{v}_{t,0}) & \overline{\hat{v}_{t,1}} & \cdots & \overline{\hat{v}_{t,p}} \\ & \ddots & & \hat{v}_{t,1} & \ddots & \ddots & \vdots \\ & \emptyset & \ddots & \vdots & \ddots & 2Re(\hat{v}_{t,0}) & \overline{\hat{v}_{t,1}} \\ & & & \hat{v}_{t,p} & \cdots & \hat{v}_{t,1} & 2Re(\hat{v}_{t,0}) \end{bmatrix}$$

The system can also be solved for positive Fourier components only. The essential observation that allows us to eliminate the negative Fourier components is given by

$$u_{-n} = Re(\hat{u}_{-n}e^{-ni\omega t}) = Re(\overline{\hat{u}_{-n}e^{-ni\omega t}}) = Re(\widehat{\hat{u}_{-n}}e^{ni\omega t})$$

A negative Fourier component becomes a positive component by taking the complex conjugate of its amplitude. We find the following form of  $\mathcal{N}$  if the negative components are eliminated

$$\mathcal{N} = \frac{1}{2} \begin{bmatrix} 2Re(\hat{v}_{t,0}) & \overline{\hat{v}_{t,1}} & \cdots & \overline{\hat{v}_{t,p}} \\ \hat{v}_{t,1} & \ddots & \ddots & \vdots \\ \vdots & \ddots & 2Re(\hat{v}_{t,0}) & \overline{\hat{v}_{t,1}} \\ \hat{v}_{t,p} & \cdots & \hat{v}_{t,1} & 2Re(\hat{v}_{t,0}) \end{bmatrix} + \frac{1}{2} \begin{bmatrix} 0 & \overline{\hat{v}_{t,1}} & \cdots & \overline{\hat{v}_{t,p}} \\ \vdots & \vdots & \ddots & 0 \\ 0 & \overline{\hat{v}_{t,p}} & 0 & \vdots \\ 0 & 0 & \cdots & 0 \end{bmatrix}$$

Note that the bandwidths of the equations with and without negative Fourier components are the same. Below, in Equation A.32, it will be shown that it is more efficient in terms of computational speed to eliminate the negative Fourier components. The model implementation nevertheless uses the negative Fourier components, because the matrices are more intuitive to implement. Future developments of the model may want to use the positive components only.

The system can be solved both analytically and numerically. The analytical solution is presented in Appendix A.6. The numerical procedure is explained below.





The forcing vectors  $\underline{f}^0$  and  $\underline{q}^0$  represent the tidal forcing and river discharge at the boundaries. Note that the addition of a leading-order river discharge is a feature of the Version 3 model, which was not included in version 1. The matrices  $A$ ,  $B$ ,  $C$  again have entries  $a_{nm}$ ,  $b_{nm}$  and  $c_{nm}$ . The matrices  $\tilde{A}$  and  $\tilde{B}$  have entries  $\tilde{a}_{nm}$  and  $\tilde{b}_{nm}$  depending on the boundary condition at  $x = L$ .

$$\begin{aligned}\tilde{a}_{nm} &= \frac{g}{\Delta x_{j_{\max}}} \int_{-H}^0 \mathcal{U} dz \\ \tilde{b}_{nm} &= -\frac{g}{\Delta x_{j_{\max}}} \int_{-H}^0 \mathcal{U} dz \\ \tilde{q}_n^0 &= \frac{Q^0}{B} \delta_{n0}\end{aligned}$$

#### A.4.2. First order

The first order solution makes use of the same definitions for  $\eta$ ,  $\gamma$  and  $\chi$  as presented in Version 1. These are repeated here for clarity.

$$\begin{aligned}\eta(x, z, t) &= u^0(x, z, t)u_x^0(x, z, t) + w^0(x, z, t)u_z^0(x, z, t), \\ \gamma(x, t) &= \zeta^0(x, t)u^0(x, 0, t), \\ \chi(x, t) &= \zeta^0(x, t)u_{zz}^0(x, 0, t).\end{aligned}$$

The resulting (scalar) functions for  $\eta$ ,  $\gamma$  and  $\chi$  are approximated by a truncated series of Fourier components similar to  $u$ ,  $w$  and  $\zeta$ ;

$$\begin{aligned}\eta(x, z, t) &= \operatorname{Re} \left( \sum_{n=-p}^p \hat{\eta}_n(x, z) e^{ni\omega t} \right), \\ \gamma(x, t) &= \operatorname{Re} \left( \sum_{n=-p}^p \hat{\gamma}_n(x) e^{ni\omega t} \right), \\ \chi(x, t) &= \operatorname{Re} \left( \sum_{n=-p}^p \hat{\chi}_n(x) e^{ni\omega t} \right).\end{aligned}$$

#### Solution for $\hat{u}$

The momentum equation in matrix notation is derived similar to the leading-order system. The equation reads

$$D\underline{\hat{u}}^1 - \mathcal{N}\underline{\hat{u}}_{zz}^1 = -g\underline{\hat{\zeta}}_x^1 - \underline{\hat{\eta}} + g\beta z \underline{\hat{s}}_x$$

This system is solved numerically. The analytical solution presented in Section A.6 can also be used, because the system matrix  $\mathcal{A}$  is the same as in the leading-order system. This results in a system

$$\mathcal{A}\underline{\hat{u}}^1 = -I_b g \underline{\hat{\zeta}} - \underline{\hat{\eta}} + g\beta z \underline{\hat{s}}_x + I_a \underline{\hat{\chi}},$$

where  $\mathcal{A}$  and  $I_b$  are the same as in the leading-order system (equation A.32) and  $I_a$ , in terms of  $2p-1 \times 2p-1$  sub-matrices, is given by

$$I_a = \begin{bmatrix} I \\ \emptyset \\ \vdots \\ \emptyset \end{bmatrix}.$$

The solution now reads

$$\underline{\hat{u}}^1 = \mathcal{A}^{-1} I_a \underline{\gamma}_{zz} - \mathcal{A}^{-1} I_b g \underline{\hat{\zeta}}_x - \mathcal{A}^{-1} \underline{\hat{\eta}}_x + \mathcal{A}^{-1} g \beta z \underline{\hat{s}}_x,$$

### Solution for $\hat{\zeta}$

The horizontal velocity field can be written as

$$\underline{\hat{u}}^1 = -\mathcal{U} g \underline{\hat{\zeta}}_x^1 + \underline{\hat{u}}_1.$$

The firstorder depth-averaged continuity equation in matrix form then becomes

$$\begin{aligned} D \underline{\hat{\zeta}}^1 - \int_{-H}^0 \mathcal{U} dz g \underline{\hat{\zeta}}_{xx}^1 - \left( \int_{-H}^0 \mathcal{U} dz \right)_x g \underline{\hat{\zeta}}_x^1 + \frac{1}{L_b} \int_{-H}^0 \mathcal{U} dz g \underline{\hat{\zeta}}_x^1 = \\ - \left( \int_{-H}^0 \underline{\hat{u}}_1 dz \right)_x - \underline{\gamma}_x + \frac{1}{L_b} \left( \int_{-H}^0 \underline{\hat{u}}_1 dz + \underline{\gamma} \right). \end{aligned}$$

This system can generally only be solved numerically. The resulting system is given by

$$\mathcal{B} \underline{\hat{\zeta}}^1 = \underline{f}^1 + \underline{q}^1 - \left( \int_{-H}^0 \underline{\hat{u}}_1 dz \right)_x - \underline{\gamma}_x + \frac{1}{L_b} \left( \int_{-H}^0 \underline{\hat{u}}_1 dz + \underline{\gamma} \right),$$

with solution

$$\underline{\hat{\zeta}}^1 = \mathcal{B}^{-1} \underline{f}^1 + \mathcal{B}^{-1} \underline{q}^1 - \mathcal{B}^{-1} \left( \int_{-H}^0 \underline{\hat{u}}_1 dz \right)_x - \mathcal{B}^{-1} \underline{\gamma}_x + \frac{1}{L_b} \mathcal{B}^{-1} \int_{-H}^0 \underline{\hat{u}}_1 dz + \frac{1}{L_b} \mathcal{B}^{-1} \underline{\gamma}, \quad (\text{A.34})$$

The vectors  $\underline{f}^1$  and  $\underline{q}^1$  represent the tidal forcing and river discharge at the boundaries and are similar to the leading order.

## A.5. Version 4: time- and space-varying viscosity

The eddy viscosity in Version 4 has the form

$$\nu_t(x, t) = \text{Re} \left( \sum_{m=0}^p \hat{\nu}_{t,m}(x, z) e^{mi\omega t} \right).$$

The difference with Version 3 is the amplitude of the eddy viscosity, which can vary in vertical direction. If  $\hat{\nu}_t$  has a parabolic profile similar to Version 2, the momentum equation can be solved analytically using hypergeometric functions according to an approach by [Tirao \(2003\)](#). The analytical solution is not implemented because of the large development time that is required to implement and test the solution. Moreover, it is expected that the computational time that is necessary to calculate the hypergeometric functions is of the same order as the time required for a high-resolution numerical calculation. This expectation is based on experience with calculations of Version 2.

The numerical calculation differs from Version 3 in only two places. Firstly, the phase of the eddy viscosity is no longer depth-averaged. Instead, the eddy viscosity adopts the phase of the velocity in every grid point. Secondly, the operator  $\mathcal{A}$  is different. This operator is derived for the Version 4 model below. The leading-order momentum equations are given by the system

$$D \underline{\hat{u}} - \mathcal{N}_z \underline{\hat{u}}_z - \mathcal{N} \underline{\hat{u}}_{zz} = -g \underline{\hat{\zeta}}_x, \quad (\text{A.35})$$

where the matrices are the same as in Version 3. The discretised equations read

$$D_{nm}\hat{u}_{n,k} - \sum_{m=1}^{2p+1} \mathcal{N}_{nm,k} \frac{1}{\Delta z_k} \left( \frac{\hat{u}_{m,k-1} - \hat{u}_{m,k}}{\Delta z_{k-1/2}} - \frac{\hat{u}_{m,k} - \hat{u}_{m,k+1}}{\Delta z_{k+1/2}} \right) - \mathcal{N}_{z,nm,k} \frac{\hat{u}_{m,k-1} - \hat{u}_{m,k+1}}{\Delta z_{k-1/2} + \Delta z_{k+1/2}} = -g\hat{\zeta}_{n,x}.$$

This is rewritten to

$$\sum_{m=1}^{2p+1} a_{nm}\hat{u}_{m,k-1} + b_{nm}\hat{u}_{m,k} + c_{nm}\hat{u}_{m,k+1} = -g\hat{\zeta}_{n,x}$$

- $a_{nm} = -\frac{1}{\Delta z_k \Delta z_{k-1/2}} \mathcal{N}_{nm,k} - \frac{1}{\Delta z_{k-1/2} + \Delta z_{k+1/2}} \mathcal{N}_{z,nm,k}$
- $b_{nm} = \left( \frac{1}{\Delta z_k \Delta z_{k-1/2}} + \frac{1}{\Delta z_k \Delta z_{k+1/2}} \right) \mathcal{N}_{nm,k} + \delta_{nm} D_{nm}$
- $c_{nm} = -\frac{1}{\Delta z_k \Delta z_{k+1/2}} \mathcal{N}_{nm,k} + \frac{1}{\Delta z_{k-1/2} + \Delta z_{k+1/2}} \mathcal{N}_{z,nm,k}$

The boundary condition on the bed is a no-slip condition. This means that the sub-matrices  $\tilde{\mathcal{A}}$  and  $\tilde{\mathcal{B}}$  in Equation A.32 are given by  $\tilde{\mathcal{A}} = \emptyset$  and  $\tilde{\mathcal{B}} = I$ .

Again a system  $\mathcal{A}\underline{\hat{u}} = -gI_b\hat{\zeta}_x$  is obtained, but with the matrix  $\mathcal{A}$  differing from that used in Version 3. The solution procedure for  $\hat{\zeta}$  and the first-order system are the same as in Version 3.

## A.6. Analytical solution to the Version 3 momentum equation

This system of Version 3 can be solved analytically, provided that the phases of the eddy viscosity are known beforehand. If this is not the case, then the system still needs to be solved iteratively by using the analytical solution method below in every iteration.

The analytical solution cannot be constructed from the system of equations A.31 directly, because the matrix  $D$  is not invertible. The equation for  $\hat{u}_0$  is therefore eliminated from the system, yielding

$$\hat{u}_{0,zz} = \frac{g}{Re(\hat{\nu}_{t,0})} \hat{\zeta}_{0,x} - \frac{1}{2Re(\hat{\nu}_{t,0})} \sum_{m=1}^p (\hat{\nu}_{t,m} \hat{u}_{-m,zz} + \overline{\hat{\nu}_{t,m}} \hat{u}_{m,zz}), \quad (\text{A.36})$$

$$\tilde{D}\tilde{\underline{\hat{u}}} = -g\hat{\zeta}_{x,red} + \mathcal{N}_{red}\tilde{\underline{\hat{u}}}_{zz}. \quad (\text{A.37})$$

The tilde over a vector in this equation signifies that the row belonging to  $\hat{u}_0$  is not included. Similarly, the tilde over matrices means that the row and column belonging to  $\hat{u}_0$  are not included. The other vectors and

matrices are defined as follows, both not including  $\hat{\nu}_{t,0}$ ,

$$\mathcal{N}_{red} = \tilde{N} - \frac{1}{2Re(\hat{\nu}_{t,0})} \begin{bmatrix} \overline{\hat{\nu}_{t,p}} \hat{\nu}_{t,p} & \overline{\hat{\nu}_{t,p}} \hat{\nu}_{t,p-1} & \cdots & \overline{\hat{\nu}_{t,p}} \hat{\nu}_{t,p} \\ \overline{\hat{\nu}_{t,p-1}} \hat{\nu}_{t,p} & \overline{\hat{\nu}_{t,p-1}} \hat{\nu}_{t,p-1} & \cdots & \overline{\hat{\nu}_{t,p-1}} \hat{\nu}_{t,p} \\ \vdots & \vdots & \ddots & \vdots \\ \hat{\nu}_{t,p} \hat{\nu}_{t,p} & \hat{\nu}_{t,p-1} \hat{\nu}_{t,p} & \cdots & \hat{\nu}_{t,p} \overline{\hat{\nu}_{t,p}} \end{bmatrix},$$

$$\hat{\zeta}_{x,red} = \tilde{\zeta}_x - \frac{1}{Re(\hat{\nu}_{t,0})} \begin{bmatrix} \overline{\hat{\nu}_{t,p}} \\ \overline{\hat{\nu}_{t,p-1}} \\ \vdots \\ \hat{\nu}_{t,p} \end{bmatrix} \hat{\zeta}_{0,x}$$

The system is rewritten to a system of first-order ODEs

$$\begin{bmatrix} \tilde{u} \\ \tilde{u}_z \end{bmatrix}_z = \underbrace{\begin{bmatrix} \emptyset & I \\ \mathcal{N}_{red}^{-1} \tilde{D} & \emptyset \end{bmatrix}}_A \begin{bmatrix} \tilde{u} \\ \tilde{u}_z \end{bmatrix} + g \begin{bmatrix} \emptyset \\ \mathcal{N}_{red}^{-1} \end{bmatrix} \tilde{\zeta}_x.$$

The general solution to this system is derived by using variation of constants. This solution is

$$\begin{bmatrix} \tilde{u} \\ \tilde{u}_z \end{bmatrix} = -g \begin{bmatrix} \tilde{D}^{-1} \\ \emptyset \end{bmatrix} \tilde{\zeta}_{x,red} + e^{Az} \underline{c}_1,$$

wherein matrix exponential  $e^{Az}$  has the following form

$$e^{Az} = \frac{1}{2} \begin{bmatrix} \cosh \left( (\mathcal{N}_{red}^{-1} \tilde{D})^{1/2} z \right) & (\mathcal{N}_{red}^{-1} \tilde{D})^{-1/2} \sinh \left( (\mathcal{N}_{red}^{-1} \tilde{D})^{1/2} z \right) \\ (\mathcal{N}_{red}^{-1} \tilde{D})^{1/2} \sinh \left( (\mathcal{N}_{red}^{-1} \tilde{D})^{1/2} z \right) & \cosh \left( (\mathcal{N}_{red}^{-1} \tilde{D})^{1/2} z \right) \end{bmatrix}.$$

The solution for  $\hat{u}$ , including  $\hat{u}_0$ , is then

$$\tilde{u} = -g \tilde{D}^{-1} \tilde{\zeta}_{x,red} + \underline{C}_1 \cosh \left( (\mathcal{N}_{red}^{-1} \tilde{D})^{1/2} z \right) + \underline{C}_2 (\mathcal{N}_{red}^{-1} \tilde{D})^{-1/2} \sinh \left( (\mathcal{N}_{red}^{-1} \tilde{D})^{1/2} z \right),$$

$$\hat{u}_0 = \frac{1}{2} \frac{g}{Re \hat{\nu}_{t,0}} \hat{\zeta}_{0,x} z^2 + \frac{1}{2Re(\hat{\nu}_{t,0})} [\hat{\nu}_{t,p} \cdots \overline{\hat{\nu}_{t,p}}] \tilde{u} + C_{01} z + C_{02}$$

Next, the  $p+2$  unknown constants  $\underline{C}, C_{01}, C_{02}$  are solved using the boundary conditions. The boundary condition at the bed is a partial-slip condition, similar to Version 1. The boundary conditions in vector form read

$$\hat{u}_z(x, 0, t) = \underline{0},$$

$$\mathcal{N} \hat{u}_z(x, -H, t) = s_f \hat{u}(x, -H, t).$$

## A.7. Numerical aspects

The Version 3, 4 and 5 models as well as the salinity and turbulence model are solved numerically. The numerical grid will be presented below, after which it is explained how derivatives and integrals are calculated on the grid.

### A.7.1. Grid

The model is called the two-directional point model (2DPM) because it consists of a sequence of 1DV models, or point models, which are connected by one horizontal grid axis. The grid is shown in Figure 44. The water levels are calculated on the grid points in the horizontal grid, while the velocities are calculated on the cell centres in the vertical grid. The velocity points are defined in the middle of a cell in order to correspond to the implementation in Delft3D-FLOW and therefore allow an extension with the  $k - \varepsilon$  model as it is implemented in Delft 3D-FLOW. Two additional velocity points are added at the surface ( $z = 0$ ) and the bed ( $z = -H$ ) in order to simplify the implementation of the boundary conditions and improve the accuracy of gradients at the bed and surface

The distances between the grid points are denoted by  $\Delta z_k$  as defined in Figure 44. Two additional distances that will be used are

$$\Delta z_{1/2} = \frac{1}{2} \Delta z_1,$$

$$\Delta z_{k_{\max}+1/2} = \frac{1}{2} \Delta z_{k_{\max}}.$$

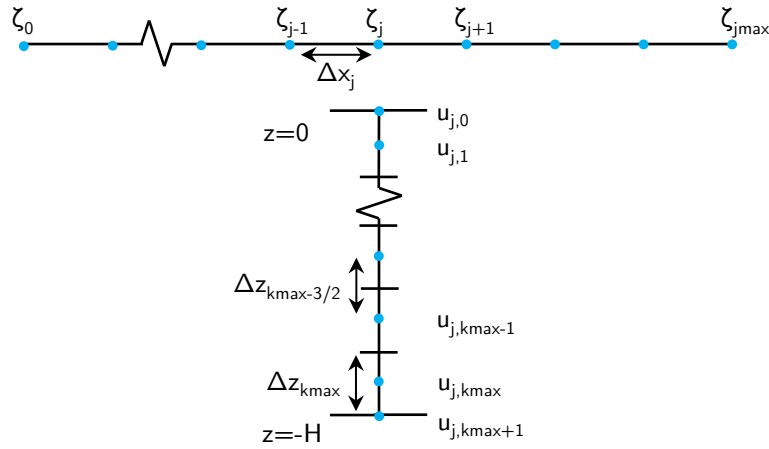


Figure 44: Grid of the 2DPM model. The dots represent velocity points (vertical grid) and water level point (horizontal grid).

The Delft 3D-FLOW  $k - \varepsilon$  model uses a staggered grid approach with the quantities  $k$ ,  $\varepsilon$  and  $\nu_t$  at the cell interfaces and  $u$  and  $\rho$  at the cell centres. The model uses the velocities from the internal velocity points, i.e. excluding the two at the boundaries. Only one grid interpolation is needed in the coupling of the perturbation model and the turbulence model, which is the interpolation of  $\nu_t$  at the cell interfaces in the turbulence model to the cell centres in the perturbation model. The eddy viscosity points at the surface and the bed can be transferred between both modules without interpolation.

### A.7.2. Derivatives & integrals

The single and double vertical derivatives of a quantity  $u$  in the internal cells of the grid are defined as

$$u_{z,k} = \frac{u_{k-1} - u_{k+1}}{\Delta z_{k-1/2} + \Delta z_{k+1/2}},$$

$$u_{zz,k} = \frac{1}{\Delta z_k} \left( \frac{u_{k-1} - u_k}{\Delta z_{k-1/2}} - \frac{u_k - u_{k+1}}{\Delta z_{k+1/2}} \right),$$

for  $k = 1, \dots, k_{\max}$ . Similarly the horizontal derivatives on the internal cells are defined as

$$u_{x,k} = \frac{u_{j-1} - u_{j+1}}{\Delta x_j + \Delta x_{j+1}},$$

$$u_{xx,k} = \frac{1}{\Delta x_j + \Delta x_{j+1}} \left( \frac{u_{j-1} - u_j}{\Delta x_j} - \frac{u_j - u_{j+1}}{\Delta x_{j+1}} \right),$$

for  $j = 1, \dots, j_{\max} - 1$ .

These definitions do not hold in the boundary cells. At the boundaries the derivatives use a one-sided approximation

$$u_{z,0} = \frac{u_0 - u_1}{\frac{1}{2}\Delta z_1},$$

$$u_{zz,0} = \frac{u_{z,0} - \frac{3}{4}u_{z,1}}{\frac{1}{2}\Delta z_1}$$
  

$$u_{x,0} = \frac{u_0 - u_1}{\Delta x_1},$$

$$u_{xx,0} = \frac{u_{x,0} - \frac{3}{4}u_{x,1}}{\Delta x_1}$$

The salinity model deviates from these definitions at a few occasions, where a first-order upwind scheme is used instead of the central scheme in order to prevent numerical oscillations.

The integral of a quantity  $u$  on the vertical grid is defined as

$$\int_{-H}^{z_k} u dz = \sum_{n=k}^{k_{\max}} u_n \Delta z_n.$$

for  $k = 1, \dots, k_{\max}$  and with  $z_k$  equal to the locations of the velocity point  $u_k$ .



# B

## Salinity model

This appendix presents the derivation and implementation of the salinity model. The model is a generalisation of the model by [McCarthy \(1993\)](#). His approach is based on the assumption that advection of salinity is small. As a result the leading-order salinity is well-mixed and vertical variations of salinity only appear in the first-order and higher-orders.

The salinity transport equation reads

$$s_t + us_x + ws_z = \frac{1}{BH} (BHK_H s_x)_x + (K_V s_z)_z,$$

where  $K_H$  and  $K_V$  are horizontal and vertical dispersion coefficients. The value of the horizontal dispersion coefficient is unknown and is used as a closure. The vertical coefficient represents turbulent mixing and is related to the eddy viscosity through a constant Prandtl-Schmidt number  $\sigma_\rho$ .

The boundary conditions to this model are no-flux conditions at the bed and at the surface. The salinity is prescribed at the mouth and is assumed to be a constant. The boundary condition at the landward boundary results from the 1DH salinity equation and is explained below. The four boundary conditions are:

$$\begin{aligned} s_z(x, \zeta, t) &= 0, \\ s_z(x, -H, t) &= 0, \\ s(0, z, t) &= s_{\text{sea}}, \\ Q \frac{1}{H} \int_{-H}^0 s(L, z, t) dz &= BHK_L \frac{1}{H} \int_{-H}^0 s_x(L, z, t) dz, \end{aligned}$$

where  $K_L$  is the salt dispersion at  $x = L$ . An expression for this coefficient is provided at the end of [Section B.1](#).

### B.1. Scaling and derivation of the model

The salinity equation is again ordered around the parameter  $\delta$ . We therefore start by scaling the equations. The typical scales are given in [Table B.1](#). This table repeats the scales given in [Table A.1](#) and adds some new scales.

The derived velocity and eddy viscosity scales in the table are the same as in [Appendix A](#). The typical vertical dispersion coefficient is related to the eddy viscosity scale by a Prandtl-Schmidt number  $\sigma_\rho$  which is  $\mathcal{O}(1)$ . It thus follows that  $K_V = \mathcal{O}(\mathcal{N})$ . The horizontal dispersion scale follows from the 1DH salt balance

$$(Qs - KHBs_x)_x = 0.$$

Scale		Dimensionless quantity
$T_{M_2}$	$M_2$ tidal period	$t = T_{M_2} t^*$
$A_{M_2}$	$M_2$ tidal amplitude at the seaward side	$\zeta = A_{M_2} \zeta^*$
$H_0$	Average depth at seaward side	$z = H_0 z^*$
$L_s$	Salt intrusion length-scale	$x = L_s x^*$
$S$	Typical salinity	$s = S s^*$

Derived scale		Dimensionless quantity
$U$	Typical horizontal velocity of the $M_2$ tide	$u = U u^*$
$W$	Typical vertical velocity of the $M_2$ tide	$w = W w^*$
$\mathcal{N}$	Typical eddy viscosity	$\nu_t = \mathcal{N} \nu_t^*$
$\mathcal{K}_V$	Typical vertical dispersion coefficient	$K_H = \mathcal{K}_H K_H^*$
$\mathcal{K}_H$	Typical horizontal dispersion coefficient	$K_H = \mathcal{K}_H K_H^*$

Table B.1: Scales and derived scales for deriving the dimensionless equations.

We expect  $K_H$  to be of the same order of magnitude as the total dispersion coefficient  $K$  (see e.g. [Fischer \(1972\)](#)). We next use that  $U_q$  is a typical scale for the velocity caused by the river discharge and find

$$\begin{aligned} \mathcal{K}_H &= U_q L_s \\ &= \frac{U_q}{U} \frac{A_{M_2}}{H_0} \frac{L_{tide} L_s}{T_{M_2}}. \end{aligned}$$

The dimensionless salinity equation is

$$\frac{S}{T_{M_2}} s_{t^*}^* + \frac{SU}{L_s} u^* s_{x^*}^* + \frac{SW}{H_0} w^* s_{z^*}^* = \frac{S\mathcal{K}_H}{L_s^2} \frac{1}{B^* H^*} (B^* H^* K_H^* s_{x^*}^*)_{x^*} + \frac{S\mathcal{K}_V}{H_0^2} (K_V^* s_{z^*}^*)_{z^*}.$$

This is rewritten to

$$s_{t^*}^* + \frac{T_{M_2} U}{L_s} u^* s_{x^*}^* + \frac{T_{M_2} W}{H_0} w^* s_{z^*}^* = \frac{T_{M_2} \mathcal{K}_H}{L_s^2} \frac{1}{B^* H^*} (B^* H^* K_H^* s_{x^*}^*)_{x^*} + \frac{T_{M_2} \mathcal{K}_V}{H_0^2} (K_V^* s_{z^*}^*)_{z^*}.$$

We then assume that  $L_s = \mathcal{O}(L_{tide})$ . This means that the salinity gradient is small so that the salinity decreases smoothly over a tidal length-scale. We also assume that  $\frac{U_q}{U} = \mathcal{O}(\delta)$ . The model is restricted to a small river discharge. This results in the equation that is given below, with the scales written under each term:

$$\underbrace{s_t^*}_{\mathcal{O}(1)} + \underbrace{u s_{x^*}^* + w s_{z^*}^*}_{\mathcal{O}(\delta)} = \underbrace{\frac{1}{BH} (BHK_H s_x)_{x^*}}_{\mathcal{O}(\delta^2)} + \underbrace{(K_V s_z)_{z^*}}_{\mathcal{O}(1)}.$$

### B.1.1. Leading-order and first-order equations

The solution  $s$  is written as a power series ordered around the small parameter  $\delta$

$$s = s^0 + s^1 + s^2 + \dots,$$

where  $s^1$  is assumed to be of order  $\delta$ ,  $s^2$  is of order  $\delta^2$  etcetera.

We then find the leading-order equation with boundary conditions

$$s_t^0 = (K_V s_z^0)_z,$$

- $s_z^0(0) = 0,$
- $s_z^0(-H) = 0.$

Integrating this equation over the vertical and applying the no-flux boundary conditions, we find  $s_t^0 = 0$  and therefore  $(K_V s_z^0)_z = 0$ . As a result we have  $K_V s_z^0 = \text{constant}$ , but with the boundary conditions this constant must be zero. We find that the leading-order salinity is uniform over the vertical and constant in time;

$$s^0(x, z, t) = s^0(x) \quad (\text{B.1})$$

The first-order salinity equation is

$$s_t^1 + u^0 s_x^0 + w^0 s_z^0 = (K_V s_z^1)_z.$$

Because  $s^0$  is z-uniform, this equation reduces to

$$s_t^1 + u^0 s_x^0 = (K_V s_z^1)_z, \quad (\text{B.2})$$

- $s_z^1(0) = 0$ ,
- $s_z^1(-H) = 0$ .

### B.1.2. Derivation of the closure equation

The above leading-order and first-order equations form a system of one equation with two unknowns  $s^0$  and  $s^1$ . McCarthy (1993) shows that the second-order depth-averaged time-averaged salinity equation can be used to close the equations. The derivation of this closure equation is presented in this section. The depth-averaged time-averaged salinity equation is

$$\left\langle \int_{-H}^{\zeta} s_t + u s_x + w s_z dz \right\rangle = \left\langle \int_{-H}^{\zeta} \frac{1}{BH} (BHK_H s_x)_x + (K_V s_z)_z dz \right\rangle,$$

where  $\langle \cdot \rangle$  denotes time averaging. This is rewritten to

$$\left\langle \int_{-H}^{\zeta} s_t + (us)_x + (ws)_z - s(u_x - w_z) dz \right\rangle = \left\langle \int_{-H}^{\zeta} \frac{1}{BH} (BHK_H s_x)_x \right\rangle,$$

where the boundary conditions are used in the process of eliminating the vertical dispersion term. Leibniz' rule and continuity are then used to obtain

$$\left\langle \left( \int_{-H}^{\zeta} s dz \right)_t \right\rangle - \langle s \zeta_t \rangle + \left\langle \int_{-H}^{\zeta} us dz \right\rangle_x + \langle -u(\zeta)s(\zeta)\zeta_x + w(\zeta)s(\zeta) - u(-H)s(-H)H_x - w(-H)s(-H) \rangle + \frac{B_x}{B} \left\langle \int_{-H}^{\zeta} us dz \right\rangle = \left\langle \int_{-H}^{\zeta} \frac{1}{BH} (BHK_H s_x)_x \right\rangle$$

Next we use  $u(-H)s(-H)H_x + w(-H)s(-H) = 0$ ,  $-u(\zeta)s(\zeta)\zeta_x + w(\zeta)s(\zeta) = s(\zeta)\zeta_t$  and the definition of time-averaging to simplify this expression to

$$\frac{1}{B} \left\langle B \int_{-H}^{\zeta} us dz \right\rangle_x = \left\langle \int_{-H}^{\zeta} \frac{1}{BH} (BHK_H s_x)_x \right\rangle$$

The second-order equation is then given by

$$\frac{1}{B} \left( B \int_{-H}^0 \langle u^0 s^1 \rangle dz \right)_x + \frac{1}{B} \left( B \int_{-H}^0 \langle u^1 s^0 \rangle dz \right)_x + \frac{1}{B} \langle \zeta B u^0(0) s^0(0) \rangle_x = \frac{1}{B} (BHK_H s_x^0)_x,$$

Next, it is used that

$$\left( B \int_{-H}^0 u^1 \right)_x + (B\gamma)_x = 0.$$

The integration of this from  $x$  to  $L$  yields

$$B(L) \left( \int_{-H}^0 u^1(L) + \gamma(L) \right) - B(x) \left( \int_{-H}^0 u^1(x) + \gamma(x) \right) = 0,$$

which is rewritten to

$$B(x) \left( \int_{-H}^0 u^1(x) + \gamma(x) \right) = Q^1.$$

This expression can be substituted in the closure equation because  $s^0$  is only a function of  $x$ . The substitution results in the final closure equation

$$\frac{1}{B} \left( B \int_{-H}^0 \langle u^0 s^1 \rangle dz \right)_x + \frac{Q^1}{B(x)} s_x^0 - \frac{1}{B} (BHK_H s_x^0)_x = 0. \quad (\text{B.3})$$

- $s^0(0) = s_{\text{sea}}$ ,
- $Qs^0(L) = BHK_L s_x^0(L)$ .

This equation corresponds to the closure equation that is obtained by [McCarthy \(1993\)](#). The boundary condition at  $x = L$  is explained below.

The boundary condition at  $x = L$  follows from an approximation of the closure equation based on the 1DH salinity equation  $(Qs - KHBs_x)_x = 0$ . This 1DH equation is integrated over  $x$  and it is assumed that the integration constant is zero. The equation is then applied at  $x = L$  to form the boundary condition. The dispersion coefficient  $K_L$  is estimated from Equation [B.3](#) as

$$HK_L s_x = HK_H s_x - \int_{-H}^0 \langle u^0 s^1 \rangle dz.$$

## B.2. Vector form of salinity model

We solve the system by using Fourier components. We therefore define

$$\begin{aligned} s^0 &= \text{Re}(\hat{s}^0(x)), & \hat{s}^0 &\in \mathbb{C} \\ s^1 &= \text{Re}\left(\sum_{n=-p}^p \hat{s}_n^1(x, z) e^{ni\omega t}\right), & \hat{s}_n^1 &\in \mathbb{C} \end{aligned}$$

The set of two equations [B.2](#) and [B.3](#) form a linear system of coupled equations that resembles the  $u-\zeta$ -system. The solution procedure that is outlined below is therefore similar to the solution procedure of the  $u-\zeta$ -system

### B.2.1. First-order salinity

First we solve the first-order system [B.2](#) in terms of the unknown  $s^0$ . This equation uses the product  $u^1 s^0$ , which can be expressed in Fourier components as follows :

$$\begin{aligned} u_n^1 s^0 &= \text{Re}\left(\frac{1}{2} \hat{u}_n^1 \hat{s}^0 e^{ni\omega t} + \frac{1}{2} \hat{u}_n^1 \bar{\hat{s}}^0 e^{ni\omega t}\right) \\ &= \text{Re}\left(\hat{u}_n^1 \text{Re}(\hat{s}^0) e^{ni\omega t}\right) \end{aligned}$$

Note that this is different from [McCarthy \(1993\)](#) who erroneously uses  $u_n^1 s^0 = \text{Re}(\hat{u}_n^1 \hat{s}^0 e^{ni\omega t})$ . We see that only the real part of  $\hat{s}^0$  appears in the equation. So we could as well say  $s^0 = \hat{s}^0$  with  $\hat{s}^0 \in \mathbb{R}$ .

Equation [B.2](#) in vector form then reads

$$D\hat{s}^1 - \frac{1}{\sigma_\rho} \mathcal{N}_z \hat{s}_z^1 - \frac{1}{\sigma_\rho} \mathcal{N}_{zz} \hat{s}^1 = -\hat{u}^0 \text{Re}(\hat{s}_x^0), \quad (\text{B.4})$$

where  $D$  and  $\mathcal{N}$  are the same as in the equations of motion A.31. This equation has one remaining degree of freedom. This degree of freedom results from the equation for the subtidal Fourier component. This equation is of the form  $(Re(\nu_{t,0})\hat{s}_{0,z}^1)_z = b$  for some forcing  $b$ . The solution to this equation with no-flux boundary conditions is  $\hat{s}_0^1 = f(x, z) + c$ , where  $f$  is a known function and  $c$  is an arbitrary constant. A compatibility relation is therefore imposed in order to close the system.

The compatibility condition can be derived by taking the time-averaged, depth-integrated form of the first-order salinity equation and applying the no-flux boundary conditions. The condition then reads

$$\int_{-H}^0 \hat{s}_0^1 dz = 0.$$

Alternatively, this condition can be derived from the depth-averaged time-averaged second-order salinity equation. This equation contains all the terms that are responsible for the net salt transport up to order  $\delta^2$ . This has been proven in Equation 3.13, which shows that the difference between the salt balance and the salt model contains only terms of order  $\delta^3$ . The compatibility condition therefore prescribes that all depth-averaged, time-averaged contributions to the salinity should be of leading-order.

### Numerical implementation

The numerical solution method is similar to the the solution method of Version 3 and 4 of the hydrodynamics model. One exception is the solution of the subtidal salinity component  $\hat{s}_0^1$ , which needs the addition of the compatibility condition. The most efficient way of solving Equation B.4 is by solving for the vector  $[\hat{s}_{-p}^1, \dots, \hat{s}_{-1}^1, \psi, \hat{s}_1^1, \dots, \hat{s}_p^1]$ , where  $\psi = \hat{s}_{0,z}^1$ . The compatibility condition is then applied to obtain  $\hat{s}_0^1$ .

The matrix system is first written as a sequence of scalar equations to make it easier to discretise. The discretised equations are of the form

$$D_{nm}\hat{s}_{n,k}^1 - \frac{1}{\sigma_\rho} \sum_{\substack{m=1 \\ m \neq p+1}}^{2p+1} \left[ \mathcal{N}_{nm,k} \frac{1}{\Delta z_k} \left( \frac{\hat{s}_{m,k-1}^1 - \hat{s}_{m,k}^1}{\Delta z_{k-1/2}} - \frac{\hat{s}_{m,k}^1 - \hat{s}_{m,k+1}^1}{\Delta z_{k+1/2}} \right) - \mathcal{N}_{z,nm,k} \frac{\hat{s}_{m,k-1}^1 - \hat{s}_{m,k+1}^1}{\Delta z_{k-1/2} + \Delta z_{k+1/2}} \right] - \frac{1}{\sigma_\rho} \mathcal{N}_{np+1,k} \psi_{z,k} - \frac{1}{\sigma_\rho} \mathcal{N}_{z,np+1,k} \psi_k = -\hat{u}_{n,k}^0 Re(\hat{s}_x^0)$$

for  $n = 1, \dots, 2p+1$ ;  $k = 1, \dots, k_{\max}$ . The subscripts  $j$  to indicate variability in the  $x$ -direction are omitted. The derivative  $\psi_z$  is implemented according to a first-order upwind scheme to prevent numerical oscillations. This scheme reads

$$\mathcal{N}_{np+1,k} \psi_{z,k} = Re(\mathcal{N}_{np+1,k}) \begin{cases} \frac{\psi_k - \psi_{k+1}}{\Delta z_{k+1/2}} & \text{if } Re(\mathcal{N}_{np+1,k}) > 0 \\ \frac{\psi_{k-1} - \psi_k}{\Delta z_{k+1/2}} & \text{if } Re(\mathcal{N}_{np+1,k}) < 0 \end{cases} + \begin{cases} \frac{\psi_k - \psi_{k+1}}{\Delta z_{k+1/2}} & \text{if } Im(\mathcal{N}_{np+1,k}) > 0 \\ \frac{\psi_{k-1} - \psi_k}{\Delta z_{k+1/2}} & \text{if } Im(\mathcal{N}_{np+1,k}) < 0 \end{cases}$$

The discretised scalar equations are put in matrix form again along the same lines as in the hydrodynamic model. This procedure yields a system in matrix form

$$\underline{\underline{\mathcal{R}}}\underline{\underline{\hat{s}}} = -\underline{\underline{\hat{u}}}^0 Re(\hat{s}_x^0),$$

where the double underlining denotes a vector in the numerical calculation with the same ordering as in the hydrodynamic model. The large matrix  $\mathcal{R}$  is a band matrix with maximum bandwidth equal to  $6p+3$ . The remainder of the solution procedure is the same as in the hydrodynamic model.

The solution for  $\hat{s}_0^1$  is obtained by integrating  $\psi$  by numerical integration such as explained in Appendix A.7.

### B.2.2. Leading-order salinity

Next we solve the closure equation B.3. This equation contains the term  $\langle u^0 s^1 \rangle$

$$\langle u^0 s^1 \rangle = Re \left( \left( \overline{\hat{u}}^0 \right)^T \hat{s}^1 \right) = Re \left( \left( \overline{\hat{u}}^0 \right)^T \zeta Re (\hat{s}_x^0) \right),$$

where  $\zeta = -\mathcal{R}^{-1} \hat{u}^0$ .

The leading-order salinity is time-independent and the equation is therefore a scalar equation. This equation reads

$$\left( \int_{-H}^0 \left( \overline{\hat{u}}^0 \right)^T \zeta dz Re (\hat{s}_x^0) \right)_x - \frac{1}{L_b} \left( \int_{-H}^0 \left( \overline{\hat{u}}^0 \right)^T \zeta dz Re (\hat{s}_x^0) \right) + \frac{Q^1}{B(x)} Re (\hat{s}_x^0) = \frac{1}{B} (BHK_H Re (\hat{s}_x^0))_x$$

or equivalently, by using  $Re (\hat{s}_x^0) = s_x^0$ ,

$$\left( \int_{-H}^0 \left( \overline{\hat{u}}^0 \right)^T \zeta dz s_x^0 \right)_x - \frac{1}{L_b} \left( \int_{-H}^0 \left( \overline{\hat{u}}^0 \right)^T \zeta dz s_x^0 \right) + \frac{Q^1}{B(x)} s_x^0 = \frac{1}{B} (BHK_H s_x^0)_x.$$

#### Numerical implementation

The closure equation is an advection-diffusion equation. This is emphasised by rewriting the equation to

$$\left( \int_{-H}^0 \left( \overline{\hat{u}}^0 \right)^T \zeta dz - HK_H \right) s_{xx}^0 + \left[ \left( \int_{-H}^0 \left( \overline{\hat{u}}^0 \right)^T \zeta dz \right)_x - \frac{1}{L_b} \left( \int_{-H}^0 \left( \overline{\hat{u}}^0 \right)^T \zeta \right) + \frac{Q^1}{B(x)} - \frac{1}{B} (BHK_H)_x \right] s_x^0 = 0.$$

This equation is simplified to

$$\text{Dif } s_{xx}^0 + \text{Adv } s_x^0 = 0,$$

- $\text{Dif} = \int_{-H}^0 \left( \overline{\hat{u}}^0 \right)^T \zeta dz - HK_H,$
- $\text{Adv} = \left( \int_{-H}^0 \left( \overline{\hat{u}}^0 \right)^T \zeta dz \right)_x - \frac{1}{L_b} \left( \int_{-H}^0 \left( \overline{\hat{u}}^0 \right)^T \zeta \right) + \frac{Q^1}{B(x)} - \frac{1}{B} (BHK_H)_x.$

The closure equation typically has a grid Péclet number  $\frac{\text{Adv} \Delta x}{\text{Dif}}$  which is greater than 2. A central scheme for the advection terms is therefore unstable and a first-order accurate upwind scheme is used in order to introduce stabilising numerical diffusion. The advection and diffusion terms are discretised according to

$$\begin{aligned} (\text{Dif } s_{xx}^0)_j &= \text{Dif}_j \frac{1}{\Delta x_{j+1/2}} \left( \frac{s_{j+1}^0 - s_j^0}{\Delta x_{j+1}} - \frac{s_j^0 - s_{j-1}^0}{\Delta x_j} \right), \\ (\text{Adv } s_{xx}^0)_j &= \text{Adv}_j \begin{cases} \frac{s_j^0 - s_{j-1}^0}{\Delta x_j} & \text{if } \text{Adv}_j > 0 \\ \frac{s_{j+1}^0 - s_j^0}{\Delta x_{j+1}} & \text{if } \text{Adv}_j < 0 \end{cases} \end{aligned}$$

for  $j = 1, \dots, j_{\max} - 1$ . The boundary condition at the landward side is discretised according to

$$Q^1 s_{j_{\max}}^0 = B_{j_{\max}} H_{j_{\max}} K_{L,j_{\max}} \frac{s_{j_{\max}}^0 - s_{j_{\max}-1}^0}{\Delta x_{j_{\max}}}.$$

The resulting system of equations forms a tridiagonal system

# C

## Implementation of the $k - \varepsilon$ turbulence model

This appendix treats the numerical implementation of the  $k - \varepsilon$  turbulence model and its coupling to the perturbation model. The assumptions that lead to the  $k - \varepsilon$  model have been outlined in Section 1.3 and 2.4 and are treated in more detail by Dijkstra (2014). First, the model equations will be repeated. Next, the discretisation will be presented.

The  $k - \varepsilon$  turbulence model solves a system of two non-linear partial differential equation for the turbulent kinetic energy (TKE)  $k(x, z, t)$  and the turbulence dissipation  $\varepsilon(x, z, t)$ . The model then uses these quantities to calculate the eddy viscosity according to

$$\nu_t = c_\mu \frac{k^2}{\varepsilon},$$

where  $c_\mu$  is a constant in Delft 3D-Flow. Some other models calculate  $c_\mu$  as a function of stratification, which is sometimes called a stability function.

The equations for  $k$  and  $\varepsilon$  are partial differential equations in three spatial dimensions. However, the model is formulated in the vertical direction only, because the gradients in the vertical direction are much greater than the gradients in horizontal direction. The  $k - \varepsilon$  model as used in Delft 3D-FLOW reads

$$k_t = \underbrace{\left( (\nu + \nu_t) k_z \right)_z}_{D_k} + \underbrace{\nu_t u_z^2}_{P_k} - \underbrace{\frac{\nu_t}{\sigma_\rho} N^2}_{B_k} - \underbrace{\varepsilon}_{\varepsilon_k}, \quad (\text{C.1})$$

$$\varepsilon_t = \underbrace{\left( \left( \nu + \frac{\nu_t}{\sigma_\varepsilon} \right) \varepsilon_z \right)_z}_{D_\varepsilon} + \underbrace{c_1 \frac{\varepsilon}{k} \nu_t u_z^2}_{P_\varepsilon} - \underbrace{c_3 \frac{\varepsilon}{k} \frac{\nu_t}{\sigma_\rho} N^2}_{B_\varepsilon} - \underbrace{c_2 \frac{\varepsilon^2}{k}}_{\varepsilon_\varepsilon}, \quad (\text{C.2})$$

where  $N$  is the Brunt-Väisälä frequency or buoyancy frequency, which is defined as

$$N = \sqrt{-\frac{g}{\rho} \rho_z}.$$

The terms on the right-hand side of the equations represent diffusion  $D$ , production by velocity shear  $P$ , production or dissipation by buoyancy  $B$  and viscous dissipation  $\varepsilon$ .

The boundary conditions of the model are

$$\begin{aligned} k(x, \zeta, t) &= 0, \\ k(x, -H, t) &= \frac{u_*^2}{\sqrt{c_\mu}}, \\ \frac{\partial \varepsilon}{\partial z}(x, \zeta, t) &= 0, \\ \frac{\partial \varepsilon}{\partial z}(x, -H, t) &= \frac{|u_*^3|}{9z_0\kappa}, \end{aligned}$$

where  $z_0$  is the roughness height,  $\kappa$  is the Von Kármán coefficient and  $u_*$  is the friction velocity which is defined as

$$u_* = \frac{\tau}{|\tau|} \sqrt{\frac{|\tau|}{\rho_0}}. \quad (\text{C.3})$$

The boundary conditions at the surface are currently implemented on the linearised surface level  $z = 0$ . It is advised to implement these boundary conditions on  $z = \zeta$  in the future.

Following the implementation in Delft 3D-FLOW (Deltares, 2014; Uittenbogaard et al., 1992), the  $k - \varepsilon$  model uses a staggered grid with  $k, \varepsilon, \nu_t$  calculated on the cell interfaces and  $u$  and  $\rho$  in the cell centres. In the equations below, all quantities with subscript and superscript denote quantities on the numerical grid, with the subscript  $k$  denoting the position on the vertical grid axis and the superscript  $n$  denoting the time step. Quantities on cell interfaces will be denoted by an index subscript  $k + 1/2$  ( $k = 0, \dots, k_{\max}$ ), while cell centres use will be denoted by subscript  $k$  ( $k = 0, \dots, k_{\max} + 1$ ). Note that the 'centre' points  $k = 0$  and  $k = k_{\max} + 1$  coincide with the interface points  $k = 1/2$  and  $k = k_{\max} + 1/2$ , see Figure 44.

The basis of the model discretisation is an implicit Euler time stepping scheme with two adjustments. First, the model is linearised. This is done by using Picard's method, i.e. by using a linear part of each term on the new time level and by using the rest on the old time level. One exception is the dissipation term  $\varepsilon_\varepsilon$ , which is linearised by Newton's method. This method takes a first-order Taylor expansion of the term around the old time level. The linearisation is done in such a way that the system of equations is decoupled, allowing for a faster computation. The linearised model is solved without iterating. Such a solution method is justified when the change of  $k$ ,  $\varepsilon$  and  $\nu_t$  is small between two time steps. Second, the  $k - \varepsilon$  model guarantees positive solutions for  $k$  and  $\varepsilon$  (Mohammadi and Pironneau, 1994). The discretisation is therefore adjusted so that the numerical implementation also guarantees positive solutions.

The discretisation for the diffusion term  $D_k$  reads

$$D_{k,k+1/2}^n = \frac{1}{\Delta z_{k+1/2}} \left( (\nu + \nu_{t,k}^n) \frac{k_{k-1/2}^{n+1} - k_{k+1/2}^{n+1}}{\Delta z_k} - (\nu + \nu_{t,k+1}^n) \frac{k_{k+1/2}^{n+1} - k_{k+3/2}^{n+1}}{\Delta z_{k+1}} \right), \quad (\text{C.4})$$

where

$$\begin{aligned} \Delta z_{k+1/2} &= \frac{\Delta z_k + \Delta z_{k+1}}{2}, \\ \nu_{t,k}^n &= \frac{\nu_{t,k-1/2} + \nu_{t,k+1/2}}{2}. \end{aligned}$$

A similar discretisation applies for  $D_{\varepsilon,k+1/2}$ .

The discretised production terms become

$$\begin{aligned} P_{k,k+1/2}^n &= \nu_{t,k+1/2}^n \left( u_{z,k+1/2}^n \right)^2, \\ P_{\varepsilon,k+1/2}^n &= c_1 c_\mu k_{k+1/2}^n \left( u_{z,k+1/2}^n \right)^2. \end{aligned}$$

The dissipation term is a sink and the buoyancy term may be a sink for TKE and can cause  $k$  to become negative. A semi-implicit method (Patankar, 1980) is used to guarantee positivity of the numerical solutions. The discretised terms read

$$B_{k,k+1/2}^n = \frac{\nu_{t,k+1/2}^n}{\sigma_\rho} \begin{cases} N^2 \frac{k_{k+1/2}^{n+1}}{k_{k+1/2}^n} & \text{if } N^2 > 0; \text{ stable stratification} \\ N^2 & \text{if } N^2 < 0; \text{ unstable stratification.} \end{cases}$$

$$B_{\varepsilon,k+1/2}^n = c_3 c_\mu \frac{k_{k+1/2}^n}{\sigma_\rho} \begin{cases} N^2 \frac{\varepsilon_{k+1/2}^{n+1}}{\varepsilon_{k+1/2}^n} & \text{if } c_3 N^2 > 0 \\ N^2 & \text{if } c_3 N^2 < 0. \end{cases}$$

$$\varepsilon_{k,k+1/2}^n = 2\varepsilon_{k+1/2}^n \frac{k_{k+1/2}^{n+1}}{k_{k+1/2}^n} - \varepsilon_{k+1/2}^n,$$

$$\varepsilon_{\varepsilon,k+1/2}^n = \frac{c_2}{k_{k+1/2}^n} \left( 2\varepsilon_{k+1/2}^n \varepsilon_{k+1/2}^{n+1} - \left( \varepsilon_{k+1/2}^n \right)^2 \right)$$

The boundary conditions use the bed friction velocity  $u_*$ . The numerical calculation of this friction velocity does not use the definition of Equation C.3. Rather, it is assumed that the flow velocity in the bottom half cell attains a logarithmic profile so that the friction velocity can be expressed as

$$u_* = \frac{\kappa u_{k_{\max}}}{\ln \left( 1 + \frac{\Delta z_{k_{\max}+1}}{z_0} \right)}.$$

The discretisation of the boundary conditions reads

$$k_{1/2}^n = 0,$$

$$k_{k_{\max}+1}^n = \frac{u_*^2}{\sqrt{c_\mu}},$$

$$\frac{\varepsilon_{1/2} - \varepsilon_{3/2}}{\Delta z_1} = 0,$$

$$\frac{\varepsilon_{k_{\max}-1/2} - \varepsilon_{k_{\max}+1/2}}{\Delta z_{k_{\max}}} = \frac{|u_*^3|}{9z_0\kappa},$$



# D

## Model verification

Several tests were done to verify the model assumptions and accuracy. In Section D.1, the error made by using a limited number of Fourier components is shown. Next, in Section D.2, it is presented how the results change when the  $M_4$  tide is moved from the first-order to the leading-order equations in order to show the validity of the scaling approach. Section D.3 describes the convergence and convergence problems associated with the coupling between the hydrodynamic and turbulence models. Finally, a guide is provided on how to use the salt balance accurately within the perturbation model in Section D.4.

### D.1. Required number of frequency components

The inclusion of temporal variations of the eddy viscosity results in a coupling of infinitely many velocity frequency components. However, the results in this thesis only use the frequencies up to the  $M_6$  frequency, because the higher frequencies are small. This is illustrated in this section by showing the result of the case of Chapter 4 with Version 5 with frequencies ranging up to the  $M_{10}$  component.

The  $M_8$  and  $M_{10}$  components of the water level and velocity are of approximately the same magnitude as the  $M_6$  component and are therefore not negligible, but rather unimportant for many applications. It was shown in Section 4.4 that the  $M_6$  component has little influence on the larger  $M_2$  and  $M_4$  components and on the exchange flow, because of its near-logarithmic profile. The same holds for the  $M_8$  and  $M_{10}$  components. Turbulence is also only weakly affected by the addition of the higher frequency components as is shown in Figure 45. The higher-frequency components are important for the flow velocity around slack tide as much as is the  $M_6$  component.

Instead of increasing the number of frequency components, the number can also be reduced. The inclusion of the  $M_6$  component is not essential for reproducing the qualitative behaviour of the model in the case that was tested in this thesis. It is useful to keep the  $M_6$  component in the model as a diagnostic for other cases; if the  $M_6$  component becomes important for the behaviour of the flow, this signals a new situation that needs more analysis. Such situation is expected for a situation with a smaller water depth, so that friction plays a greater role and the  $M_4$  eddy viscosity becomes more important. The interaction between this eddy viscosity and the  $M_2$  velocity then creates a strong  $M_6$  velocity. In general, it is advised to keep one frequency component that is expected to be unimportant for the qualitative behaviour of the flow for such signalling purposes.

### D.2. Validity of the scaling

The first-order  $M_4$  tide in the case of Section 4.2 grows to an amplitude of 0.4 m at the end of the estuary, which amounts to 2 % of the water depth. The scaling approach requires the first-order tide to be of order

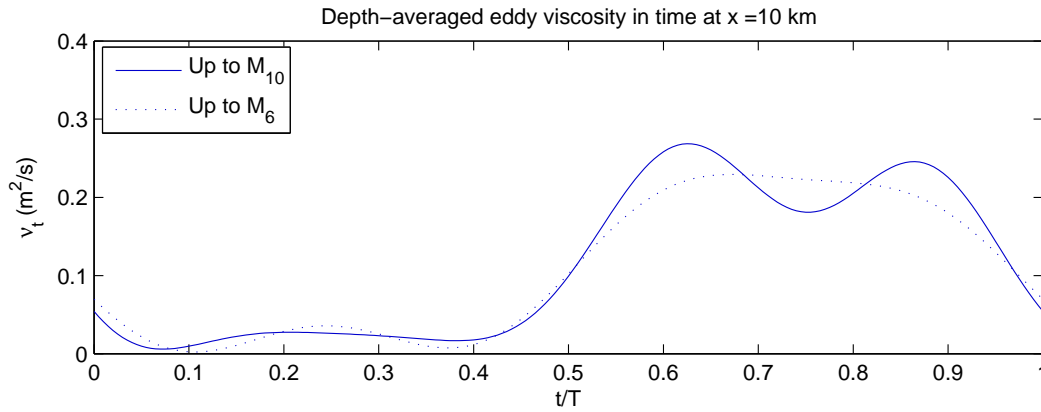


Figure 45: Depth-averaged eddy viscosity at  $x = 10$  km with the  $k - \varepsilon$  model and prescribed well-mixed salinity. The model resolves tidal components up to  $M_{10}$  (solid line) and  $M_6$  (dotted line).

$\delta^2$ , which is satisfied in this case if  $\delta = 0.1$ . The validity of the scaling approach will be shown by comparing this case with the case where the  $M_4$  tide is moved to the first order, while keeping the same magnitude. This section uses Version 2, i.e. with a temporally constant parabolic eddy viscosity, of the model with prescribed salinity field.

The results are displayed in Figure 46. The figure shows the difference between the water level amplitude if the  $M_4$  tide appears in the leading order and if the  $M_4$  tide appears in the first order. The main difference is the  $M_6$  component, which shows a difference of 0.1 m at the end of the basin. The velocity has a maximum difference of 4 cm/s, also originating from the  $M_6$  component. This  $M_6$  component is contained in  $u_{\text{return}}$  flow, the return flow to compensate for Stokes drift. These water level and velocity amplitude differences are small compared to the total water level and velocity.

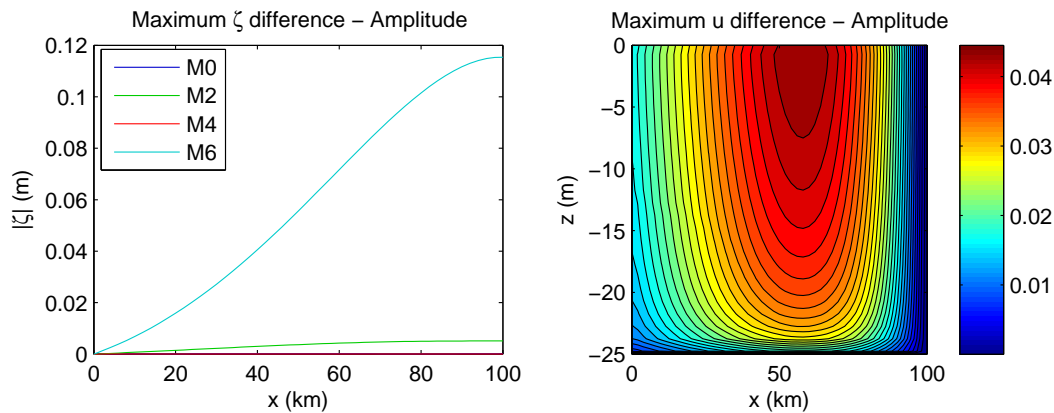


Figure 46: Water level and velocity difference between the case where the  $M_4$  tide is positioned in the leading order and first order in Version 2. Left: difference of water level amplitude. Right: maximum difference of the velocity amplitude.

### D.3. Model convergence and limitations

The coupling of the perturbation model to any turbulence model that depends on the velocity or salinity converts the otherwise linear model to a non-linear model. This non-linear model is solved iteratively. The convergence of several of such iterative solution procedures will be discussed below. Convergence is measured by the supremum norm of the eddy viscosity difference between two consecutive iterations, i.e. the maximum absolute difference in time and space.

The model Versions 3 and 4 become non-linear when the phase of the eddy viscosity is not prescribed, but depends on the velocity. The iterative process of solving this non-linear model converges quickly; within three

to six iterations in all cases that were tested in this research. The simulation is considered to be converged when the phase difference between the phase of the eddy viscosity in the model and the desired phase is less than 0.1 degrees.

The convergence becomes slower when the perturbation model is coupled to a  $k - \varepsilon$  turbulence model. Such slow convergence is caused for a significant part by the under-relaxation procedure (see Section 2.4) which is required in order to establish convergence. The convergence for the case of Section 4.3 is shown in Figure 47. The figure shows the supremum norm of the eddy viscosity difference between subsequent iterations, corrected for under-relaxation. The under-relaxation was 0.9 in this case, which means that the real supremum norm is a factor 10 smaller than is shown in the figure. The convergence is measured directly from the  $k - \varepsilon$  model output (before FFT) and from the signal that is used in the hydrodynamic model (after FFT). The iteration appears to be diverging in the first 30 to 40 iterations, but ultimately reaches linear convergence.

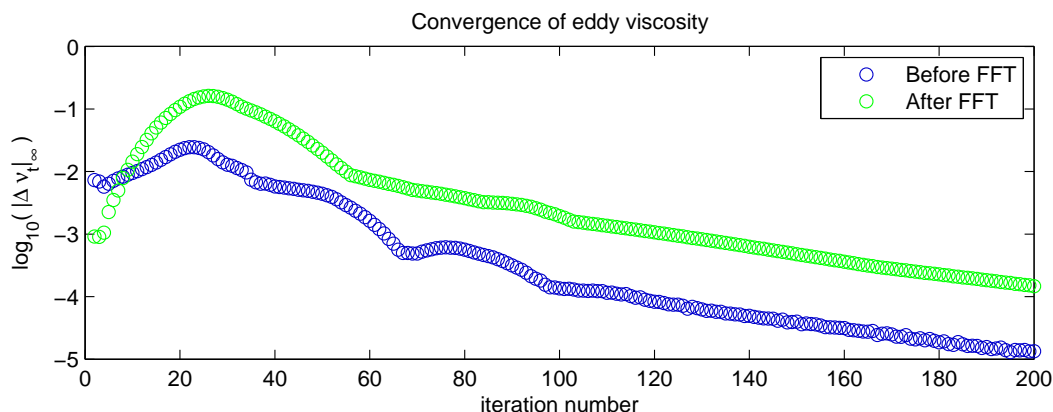


Figure 47: Supremum norm of the difference in the eddy viscosity in subsequent iterations in the case of Section 4.3. The norm is corrected for the under-relaxation factor.

Convergence of the coupled model is not guaranteed for all parameter settings. The convergence of the model stagnates, for example, after 80 to 100 iterations if the roughness coefficient is changed to  $z_b = 0.1$  m. Such stagnation of convergence also happens when the model is coupled to the salinity model and the  $k - \varepsilon$  turbulence model without buoyancy as is shown by Figure 48. The convergence stops after 130 to 150 iterations with a supremum norm of  $6 \cdot 10^{-3}$  m<sup>2</sup>/s after FFT.

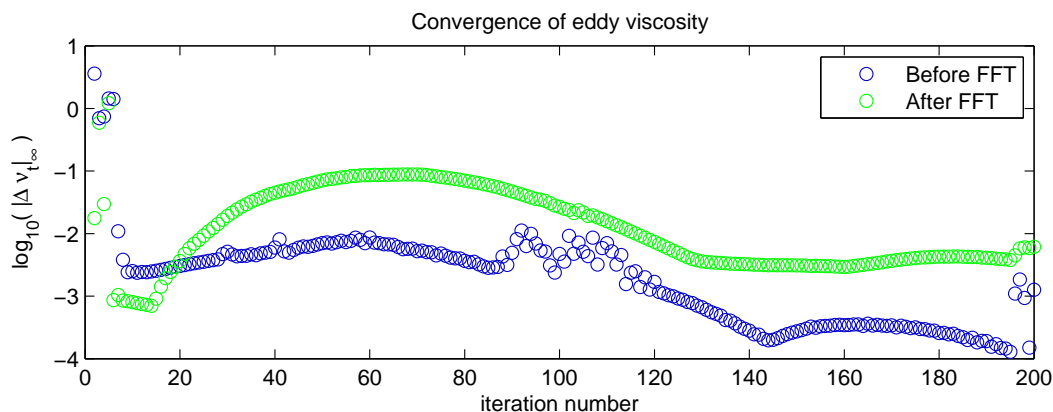


Figure 48: Supremum norm of the difference in the eddy viscosity in subsequent iterations in the case of Section 5.2. The norm is corrected for the under-relaxation factor.

The model diverges when it is coupled to the salt model and the  $k - \varepsilon$  model with buoyancy effects. A possible factor that influences this divergence could be the fast variations of the eddy viscosity due to stable and unstable stratification, which cannot be reproduced by a limited number of Fourier components. Another reason could be the strong sensitivity of the salinity to the eddy viscosity and vice versa.

## D.4. Closure of the salt balance

The salt balance introduced in Section 3.4 uses a grouping of terms which will be explained in this section. The salt balance needs to be used carefully in the perturbation model, because the second-order velocity is not resolved. This will also be explained below.

The full decomposition of the model resolved salt flux  $\langle B(H + \zeta)\overline{u\bar{s}} \rangle$  using the Fischer (1972) decomposition of equation 3.11 contains 16 terms and reads

$$\begin{aligned} \langle B(H + \zeta)\overline{u\bar{s}} \rangle = & BHu_a s_a + Bs_a \langle \zeta u_b \rangle + Bs_a \langle \zeta u_d(0) \rangle \\ & + BH\overline{u_c s_c} + Bs_c(0) \langle \zeta u_b \rangle + Bs_c(0) \langle \zeta u_d(0) \rangle \\ & + BH \langle u_b s_b \rangle + Bu_a \langle \zeta s_b \rangle + Bu_c(0) \langle \zeta s_b \rangle + B \langle \zeta u_b s_b \rangle + B \langle \zeta u_d(0) s_b \rangle \\ & + BH \langle \overline{u_d s_d} \rangle + Bu_a \langle \zeta s_d(0) \rangle + Bu_c(0) \langle \zeta s_d(0) \rangle + B \langle \zeta u_d(0) s_d(0) \rangle + B \langle \zeta u_b s_d(0) \rangle. \end{aligned} \quad (D.1)$$

Many of these terms represent a Stokes drift transport. It is chosen to combine the Stokes drift terms with the depth-averaged term that contains the same salinity component, i.e.

$$\begin{aligned} Qs_a &= BHu_a s_a + Bs_a \langle \zeta u_b \rangle + Bs_a \langle \zeta u_d(0) \rangle, \\ BH \langle u_b s_b \rangle^* &= BH \langle u_b s_b \rangle + Bu_a \langle \zeta s_b \rangle + Bu_c(0) \langle \zeta s_b \rangle + B \langle \zeta u_b s_b \rangle + B \langle \zeta u_d(0) s_b \rangle, \\ BH\overline{u_c s_c}^* &= \zeta \overline{u_c s_c} + Bs_c(0) \langle \zeta u_b \rangle + Bs_c(0) \langle \zeta u_d(0) \rangle, \\ BH \langle \overline{u_d s_d} \rangle^* &= B \zeta \langle \overline{u_d s_d} \rangle + Bu_a \langle \zeta s_d(0) \rangle + Bu_c(0) \langle \zeta s_d(0) \rangle + B \langle \zeta u_d(0) s_d(0) \rangle + B \langle \zeta u_b s_d(0) \rangle. \end{aligned}$$

The idea behind this grouping stems from the first line, in which all terms involving  $s_a$  are grouped. The terms on this line have a clear meaning. Let us consider the situation of homogeneous flow and let us replace  $s$  by a constant density  $\rho$ , then the mass reduces to

$$\langle B(H + \zeta)\overline{u\bar{\rho}} \rangle = BHu_a \rho + B\rho \langle \zeta u_b \rangle + B\rho \langle \zeta u_d(0) \rangle. \quad (D.2)$$

This equation equals the water balance. The last two terms are Stokes drift terms. These Stokes drift terms are compensated for by a return flow that is contained within  $u_a$ . The net result should be equal to the salt transport by the river discharge  $Q\rho$ , so it is physically meaningful to group terms that contain  $s_a$ . Similar arguments do not exist for grouping the other terms, because the remaining Stokes drift terms do not vanish.

The salt balance should be used with care within the perturbation approach, because of the Stokes drift terms. It was shown above in the water balance of Equation D.2 that the Stokes drift term cancels against a return flow. The other Stokes drift terms cancel partly against a return flow. Stokes drift results from the interaction of the velocity and water level elevation at the  $i^{\text{th}}$  order ( $i = 1, 2, \dots$ ), but the corresponding return flow appears only at order  $i + 1$ . This means that the Stokes drift in the first order lacks its corresponding return transport, which appears in the unresolved second-order velocity. All Stokes drift related terms by all first-order velocity components are therefore excluded from the salt balance. This holds for the Fischer decomposition as well as for the decomposition in physical contributions (Section 3.4.2).

Figure 49 is included to illustrate the importance of removing the Stokes drift related terms from the mass balance. The figure shows the salt transport in terms of equivalent dispersion coefficients for the case of Chapter 5 with  $k - \varepsilon$  model without buoyancy. The top-left panel is the same as figure 37 except for the return flow. This return flow is almost fully compensated for by the resolved leading-order Stokes drift shown in the top-right panel. The bottom-left panel shows all higher-order Stokes drift transport terms. These terms are not small and the erroneous inclusion of these terms in the salt balance would therefore have shown a completely different result. It is expected that the second-order and third-order return flows largely compensate for these higher-order Stokes terms.

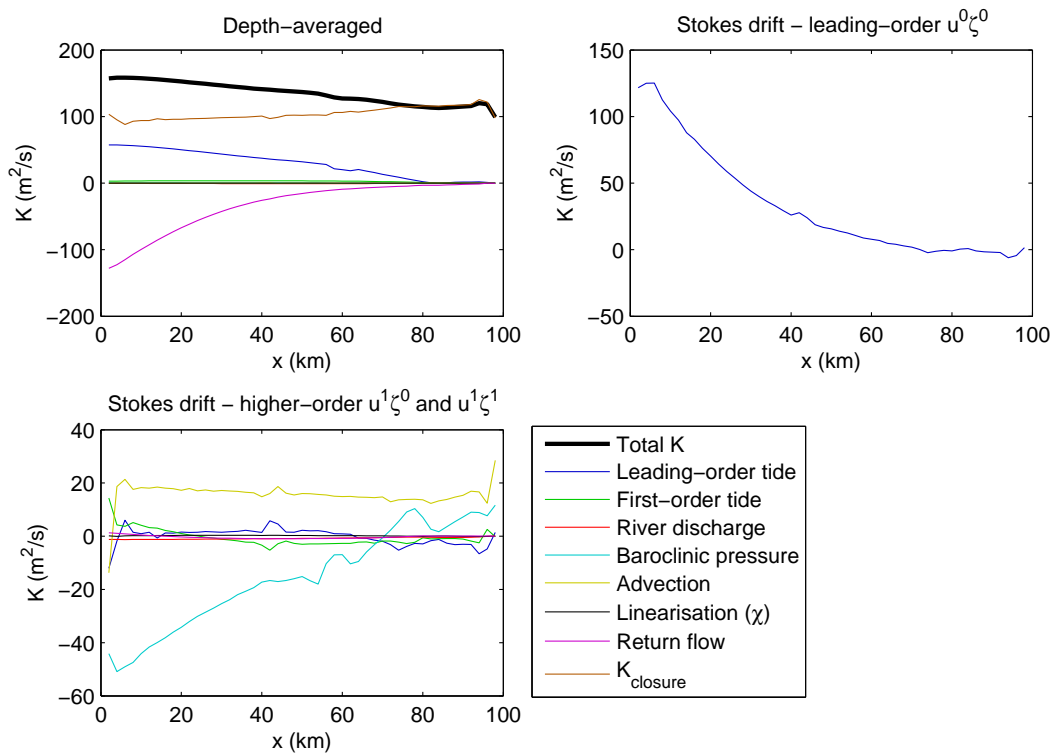


Figure 49: Salt balance separated according to physical contribution. Top-left: transport by flow in interval  $[-H, 0]$ . Top-right: Stokes drift in leading order ( $u^0_{\zeta^0}$ ). Bottom-left: Stokes drift in higher orders ( $u^1_{\zeta^0}$  and  $u^1_{\zeta^1}$ ).



# E

## Approximate analytical solutions to the straining circulation

Section 4.5 uses the analytical solution to the tidal straining circulation that results from the  $M_2$ - $M_2$  interaction of the leading-order tide in with a vertically constant and arbitrary eddy viscosity (Version 3 and 4). The derivations of these solutions are given in Sections E.1 and E.2. Section E.3 will show the proof that the gravitational straining circulation is independent of the phase of the eddy viscosity. In all cases it is assumed that the eddy viscosity and the flow velocity can be described by the residual and  $M_2$  components only.

### E.1. Tidal straining circulation with a constant eddy viscosity profile

We will assume that the eddy viscosity and velocity can be described by an  $M_2$  tide and the residual velocity. These two constituents are assumed to form a strictly weakly interacting system in which the  $M_2$  tide affects the residual flow, but not vice-versa. The eddy viscosity is assumed to be constant in the vertical direction. The solution for arbitrary eddy viscosity profiles will be derived in Section E.2.

The momentum equation for the the leading-order residual flow is

$$-\hat{\nu}_{t0}\hat{u}_{0,zz}^0 = -g\hat{\zeta}_{0,x}^0 + Re\left(\overline{\hat{\nu}_{t1}}\hat{u}_{1,zz}^0\right). \quad (\text{E.1})$$

The general solution is obtained by integrating Equation E.1 twice.

$$\hat{u}_0^0 = \frac{1}{2}\frac{g\hat{\zeta}_{0,x}^0}{\hat{\nu}_{t0}}z^2 - Re\left(\frac{\overline{\hat{\nu}_{t1}}}{\hat{\nu}_{t0}}\hat{u}_1^0\right) + c_1z + c_2.$$

The no-stress boundary condition at the surface is applied to this equation, which results in  $c_1 = 0$ . The partial slip condition at the bed reads

$$\hat{\nu}_{t0}\hat{u}_{0,z}^0(-H) = -Re\left(\overline{\hat{\nu}_{t1}}\hat{u}_{1,z}^0(-H)\right) + s_f\hat{u}_0^0(-H).$$

An expression for  $c_2$  is obtained by substituting the equation in this boundary condition.

$$-\hat{\nu}_{t0}\frac{g\hat{\zeta}_{0,x}^0}{\hat{\nu}_{t0}}H - Re\left(\frac{\overline{\hat{\nu}_{t1}}}{\hat{\nu}_{t0}}\hat{u}_{1,z}^0(-H)\right) = -Re\left(\overline{\hat{\nu}_{t1}}\hat{u}_{1,z}^0(-H)\right) + s_f\frac{1}{2}\frac{g\hat{\zeta}_{0,x}^0}{\hat{\nu}_{t0}}H^2 - s_fRe\left(\frac{\overline{\hat{\nu}_{t1}}}{\hat{\nu}_{t0}}\hat{u}_1^0(-H)\right) + s_fc_2,$$

with solution

$$c_2 = -g\hat{\zeta}_{x,0}^0\left(\frac{H}{s_f} + \frac{H^2}{2\hat{\nu}_{t0}}\right) + Re\left(\frac{\overline{\hat{\nu}_{t1}}}{\hat{\nu}_{t0}}\hat{u}_1^0(-H)\right).$$

The solution for  $\hat{u}_0^0$  is then

$$\hat{u}_0^0 = -g\hat{\zeta}_{0,x}^0 \left( \frac{H}{s_f} + \frac{H^2 - z^2}{2\hat{\nu}_{t0}} \right) + Re \left( \frac{\overline{\hat{\nu}_{t1}}}{\hat{\nu}_{t0}} (\hat{u}_1^0 - \hat{u}_1^0(-H)) \right).$$

A closure for  $\hat{\zeta}_{x,0}^0$  is easily obtained, because we require that the net residual flow is zero. This condition is

$$\int_{-H}^0 \hat{u}_0^0 dz = -g\hat{\zeta}_{0,x}^0 \left( \frac{H^2}{s_f} + \frac{H^3}{3\hat{\nu}_{t0}} \right) + Re \left( \frac{\overline{\hat{\nu}_{t1}}}{\hat{\nu}_{t0}} \left( \int_{-H}^0 \hat{u}_1^0 dz - H\hat{u}_1^0(-H) \right) \right) = 0,$$

so that we find

$$\hat{\zeta}_{0,x}^0 = Re \left( \frac{1}{g} \frac{\overline{\hat{\nu}_{t1}}}{\hat{\nu}_{t0}} \left( \int_{-H}^0 \hat{u}_1^0 dz - H\hat{u}_1^0(-H) \right) \right) \left( \frac{H^2}{s_f} + \frac{H^3}{3\hat{\nu}_{t0}} \right)^{-1}$$

So the final solution for  $\hat{u}_0^0$  is

$$\hat{u}_0^0 = Re \left( \frac{\overline{\hat{\nu}_{t1}}}{\hat{\nu}_{t0}} \left( \frac{1}{H} \int_{-H}^0 \hat{u}_1^0 dz - \hat{u}_1^0 + \kappa(z) \left( \frac{1}{H} \int_{-H}^0 \hat{u}_1^0 dz - \hat{u}_1^0(-H) \right) \right) \right), \quad (\text{E.2})$$

where

$$\begin{aligned} \kappa(z) &= H \left( \frac{H}{s_f} + \frac{H^2 - z^2}{2\hat{\nu}_{t0}} \right) \left( \frac{H^2}{s_f} + \frac{H^3}{3\hat{\nu}_{t0}} \right)^{-1} - 1, \\ &= \frac{1}{2} \frac{s_f}{H} \frac{H^2 - 3z^2}{Hs_f + 3\hat{\nu}_{t0}} \end{aligned}$$

The function  $\kappa(z)$  has a depth-averaged value of zero. The value of  $\kappa$  at the bed is in the range  $(-1, 0]$  and its value at the surface is in the range  $[0, \frac{1}{2})$ .

## E.2. Tidal straining circulation with an arbitrary eddy viscosity profile

We will use the same assumptions as in Section E.1, but the eddy viscosity now has an arbitrary vertical profile. It is assumed that the profiles of the residual and  $M_2$  eddy viscosity are the same.

The derivation of the solution to Version 4 is similar to the derivation above. The equation for Version 4 reads

$$-(\hat{\nu}_{t0}\hat{u}_{0,z}^0)_z = -g\hat{\zeta}_{0,x}^0 + Re \left( (\overline{\hat{\nu}_{t1}}\hat{u}_{1,z}^0)_z \right). \quad (\text{E.3})$$

This equation is integrated once. Next, the boundary at the surface can be applied to eliminate the constant of integration:

$$\hat{u}_{z,0}^0 = g\hat{\zeta}_{x,0}^0 \frac{z}{\hat{\nu}_{t0}} - Re \left( \frac{\overline{\hat{\nu}_{t1}}}{\hat{\nu}_{t0}} \hat{u}_{z,1}^0 \right).$$

The model uses parabolic vertical eddy viscosity profiles with a similar shape and the same roughness parametrisation for  $\hat{\nu}_{t0}$  and  $\hat{\nu}_{t1}$ . So the ratio of the two eddy viscosity components is constant in the vertical direction. This constant is defined as  $\mu$ ;

$$\mu = \left( \frac{\hat{\nu}_{t1,0}}{\hat{\nu}_{t0,0}} \right).$$

The solution for  $u_0^0$  then reads

$$\hat{u}_0^0 = g\hat{\zeta}_{x,0}^0 \int \left( \frac{z}{\hat{\nu}_{t0}} \right) dz - Re (\overline{\mu}\hat{u}_1^0) + c_2. \quad (\text{E.4})$$

For ease of notation we define  $f(z) = \int \left( \frac{z}{\tilde{\nu}_{t0}} \right) dz$ .

The no-slip boundary condition at the bed results in

$$c_2 = -g\hat{\zeta}_{x,0}^0 f(-H).$$

The closure  $\hat{\zeta}_{x,0}^0$  is again derived by requiring a vanishing depth-averaged residual velocity. This yields

$$\hat{\zeta}_{x,0}^0 = \frac{1}{g} Re \left( \bar{\mu} \frac{1}{H} \int_{-H}^0 \hat{u}_1^0 dz \right) \left( \frac{1}{H} \int_{-H}^0 f(z) dz - f(-H) \right)^{-1}.$$

The final solution is then

$$\hat{u}_0^0 = Re \left( \bar{\mu} \left( \frac{1}{H} \int_{-H}^0 \hat{u}_1^0 dz - \hat{u}_1^0 + \kappa(z) \frac{1}{H} \int_{-H}^0 \hat{u}_1^0 dz \right) \right),$$

where

$$\kappa(z) = - \frac{\frac{1}{H} \int_{-H}^0 f(z) dz - f(z)}{\frac{1}{H} \int_{-H}^0 f(z) dz - f(-H)}.$$

### E.3. Phase independence of the gravitational straining circulation

It will be shown that the gravitational straining circulation is independent of the phase of the  $M_2$  eddy viscosity. It is assumed that the velocity and eddy viscosity consist of a residual and an  $M_2$  component. For simplicity of notation it is also assumed that the eddy viscosity is constant in the vertical direction, but a similar derivation holds for general eddy viscosity profiles.

The momentum and depth-averaged continuity equations are reduced to the baroclinic pressure forcing and the balancing barotropic forcing only. We will only consider the interaction between the residual component and the positive Fourier component corresponding to the  $M_2$  tide. The residual flow also interacts with a negative Fourier component of the  $M_2$  tide. This interaction is fully symmetric to the derivation given below. The equations read:

$$\begin{aligned} -\tilde{\nu}_{t0} \hat{u}_{0,zz}^1 &= -g\hat{\zeta}_{0,x,s_x}^1 + \frac{1}{2} \overline{\tilde{\nu}_{t1}} \hat{u}_{1,zz} + g\beta s_{0,xz}, \\ \int_{-H}^0 \hat{u}_0^1 dz &= 0, \\ i\omega \hat{u}_1^1 - \tilde{\nu}_{t0} \hat{u}_{1,zz} &= -g\hat{\zeta}_{1,x,s_x}^1 + \frac{1}{2} \tilde{\nu}_{t1} \hat{u}_{0,zz}^1, \\ i\omega \hat{\zeta}_1^1 + \left( B \int_{-H}^0 \hat{u}_1^1 dz \right)_x &= 0. \end{aligned}$$

The last equation uses  $B$  to denote the width of the estuary. The equations contain both the gravitational circulation (GC) and the gravitational straining circulation (GSC). In order to separate these parts we separate the subtidal water level gradient according to

$$\hat{\zeta}_{0,x,s_x}^1 = \hat{\zeta}_{0,x,GC}^1 + \hat{\zeta}_{0,x,GSC}^1.$$

The  $M_2$  water level gradient contains only the GSC part, because it is not directly forced by the salinity gradient.

The momentum equations are rewritten to

$$-\tilde{\nu}_{t0} \hat{u}_{0,zz}^1 = \underbrace{-g\hat{\zeta}_{0,x,GSC}^1}_{(GSC)} + \underbrace{-\frac{1}{2} \bar{\mu} \left( -g\hat{\zeta}_{1,x,GSC}^1 - i\omega \hat{u}_1^1 \right)}_{(GC)} - \underbrace{g\hat{\zeta}_{0,x,GC}^1 + g\beta s_{0,xz}}_{(GC)} \quad (E.5)$$

$$i\omega \hat{u}_1^1 - \tilde{\nu}_{t0} \hat{u}_{1,zz}^1 = \underbrace{-g\hat{\zeta}_{1,x,GSC}^1 - \frac{1}{2} \mu \left( -g\hat{\zeta}_{0,x,GSC}^1 - g\hat{\zeta}_{0,x,GC}^1 + g\beta s_{0,xz} \right)}_{(GSC)}, \quad (E.6)$$

where

$$\mu = \frac{\hat{\nu}_{t1}}{\nu_{t0}},$$

$$\tilde{\nu}_{t0} = \hat{\nu}_{t0} - \frac{1}{4} \frac{|\hat{\nu}_{t1}|^2}{\hat{\nu}_{t0}} = \hat{\nu}_{t0} \left( 1 - \frac{1}{4} |\mu|^2 \right).$$

The depth-averaged continuity equations can be rewritten in an abstract notation to

$$\mathcal{B}_0 \zeta_0^1 = -\bar{\mu} \underbrace{\int_{-H}^0 \mathcal{A}_0^{-1} \left( -g \hat{\zeta}_{1,x,GSC}^1 - i\omega \hat{u}_1^1 \right) dz}_{(GSC)} - \underbrace{\int_{-H}^0 \mathcal{A}_0^{-1} g \beta s_{0,xz} dz}_{(GC)} \quad (\text{E.7})$$

$$\mathcal{B}_1 \zeta_1^1 = - \left( \mu B \int_{-H}^0 \mathcal{A}_0^{-1} \left( -g \hat{\zeta}_{0,x,GSC}^1 - g \hat{\zeta}_{0,x,GC}^1 - g \beta s_{0,xz} \right) \right)_x dz,$$

$$\approx -\mu \underbrace{\left( B \int_{-H}^0 \mathcal{A}_0^{-1} \left( -g \hat{\zeta}_{0,x,GSC}^1 - g \hat{\zeta}_{0,x,GC}^1 - g \beta s_{0,xz} \right) \right)_x}_{(GSC)} dz \quad (\text{E.8})$$

The abstract operators are linear operators of which the exact formulation is not important for the present purposes. In the final equation it is assumed that  $\mu_x$  is negligible<sup>1</sup>.

Equations E.5 and E.7 describe the subtidal velocity and water level. The  $M_2$  velocity and water level act as a forcing in these equation via the factor  $\mu$ . Similarly, the subtidal velocity and water level acts as a forcing in Equations E.6 and E.8 via  $\bar{\mu}$ . So the variable  $\mu$  acts as a coefficient that regulates the interaction between the frequency components.

We will focus on the dependency of the solution of the GSC part on the eddy viscosity. The residual GSC velocity and water level depend linearly on the forcing from the  $M_2$  velocity and water level. Similarly, the  $M_2$  velocity and water level depend linearly on the forcing from the residual component. We can therefore write

$$\hat{u}_{0,GSC}^1 \sim \bar{\mu} \left( f_1(\hat{\zeta}_{1,GSC}^1, \hat{u}_{1,GSC}^1) \right),$$

$$\hat{\zeta}_{0,GSC}^1 \sim \bar{\mu} \left( f_2(\hat{\zeta}_{1,GSC}^1, \hat{u}_{1,GSC}^1) \right),$$

$$\hat{u}_{1,GSC}^1 \sim \mu \left( f_3(\hat{\zeta}_{0,GSC}^1, \hat{u}_{0,GSC}^1) \right),$$

$$\hat{\zeta}_{1,GSC}^1 \sim \mu \left( f_4(\hat{\zeta}_{0,GSC}^1, \hat{u}_{0,GSC}^1) \right),$$

where the functions  $f_n$ ,  $n = 1, 2, 3, 4$  are some functions that do not depend on the  $M_2$  eddy viscosity and that depend linearly on their two arguments. The variables can be substituted to obtain the following dependency of the subtidal and  $M_2$  velocity and water level. This yields

$$\hat{u}_{0,GSC}^1 \sim |\mu|^2 \left[ f_1 \left( f_4(\hat{\zeta}_{0,GSC}^1, \hat{u}_{0,GSC}^1), f_3(\hat{\zeta}_{0,GSC}^1, \hat{u}_{0,GSC}^1) \right) \right],$$

$$\hat{\zeta}_{0,GSC}^1 \sim |\mu|^2 \left[ f_2 \left( f_4(\hat{\zeta}_{0,GSC}^1, \hat{u}_{0,GSC}^1), f_3(\hat{\zeta}_{0,GSC}^1, \hat{u}_{0,GSC}^1) \right) \right],$$

$$\hat{u}_{1,GSC}^1 \sim |\mu|^2 \left[ f_3 \left( f_2(\hat{\zeta}_{1,GSC}^1, \hat{u}_{1,GSC}^1), f_1(\hat{\zeta}_{1,GSC}^1, \hat{u}_{1,GSC}^1) \right) \right],$$

$$\hat{\zeta}_{1,GSC}^1 \sim |\mu|^2 \left[ f_4 \left( f_2(\hat{\zeta}_{1,GSC}^1, \hat{u}_{1,GSC}^1), f_1(\hat{\zeta}_{1,GSC}^1, \hat{u}_{1,GSC}^1) \right) \right].$$

The only parameter that contains phase information of the eddy viscosity is  $\mu$ , which appears only in its absolute value in this equation. The phase of the eddy viscosity therefore cancels from the equations. So the GSC components of the velocity and water level are independent of the phase of the eddy viscosity. A sensitivity test shows that this conclusion indeed holds in Version 3 and also for the depth-averaged phase of the eddy viscosity in Version 4 and 5.

<sup>1</sup>The same structure would also be obtained under the weaker assumption that  $|\mu|_x$  is negligible, i.e. the ratio of the subtidal and  $M_2$  eddy viscosity amplitudes remains constant.